# Mind the Traffic: Validation and characterisation of artemisinin resistance pathways in *Plasmodium falciparum* by genome editing

Ryan Christopher Henrici

Thesis submitted in accordance with the requirements for the degree of Doctor of Philosophy of the University of London

May 2018

Department of Immunology and Infection
Faculty of Infectious and Tropical Diseases
LONDON SCHOOL OF HYGIENE & TROPICAL MEDICINE

Funded by Her Majesty's Government, UK Foreign and Commonwealth Office
Marshall Aid Commemoration Commission

Research Group Affiliations: Colin Sutherland Laboratory

Supervisor: Professor Colin J. Sutherland

London School of Hygiene & Tropical Medicine

# Declaration

I, Ryan Christopher Henrici, declare that the work presented in this thesis is my own. Where information has been derived from other sources, I confirm that this has been indicated in my thesis.

# Acknowledgements

They say that completing a PhD is a lonely endeavour. That you spend three to four years immersed 30,000 leagues under the sea examining your corner of the natural world under, quite literally in this case, a microscope. One might argue that is isolating over time. But looking back on the last nine hundred fifty-seven days, the process somehow seems like the worldliest thing I have ever done. In large part, this is due to the people with whom I have worked shoulder to shoulder on this project, on their project, on the global effort against malaria. This project is not complete, but without the support of these people, this project simply would not be. LSHTM does not have the shiniest labs or the newest equipment, however LSHTM is unique because of its people. I have had the distinct privilege of meeting and working alongside scientists and physicians from around the world, particularly from endemic countries. I have learned about health systems, discussed politics, and enjoyed culture unique to all of these countries. As an American in London, I am forced to confront these features of my own identity, and reflecting now, there is no other institution at which I would have rather studied. Here is my attempt to thank those who have played a part in this grand adventure.

The thanks necessarily start with the mentorship of Drs Wood and Best at Conestoga High School. We built incredible machines and performed the tiniest reactions, and together, we turned new pages in the science of coffee and caffeine. You showed me that the pursuit of science was worthy. That funding did not matter. That with a bit of cleverness and determination, one could achieve great things. Those basic lessons have enabled my success.

Throughout my PhD, there have been dark days that challenged my will to complete this project. On those days, I often turned to Prof Song Tan. Song, you have been there every step of the way to celebrate my success, to voice reason, and above all to be a sincere and genuine friend. You have taught me too many things about life and science to list, and I am truly honoured to have followed in your footsteps as a Marshall Scholar. It has been the experience of a lifetime. On a very practical note, thank you for making the pSLI-Ubp1-GFP-neo$^{R}$ plasmid described in Chapter 7. I tried for months to create that plasmid with no success, and without your sacrifices to the gremlins, Chapter 7 may never have happened.

Now to Lab 318 at LSHTM. Khalid, Julian, and Mary, you have all been wonderful labmates. It's been a privilege to watch you all develop your projects and careers, and you have all provided counsel and made me feel at home. Don, you have been an invaluable pillar of support in the culture lab. You are a senior post-doc but still volunteered to help me

with some horrible timecourse experiments and have stepped in to take care of cultures for me throughout my time here. Our chats while working in the hoods have been great fun, and I wish you all the best as you develop your own lab.

Christian, Avi, and Steph, you three have been my first line go-to guys for help and advice in the lab. You all have been invaluable sounding boards for shaping ideas and rationalising data. To the entire Baker lab, thank you for opening your fridges, freezers, and equipment to me. Enzymes, antibodies, and reagents are the bread and butter of any thesis, and your laboratory generously treated me as one of their own. I am very much indebted to you all. Our friendships and the shenanigans we got up to have formed memories to last a lifetime. I hope our paths cross again.

Melissa, Franziska, and Rob – though we have turf wars in 318 and 310c, we've developed a remarkable collaboration and friendship. Your help with the *P. knowlesi* work described in this thesis was instrumental. Melissa, I cannot state how much I appreciate you taking time out of your own PhD to help with the transfections and our brief foray into immunoEM. We've done some incredible work together, and I can't wait to see how your work wraps up over the next year. Rob, thank you very much for your counsel, experimental and personal throughout my time here, and your editing of this thesis.

I would be remiss if I did not acknowledge the efforts of the Mark Field and Audrey Odom-John laboratories. Mark and Martin, you took me into your lab to learn cryomilling and IP-MS pipelines and made me feel at home. Your help with the pulldowns and mass spectrometry has taken my PhD and the manuscripts that will result from it to a new level. We're turning new pages in *Plasmodium* biology, and I am very excited to see where this new collaboration goes. The IEMs described in this thesis would not have been possible without the efforts of Audrey Odom-John and Rachel Edwards at Washington University, St Louis. Your efforts and attention to detail have complemented our collaboration with Mark and Martin to clarify the fascinating biology of AP-2 and Clathrin, and we are indebted to you.

To Prof Tobias Spielmann, your provision of µ2-GFP and Clathrin-GFP parasite lines have made several lines of work in this thesis possible. Prof Frances Brodsky, your clathrin heavy chain antibody was an unexpected gift that has allowed us to pursue connections between clathrin and AP-2.

To the David Fidock laboratory, thank you for taking me into your lab last spring as we sought answers to fundamental questions about K13 and AP-2. Your monoclonal antibody against K13 helped kick this project forward into new and interesting territory. Most importantly, you've taught me invaluable lessons about how to and how not to do science.

To Prof Andrew Osbourne, you have been like a second supervisor at times. You have guided my scientific intuition, and your scepticism has pushed me to be ruthless with my data. I greatly appreciate our long discussions and your edits on this thesis.

The last person to thank is perhaps the most difficult. Prof Colin Sutherland, you've been an incredible mentor to me since I started. I know I am unruly and tough to work with, and you have somehow carefully guided me through this process from start to finish. You have been a champion of my success and pushed me to become the scientist I am today. I am very grateful for your patience and support. You have stuck your neck out for me when others would not have, while simultaneously giving me the space and resources to chase wild theories at the fringes of malaria biology. We've accomplished incredible things together, and I hope we can continue to push these stories forward. Thank you for everything.

Last but certainly not least, I want to thank my family. Despite the distance and time differences, you have been there for me every step of the way. I can't wait to celebrate this textbook I'm calling a thesis with you in July. You all know every high and every low, and I miss you all incredibly. Kelley, you are family to me. I cannot repay or describe the sacrifices you have made to support me. The longest nights in the lab and 7-day schedule I maintained for months on end took tolls from both of us, but you handled it without complaint. I love you all to the moon and back. Now back to the Philly…

-

R. Henrici is funded and supported by a Marshall Scholarship, granted by the Marshall Aid Commemoration Commission and Her Majesty's Government and funded by the Foreign and Commonwealth Office.

-

*"If I have seen further it is by standing on the shoulders of giants."*

- Sir Isaac Newton, 1675

# Abstract

Artemisinin susceptibility in Plasmodium falciparum is modulated by mutations in the gene *pfk13*, which encodes a kelch propeller domain protein of unknown function. Reduced susceptibility is demonstrated *in vitro* by elevated parasite survival after short exposures to physiologic concentrations of drug in the early ring stage. Using CRISPR-Cas9 genome editing, we provide the first evidence of a similar but K13-independent *in vitro* artemisinin resistance caused by single base changes in the genes encoding the AP-2 adaptor complex µ-subunit (*pfap2mu*) and the deubiquitinase Ubp1. Through extensive fluorescence and electron microscopy and proteomics, functional characterisation of PfAP2µ shows that gene as encoding a non-canonical AP-2 trafficking factor that may interact with K13 and other important factors in the cytosol and near the ER and is essential for asexual parasite survival. This thesis provides evidence that disruption of trafficking in early rings initiates an ER-based stress response that underlies artemisinin resistance and induced dormancy. A model depicting a role for ER trafficking components in ring-stage artemisinin action is proposed. Brief characterisations of Ubp1 and clathrin heavy chain are also provided, showing for the first time that clathrin may support multiple key secretory organelles and that malarial deubiquitinases are attractive drug targets.

# Table of Contents

## Summary

Despite considerable reductions in malaria mortality achieved by collective parasite and vector control efforts over the last 20 years, malaria still remains one of the top causes of death among children under the age of 5 globally[1]. Further, important gains against *Plasmodium falciparum*, the species responsible for the majority of malaria deaths, are currently threatened by growing parasite resistance to frontline chemotherapies[1]. Genomic investigations into the roots of resistance in our lab and many others have correlated parasite drug responses with a complicated web of polymorphisms in many genes including *pfk13*, *pfcrt*, *pfmdr1*, *pfdhfr*, *pfdhps*, *pfap2μ*, and *pfubp1*. Though statistically significant, these correlations cannot prove causation. Therefore, studies that blend *in vitro* biochemical assays with manipulation of the parasite genome could shed important light on the biological roles of individual or combinations of mutations in modulating drug sensitivity *in vivo*.

This thesis will characterize the phenotypic impacts of mutations in the *pfap2μ* and *pfubp1* genes that have been tracked over the past several years in our laboratory through high-throughput PCR-seq studies of parasite DNA samples from sub-Saharan Africa and *in vitro* transgenesis. Specifically, I will perform a retrospective genetic analysis on blood samples from patients who have undergone ACT treatment to evaluate the prevalence, distribution, and dynamics of SNPs in these alleles in East Africa. Informed by these studies, I will use the CRISPR-Cas9 genome manipulation system recently established in *P. falciparum* to perform reverse genetics experiments by engineering mutations that have been correlated with resistant phenotypes *in vitro* and *in vivo* into parasites and fully characterise their sensitivity profiles to chloroquine, artemisinin, and ACT partner drugs such as lumefantrine and mefloquine. I will then characterise the biological role of these proteins and seek to provide mechanistic insight into how artemisinin resistance occurs. This thesis will contribute to our understanding of the molecular and genetic determinants of drug resistance and provide critical information to healthcare practitioners and regional health experts about the roles of particular mutations in their surveillance networks.

## List of Tables

## List of Figures

# Chapter 1

# Introduction

## 1.1 Malaria as a global problem

Malaria is the clinical term for the human and animal infectious disease caused by infection with one of several parasites of the genus *Plasmodium*. Although malaria symptoms were first recorded nearly five thousand years ago in ancient Chinese medical texts, *Plasmodium* parasites are believed to have existed on Earth for more than thirty million years[1,2]. In 2015, the World Health Organization estimated 214 million clinical cases and 438,000 deaths occurred worldwide while nearly 3.2 billion people were at risk of developing malaria[3]. Of these cases and deaths, the vast majority occur in young children. Though these data represent a 48 per cent decline in mortality since 2000, malaria remains a major oppressive force in tropical developing nations.

## 1.2 Several *Plasmodium* species cause clinical malaria

While there are more than 250 members of the *Plasmodium* genus, only six species are known to cause naturally-occurring malaria in humans: *P. falciparum*, *P. vivax*, *P. malariae*, *P. knowlesi*, *P. ovale curtisi*, and *P. ovale wallikeri*. Recent evidence suggests that other species including *Plasmodium cynomolgi*, *Plasmodium simium*, *Plasmodium inui*, and *Plasmodium brasilianum*, which were previously

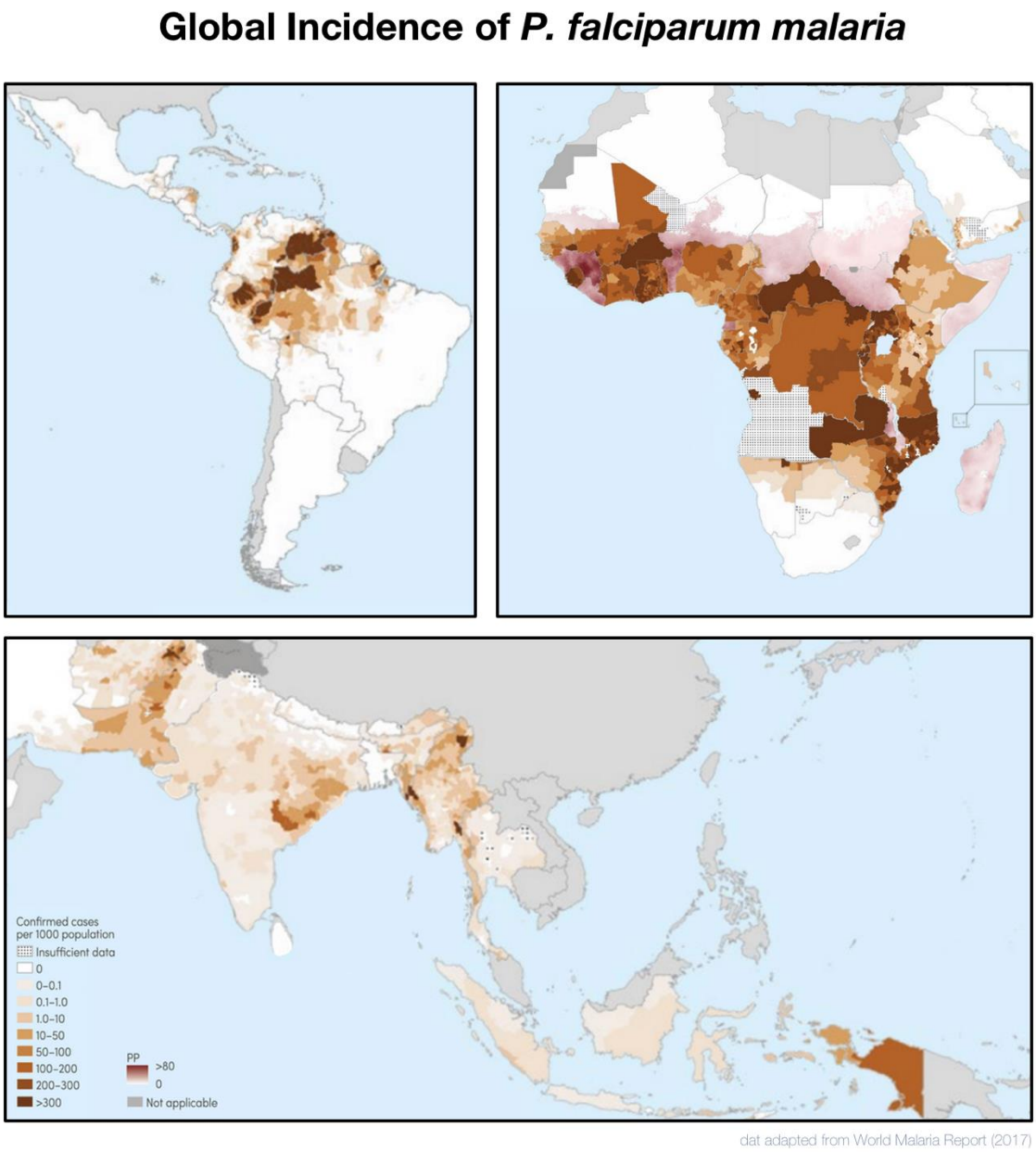


**Figure 1 Global Incidence of *P. falciparum***
Global distribution map of *Plasmodium falciparum* based on data from the 2017 World Malaria Report[3].

thought to exclusively infect non-human primates, may also be able to infect human hosts, though further investigation is needed [4–7]. Although the distribution of species varies geographically, *P. falciparum* is responsible for the vast majority of cases worldwide. *P. vivax* is the next most prevalent parasite at roughly 1 in 5 cases, and the other *Plasmodium* spp. contribute the remaining incidence. Polyclonal and multi-species infections also contribute to this incidence.

Recent evidence suggests that these data may not reflect the true distribution of cases for several reasons. For example, *P. ovale* spp. are sympatric and can only be differentiated by PCR[8]. Morphologically, they resemble *P. vivax.* Likewise, the morphology of *P. knowlesi* is nearly identical to *P. malariae.* Interestingly, though *P. malariae* is thought to be responsible for a small portion of the overall malaria disease burden, it has been found as a co-infecting species in as many as 50% of RDT-confirmed *falciparum* infections in Southern Uganda and 4-8% of infections in other parts of equatorial Africa [9–12]. These underlying *P. malariae* infections are less likely to be cleared during standard ACT treatment and presumably account for an unknown number of asymptomatic infections[13]. Therefore, while *P. ovale*, *P. knowlesi*, and *P. malariae* may be less prevalent than *falciparum* infections overall, these species are likely underreported and remain important contributors to human malaria infection[12].

### 1.2.1 The *Plasmodium* lifecycle

Though there are divergences in morphology and geographic localization, the life cycles of all six *Plasmodium* species can be understood as slight variations on the *P. falciparum* stages (Fig 2). In the blood, merozoites, the short-lived,

exoerythrocytic parasite stage, quickly adhere to and invade an uninfected red blood cell. Once inside a red blood cell, the parasites have a roughly 48 hour life cycle during which the parasite undergoes considerable morphologic, metabolic, and gene regulatory changes as it progresses from the early ring stage to the later trophozoite and schizont stages [14,15]. In *P. knowlesi* and *P. malariae*, the asexual cycle progresses over 24 and 72 hours, respectively. Near the end of this asexual cycle, the parasite undergoes several rounds of asexual, nuclear replication and division followed by a specialised cytokinesis in a process called schizogony, producing up to, in *P. falciparum*, 16-24 daughter merozoites primed for release. Shortly thereafter, the blood cell ruptures, and the merozoites egress.

Thus, a patient's total parasitaemia (percentage of infected red cells) can increase quite rapidly over the course of a few days in an untreated or drug resistant infection and in some cases lead to cerebral malaria, severe anaemia, and/or death. Because this blood stage is responsible for the clinical symptoms and mortality of malaria, most pharmacologic interventions aim to rapidly reduce the parasite burden in the periphery.

During the course of an infection, some of these asexual parasites will differentiate into male and female gametocytes. In *P. falciparum*, cyclic nucleotide signalling cascades initiated by cGMP-dependent protein kinase in schizonts control this process, which ultimately concludes in the development of elongated Stage V gametocytes. In other species, gametocytes are present throughout the infection, and the mechanisms underpinning their development are less clear. Gametocytogenesis is the subject of intense investigation from perspectives of basic biology, drug design, and vaccine development. By targeting the gametocyte stages, drugs or vaccines could block transmission. Recent analysis of these so-called transmission-

blocking drugs and vaccines by Andrew Blagborough suggests, unlike drugs or vaccines that target the blood-stage, the efficacy of transmission-blocking agents can be low and still have a remarkable impact on transmission[16].

Once gametocytes taken up during a bloodmeal by a female Anopheline mosquito reach the gut, 8-12 male gametes undergo egress and exflagellation into male microgametes. Each microgamete is capable of fertilising the female macrogamete and producing a zygote, which matures into an ookinete. Mature ookinetes exit the insect midgut through the basement membrane of the gut epithelium via the action of secreted prochitinases (activated by trypsin in the gut) and traverse the gut wall, forming oocysts. Oocysts divide into multiple sporozoites via a division process resembling schizogony called sporogony, and these sporozoites migrate to the mosquito salivary glands. This entire process can take up to two weeks.

The number of sporozoites that an infective mosquito injects into a host during a bloodmeal varies from less than ten to potentially more than one hundred [17]. Sporozoites in the host bloodstream or lymphatics will infect hepatocytes in the liver and undergo multiple rounds of asexual replication during the pre-erythrocytic liver stage of the infection. After several divisions, merozoites will enter peripheral circulation and infect erythrocytes, beginning a new bloodstage infection.

Interestingly, by an unknown mechanism, *P. vivax* and *P. ovale* spp. are able to differentiate some liver stage parasites into dormant hypnozoite parasites that awaken periodically to release new infectious merozoites, which trigger a new blood stage infection even after a previous blood stage infection has been successfully cured or cleared or supressed by immunity.

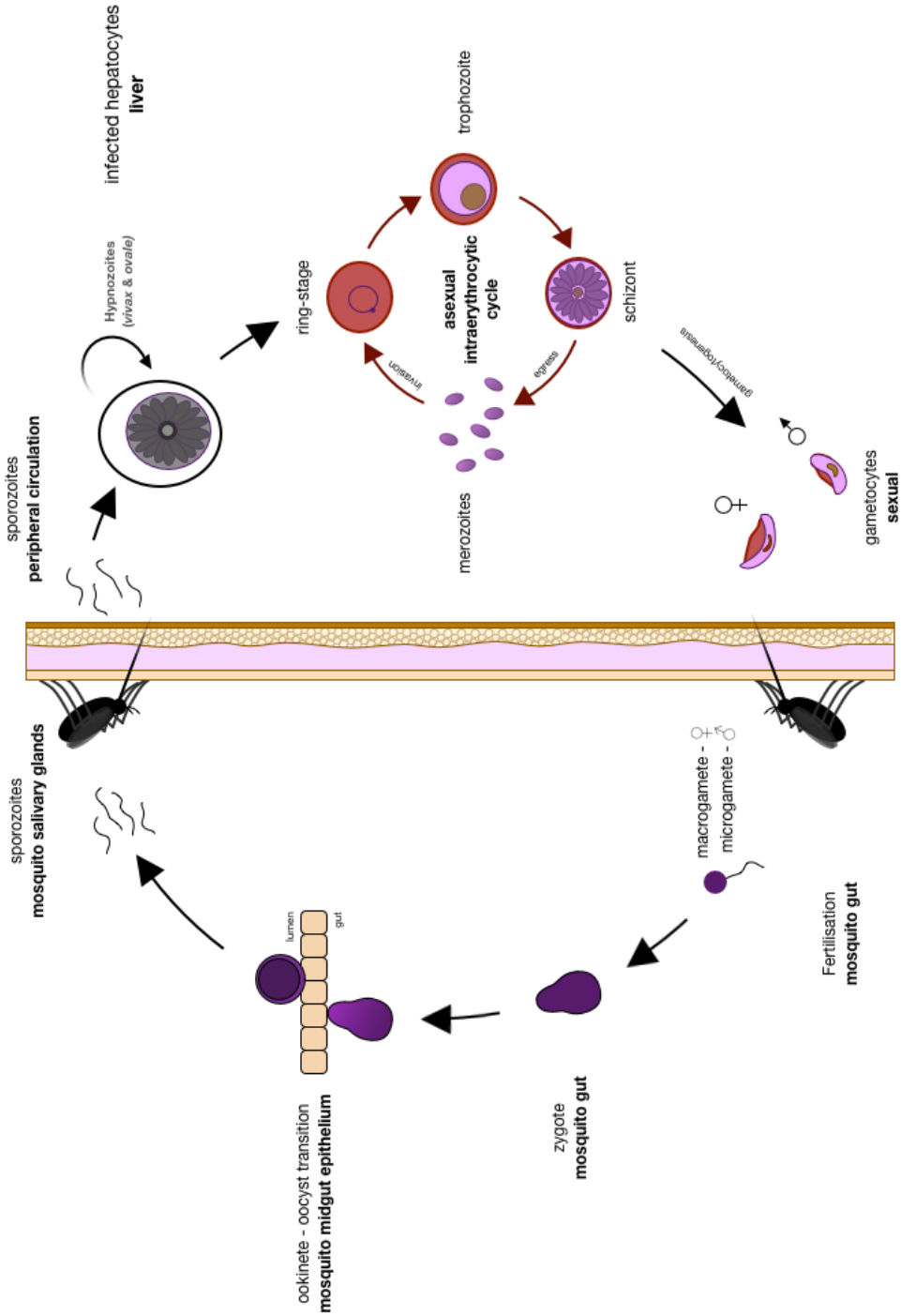


**Figure 2 Full lifecycle of Plasmodium species**
The lifecycle of the human-infecting *Plasmodium* species exists between two hosts. Mosquitos inject mature sporozoites via a bite. These sporozoites infect the liver and ultimately differentiate into asexual merozoites, which infect red blood cells in circulation. During the course of the bloodstage infection, some of these parasites differentiate into sexual gametocytes, which are taken up by a mosquito bite.

## 1.3 Current anti-malaria efforts and challenges

On the most fundamental level, malaria infections involve people, parasites, and mosquitoes. These basic groups represent the major focal points for interventions to treat, prevent, and eradicate malaria. Parasites can be eliminated with drugs; new infections can be prevented with vaccine-induced host immunity; transmission can be blocked with insecticides, bed nets, and transmission-blocking drugs and vaccines (Fig 3). Each avenue is currently subject to intense scientific investigation, and while great advances have been made in each category, some considerable challenges still frustrate global malaria eradication efforts.

### 1.3.1 Drugs and drug resistance

Malaria chemotherapy has a long and storied history. For centuries, medical practitioners successfully treated malaria fevers and symptoms using herbal remedies derived from *cinchona* bark and the *qinghao* plant, which we now know to contain quinine and artemisinin (qinghaosu), respectively. These drugs were eventually isolated from their natural sources, and quinine dominated malaria therapy into the 20$^{th}$ century. In support of the soldiers and efforts of many countries involved in the World Wars, analogues of quinine and novel anti-malarials were developed and deployed to great success [18]. Widespread use during the first half of the century led to evidence of drug resistance by the late 1950s. By implementing state-level malaria drug schedules and distributing novel "artemisinin-combination therapies" (ACT) where an artemisinin is co-administered with a partner drug, we have temporarily regained the upper hand over the *Plasmodium* parasites and dramatically reduced infection rates and mortality, especially in children. Further, by administering

antimalarials as prophylaxis to pregnant mothers and infants through intermittent preventative treatment regimens (IPTp and IPTi), millions of cases of placental malaria and severe anaemia have been avoided across Sub-Saharan Africa [19–23]. However, recent evidence suggests that even the effectiveness of frontline ACTs are decreasing. A better understanding of parasite evolution dynamics and drug resistance pathways are needed to inform national malaria elimination programs, improve the regimens of our existing drugs, and design novel antimalarials to overcome the parasites' adaptive and persistent nature. Specific details about frontline chemotherapies and resistance are discussed in Sections 1.4 and 1.5, respectively.

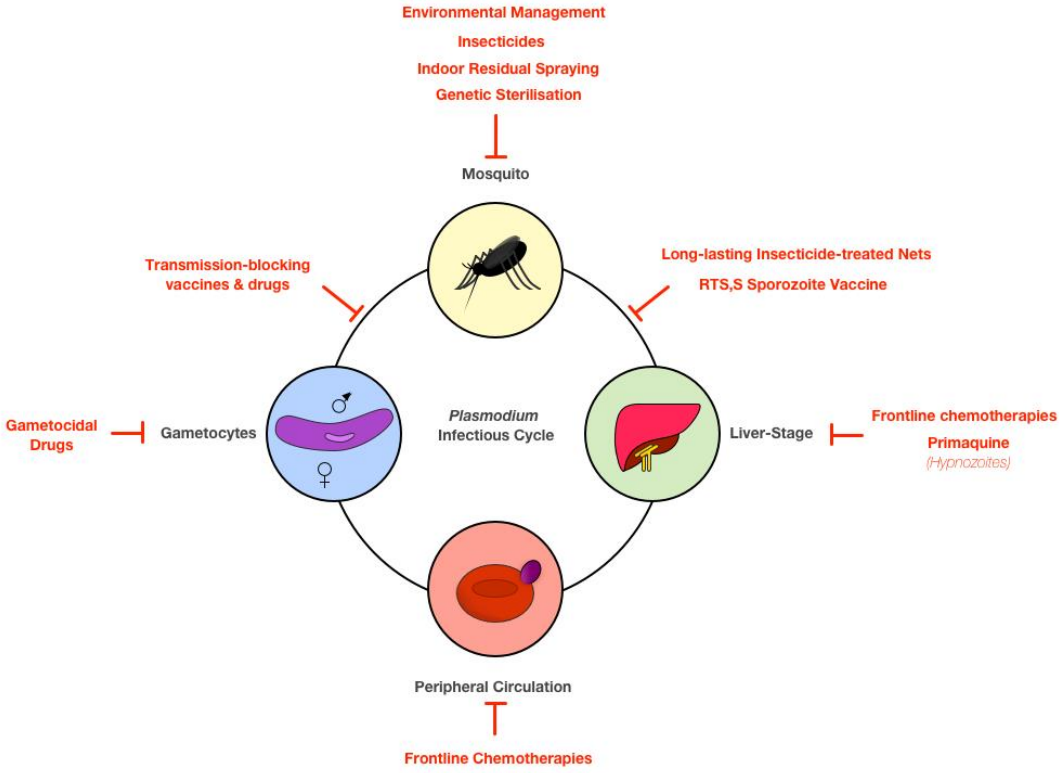


**Figure 3 Common antimalarial interventions**
Many interventions have been deployed in the fight to eradicate malaria. These involve targeting the parasite in both the human host and mosquito vector but also encompass environmental interventions.

### 1.3.2 A malaria vaccine

As with smallpox, the best hope for eradication of malaria worldwide is a vaccine. However, the malaria parasite presents several layers of greater complexity over the smallpox virus. There are several *Plasmodium* parasites that cause malaria, and exposed antigens are highly polymorphic even within a single life cycle stage. The parasite undergoes dramatic changes throughout its infectious cycle, and many of the presented antigens are not sufficiently immunogenic to stimulate a strong immune response that provides long-lasting memory. Although the first vaccine was proposed back in the 1960s, these issues continue to complicate vaccine development [24]. Today, the RTS,S vaccine (Mosquirix) pioneered by GlaxoSmithKline and the US Army is the best candidate and uses a unique recombinant fusion between a *P. falciparum* surface protein and the highly immunogenic HepB surface antigen along with adjuvant to stimulate an immune response. However, data from the latest clinical trials show RTS,S is only 25-50% effective in preventing liver infections in very young children and is not effective in adults [25–27]. These recombinant technologies and lessons learned from the current iteration of the RTS,S vaccine may give way to a more broadly effective next-generation vaccine.

Additionally, other approaches to vaccine development include the use of attenuated whole sporozoites and exposure under drug cover. The pharmaceutical giant Sanaria is currently pioneering PfSPZ-CVac, a vaccine based on irradiated *P. falciparum* sporozoites. Initial results suggested this type of vaccine could provide protective immunity, and larger trials with heterologous *P. falciparum* challenges are underway [28]. These data suggest PfSPZ-CVac may induce greater protection than RTS,S. A 2013 study described the second approach in rodents using a live

sporozoite challenge from an infected mosquito [29]. After infection, the animals were administered chloroquine to prevent a bloodstage infection. Interestingly, these rodents developed immunity against subsequent challenges suggesting that an adaptive immune response with memory can result from a liver-stage infection and the presence of a bloodstage infection may normally suppress this immune response. Further work will be needed to evaluate this approach in higher order mammals and humans.

### 1.3.3 Insecticide spraying, bed nets, and genetic manipulation of mosquitos

As previously discussed, the female members of about 40 species of anopheline mosquitoes are responsible for the transmission of *Plasmodium* parasites to humans. Of all the interventions that have been deployed against malaria over the past century, vector control had the most dramatic effects in reducing the global malaria burden. In the United States, a highly organised and well-funded effort combining insecticide dumping, swamp drainage, mosquito screen installation, indoor residual spraying (spraying of insecticides on indoor surfaces where mosquitos rest at night typically after blood meals), and personal protection measures culminated in the eradication of malaria over the course of four years from 1947-1951 [18]. Indeed, bed net usage, environmental management to reduce vector populations, and indoor residual spraying were all key to the reductions in malaria incidence achieved over the last decade. However, despite it being nearly universally recommended under national malaria programmes, the 2017 World Malaria Report indicates that the number of households using indoor spraying has dropped by nearly

50% around the world since 2010. This drop is concerning and should be further investigated to improve compliance because IRS remains an indispensable tool in the fight to reduce vector populations.

Broadly, malaria occurs on an entirely different scale in Sub-Saharan Africa than the American South, and political willpower, commitment, and organisation have long been stumbling blocks for managing sustainable and effective environmental vector control programs [30]. Further, continuous use of some insecticides for public health programs and agricultural practises has contributed to the rise of insecticide-resistant mosquito populations [30]. Insecticide-resistant vectors do not necessarily predict the return of malaria to areas that previously were malaria-free – some studies question the vectorial capacity of resistant mosquitoes [31,32]. However, they certainly pose a challenge to communities struggling to reach malaria elimination targets.

Most recently, groups of scientists have developed and adapted various approaches to genetically modify anopheline mosquitos so that they are incapable of transmitting malaria [33–36]. Although promising, these studies are still in their infancy and may not be robust enough to be used as a global solution. Instead, long lasting insecticide-treated nets (LLINs) will remain one of the best transmission-blocking interventions. These nets protect both the user underneath them by providing a barrier that the mosquito cannot penetrate and the community at large by reducing access of mosquitos to infected people. Insecticide-resistant mosquitos and improper use of LLINs such as for fishing are two significant challenges to their effectiveness [37–40].

## 1.4 Antimalarial drugs

Though they are all structurally very different, frontline antimalarial compounds can be broadly classified based on core chemical scaffolds and shared molecular targets as aryl-amino alcohols, quinoline derivatives, antifolates, antimicrobials, or endoperoxides. Within these major groups, all of the antimalarial drugs can be sub-classified based on their unique chemical structures and properties. This section will only provide background on antimalarials discussed in this thesis. There are hundreds of compounds with antimalarial properties at various stages of investigation and implementation, and the molecules not reviewed below are well reviewed elsewhere.

### 1.4.1 Aryl-Amino Alcohols: quinine, mefloquine, and lumefantrine

When discussing the history of modern antimalarial treatment, it is appropriate to begin with the aryl-amino alcohols, namely quinine. Quinine was the first chemical compound isolated and used to successfully treat clinical malaria [41]. Structurally, the quinine molecule is comprised of a bicyclic quinuclide group conjugated to a quinoline ring group by an alcoholic carbon. Together, this chiral alcoholic carbon centre forms the core amino alcohol with the nitrogen atom of the bicyclo-ring [42].

Quinine was isolated as the active chemical in the bark of the *Cinchona* tree in 1820 by Pierre Joseph Pelletier and Joseph Bienaimé Caventou, though extracts of this bark had been used to treat malaria since the mid-17$^{th}$ century [41]. Extracts of *Cinchona* bark had previously been used as a muscle relaxant and anti-diarrhoeal by indigenous populations in South America and eventually the Spanish in the 1500s.

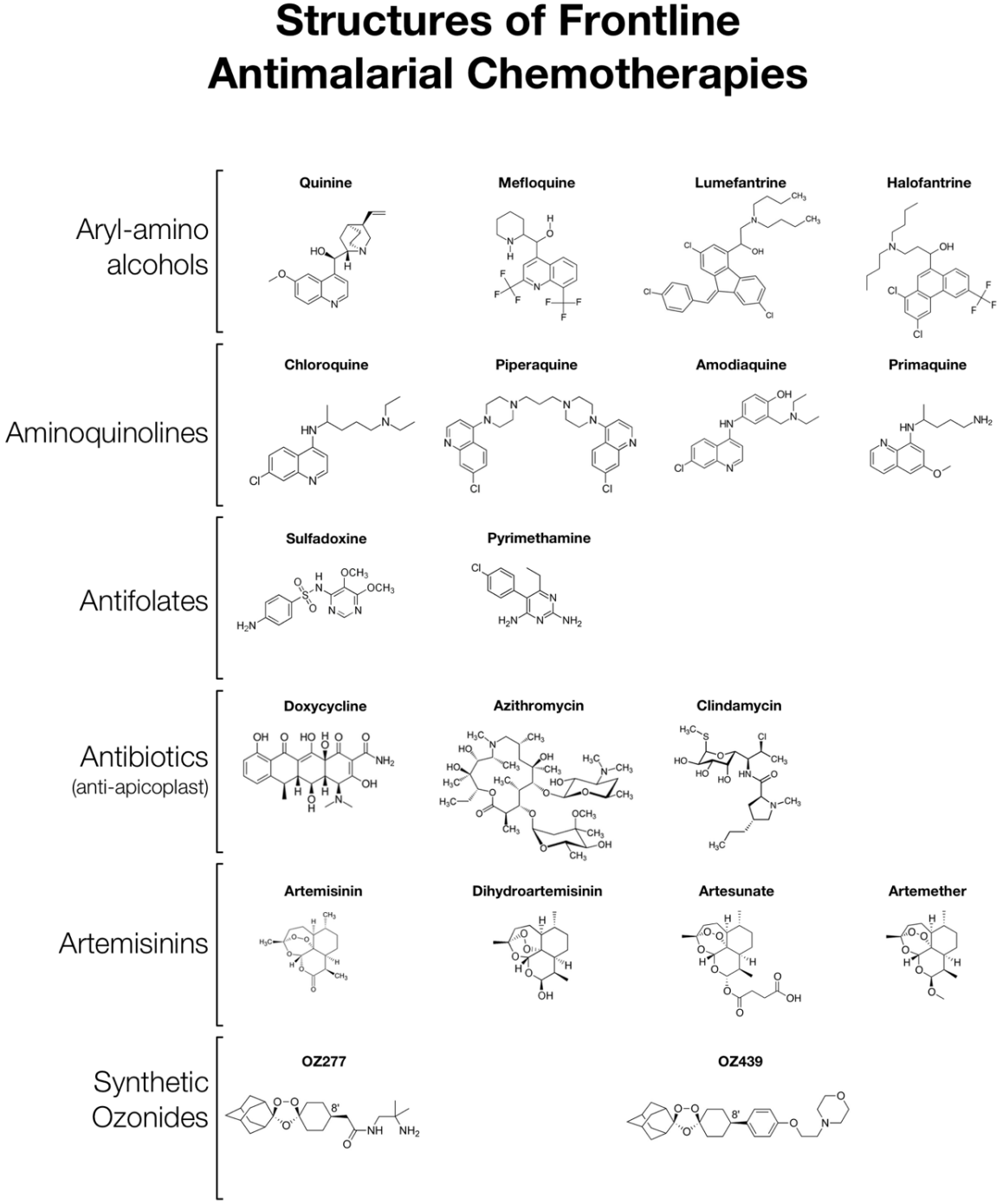


**Figure 4 Structures of common antimalarials**

The structures of several representative molecules of frontline chemotherapy classes are presented. These antimalarials cover compounds used as monotherapy, combination therapy, and rescue therapy as well as compounds which are currently under research and development.

Jesuit missionaries realised the antimalarial properties of the bark and sent samples to Rome where these properties were confirmed. Over the course of the next one hundred years, quinine in these extracts saved the lives of countless Europeans, including King Charles II. By 1850, some had begun to use quinine as a prophylactic.

Despite repeated attempts over the years, nobody has been able to successfully synthesise quinine at mass-production scale more cheaply than extracting the molecule from the bark of the trees. Consequently, South American countries held a monopoly over the supply of the raw product to the rest of the world [18]. Eventually other countries throughout the tropics were able to grow the trees and compete for market share. Throughout the war years, hostilities in the Pacific Theatre restricted production of quinine, and the Dutch were able to corner the market by establishing *Cinchona* seedlings in Indonesia. The Americans attempted to begin production out of Costa Rica, but these supplies ultimately arrived too late [18]. Despite its success, early reports of resistance surfaced in the early 1900s [43]. The discovery of synthetic drugs like chloroquine and ultimately artemisinins led to reduced reliance on quinine worldwide; however, quinine remains an indispensable rescue treatment for severe or drug-resistant malaria.

The mechanism of action of quinine remains poorly understood despite its storied history. At present, quinine is thought to exert its cytotoxic effect by somehow interfering with haemoglobin metabolism, like many other antimalarial drugs. Chloroquine accumulates and blocks haem detoxification in the digestive vacuole, and quinine seems to similarly accumulate in this organelle [42].

As chloroquine-resistant parasites began to emerge and spread, the United States, while deeply embattled in the Vietnam War, began searching for alternatives

[18]. During the 1960s, the Walter Reed Army Institute of Research in Maryland screened nearly a quarter of a million compounds in search of molecules that displayed high potency against malaria parasites [44]. The researchers found mefloquine and halofantrine, both amino alcohols like quinine. Due to the urgency of the situation, the Army partnered with F. Hoffman-La Roche and Smith Kline Beecham to push the drugs forward. Safety and tolerability trials were skipped, and mefloquine was swiftly approved for prophylaxis by the FDA in the late 1980s, unfortunately too late for the war effort [44]. Initial data suggested mefloquine could be a single-dose radical cure because of its very long half-life in the body of about 3 weeks [45,46]. However, reports quickly surfaced of substantial neurological and psychological side effects. Work at the end of the century suggested combining mefloquine with artemisinin derivatives to potentially lower the required dose of mefloquine and improve safety [47].

As we now know, mefloquine is neurotoxic and is associated with potentially severe neuropsychiatric side effects [44,48]. Recent concerns about neurotoxicity and side effects led the British Government to ban the use of mefloquine for prophylaxis in soldiers in 2016, citing potential increased risk of suicide [49]. However, to this day, mefloquine remains a key part of artemisinin combination therapies for treating clinical cases, when paired with artesunate, around the developing world. Like most antimalarials, the mechanism of action is still unknown, though believed to involve haemoglobin detoxification.

On the other side of the Pacific, the People's Republic of China was also busy generating and studying new antimalarial compounds also in support of the Vietnam War effort, though for the North Vietnamese. "Project 523" was highly productive and led to the discovery and isolation of artemisinin, artemether,

artesunate, pyronaridine, napthoquine, and lumefantrine. Lumefantrine in particular, discovered in 1976, belongs to the same aryl amino alcohol family as quinine, though its substituent groups are quite different. *In vivo*, lumefantrine has a half-life of approximately 3-6 days, but must be taken with food to increase bioabsorportion[50]. Given its shorter half-life and poor uptake, lumefantrine was never used as monotherapy, unlike mefloquine. At the turn of the century, lumefantrine was paired with artemether in the artemether/lumefantrine ACT and commercialised and since then has been widely used around the world [51–53].

Aryl amino alcohols do not have activity against liver stage parasites, and while they do kill other *Plasmodium* species including *vivax* in the blood stages, they must be combined with primaquine to cure a relapsing infection.

### 1.4.2 4-Aminoquinolines: chloroquine, piperaquine, and amodiaquine

After quinine, the next most successful antimalarial drug of the 20th century was chloroquine. Chloroquine was discovered between the Wars in 1934 by Hans Andersag in Germany at Bayer Labs as part of an effort to discover and evaluate new molecules to replace quinine. At the time, Bayer produced resochin and sontochin, but shelved both compounds because they were believed to be toxic. The detailed history of chloroquine is intimately tied with pre-World War II political alignments between Allied and Axis powers. This history is well reviewed by Karen Masterson [18]. But in short, American drug manufacturers Merck & Co and Winthrop Chemical Co. had a working relationship with the German firms IG Farben and Bayer before hostilities broke out in Europe. Afterwards, the American chemists were left totally

cut off from their more skilled German colleagues once anti-Nazi financial regulations were levied by the US Treasury.

German scientists had been testing sontochin in North Africa when the Allies invaded in 1943. During the invasion, a German scientist, Professor Schneider, surrendered his data and compounds to the Americans, who shortly thereafter synthesised chloroquine and realised its gamechanging potential [18,54]. Successful efficacy and safety trials after the war led to global adoption. Chloroquine currently costs only $0.04 per dose in the developing world, and chloroquine monotherapy dominated clinical treatment recommendations. However, reports of resistance in 1960 inspired the search for alternative drugs. Investigation into resistance mechanisms uncovered key aspects of chloroquine's mechanism of action, which involves accumulation in the digestive vacuole. In the digestive vacuole, chloroquine blocks haem polymerisation into crystalline haemazoin, which leads to accumulation of toxic haem molecules and ultimately cell death. Currently, chloroquine is still available in many countries across the tropics, even though National Malaria Programmes and the WHO endorse artemisinin combination therapies.

As part of efforts to find a replacement for chloroquine, Chinese and French researchers independently created piperaquine in the 1960s [55,56]. The molecule belongs to the same 4-aminoquinoline class of compounds and was potent against circulating, multi-drug resistant parasites. Piperaquine monotherapy was used for prophylaxis and acute treatment throughout the later 1960s and 70s, in particular replacing chloroquine in China [56]. Despite reports of resistance, piperaquine was used in China through the mid-90s. Apparently resistance to piperaquine is unstable, as sensitivity returned quickly after monotherapy was replaced. As interest in artemisinins increased through the 1990s, piperaquine was explored as a potential

partner drug. Dihydroartemisinin-piperaquine (DP) was rolled out in the 2000s. DP was effective against multi-drug resistant strains in Southeast Asia, but recent evidence shows efficacy in the Greater Mekong Subregion (GMS) is declining dangerously. As with chloroquine, piperaquine is expected to interfere with haem detoxification in the digestive vacuole.

Shortly after the war, another 4-aminoquinoline, amodiaquine, was synthesised as part of a new chemical scheme to create aminoalkylphenols by American chemists Burckhalter *et al* [57,58]. In 1946, amodiaquine was created, and from shortly thereafter, it was used to treat patients. In the body, amodiaquine is metabolised to desethylamodiaquine, which kills the parasite presumably by a similar haem-mediated cytotoxic mechanism as cross-resistance with piperaquine has been reported [59]. However, the WHO withdrew its recommendation for amodiaquine prophylaxis in the 1990s because of complications with liver toxicity and agranulocytosis. In 2008, amodiaquine was re-approved as a partner drug in ACT cocktails when paired with artesunate. Artesunate-amodiaquine (AS-AQ) is commonly used throughout Africa [59].

Project 523 in China discovered another 4-aminoquinoline, naphthoquine, in 1986 [60]. While naphthoquine has never been used as monotherapy, current studies are examining potential efficacy as a partner drug in future ACT cocktails [61]. Very little is known about how it functions.

### 1.4.3 8-Aminoquinolines: primaquine

Though the first 8-aminoquinoline, plasmochin, was synthesised in 1925, the most noteworthy 8-aminoquinoline is primaquine. Primaquine was discovered in

1946 by American chemistry Robert Elderfield at Columbia University [62,63]. Primaquine is most useful in killing the relapsing liver stage parasites in *Plasmodium vivax* and *Plasmodium ovale* infections, but the drug is also a potent gametocytocide. Primaquine cannot be used for chemoprophylaxis but remains in use for relapsing infections. To date, primaquine is the only approved compound that targets these liver stages; preserving its efficacy is crucial.

During the Korean War, Army scientists experimented with administering primaquine as a combination therapy with chloroquine to treat *P. vivax* infections with great success [62]. Uniquely, primaquine is contraindicated for use in patients with glucose-6-phosphate dehydrogenase (G6PD) deficiency as the drug causes dangerous haemolysis [64].

### 1.4.4 Antifolates: sulfadoxine and pyrimethamine

Sulfadoxine and pyrimethamine are two antimalarials of great importance even though resistance evolves very quickly. Pyrimethamine was first discovered in the 1940s by Gertrude Elion in the United States [65]. Elion sought to exploit biochemical differences between organisms in her effort to design drugs. In the case of pyrimethamine, Elion took aim at differences in metabolism and DNA replication. For her work on pyrimethamine and several other key drugs, Elion shared the Nobel Prize in Chemistry in 1988.

Pyrimethamine inhibits dihydrofolate reductase (DHFR) and interferes with folate biosynthesis. Folate is required for nucleotide biosynthesis and DNA methylation. Around the same time, sulfadoxine was discovered and shown to inhibit dihydropteroate synthase (DHPS) [65]. DHPS lies in the same synthetic cascade as

DHFR; therefore, sulfadoxine and pyrimethamine synergise when used together. This combination therapy (SP) was rolled out as chloroquine resistance began to sweep through the tropics as a promising alternative therapy. However, resistance to SP evolved even faster [66]. Even though parasites harbouring the mutations required for resistance to both drugs are globally prevalent, SP is used in intermittent preventative treatment in pregnant women and infants (IPTp and IPTi). IPTp and IPTi were officially recommended by the WHO in 2010 after several years of study and debate [67]. Both involve administering a full round of SP treatment to asymptomatic pregnant mothers and newborns in endemic areas to prevent infection during and shortly after the pregnancy, even when resistance-causing mutations approach 50% prevalence. In these areas, SP is not used to treat clinical infections, and the prophylactic benefit of administering SP in the context of IPTi and IPTp outweighs continuing to select for resistance-causing mutations. Infection of the placenta interferes with the flow of nutrients to the foetus and frequently results in spontaneous abortion or stillbirth. Around the same time, research primarily led by Sir Brian Greenwood and Prof Alassane Dicko examined the efficacy of prophylactic administration of SP-amodiaquine in high transmission areas during the dry season to reduce the human infectious reservoir heading into the wet season [68–70]. This work turned into what is now called Seasonal Malaria Chemoprevention (SMC), which is used across the Sahel and has saved hundreds of thousands of lives over the last five years. For his contributions to this work, Dicko was awarded the Africa Prize by the Royal Society in 2017. Current work aims to combine SMC and IPTp/IPTi with the RTS,S vaccine.

Sulfadoxine and pyrimethamine are unique amongst antimalarials because the mechanisms of action and resistance are known. As mentioned above, the drugs

are substrate analogues that specifically inhibit *Plasmodium* isoforms of DHPS and DHFR, respectively. Several structures of these enzymes have been resolved in complex with drugs and small molecule cofactors, indicating precisely how the drugs interact with the catalytic machinery [71–73]. These drugs select variants of *dhps* and *dhfr* with mutations that sterically block drug molecules from accessing their binding pockets. *In vivo*, the evolution of resistance to SP is complicated, but canonically involves variants at codons 437, 540, and 581 in *dhps* and 51, 59, and 108 in *dhfr*, though other haplotypes associated with clinical treatment failure have been observed [74]. Crystal structures of some of these mutant proteins have been solved and provide insight into how the structural changes prevent drug access [71,72]. Haplotypes vary by continent, indicating resistance has arisen independently [66].

Other antifolates have seen usage in the clinic and laboratory, including WR99210 and proguanil. WR99210 is a potent inhibitor of *P. falciparum* DHFR and is used commonly in transfection studies, though is too toxic for use in humans. Human DHFR can complement loss of *P. falciparum* DHFR activity and rescue parasite growth in the presence of WR99210 in culture [75]. Proguanil is used as a combination with atovaquone, and its active metabolite cycloguanil inhibits *Plasmodium* DHFR. Though these drugs are all active against *falciparum*, *vivax* and *knowlesi*, there are differences in sensitivity between species [76]. Potency against *ovale* spp. and *malariae* remains to be characterised.

### 1.4.5 Antimicrobials: doxycycline, clindamycin, and azithromycin

Though tetracyclines, macrolides, and lincosamides were all originally developed for prokaryotic bacterial infections, some have potency against protozoa.

Tetracyclines were originally discovered in the 1940s, and in 1950, initial trials in consenting human volunteers indicated doxycycline may have anti-*falciparum* and anti-*vivax* properties [77,78]. Just like with the antifolates, tetracycline use was revisited by health authorities as chloroquine resistance began to spread in the 1960s. In addition to tetracyclines, macrolides and lincosamides were also considered, and clindamycin and azithromycin were found to have antimalarial properties [79]. In 1985, the CDC formally recommended the use of doxycycline for chemoprophylaxis [77]. Recommendations to include clindamycin and azithromycin followed thereafter.

These drugs are not recommended for treatment of acute clinical infections because they exhibit delayed action. In bacteria, these three classes target ribosomes and block protein synthesis. In *Plasmodium*, these drugs target the bacteria-like organelle called the apicoplast. The apicoplast is a four-membrane organelle in the parasite cytoplasm derived from an evolutionary endosymbiotic engulfment of a red alga[80]. This prokaryotic alga had prokaryotic ribosomal machinery, which the apicoplast retained. These ancient ribosomes are susceptible to antibiotics in the same way as bacteria[81]. However, unlike bacteria, the parasite also has eukaryotic ribosomes, which do the bulk of the protein synthesis in the cell. Parasites can survive one entire lifecycle without a functional apicoplast [81]. Because the apicoplast in these treated parasites is not functional, it cannot replicate and segregate properly into the daughter parasites. Therefore, these next-generation parasites lack an apicoplast and are not viable. Interestingly, *in vitro* antibiotic-mediated cytotoxicity can be overcome by supplementing the parasites with isopentenyl pyrophosphate (IPP) [82]. In the asexual stage, the only essential function of the apicoplast is to produce IPP for use in post-translational protein prenylation. Replacing this

metabolite in culture medium allows parasites to grow without an apicoplast, indefinitely [82].

Therefore, except at micromolar concentrations of drug, parasites replicate normally in the presence of antibiotics over one life cycle. This "delayed death effect" renders antibiotics unsuitable for treating acute infections where rapidly reducing peripheral parasitaemia is required [81]. However, they do work well as prophylaxis when any infection is in the liver-stage or asymptomatic and peripheral parasitameia is very low. I.V. quinine and doxycycline is used in some cases as a rescue therapy for complicated malaria patients. Some prophylactic failures and putative markers for doxycycline resistance have been reported, but these *in vitro* experiments were not performed to look at the delayed death effect exerted by doxycycline [83–87]. Therefore these data are difficult to interpret. It is not clear how a difference in $EC_{50}$ to a 48-hour exposure of doxcycyline translates to the accepted 96-hour $EC_{50}$.

### 1.4.6 Endoperoxides: Artemisinins and Synthetic Ozonides

Though artemisinin was not properly extracted and identified until the twentieth century, records show Chinese herbal practitioners had been using preparations of the qinghao plant (*Artemisia annua*) to treat a variety of ailments for nearly 2000 years [88]. The active metabolite, dihydroartemisinin, was only discovered in the 1970s by scientists led by Tu Youyou under Project 523 in China. These scientists also created the more stable versions of the artemisinin pro-drug artemether and artesunate. After the Cultural Revolution, Chinese science was opened to the West, and publications in the 1990s began to describe the efficacy of

artesunate, artemether, and dihydroartemisinin as superior to chloroquine and quinine [88]. Nicholas White, Keith Arnold, and others were early European champions of the artemisinins and helped bring the drugs to the global marketplace .

Artemisinin and its derivatives are unique molecules possessing a hallmark endoperoxide bridge in a sesquiterpene lactone tricyclic ring. These molecules are highly potent against *P. falciparum, P. knowlesi,* and *P. vivax* but their efficacy against *P. ovale* spp. and *P. malariae* remains to be characterised. So far, the mechanism of action of artemisinin is unclear, though its cytotoxic effect is largely believed to result from overwhelming oxidative stress caused by opening of the endoperoxide, forming reactive radical oxygen atoms. Parasites treated with artemisinin *in vitro* display increased levels of total ubiquitylation, consistent with systemic protein damage and turnover [89]. Studies have suggested that haemoglobin metabolism catalyses the activation of the endoperoxide, but this remains to be validated and clarified [90]. It is accepted that, though all asexual stages are susceptible to artemisinin, there is a period of hypersensitivity in the very early ring stage, which gives way to a period of relative insensitivity that arcs back towards sensitivity in the trophozoite phase. The schizont stage is again relatively insensitive. Throughout the lifecycle, potency of artemisinin, as determined by 6-hour pulses of drug, ranges from approximately 1 nM to greater than 100 nM [91]. Artemisinins show variable activity against male and female gametocytes, seeming to only inhibit male gametocytes [92].

In the clinic, artemisinin monotherapy was used briefly in the late 1990s before it was condemned by the WHO in 2006. Even so, monotherapies are still available in many endemic countries [3]. The recommended treatment guidelines since then specify that artemisinin should be used in combination with another, longer-

lasting drug in a three-day artemisinin combination therapy (ACT). Currently the most common ACTs available are mefloquine-artesunate (MA; Artequin), artemether-lumefantrine (AL; Coartem), artesunate-amodiaquine (AS-AQ; Camoquin), and dihydroartemisinin-piperaquine (DP; Artekin). Other formulations include amodiaquine and pyronaridine. ACTs remain effective throughout Africa, though there are recent reports of concerning treatment failure [93–96]. However, in Southeast Asia, artemisinin resistance is well established, and there are increasing reports of partner drug failure. Efficacy in South America remains high. Preliminary evidence indicates that the basis for reduced artemisinin susceptibility in Africa, where it occurs, differs from that in Southeast Asia [93]. Further discussion of artemisinin resistance can be found in Section 1.5.3.1. Currently, the TRAC II project in Southeast Asia is examining the safety and efficacy of triple ACT formulations. Other proposed interventions include a six-day sequential ACT regimen with two different ACT formulations, though compliance may be low [97].

Several synthetic endoperoxide compounds based on the chemical scaffold of artemisinin are currently at various stages of the development pipeline. The most promising candidates include OZ277 and OZ439. These compounds are so far tolerated well and are highly effective against parasites [98]. One report indicates OZ277 may be susceptible to K13(C580Y)-mediated cross-resistance with dihydroartemisinin as determined by the ring-stage survival assay (Section 1.6), though OZ439 is effective against these strains in this assay format [99,100]. This assay format may not be appropriate for the synthetic compounds because the RSA was designed for artemisinin, which displays a very short, six-hour half-life, and these ozonides have a much longer half-life. Further work is needed to move these

compounds to market, but their high potency and long half-life represent promising developments in a much-needed space of malaria control efforts.

## 1.5 Genetic and molecular mechanisms of antimalarial resistance

Despite our best efforts to eradicate malaria, the malaria parasite has kept pace, tuning its genome to block or circumvent drug action (Fig 5). Over the last several decades, molecular tools such as whole genome sequencing and PCR have allowed researchers to comb through the parasite genome to study changes during drug pressure *in vitro* and *in vivo*. These studies have quantified the parasite's basal mutation rate at approximately $1 \times 10^{-10} – 1 \times 10^{-9}$ per base per parasite division [101,102]. However, these genome-wide estimates are extrapolated from the analysis of mutations and recombination in specific gene families rate, and some studies show this rate varies based on the parasite strain[103–105]. Given that parasite burdens can exceed $1 \times 10^{9}$ in a typical acute infection, individual mutations are constantly arising and may be selected based on the fitness costs of the mutation and drug pressure [101]. For this reason, drug resistance can develop unexpectedly and expand suddenly and rapidly. Clinical resistance has been observed for nearly every antimalarial drug ever rolled out. Understanding the molecular changes in the parasite that underpin resistance has helped scientists track resistance and design novel chemotherapies. This section will only discuss quinine, mefloquine, lumefantrine, chloroquine, piperaquine, doxycycline and clindamycin, and artemisinin because these are the only drugs that are discussed extensively in this thesis and therefore warrant a detailed introduction. A brief discussion of other common antimalarials can be found above.

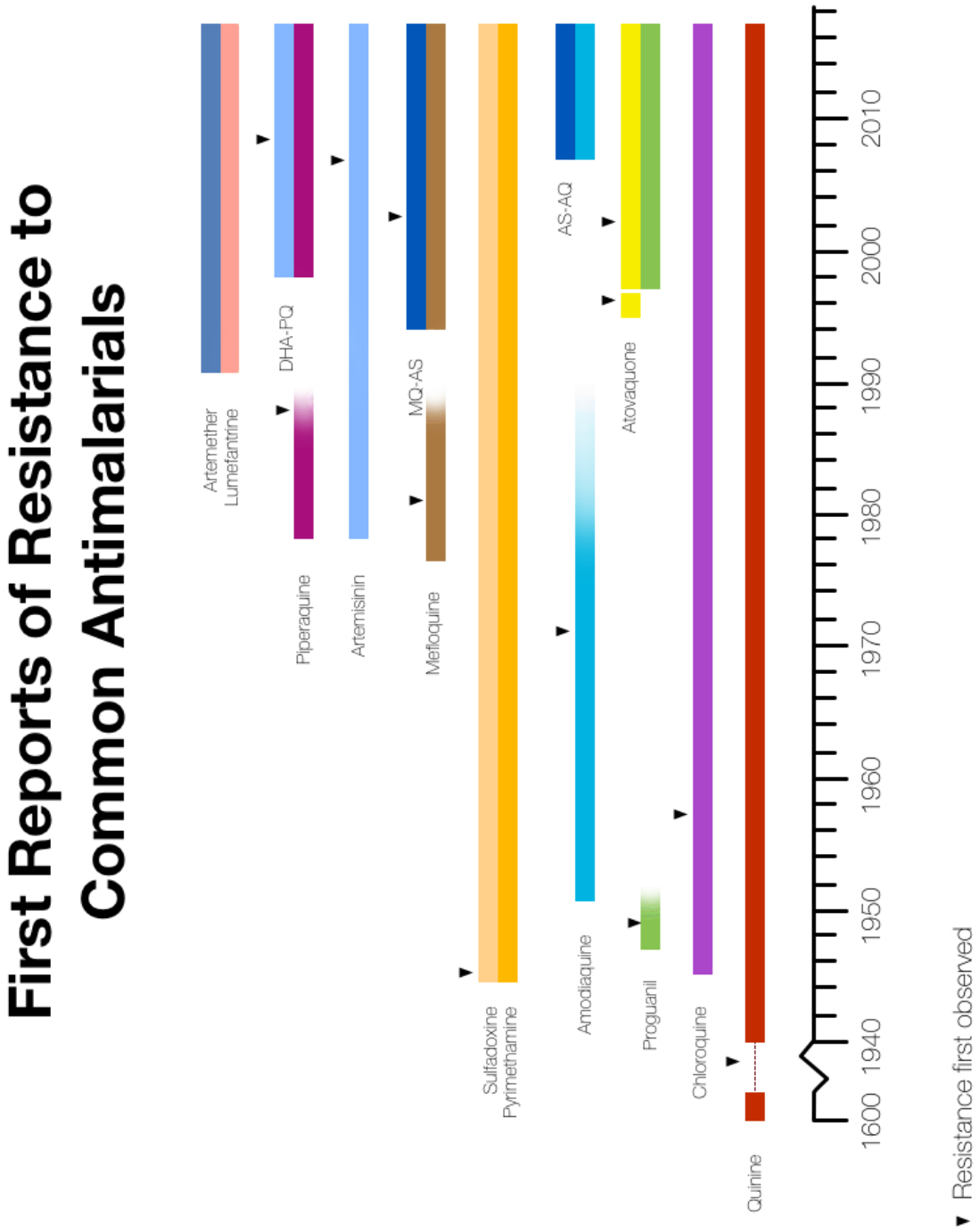


**Figure 5 Timeline of the emergence of parasite resistance to frontline chemotherapies**

*Plasmodium falciparum* has evolved resistance to nearly every drug that has been introduced for treating human infections. The length of the coloured bars indicates the approximate duration of use of each annotatd chemotherapy. The edges of the bars indicate the approximate dates of introduction and withdrawal. A fading bar indicates waning use of the given chemotherapy. Black arrows indicate the first reports of parasite resistance to the compound in humans. The specific years indicated by these black arrows are referenced in the following sections.

### 1.5.1 Resistance to aryl-amino alcohols

#### *1.5.1.1 Quinine Resistance*

Despite its first recorded use dating back to the 1600s, the first clinically confirmed quinine resistance occurred in the early 1900s. In 1907, Arthur Neiva first observed quinine-resistant infections in workers returning from construction teams working on the "The Devil's Railway" deep in the Amazon Rainforest in Brazil [43]. These observations were later confirmed and reported in Germany by Bernhard Nocht and Heinrich Werner in 1910 as workers stationed in Brazil were ordered back to Hamburg, infirm [43]. Concerns about quinine resistance persisted and worsened throughout the 1910s as the First World War erupted across Europe. Although sparse, military records indicate that one to two million soldiers across Allied and Axis powers were affected. As the War continued, quinine efficacy declined dramatically, particularly on the Eastern Balkan front. Due to the lack of understanding and tools at the time, it is not clear if these parasites were of a similar genetic background or susceptibility profile as those reported in Brazil earlier [41,43,106]. Particularly in the Brazil context, at least some of these quinine-resistant cases were diagnosed as multiple infections. It is possible that the same was true in the War theatres – indeed most of the relapsing cases which presented in hospital were *P. vivax* [106]. Although quinine does not kill *vivax* hypnozoites, these documented cases of recrudescence suggested clinical treatment failure as they occurred too soon for reinfection with *P. falciparum* or *P. vivax* relapse[106].

Since the War, quinine use, and resistance, has declined and to date is mostly confined to rare occurrences in South America and Southeast Asia. Domestic cases in Africa are very rare, and quinine retains efficacy on the continent. Consequently, quinine is considered frontline chemotherapy for treatment of severe malaria and

multi-drug resistant infections, typically in combination with an antibiotic or antifolate [107,108].

### *1.5.1.2 Mefloquine Resistance*

As described previously, mefloquine was discovered by the US Army in the mid-1960s, trialed, and rolled out several years later [44]. However, within a few years of use, resistance was reported in the Thai-Cambodian border region in the Greater Mekong Subregion. By 1990, researchers reported a 30% treatment failure rate with mefloquine monotherapy [109]. Since then, resistance has been reported in South America and sporadically in West Africa, possibly due to less common use [110–112]. Shortly after the initial detection and report of mefloquine resistance moving through the GMS, trials of combination therapy with artesunate showed the progression of resistance could be halted and mefloquine efficacy rescued, presumably because the burden of parasite density reduction is mainly accomplished by the fast-acting artemisinin with support and long-term protection from mefloquine [109]. Currently, mefloquine-artesunate combination therapy enjoys widespread success throughout Africa and South America, though the combination is failing in Southeast Asia[94,113–119].

### *1.5.1.3 Lumefantrine Resistance*

Where mefloquine was discovered by the Americans, lumefantrine, and a host of other drugs, was discovered by the Chinese in an analogous clandestine

project around the same time in 1976 [120]. Unlike quinine and mefloquine, lumefantrine has never been used as a monotherapy and has only been coadministered with the artemisinin-derivative artemether as Coartem (artemether-lumefantrine, AL). Therefore, it is difficult to obtain direct evidence of resistance *in vivo*. As noted previously, artemisinin combination therapies in general, and Coartem specifically, have been widely successful outside of the Greater Mekong Subregion [121–123]. Evidence of resistance outside this region, particularly in East Africa where AL is frontline under some national malaria control programs, is limited and, in some cases, controversial, though cannot be ignored and demands further investigation [93,124–130].

#### *1.5.1.4 Mechanism of resistance to aryl-amino alcohols*

So far, decreased susceptibility to aryl-amino alcohols has been linked to genomic amplifications of the *pfmdr1* gene. This gene was first identified in *falciparum* in 1989 by Wilson *et al* following a search for orthologues of the multi-drug resistance transporters found in mammalian organisms. This seminal study followed on the back of work in 1987 showing chloroquine-resistant (CQR) parasites accumulated dramatically less chloroquine than sensitive parasites [131]. This accumulation and CQR phenotype could be reversed with Verapamil, which had previously been shown to block the release of anticancer drugs from tumour cells via MDR-dependent pathways, suggesting an underlying efflux mechanism in CQR parasites [131]. Therefore, Wilson *et al* identified the two orthologues of the mammalian *mdr*: *pfmdr1* and *pfmdr2,* which share 59% homology [132]. Northern blotting revealed *mdr1* was overexpressed in their mefloquine-resistant parasite,

whereas *mdr2* was not. On the basis of chloroquine sensitivity, subsequent comparative studies identified copy-number variations in CQ-sensitive and -resistant strains without a clear trend delineating the two phenotype classes [132–134].

*Pfmdr1* encodes a P-glycoprotein family protein, Pgh1, which is localised to the digestive vacuole in *P. falciparum* [135]. Several years later in 1994, Cowman *et al* also experimentally derived mefloquine-resistant parasites *in vitro* on a CQR background and showed these parasites overexpressed *mdr1*. Interestingly, this CNV also correlated in this study with potentiation of chloroquine and cross-resistance to quinine and the related molecule, halofantrine [136]. Several studies from the late 1990s well into the 2000s continued to question and redefine the role of PfMDR1 in modulating drug sensitivity [137,138]. Transfection studies suggested that mutations in the C-terminal region of the protein encoding S1034C, N1042D, and D1246Y could, together, modulate susceptibility to mefloquine and quinine [137,139]. Parasites harbouring *pfmdr1* copy number variants were also shown to have reduced susceptibility to lumefantrine, mefloquine, and quinine [140]. However, the prevalence of these SNPs and CNVs is highly-region specific. Recent genome editing using zinc finger nucleases clarified the role of certain globally prevalent mutations in modulating sensitivity to frontline chemotherapies. Specifically, N86 reduces susceptibility to lumefantrine and mefloquine but may potentiate quinine, whereas N86Y causes parasites to become less sensitive to chloroquine [8].

Synthesizing these results and the current understanding about the complex dynamics in multidrug-resistant parasites, Veiga *et al* propose that PfMDR1(N86) weakly imports lumefantrine into the DV away from its cytosolic target where it is protonated and sequestered, whereas the N86Y mutant cannot import lumefantrine and thus increases the effective cytosolic drug concentration (Fig 7) [141]. This may

make sense because lumefantrine and mefloquine do partly accumulate in the DV[142]. However, this mechanism does not account for differences observed in quinine susceptibility. At this point, it is difficult to speculate how PfMDR1 affects mefloquine and quinine activity because very little is known about their mechanisms of action in the cell. A recent study showed that mefloquine may inhibit the 80S ribosome, though further work is required (Fig 7)[143]. With the arrival of molecular forward and reverse genetic tools for *Plasmodium*, these important mechanisms will likely begin to be unravelled.

### 1.5.2 Resistance to 4-aminoquinolines

This section will only discuss the 4-aminoquinolines chloroquine and piperaquine, because the 8-aminoquinolines were not used in the work described by this thesis. A brief discussion of these other related compounds is included above.

#### *1.5.2.1 Chloroquine Resistance*

Chloroquine enjoyed widespread use during and after World War II until the late-1950s when pockets of resistance emerged along the Thai-Cambodian border and in Northern South America. These pockets quickly spread into tracks of resistance that began to sweep across both regions. By 1960, chloroquine-resistant (CQR) infections were documented and confirmed in Colombia, Venezuela, Thailand, and Cambodia, ultimately reaching Africa in the late 70s [144] (Fig 6). By the mid-80s, resistant strains dominated Sub-Saharan tropical Africa [144,145]. At the height

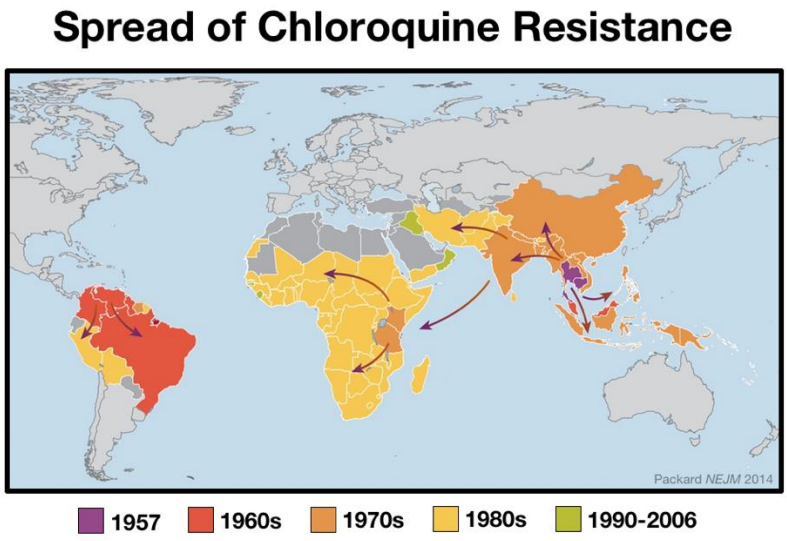


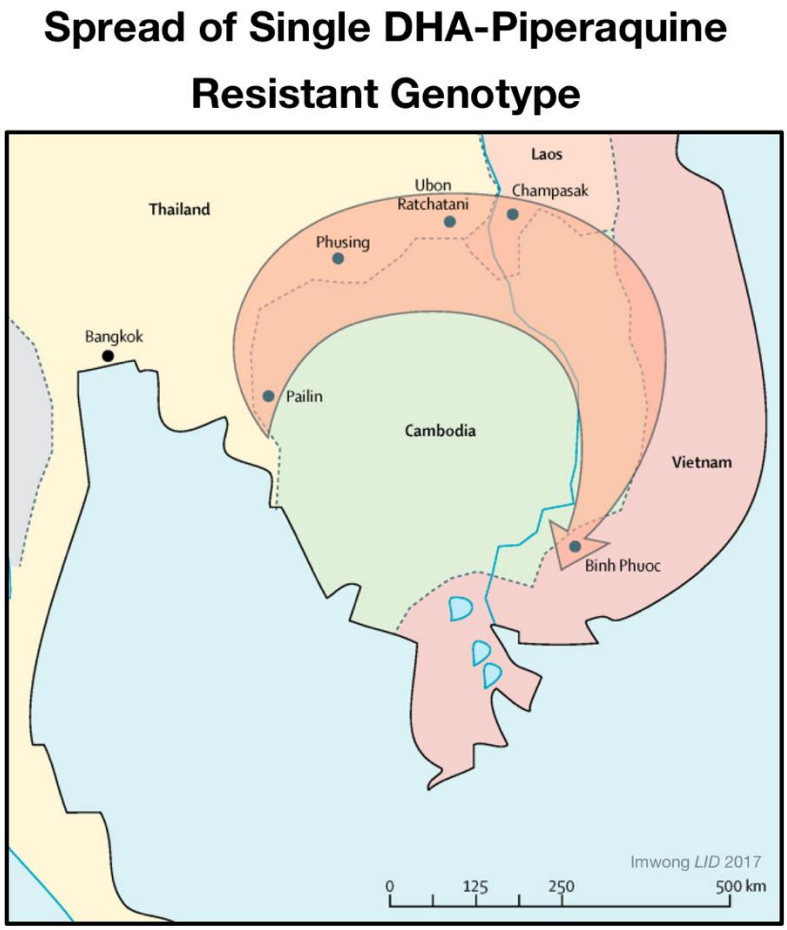


**Figure 6 Spread of chloroquine- and DHA-Piperaquine-resistant genotypes over geographic areas**

The top panel depicts how chloroquine-resistant genotypes encoding PfCRT(K76T) spread across the world over time, emanating from Southeast Asia beginning in 1957. The bottom panel describes how a single lineage of parasites resistant to dihydroartemisinin-piperaquine combination therapy harbouring K13(C580Y) and *plasmepsin II* amplification is spreading around the Greater Mekong Subregion along Cambodia's borders. These figures are adapted from data presented by Packard *et al* and Imwong *et al* respectively.

of the resistance crisis, childhood (under the age of 10) mortality was up nearly 6-fold in some parts of Africa, and no cheap, effective alternatives were available [146].

### *1.5.2.2 Mechanism of resistance to chloroquine*

Chloroquine resistance likely arose independently several times, first in the Greater Mekong Subregion, then in South America, the outlying Pacific Rim, and East Africa, rather than sweeping around the tropics as a single genetic lineage [147]. That this process took decades is interesting. The antifolates sulfadoxine and pyrimethamine, which were intended as replacements for CQ, failed as acute clinical therapies very quickly because the parasite was able to evolve point mutations to sterically block access to the drug-binding pocket on their target enzymes. When a drug retains its efficacy for many years, this indicates that the underlying mechanism of action and resistance may be complicated at the subcellular level or cause a significant fitness deficit.

Initially, investigators believed there was a "chloroquine receptor" that mediated the drug's cytotoxicity and resistance after detailed reports of host cell membrane involvement and collapsed digestive vacuoles, a phenomenon called "clumping". At the time, studies had shown that chloroquine accumulated in the acidic digestive vacuole [148]. These initial investigations were particularly difficult because there was no *in vitro* culture system for *P. falciparum*. Once Trager and Jensen described the successful, long-term passage of *P. falciparum* in human erythrocytes in 1976, the field of molecular parasitology began in earnest, starting with attempts to unravel chloroquine resistance [149].

In 1980, Chou *et al* proposed ferriprotoporphyrin IX as a candidate chloroquine receptor[150]. The group showed chloroquine binds ferriprotoporphyrin IX (FP), which is naturally produced by the parasite during haemoglobin degradation *in vitro* and accelerates FP-mediated cell lysis [150]. They proposed that, while FP is naturally produced and inherently toxic to cells, there is a factor in the cell that further modifies FP into malaria pigment and mitigates its cytotoxicity. It followed that CQ interacts with FP and forms stable FP-CQ complexes that retain cytotoxicity and cannot be sequestered as nontoxic complexes [150–152].

D.C. Warhurst countered with an alternative view that chloroquine is carried down a pH gradient in the cytoplasm towards the acidolysosome [42]. There, CQ blocks haemoglobin degradation and starves parasites of amino acids. This view is consistent with known cytotoxicity in mammalian cells that lack FP but fails to explain multi-fold differences in sensitivity between parasites and mammalian cells.

Through the vigorous debate on mechanisms of action, it was clear that chloroquine targeted the digestive vacuole and resistant parasites retained dramatically less chloroquine, despite normal accumulation kinetics [131,153]. As stated in Section 1.5.1.3, investigators looked for mechanisms of drug efflux and identified *pfmdr1*, an orthologue of the mammalian chemotherapy efflux gene, and observed that the calcium channel blocker Verapamil potentiated chloroquine accumulation and sensitivity specifically in CQR strains, just like in drug-resistant cancer cells [131,154]. As mentioned above, field studies in the late 1990s provided mixed evidence linking mutations in *pfmdr1* to chloroquine susceptibility [155]. Later work argued against a resistance mechanism involving expulsion of CQ from the cell, but confirmed accumulation defects in the digestive vacuole, suggesting Verapamil targeted mutant-PfMDR1 [154–156].

At the end of the century, field and genetic studies identified a strong genetic selection on a region of chromosome 7 corresponding to *pfcg2* [157,158]. Transgenic experiments ruled out a role for this protein but showed mutations in the neighbouring *pfcrt* gene may determine chloroquine sensitivity [159,160]. Field work then confirmed the association of a locus, PfCRT(K76), with chloroquine resistance around the world. While K76T is the major causal allele, K76I and K76N have also been observed in the laboratory and correlated with reduced susceptibility to chloroquine [159,161]. Interestingly, this mutation was found on diverged backgrounds, and mutations in *pfmdr1* and *pfcg2* did not improve the association, corroborating evidence that these genes are not predictive in determining the resistance status, though *pfmdr1* may be involved in fine tuning resistance in some parasite backgrounds [155].

Subsequent genetic investigation has revealed that PfCRT is a transmembrane protein located in the digestive vacuole membrane, like PfMDR1 [159]. Sequence analysis indicates that the protein has 10 transmembrane domains and shares homology with known membrane channels and transporters. Despite a decade of intense work, the native function of PfCRT remains unclear. Several roles have been proposed including export of haemoglobin-derived peptides to the cytosol and as an ion channel or proton pump [162,163]. Mutations predicted to have inactivating, steric consequences on protein folding which cause hypersensitivity to CQ have been shown to cause the DV to swell, supporting a role for the wild type protein in transporting some natural substrate towards the cytosol [163]. As described above, CQ is known to diffuse into the DV where it is protonated and trapped in the acidic environment. The globally prevalent K76T mutation likely enhances the activity of the transporter or reduces its specificity, allowing the efflux of protonated, charged

chloroquine, and thereby reduces intra-DV CQ levels to a sub-therapeutic concentration [163,164]. Indeed, an earlier study in *Xenopus* oocytes showed mutant PfCRT could transport non-protonated CQ whereas wild type PfCRT could not [164]. The identification of mutations which increase sensitivity of already-sensitive strains suggests the wild type protein has the ability to export small amounts of protonated

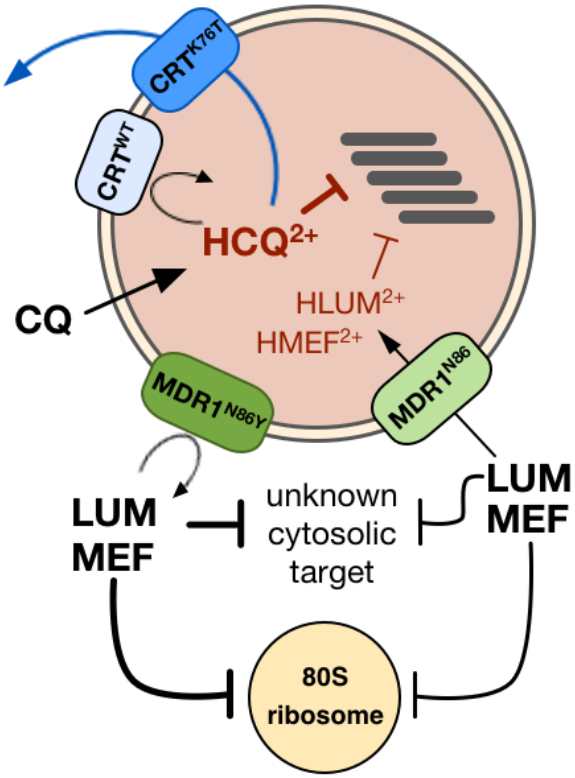


**Figure 7 Schematic representation of the mechanism of lumefantrine, mefloquine, and chloroquine action and resistance**
Chloroquine and lumefantrine are believed to inhibit parasite haemoglobin detoxification by similar processes. Chloroquine diffuses into the digestive vacuole where it is spontaneously diprotonated in the acidic environment into $HCQ^{2+}$ which blocks haem detoxification. Wild type PfCRT is incapable of effluxing the charged chloroquine molecule. The mutant PfCRT(K76T) molecule, which confers chloroquine resistance, is capable of pumping protonated chloroquine out of the vacuole, thus reducing the effective concentration of $HCQ^{2+}$ in the digestive vacuole. Lumefantrine is believed to be pumped into the vacuole by PfMDR1 where it is similarly protonated to $HLUM^{+}$, which interferes with haem detoxification. PfMDR(N86Y) is believed to block the import of LUM into the digestive vacuole. However, lumefantrine in the cytosol may still inhibit an essential process which explains why N86Y only confers reduced parasite susceptibility to lumefantrine. Mefloquine sensitivity follows a similar trend and may inhibit the 80S ribosome in the cytosol. These data are adapted from Veiga *et al*[141] and Wong *et al*[143].

CQ to the cytosol at steady state, and any mutations which inactivate the protein would cause super-lethal accumulation of CQ in the DV (Fig 7). Still, further investigation is required to improve our understanding of how this complex process occurs and elucidate any involvement of other factors in tuning CQR phenotypes.

A similar mechanism may be involved in mediating amodiaquine resistance as PfCRT(K76T) has been reported to be associated with clinical treatment failure in patients in the Greater Middle East treated with amodiaquine monotherapy [165,166]. Additionally, mutant CRT, albeit with a different mutation encoding H95P, is associated with loss of amodiaquine sensitivity in *P. berghei* [167]. Further investigation will be required to unravel the mechanisms mediating amodiaquine resistance and its underlying mechanism of action.

#### *1.5.2.3 Piperaquine Resistance*

Currently, piperaquine is used in combination with artemisinin as dihydroartemisinin-piperaquine, though it was previously used as a monotherapy in China from the 1960s until reports of resistance in the 1980s [168,169]. Dihydroartemisinin-piperaquine combination therapy (DP) has found success where other ACTs have started to fail, namely in the Greater Mekong Subregion. However, as early as 2010, PCR-corrected trials indicated that failure rates to DP were as high as 25% in some parts of Cambodia [170,171]. Efficacy of DP has continued to decline, and recent reports suggest a single artemisinin- and piperaquine-resistant *P. falciparum* lineage may be sweeping across the GMS [172,173]. To date, there have been no reports of piperaquine failure outside of the GMS.

### *1.5.2.4 Mechanism of resistance to piperaquine*

Unfortunately, there are no culture-adapted clinical isolates from the 1980s when resistance to piperaquine monotherapy in China was first reported. *Ex vivo* studies of piperaquine-resistant parasites in the late 1990s, largely carried out by one group led by H Yang, suggested cross-resistance to chloroquine and piperaquine [169]. Indeed, the piperaquine molecule is also a weak base and shares a quinoline structure with chloroquine. However, a more recent study of 280 isolates from French travellers reported that chloroquine and piperaquine resistance are not linked and that any early associations were simply co-occurences [174].

Early attempts to generate a piperaquine-resistant parasite *in vitro* succeeded and identified a novel SNP in *pfcrt* encoding C101F, deamplification of *pfmdr1*, and a novel amplification on chromosome 5 in two independent clones [175]. Both clones displayed decreased accumulation of the drug in the parasite. However, this resistance was unstable and reverted in the absence of piperaquine pressure. Recent *in vitro* investigation and genome editing definitively showed this C101F mutation in PfCRT could mediate piperaquine resistance [176]. This data provides insight into a mechanism of piperaquine action in the haem detoxification process much like chloroquine. A mutant PfCRT could pump the drug out of the DV. However, this causative mutation has not yet been observed in the field [177].

A recent phenotype-genotype association study conducted by Benoit Witkowski showed *ex vivo* piperaquine sensitivity is associated with *plasmepsin II* copy number. Plasmepsin II is a haemoglobinase localised to the parasite DV [178,179]. Parasites with duplicated *plasmepsin II* displayed 100-fold greater survival than parasites harbouring single copies of the gene in the novel Piperaquine Survival Assay [180]. Another study of isolates from Cambodia re-identified this duplication and

also associated a novel mutation encoding E415G in Exonuclease I with reduced piperaquine susceptibility [181]. While polymorphisms in Plasmepsin II seem consistent with what is known and proposed about piperaquine's mechanism of action, mutations in Exonuclease I are harder to explain. However, a recent study by Andrew Lee and David Fidock showed that Cambodian parasites lacking ExoI displayed a mild mutator phenotype. To date, no polymorphisms in *plasmepsin II* or *exoI* have been detected in parasites outside of Southeast Asia, though these markers have been used to track resistance throughout the GMS [172]. However, currently there are fears of a parasite lineage bearing *plasmepsin II* CNVs and *pfk13* mutations sweeping across the GMS, entrenching artemisinin and piperaquine resistance. Further work is needed to examine how these and other mutations may impact piperaquine accumulation and action.

### 1.5.3 Resistance to artemisinins

As described above, artemisinin combination therapies (ACT) are used universally around the world in malaria endemic regions. The artemisinin component of ACT is one of several molecules but all are metabolised *in vivo* into dihydroartemisinin. These compounds have high potency on the early ring stage of *P. falciparum* and rapidly reduce peripheral parasitaemia. However, due to the dramatic differences in stage-specific cytotoxicity, parasites of other stages by not be completely killed off by the time the drug is completely degraded in the body.

ACTs have had excellent success worldwide since their deployment in the mid 1990s—however widely reported resistance in Southeast Asia threatens their global efficacy [182]. Noedl and Dondorp first reported clinical treatment failures in

Western Cambodia along the Cambodian-Thai border in 2008 and 2009 [183,184]. Since then, treatment failures have been reported widely across Mekong, and as mentioned above, some fear the spread of a single, multi-drug resistant strain across the region [3,172]. To date, ACTs remain highly effective throughout Africa and South America. One study in the *New England Journal of Medicine* in July 2017 described the emergence of an artemisinin-resistant parasite in Equatorial Guinea in a Chinese worker [185]. *In vitro* culture adaptation and examination showed this parasite had an elevated ring-stage survival phenotype similar to but less dramatic than parasites of Southeast Asian origin. While this report is certainly concerning, the mutations in the parasite genome noted in this report have never been observed previously nor observed since, either in Africa or the GMS. Several recent studies of imported *P. falciparum* malaria cases in Europe suggest that ACT efficacy may be declining in sub-Saharan Africa. These studies beg continued investigation.

Interestingly, when artesunate was first used as a monotherapy in the late 1990s, nearly one in five patients had recrudescent parasitaemia. Even when artemisinin is administered for seven days, one in ten patients display recrudescent parasitaemia [186]. This sparks an interesting debate as to whether the treatment failure observed in Southeast Asia is truly artemisinin resistance or just partner drug failure. The consensus in the field is that the ring-stage survival phenotype quantified in the lab is indicative of clinical treatment outcome, though this association needs to be further investigated.

Currently, extended ACT regimens and triple ACTs (combinations of three drugs) are under examination for their efficacy in regions with multi-drug resistant parasites. Additionally, synthetic endoperoxides with longer *in vivo* half-lives are

under development and show great promise, particularly on these artemisinin-resistant strains.

### *1.5.3.1 Mechanism of resistance to artemisinins*

So far, very little is known about how the *falciparum* parasite tunes its biology to evade artemisinins. Artemisinins have remarkably short, 2-5-hour half-lives both in the body and *in vitro* [187]. As a result, it is inappropriate to study resistance over a 48-hour lifecycle like chloroquine. Instead, small windows of the lifecycle should be examined. A seminal work by Witkowski *et al* in 2013 showed that a 6-hour pulse of 700 nM dihydroartemisinin administered to cultures of early ring-stage *P. falciparum* parasites distinguished between slow-clearing parasites from Pailin, Cambodia and sensitive, normally-clearing parasites from Ratanakiri, Cambodia [188]. This *in vitro* correlation with clinical phenotype laid the foundations of the subsequent efforts to understand this ring-stage phenomenon. A later study by Klonis *et al* showed an oscillating artemisinin sensitivity profile of the 3D7 isolate across a 48-hour lifecycle [91] (Fig 8). This work revealed a period of hypersensitivity in the first few hours of the lifecycle immediately followed by a brief period of relative resistance in the late ring/early trophozoite stage, which progresses back towards sensitivity in the trophozoite stage. The basis of this early ring-stage hypersensitivity and thereby resistance is the subject of intense investigation.
It has been long proposed that the haem-derived iron atoms activate the endoperoxide in dihydroartemisinin. This therefore would support a mechanism of resistance involving altered haemoglobin uptake or degradation.

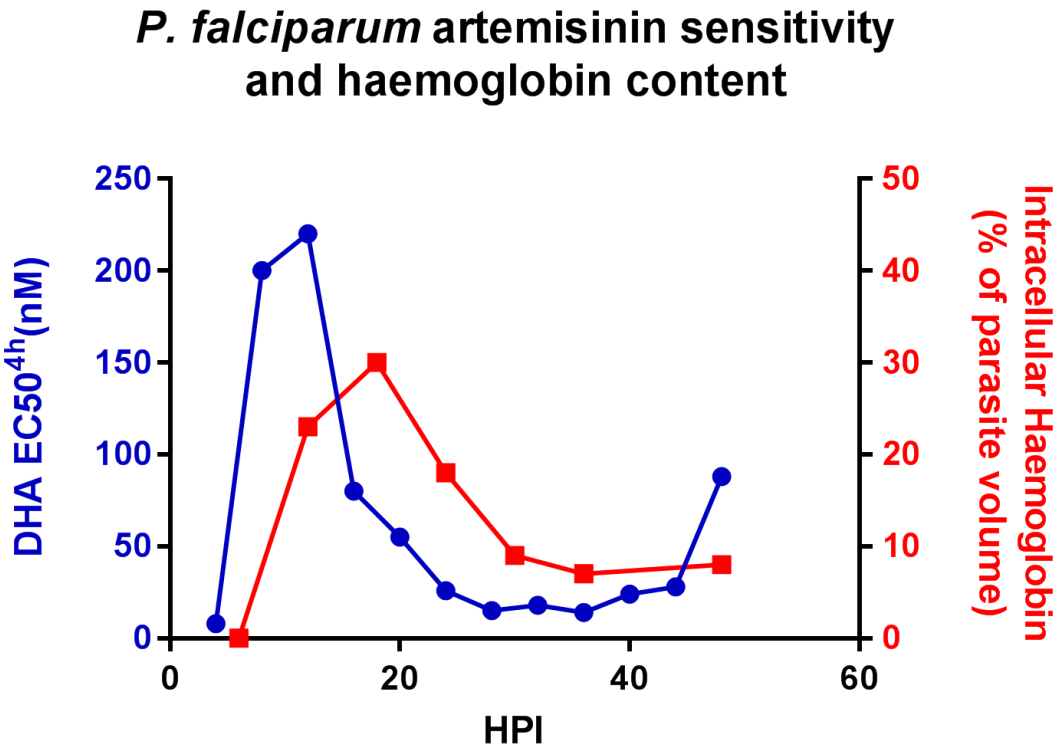


**Figure 8 Comparison of time-dependent relationship between haemoglobin uptake and artemisinin resistance**
Overlaid data, derived from Klonis *et al* (DHA $EC_{50}$'s) and Elliott *et al* (haemoglobin content), show how parasite sensitivity to artemisinin seems to negatively correlate with haemoglobin content. Parasites are more susceptible to artemisinin when there is less haemoglobin in the parasite cell. These studies were conducted by different laboratories making it difficult to directly compare the exact temporal relationship between artemisinin susceptibility and haemoglobin content. However, as haemoglobin is degraded in the trophozoite stage, haem and haemazoin may activate artemisinin's endoperoxide. Interestingly, the period hypersensitivity in the ring-stage does not correlate with haemoglobin content as even by microscopy, there is little to no haemoglobin in the parasite cell.

Indeed, several studies have shown that interfering with haemoglobin degradation by knocking out falcipain proteases or treating cells with protease inhibitors dramatically affects parasite susceptibility to artemisinins[90,189,190]. However, questions remain regarding how haemoglobin degradation could affect cells in the first few hours of life when the digestive vacuole is still forming, and studies have shown that there is virtually no haemoglobin in the parasite at this stage[191] (Fig 8).

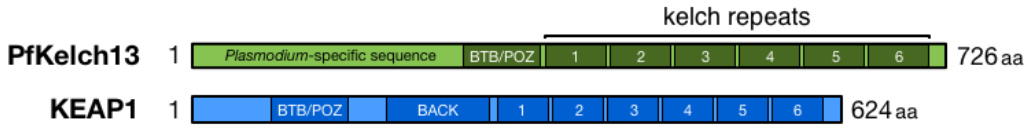


**Figure 9 Protein map of pfkelch13 and hkeap1**
A schematic representation of PfKelch13 protein, the confirmed modulator of artemisinin resistance *in vitro* and *in vivo*, and its human orthologue, hKEAP1. PfKelch13 (K13) and KEAP1 both have a 6-bladed β-propeller kelch-domain at their C-terminus as well as a BTB/POZ domain upstream of this propeller domain. In the context of the BTB/POZ dimerization domain, the propeller domain mediates interactions with ubiquitylation machinery in KEAP1. The BACK domain may help orient substrates. K13 lacks the BACK domain but contains an approximately 200 amino acid N-terminal sequence with little homology to KEAP1 or other mammalian factors.

Clinical resistance has been linked to several mutations in *pfkelch13*, which produces the Kelch13 (K13) protein, with the C580Y mutation being the most common K13 mutation in Southeast Asia. On the molecular level, K13 is a WD40-repeat containing factor, which shares some homology with the KEAP1 transcriptional regulator in mammalian cells (Fig 9). KEAP1 regulates the NRF2 transcription factor, which activates stress response and cell survival pathways.

However, K13 does not seem to be involved directly in transcriptional regulation. Instead, a recent study localised K13 to a conspicuous cytoplasmic compartment closely apposed to the digestive vacuole [192].

Multi-omic investigation suggests that cells expressing K13 mutations associated with artemisinin resistance seem to have a more robust oxidative stress response, consistent with the proposed mechanism of artemisinin-mediated cytotoxicity. These cells display elevated levels of glutathione, an important antioxidant, lower abundance of haemoglobin-derived peptides, and a transcriptional response tuned towards expression of mitochondrial redox factors [193,194]. Artemisinin-treated parasites also display significantly increased global

ubiquitylation, consistent with a response involving the ubiquitin-proteasome system and increased protein turnover [89,195].

The only mechanistic information on K13-mediated protection comes from a 2015 study by Mbengue *et al* [196]. In this work, the authors propose that K13 regulates PI3K, which produces the lipid signalling molecule phosphatidylinositol-3-phosphate (PI3P). They show that parasites with K13 mutations have elevated levels of PI3P, and artificial induction of PI3P in the absence of K13 mutations phenocopies the K13(C580Y)-mediated ring-stage protection from artemisinins. PI3P localises to the digestive vacuole and apicoplast membranes, though it is known to participate in a wide variety of intracellular processes in other organisms [196–199]. One 2018 study published by Bhattacharjee *et al*, also from this laboratory, demonstrated that K13 localises to PI3P-labeled vesicles and structures emanating from the endoplasmic reticulum, which increase in number during artemisinin-induced stress [200] (Fig 10). Apparently, these vesicles contain exported proteins, namely PfEMP1, an important family of cytoadhesion molecules that are secreted to the red cell surface and mediates virulence. In their study, K13 copurifies with these factors and many other factors involved in proteostasis. Additionally, red cells infected with parasites expressing resistance-associated *pfkelch13* mutations have different cytoadherence properties. However, a previous study in 2016 by six prominent laboratories each independently confirmed that no PI3P could be detected in the ER, and PI3P does not have a role in export to the red cell, which questions these results [201]. Additionally the cryoimmunoelectron micrographs presented as strong evidence in Bhattacharjee's work seem to show both PI3P and K13 signal essentially everywhere inside and outside of the parasite and red cell in DHA-treated samples suggesting that these antibodies may also recognise off-target epitopes [200].

Another recent work addressed the mechanisms underlying artemisinin-induced dormancy [202]. Zhang *et al* demonstrated that artemisinin stress causes BiP, an ER-resident chaperone, to mediate PK4 dimerisation in the ER membrane. This dimerised PK4 phosphorylates and activates eukaryotic initiation factor 2a (eIF2α), which induces translational repression. Normally, eIF2α is only phosphorylated in schizonts in preparation for cytokinesis and egress. However, in parasites with K13 mutations associated with artemisinin resistance, PK4 either remains phosphorylated or is prematurely phosphorylated in early ring-stage parasites. By extension, these cells exhibit a type of dormancy in the early ring-stage that allows them to evade some of artemisinin's cytotoxicity and propagate into the next cycle. Chemically inhibiting PK4 restores sensitivity in artemisinin-resistant strains [202] (Fig 10).

The Zhang study revealed important information about the mechanisms of dormancy, but do not clarify how the parasite resumes its normal growth. Around the same time, a third paper by Duvalsaint *et al* examined the role of phytohormones and isoprenoids in enabling the parasite to resume its growth after artemisinin-induced dormancy [203]. This work showed that apicoplast-derived isoprenes were required for exiting the artemisinin-induced dormant state.

A number of other factors have been proposed to be involved in modulating drug response and be associated with clinical treatment failure. Some of these proteins include Ubp1 and AP2μ, which are the subjects of this thesis, as well as ATP6, the SERCA calcium pump [204–208]. The role of ATP6 has been seriously questioned lately, and there is no evidence of association with resistance in the field [120,209–211]. It is likely that the mechanism of artemisinin resistance is subtle because only a fraction of "resistant" parasites actually survive to the next cycle after artemisinin exposure. From the evidence presented so far, it probably involves some

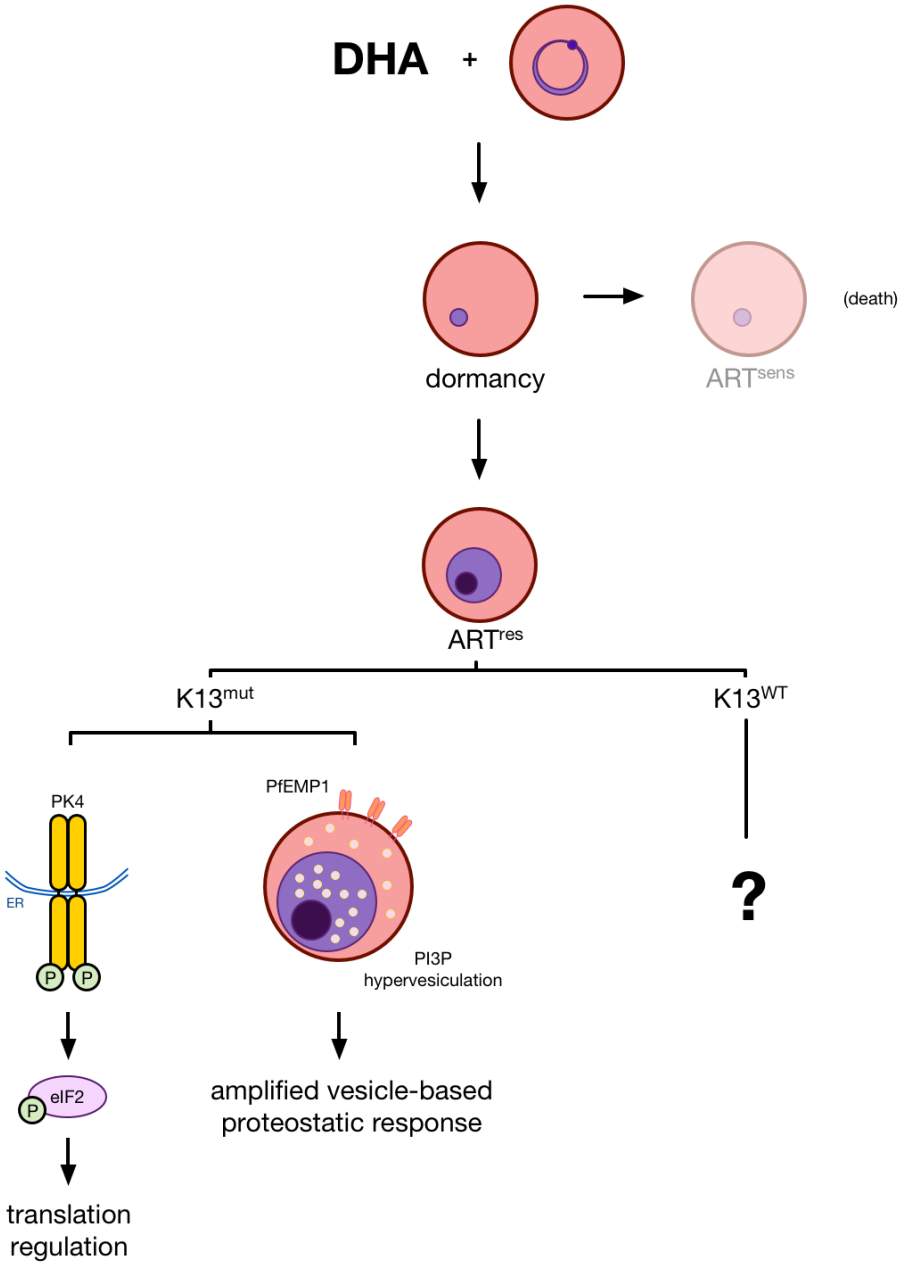


**Figure 10 Schematic representation of artemisinin response and resistance mechanisms**
Artemisinin exposure is believed to induce a type of dormancy in *Plasmodium falciparum*. How the cell recovers from this dormancy and the characteristics of this dormancy are mostly unknown. K13 mutations cause resistance either by enhancing the ability of parasite cells to endure artemisinin-induced stress or escape ART-induced dormancy. Two mechanisms have been offered: induction of ER stress response and translational dormancy factors BiP, PK4, and eIF2α as well as a PI3P-dependent hypervesiculation and export of key virulence factors. Reduced parasite susceptibility to artemisinin has been reported in the absence of K13 mutations. However, it is unclear how this would occur.

modulation of protein synthesis and turnover centred at the ER and may require additional antioxidant cofactors or signalling molecules. Overall, considerable study is still required to elucidate the mechanisms of artemisinin activation, action, and resistance in order to preserve their efficacy worldwide.

## 1.6 Evaluation and Surveillance of Drug Resistance

Currently, surveillance of drug resistance predominantly relies on active case detection and reporting through drug efficacy studies in the field and *in vitro* or *ex vivo* assessment of drug susceptibility of parasite isolates in the lab.

Evaluation of drug efficacy in the field involves treating symptomatic patients with a frontline chemotherapy and monitoring these patients' clinical and parasitological responses over 4 to 6 weeks. Namely, investigators examine progression of clinical symptoms, resolution of peripheral, acute parasitaemia, and long-term protection from reinfection or recrudescence. The sum of these indicators provides evidence of early treatment failure, late treatment failure, delayed clearance, and adequate clinical and parasitological response. While blood smears are taken and read in the field for microscopic diagnosis of infection and treatment monitoring, peripheral blood samples are usually taken as filter paper blood spots or venous blood samples for subsequent PCR-based investigation of parasite clearance and molecular markers of drug resistance. PCR and Sanger Sequencing are also used to separate new infections or multi-species infections from parasite recrudescence after treatment. This genotyping across a region can provide insights into the spread of resistance-associated parasite genetic haplotypes.

In the lab, cryopreserved or live samples of infected blood can be cultured and examined for *ex vivo* drug susceptibility. Some of these isolates may be adapted

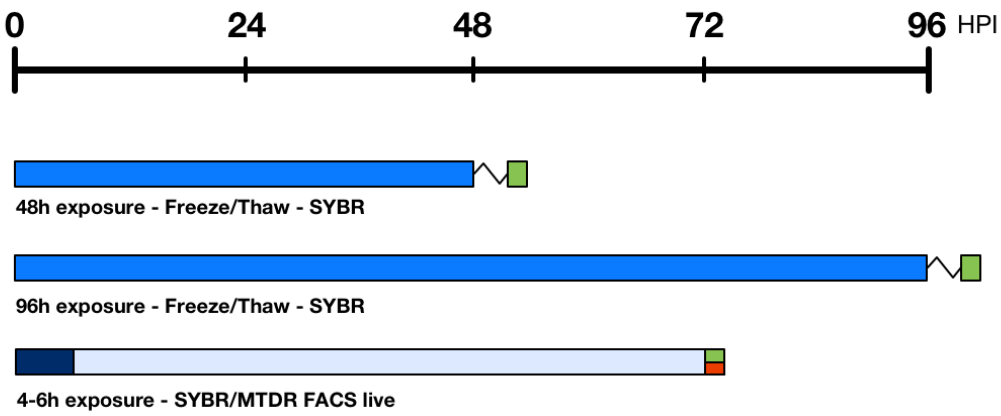


**Figure 11 Common antimalarial drug sensitivity assays**

Schematic representation of common antimalarial drug sensitivity assays. The 48-hour and 96-hour assays involve exposing parasites to serial dilutions of compounds in 96 well plates for the stated length of time beginning when parasites are in the ring stage. After the stated time, these plates are frozen, thawed, and lysed. Parasite growth is quantitated by proxy with SYBR-Green, which stains DNA. Total DNA correlates with parasite proliferation. Short exposure assays (third assay) involve exposing parasites to fixed concentrations or serial dilutions of a chemotherapy for 4 to 6 hours. Drugs are then washed off and parasite growth is assessed directly by live cell FACS using SYBR Green and MitoTracker Deep Red (MTDR), which stains total parasite DNA and mitochondria of live cells.

to long-term *in vitro* culture and used for advanced genetic or molecular research, including genome editing. Three main assay formats are used to examine drug susceptibility in the lab: 48-hour dose response, pulsed dose response, and single pulse survival (Fig 11). The type of assay and the method of assay readout chosen depends on the drug under examination. Drugs with half-lives like chloroquine or pyrimethamine are assayed using the 48-hour approach. This is because these drugs remain at a near constant concentration in the body over a single parasite lifecycle. Quantitating the reduction in parasitaemia over a single lifecycle provides insight into how the parasites will be cleared over multiple days *in vivo*. However, this 48-

hour format is not appropriate for drugs with shorter half-lives. In particular, artemisinins are exceptionally unstable and rapidly degrade in the body and in culture. Therefore a 48-hour exposure is not physiologically relevant. Witkowski *et al* first described a pulsed assay format where parasites are exposed to the artemisinin compound for 6 hours, which more closely resembles the *in vivo* half-life of the drug, and then extensively washed [212]. Shorter pulses have also been explored for artemisinins with equal ability to discriminate resistant and sensitive parasite populations [213]. Incorporation of serial dilutions of a drug either in a pulsed or 48-hour exposure format allows investigators to determine $EC_{50}$ or $EC_{90}$. In general, a FACS-based readout using a live/dead stain like MitoTracker and a DNA stain like SYBR Green provides a reproducible and robust quantitation of parasite survival. However, FACS machines are expensive to maintain and may not be available. In this case, SYBR Green-based quantitation of parasite proliferation in a plate reader is an affordable and high-throughput. However, this method is sensitive to the exact concentration of parasite material in each well—evaporation or sample loss will lead to overcounting of parasite DNA—whereas FACS counts the same number of gate-stopping events per sample. In practice, the difference is small, though FACS is particularly useful when looking at artemisinins because these drugs render a subpopulation of cells pyknotic whereby they are nonreplicative but still retain DNA. SYBR Green methods will count these parasites as alive, whereas FACS with MitoTracker will not.

When carried out in the ring stage, the pulsed assay format, also known as the ring-stage survival assay (RSA), is the only validated assay for examining the sensitivity of a given parasite isolate or strain to artemisinin. With clinical parasite isolates, the *ex vivo* RSA survival (percentage of cells surviving the drug pulse)

correlates well with *in vivo* parasite clearance and clinical outcome. However, it is not clear whether elevated survival rates in this assay format are good predictors of clinical outcome (i.e. would a novel mutation identified in the laboratory be clinically relevant?). Additionally, this assay does not capture important aspects of host environment during ring-stage infection, namely environmental temperature (Fever conditions). Ring-stage resistance must occur in the context of hyperthermic conditions, and the RSA is only performed at 37C. Therefore, while the RSA is the best assay we currently have to examine parasite sensitivity to artemisinin, there is clear room for improvement, and it will be important to understand how predictive the RSA survival rates are of clinical outcome.

For antimicrobial agents such as doxcycyline and azithromycin, *in vitro* studies of parasite susceptibility require longer 96-hour exposures because these agents exert cytotoxic effects on second-generation parasites. In general, the assay formats described here are robust and basic parameters can be manipulated to provide an optimised readout of parasite survival.

This thesis uses $EC_{50}$ to refer to the concentration of a compound required to reduce parasite growth by 50% with respect to a solvent-treated control. Though it may seem pedantic, it is important to distinguish cytocidal and cytostatic killing when studying the cytotoxicity of compounds in live cells. Because the assays in this thesis quantify cellular proliferation, it is inappropriate to use $IC_{50}$, which canonically refers to inhibition of a specific pathway or enzyme.

## 1.7 Endocytosis in *P. falciparum*

Many of the most common antimalarial drugs leverage the malaria parasite's dependence on haemoglobin. Despite its importance to drug action and broader parasite biology, relatively little is known about how malaria parasites sample their extracellular and intraerythrocyte environments.

The term endocytosis encompasses any mechanism of uptake of material from the extracellular space and takes many forms in higher order eukaryotes[214]. Broadly, there are three types of endocytosis: phagocytosis, pinocytosis, and receptor-mediated endocytosis (Fig 12)[214]. Phagocytosis describes the active, ATP-dependent process of invagination and uptake of molecules other than solutes from outside the cell through a structure called the cytostome. This is commonly associated with the behaviour of macrophages engulfing entire diseased or disease-causing cells, but also includes the uptake of macromolecules, excluding solutes. Pinocytosis is also an ATP-dependent process but only concerns the uptake of extracellular fluid and solutes[214]. Receptor-mediated endocytosis (RME) is a

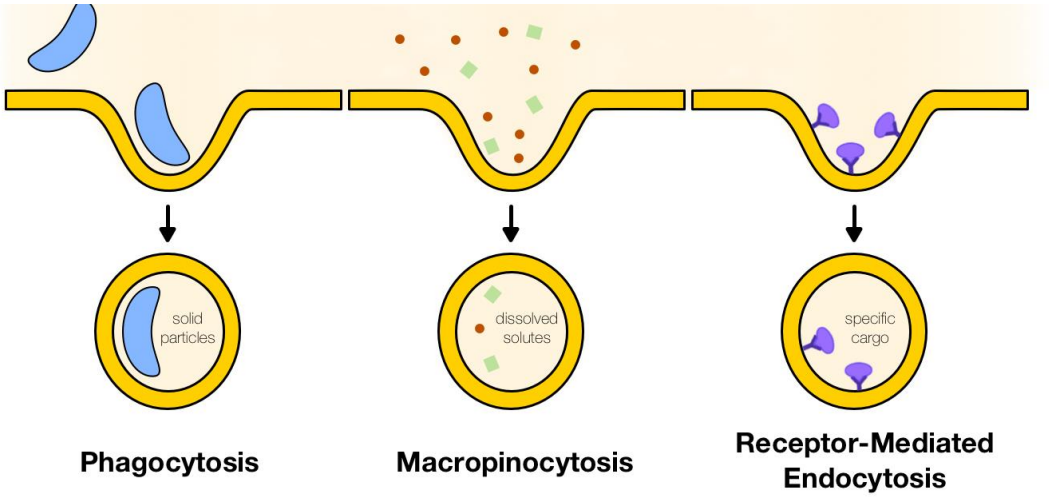


**Figure 12 Three types of endocytosis in eukaryotes**
Three major pathways for endocytosis exist in eukaryotes. Phagocytosis involves the uptake of solid particles from an extracellular space, including other cells and proteins. By contrast, macropinocytosis allows cells to sample soluble, dissolved small molecules in the extracellular space. Receptor-mediated endocytosis refers to the uptake of extracellular ligands via interaction with ligand-specific, transmembrane receptors.

specialised mechanism, which internalises receptor-bound cargo and therefore is a cargo-specific process. RME is a highly regulated process and encompasses a wide variety of uptake pathways across eukaryote cells. All RME pathways involve a controlled invagination of the plasma membrane around a critical mass of cargo-bound receptors[214]. This invagination is directed by several factors including a coat protein, which polymerises into a cage-like structure on the cytoplasmic face of the budding membrane[215]. Via ATP-dependent membrane scission, the membrane droplet is cleaved from the plasma membrane and trafficked into early endosomal compartments or hydrolytic lysosomes. The cargo molecule is dissociated from the receptor molecule, and the receptor molecule is, in some cases, shuttled back to the plasma membrane[216]. All of these processes originate at the plasma membrane and therefore differ from transcytosis, which describes the budding and traffic of membrane bound vesicles between organelles inside the cell[214].

Mechanisms of endocytosis in *Plasmodium* are generally unclear. To date, the study of endocytosis revolves around the examination of haemoglobin uptake. The parasite engulfs an enormous amount of haemoglobin from the host erythrocyte cytoplasm during the asexual lifecycle. It is not immediately clear if this is by a continuous, dedicated phagocytic process or simply one major phagocytic event, which happens to ingest a large volume of haemoglobin, since the erythrocyte cytoplasm contains so much of it. A seminal study by Elliott *et al* in 2007 showed the parasite has four separate pathways for haemoglobin uptake, which take place over different stages of the asexual cycle [191] (Fig 13). They major mechanism is what the authors describe as the "Big Gulp." They time this process to occur between hours 6 and 30 of development and describe it as the invagination of a single, massive vacuole, formed during the developmental "folding" of the very-early

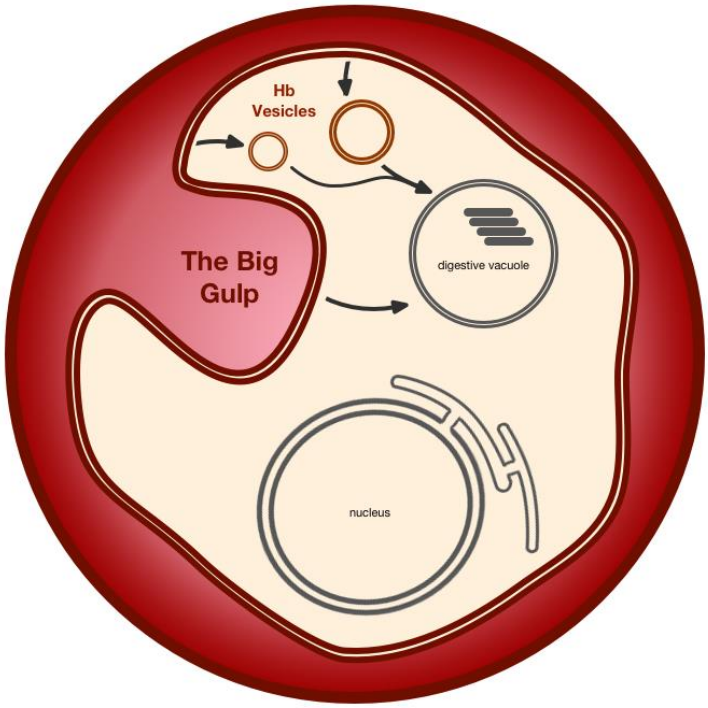


**Figure 13 Several distinct pathways for haemoglobin uptake**
During *Plasmodium falciparum* development, the parasite cell ingests haemoglobin through four major means. The Big Gulp is a large endocytic event mediated by unknown factors occurring in the ring stage. Throughout the asexual cycle small vesicles, cytostomal tubules, and phagotrophs also mediate uptake. Phagotrophs are similar to The Big Gulp but is actin-independent.

parasite into the canonical ring shape observed by Giemsa staining. This process seems to be actin independent and accounts for nearly 95% of the haemoglobin uptake. Other mechanisms of haemoglobin ingestion include small haemoglobin-containing vesicles, which can be observed budding from the cytostome by electron microscopy before, during, and after the Big Gulp; cystostomal tubules, which form direct channels from the cytostome into the cytoplasm; and phagotrophs, which define large haemoglobin-containing vesicles [191].

Though clathrin heavy chain is encoded in the parasite genome, it has not yet been characterised, so the involvement of clathrin in haemoglobin endocytosis is unknown. However, by electron microscopy, haemoglobin-containing vesicles seem to be too small to be consistent with clathrin-coated vesicles in higher-order eukaryotes[191]. In 2010, Bakar *et al* recapitulated some of these results and showed that the parasite does not begin to sample the host cell cytoplasm until the mid-ring

stage [217]. This group also showed haemoglobin is first internalised into small vesicular structures that then coalesce into the digestive vacuole.

The role of actin in parasite endocytosis is subject to some debate. The original Elliott study suggested the Big Gulp is not affected by actin inhibitors and that only some of the mechanisms of endocytic uptake were actin-dependent[191]. However, multiple studies have shown that interfering with actin dynamics does seem to affect haemoglobin levels in the cell and digestive vacuole size, leading to the conclusion that an actomyosin motor is somehow required in the traffic of haemoglobin-containing endocytic vesicles to the digestive vacuole [191,217–220]. Another study recently suggested that Dyn1, a dynamin family member, is required for cleaving vesicles from the plasma membrane for parasite endocytic sampling of the erythrocyte cytosol, much like in other eukaryotes [220].

Through all of this work, it is still not clear what factors mediate these different pathways of haemoglobin uptake and whether they all proceed via the cytosome. It is also not clear if there are any receptor-mediated pathways. Across nearly all eukaryotic taxa, the AP-2 adaptor protein complex mediates clathrin-dependent endocytosis from the plasma membrane to the early endosome compartment of specialised cargo molecules, including the transferrin receptor. An early study in 1986 reported that the parasite produces a transferrin receptor, which allows the parasite to ingest ferric iron bound to transferrin [221]. However, a later study in 1992 showed that parasites did not take up transferrin, suggesting any encoded transferrin receptor is either dispensable or behaves in an unknown way [222]. Therefore, to date, the only mechanistic insights into endocytic processes in the parasite exist in the context of haemoglobin uptake, which seems to largely be an active, but non-specific sampling of the erythrocyte cytosol. A detailed

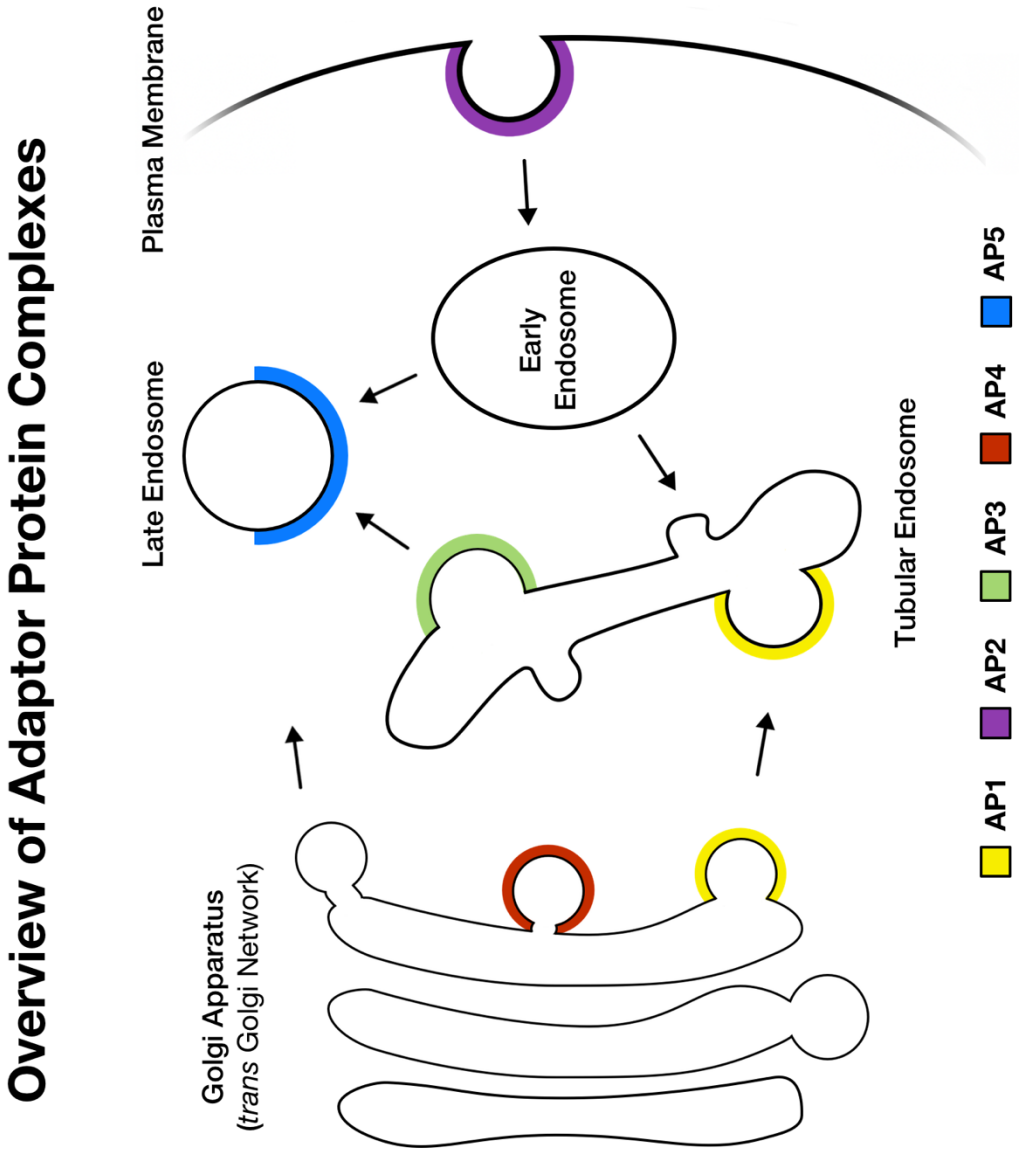


**Figure 14 Overview of adaptor protein complexes**
Eukaryotes have several adaptor protein complexes that mediate compartment-to-compartment vesicular traffic. AP-1 mediates Golgi-to-endosome traffic, AP-2 plasma membrane endocytosis, and AP-3 intra-endosomal traffic. AP-1, AP2, and AP-3 functionality is conserved across eukaryotes. AP-4 and AP-5 are not necessarily found in all eukaryotes and are involved in specialised traffic in the Golgi and endosomal network. COPI and COPII (not pictured) mediate traffic between the ER and the Golgi.

characterisation of clathrin heavy chain and the transferrin receptor are necessary to further elucidate potential roles of canonical endocytic machinery in the parasite.

## 1.8 Adaptor Protein Complexes

Where endocytosis refers to the process of moving material from the extracellular space into the cell, transcytosis refers to a similar process, which moves material from compartment to compartment within the cell. In many cases, this cargo shuttling is mediated by specialised adaptor protein complexes that recognise cargo molecules and coat proteins[223]. These complexes and their associated traffic define major cargo highways in the cell.

The adaptor protein complexes are composed of the four heterotetrameric complexes, AP-1-AP-4, and the heterohexameric AP-5 which associate with clathrin or another coat protein to direct intracellular vesicular traffic [224] (Fig 14). Not all eukaryotes have all five complexes, but all sequenced organisms have AP-1, AP-2, and AP-3, reflecting their evolutionary functional importance[214,223]. AP-1 traffics between the *trans*-Golgi network (TGN) and endosomes. AP-2 canonically mediates endocytosis of bound cargo from the plasma membrane to the early endosome. AP-3 moves cargo from the early endosome further along the endosomal system to multivesicular bodies, late endosomes, or lysosome-like organelles. AP-1-AP-3 all interact with clathrin cages [224]. AP-4 resembles AP-1 in that it traffics from the *trans*-Golgi to the endosomal network, but it has functionally diverged and is utilised in unique, cell type-specific pathways, such as neural signalling and polarised intracellular traffic. Notably, AP-4-containing vesicles do not utilise a clathrin coat [224,225]. AP-5 is the most recently discovered complex in the adaptor complex family.

Like AP-4, AP-5 does not seem to associate with clathrin and is also localised to the TGN. Although it is expressed throughout mammalian development and is essential for cell survival, its trafficking destination and cargo are still unknown [225,226]. The monomeric GGA proteins are also clathrin adaptins, share some homology with the gamma subunits of the APs, and participate in similar trafficking pathways. However, these are well outside the scope of this thesis and will not be discussed or reviewed.

Architecturally, the adaptor protein complexes are heterotetramers consisting of two large (α/γ/δ/ε, β) , one medium (μ), and one small subunit (σ) (Fig 15). The large subunits are made of a large trunk domain consisting primarily of a twisting L-

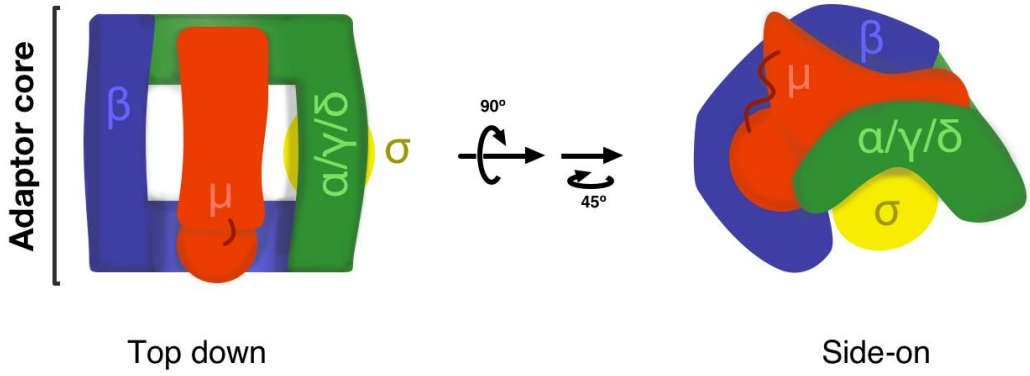


| | Large Subunit | | Large Subunit | | Medium Subunit | | Small Subunit | |
|---|---|---|---|---|---|---|---|---|
| | Name | PFID | Name | PFID | Name | PFID | Name | PFID |
| **AP-1** | γ | PF3D7_1455500 | β | PF3D7_0528100 | μ | PF3D7_1311400 | σ | PF3D7_1118100 |
| **AP-2** | α | PF3D7_0617100 | β | *not annotated* | μ | PF3D7_1218300 | σ | PF3D7_0217300 |
| **AP-3** | δ | PF3D7_0808100 | β | PF3D7_0613500 | μ | PF3D7_1440700 | σ | PF3D7_1250500 |
| **AP-4** | ε | PF3D7_0904100 | β | PF3D7_0730200 | μ | PF3D7_1119500 | σ | PF3D7_0423100 |

**Figure 15 Architecture of adaptor protein complex core**
(Top panel) The adaptor protein complexes are heterotetrameric complexes consisting of large (α/γ/δ, β) subunits that provide architectural support and interact with the coat protein and vesicle membrane via appendage domains. The structure of these appendages have not been resolved and therefore are not depicted. The μ subunit interacts with the cargo molecules, and σ provides regulatory and structural functionality. μ resides in a saddle formed by the large subunits. (Bottom panel) A list of the expected components of each adaptor protein complex and the respective *P. falciparum* gene identifiers. No gene for AP-2β has been annotated in the *P. falciparum* genome.

shaped, α-helical solenoid connected to an appendage, "ear" domain by a protease-sensitive linker [224,227]. The trunk domains of each large subunit are primarily structural and make contacts with each other and the μ and σ subunits. The ear appendages are more functional and are responsible for interaction with the coat protein and other factors [227]. The L-shaped curvature of the superhelical trunks form pockets that cradle σ and μ subunits within the assembled complex [227,228].

The σ subunit shares structural homology with the N-terminal domain of the μ subunit [228]. The overall function of σ within an AP complex remains under investigation. It is probably involved in complex stability. Mutations in this subunit in the context of most adaptor complexes have been linked with developmental pathologies in humans [229,230]. The μ subunit is directly responsible for cargo binding on the C-terminal domain of the subunit and harbours phosphoregulatory sites on the flexible linker bridging the N- and C-terminal domains. Structurally, μ sits in a saddle formed by the two large subunits until a cargo molecule is present, at which point, the μ subunit undergoes a large translocation and rests "open" on the solvent-exposed surface of large, β subunit [227,228]. The μ and β subunits directly bind C-terminal dileucine (D/ExxxLL) and tyrosine-hydrophobic (Yxxϕ) sorting motifs. μ also interacts with phospholipids.

Mechanistically, the adaptor complex weakly associates with phosphatidylinositol-labelled membranes, with the lipid type specific to each complex. Phosphorylation of a threonine residue on the linker in the μ subunit triggers a conformational change, which enables the μ and β subunits to interact with cargo molecules [231,232]. These cargo-loaded complexes interact with other factors involved in the budding process including the coat protein. The budding process continues as the coat polymerises around the budding vesicle until dynamin cleaves

the neck of the invagination, forming the free vesicle and resealing the parental membrane [231]. A large number of other factors including auxulin, epsin, AP180, and amphiphysins are recruited to the sites of the initial invagination after cargo recognition and binding. These factors are complex-specific and regulate how the budding process proceeds and where the vesicle ultimately goes.

The adaptor protein complexes and clathrin support the late secretory pathway and endocytosis between the *trans*-Golgi, cell surface, and endosomal network as described. Upstream of these pathways, the coatomer complexes COPI and COPII mediate anterograde and retrograde traffic between the endoplasmic reticulum and the *cis*-Golgi[233]. COPI also mediates traffic within the Golgi. Unlike the adaptor protein complexes, COPI and COPII both aggregate and interact with cargo molecules and act as vesicular coats[233].

Though these processes are reasonably well defined in mammalian cells, it is unclear how this canon translates to Apicomplexans. Apicomplexa are, at least for some of their lifecycles, intracellular and exist within a parasitophorous vacuole and have unique organelles in the post-Golgi secretory pathway. Cargo will need to get to these organelles, and it is possible that traditional Golgi-to-endosome sorting pathways have been redirected towards these organelles. In *Toxoplasma gondii*, ap-1 has been shown to target to the apical secretory organelles from the TGN, and limited evidence suggests the same may be true in *Plasmodium falciparum* [234,235]. In *Dictyostelium*, the large β subunit of AP-1 plays a dual role in AP-2 [236]. Though no additional studies of adaptins in *Apicomplexa* have been reported, this may suggest an evolutionary multi-purposing of some adaptins in multiple adaptor complexes as a result of genome streamlining.

AP-2 in *Plasmodium* has been implicated in artemisinin resistance in the field and in rodent model studies [204–206,208]. In 2007, Hunt *et al* evolved an artemisinin-resistant *P. chabaudi* malaria parasite by a series of sequential drug selections and *in vivo* crosses[208]. Genome sequencing identified a mutation of interest in the *pfap2mu* gene, encoding PcAP-2μ(I568T). Subsequent analysis of *P. falciparum* parasites from patients in East Africa identified evidence of selective pressure on a separate mutation of interest encoding PfAP-2μ(S160N), and preliminary reverse genetics work suggested this mutation may alter parasites susceptibility to several drugs[205]. These studies argued a putative mechanism in haemoglobin endocytosis by homology with mammalian AP-2, which performs receptor-mediated endocytosis from the plasma membrane, but how receptor-mediated endocytosis could occur in the context of a double membrane at the parasite periphery is unclear. Specific investigations of these putative factors are needed to determine the nature and extent of their involvement in endocytic events.

## 1.9 Roles of ubiquitin and ubiquitin turnover *P. falciparum*

Ubiquitin, as its name suggests, is involved in nearly every process in the cell. The small, 76-amino-acid protein is a post-translational modification, ligated onto lysine sidechains of a protein target via an enzymatic ubiquitylation cascade. Ubiquitylation is a dynamic and reversible process, and understanding how ubiquitin ligation and removal occurs throughout the parasite is important as artemisinin susceptibility has been linked to ubiquitylation and protein turnover.

### 1.9.1 Ubiquitin conjugation is a dynamic process

Generally, ubiquitylation is catalyzed by a cascade of ubiquitin-activating E1, ubiquitin-conjugating E2, and ubiquitin-ligating E3 enzymes[237]. An E1 first generates an activated, ubiquitin adenylate through ATP hydrolysis. The E1 then transfers this ubiquitin intermediate to a cysteine side chain in the E2 active site via a transthioesterification reaction. With the help of one or more E3 enzymes, the C-terminus of ubiquitin is finally covalently ligated to the ε-$NH_3$ of the target lysine side chain on the substrate (Fig 16).

The final step of the ubiquitin ligation cascade occurs through one of two mechanisms depending on the ligation domain of the E3 protein. HECT (Homologous to the E6-AP Carboxyl Terminus) domain-containing E3s catalyse a transthioesterification between the E2 active cysteine and a cysteine in their active site, and subsequently, ligate ubiquitin to the target protein. In contrast, RING (Really Interesting New Gene) domain-containing E3s never covalently possess ubiquitin but rather guide direct ligation of ubiquitin from the E2 cysteine to the target lysine.

Despite the differences in the molecular size of each modification, ubiquitylation is a dynamic modification like acetylation, phosphorylation, and methylation, and like methylation, a substrate can be mono- or polyubiquitylated. In all cases, ubiquitylation begins with ligation to a lysine side chain of the target protein by one of the mechanisms previously discussed. Successive ubiquitylation can then form chains on different and alternating lysine side chains of the previous ubiquitin (K6, K11, K29, K48, K63 etc.).

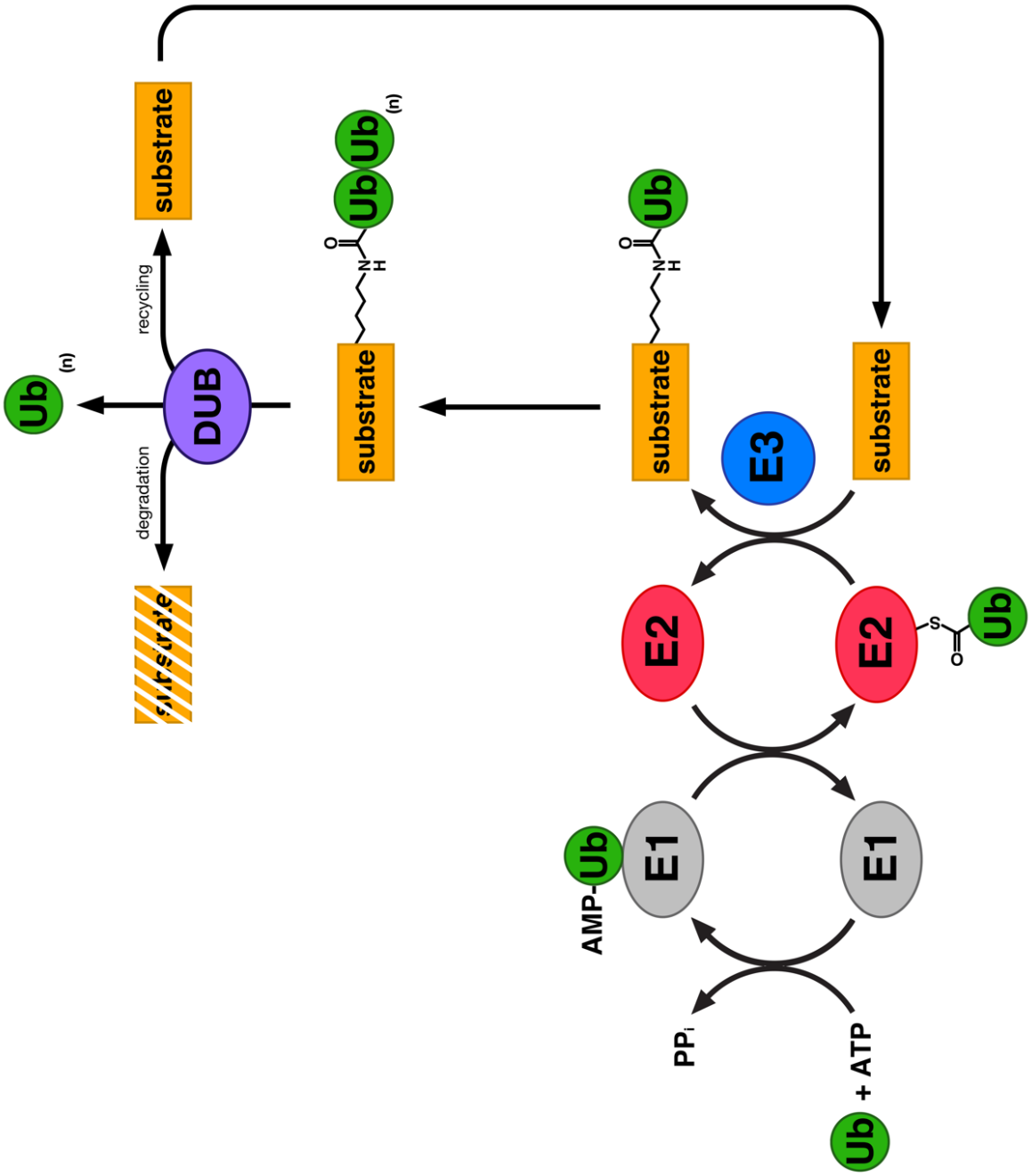


**Figure 16 Conjugation and cleavage of ubiquitin chains from target substrates**
Conjugation and cleavage of ubiquitin chains from a target substrate requires several enzymatic steps. E1 ubiquitin-activating, E2 ubiquitin-conjugating, and E3 ubiquitin-ligating enzymes all work in concert to retrieve free ubiquitin from solution and covalently attach it to the ε-NH3 of a lysine sidechain of a target protein in an ATP-dependent process. The specificity of this reaction is derived by combinatorial diversity resulting from the pairing of E2 and E3 enzymes into a catalytic holoenzyme. Removal of ubiquitin requires the activity of a deubiquitinase (DUB) which catalyses a hydrolysis reaction to cleave the thioester linking ubiquitin and a substrate sidechain. Ubiquitin conjugation and cleavage is involved in cell signaling, chromatic modification, and protein turnover.

In the cell, the degree and type of ubiquitylation determines the fate of the ubiquitylated substrate. Polyubiquitylation on K48 always marks a protein for proteolysis by the 26S proteasome [237]. K63-linked polyubiquitin chains are involved, in humans, in intracellular targeting and transportation of vesicles, inflammation, and other tasks [237,238]. Other types of polyubiquitylation, including branched chains and monoubiquitylation, are much less well understood [239,240].

Much of the substrate specificity of the ubiquitin ligation cascade is believed to be derived from the E3 enzyme interactions with the target protein. Although many HECT-type E3 ubiquitin ligases function as monomers to receive ubiquitin from an E2 and modify a target protein, evidence now indicates that many E3's form $E2_n$:$E3_n$ multisubunit complexes. These modular complexes take advantage of combinatorial diversity to allow a single E3 to toggle between substrates or poly- and monoubiquitylation of the same substrate [241]. The *Plasmodium falciparum* genome is reported to encode 8 E1s, 14 E2s, and 54 E3s [195].

Recent work suggests that nearly half of the proteome may be ubiquitylated, with overall ubiquitylation peaking in the trophozoite stage [242]. Mass spectrometry on *P. falciparum* whole ubiquitome extracts reveals components of nearly every cellular process ranging from chromatin structure to transcription factors to redox metabolism maybe ubiquitylated [242]. A large number of factors identified in this screen are currently of no putative function.

There is also considerable interest in ubiquitin-like modifiers including SUMO and Nedd8. These proteins are conjugated to target factors in mechanistically similar ways, and some machinery has been identified in *falciparum*, leading to the speculation that they are actively involved in regulation of the parasite cell.

However, these related systems are beyond the scope of this thesis and will not be discussed further.

As mentioned above, ubiquitylation and protein turnover has been linked to artemisinin susceptibility. In particular, K13 is a proposed E3 ligase scaffold factor, mediating substrate-ligase interaction [196]. Additionally, recent work has associated mutations in an E2 (PF3D7_1243700) and HECT H3 (PF3D7_0826100) with artemisinin resistance in a GWAS study of 45 parasites from Senegal, but these data require further evaluation [243,244].

### 1.9.2 Deubiquitylation as a process, exploitable for cell survival

Just as ubiquitin monomers are ligated to target proteins and polymerised by an E1-E2-E3 cascade, ubiquitin monomers can be removed from proteins or poly-Ub chains by specialised proteases called ubiquitin hydrolases (Fig 16). These enzymes hydrolyse the isopeptide bond formed between the target lysine side chain and C-terminal Gly76. The foundational mechanistic biology is well reviewed by Wilkinson, but there are two general classes of cysteine hydrolases that operate on ubiquitylated substrates: ubiquitin C-terminal hydrolases (UCH-family) and ubiquitin-specific proteases (USP/UBP-family) [245]. UCH-family proteases resemble papain proteases and prefer substrates with single ubiquitin modifications or with flexible linkers between the globular domain of the target protein and the isopeptide bond. In contrast, UBP-family members prefer polyubiquitylated substrates [245].

In general, these factors, and UBPs in particular, play an important role in the ubiquitin-proteasome system. Since the majority of cellular energy is devoted to protein synthesis and recycling, it makes sense that the cell would aim to limit

unnecessary turnover. UBPs remove ubiquitin monomers from proteins destined for degradation immediately before entry into the proteasome to preserve a free ubiquitin pool. Proteasome activity, and the turnover of this ubiquitin pool, has been linked with rates of protein synthesis. Therefore, DUBs have been explored as possible drug targets for diseases involving immortal or rapidly dividing cells, including many cancers [246,247].

Very little is known about how deubiquitylation occurs in *Plasmodium* spp [248]. To date, only one deubiquitinase (DUB) has been characterised. In 2010, Artavanis *et al* presented the first structural and biochemical characterisation of PfUCHL3 (PF3D7_1460400) with and without an ubiquitin substrate bound to the active site [249,250]. PfUCHL3 is unique in that it is has dual specificity for ubiquitin and Nedd8 and is the only deNeddylase in the parasite genome, by inference with sequence homology to other taxa. Additionally, PfUCHL3 has similar activity *in vitro* as compared to the human orthologue.

The proteasome and DUB system is known to have redundancies in other organisms. Therefore, though some DUBs are chemotherapy targets, some may be dispensable. The high-resolution structure provided by Artavanis highlights important differences between the *P. falciparum* protein and the human orthologue indicating that at least some hydrolases may be druggable. Additionally, ectopically overexpressing a catalytically dead mutant of PfUCHL3 in cells is lethal, indicating the protein may be essential, though this may be due to a dominant negative effect [250]. Artvanis did not undertake a cell biology approach to examine localisation or factors that may interact with PfUCHL3. This work provides a platform into the functional characterisation of other *P. falciparum* DUBs, but to date no other studies have been published.

In *P. falciparum*, components of the DUB/proteasome system have been linked to drug resistance. Proteasome inhibitors have been shown to be cytotoxic on their own and synergise with artemisinins, supporting a mechanism of action of artemisinin involving oxidative insult and resistance requiring an enhanced stress response. The DUB Ubp1 has been linked in multiple studies in *Plasmodium chabaudi* and *Plasmodium falciparum* to artemisinin and chloroquine resistance [205,208,251–253]. *Pfubp1* potentially encodes a 416 kDa polypeptide over three exons. The C-terminal third of PfUbp1 shares some homology with USP7/HAUSP in humans, which is widely targeted by chemotherapies (Fig 17). USP7 regulates Mdm2, which regulates p53, a well-characterised tumour suppressor [246]. In this case, USP7 prevents Mdm2 from being degraded, rather than being a general hydrolase targeting polyubiquitin chains at the proteasome. Whether PfUbp1 shares functional homology with USP7 and whether the mutations of interest identified in this gene have any functional and clinical relevance remains to be investigated.

General protein turnover and recycling are only two of the important cellular roles of deubiquitylation activity. DUBs are also important components of protein quality control at the ER and protein import into the apicoplast (Fig 18). Both of these roles involve ubiquitylation of a substrate, unfolding of the polypeptide, and feeding into a protein channel. In the case of ER-associated degradation (ERAD), misfolded proteins are first recognised in the ER lumen, where these polypeptides are recognised by an E2-E3 complex made up of PfUbc7 and PF14_0215 in *P. falciparum* and polyubiquitylated [254]. The ubiquitin polymer is then recognised by chaperones, which guide the protein to the 26S proteasome in the cytosol where the protein is unfolded and degraded, and the ubiquitin polymer is disassembled by DUBs.

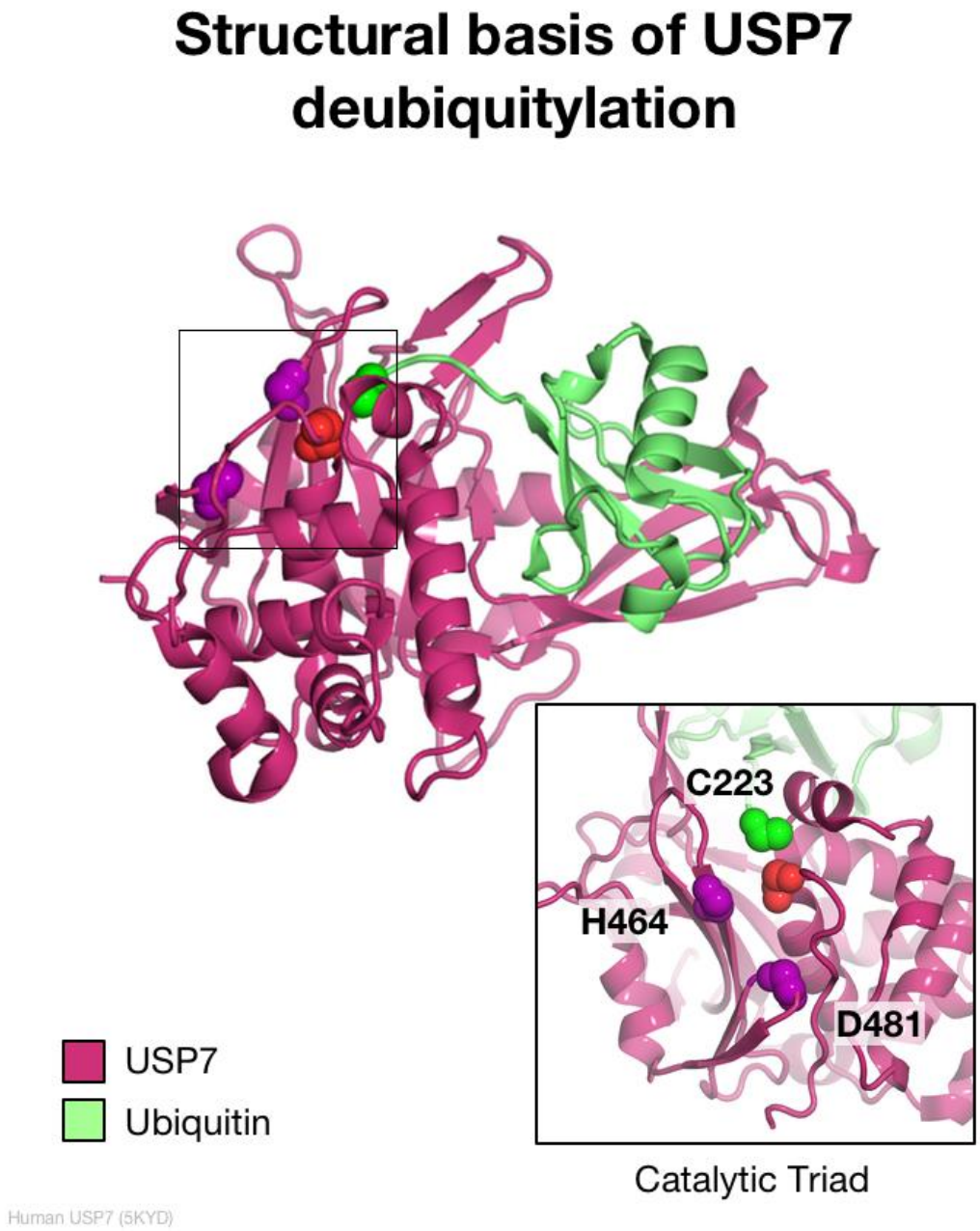


**Figure 17 Structure of USP7 catalytic core**
The crystal structure of the catalytic core of USP7 (pink, RCSB: 5KYD) provides insights into how recognition and hydrolysis of ubiquitin (green) occurs. The ubiquitin molecule docks into a pocket formed by b sheets which form a hand-like structure. The C-terminus of ubiquitin does not have secondary structure and extends through a scissor-like catalytic pocket made up of C223, H464, and D481. H464 and D481 provide electrostatic stabilisation and help to orient the incoming ubiquitin tail with respect to the catalytic cysteine, C223. The reactive sulfhydryl group of C223 catalyses a hydrolysis reaction to cleave the thioester linking Gly76 of ubiquitin to a target lysine sidechain.

This system is adapted to the import of proteins across the unusual 4-membrane structure of the apicoplast. The apicoplast is the relict plastid organelle in the parasite most likely acquired through a symbiotic engulfment of a photosynthetic red alga. In recent years, studies have revealed that some proteins are localised in specific membranes or lumens of this 4-membrane structure, suggesting a functional significance of this structure rather than just evolutionary coincidence [255,256]. To facilitate this sub-compartment-specific targeting, each membrane has a specialised "doorway" to the next lumen [256,257]. The mechanism by which cargo is first delivered through the outermost membrane is unknown, however a 2009 study by Spork *et al* indicated that a modified ERAD pushes proteins through the second outermost membrane [257]. CDC48, a AAA-type ATPase partners with Der1p, a membrane channel, to force proteins through this membrane with the help of an ubiquitylation cascade leading to the linearisation of the polypeptide. Proteins are then refolded on the other side of the channel. In *Toxoplasma gondii*, this process makes use of a special, apicoplast-localised ubiquitin molecule [256]. Apicoplast-localised DUBs remove this specialised ubiquitin immediately before translocation.

Each ubiquitylation process requires a deubiquitylation step, at some point. We know that ubiquitylation also plays key roles in regulating endocytosis, propagating signal transduction, and modifying chromatin architecture, but at this point, nothing has been published to shed light on these pathways and how they might be similar, different, or druggable when compared with the widely studied mechanisms and machinery of the higher order eukaryotes.

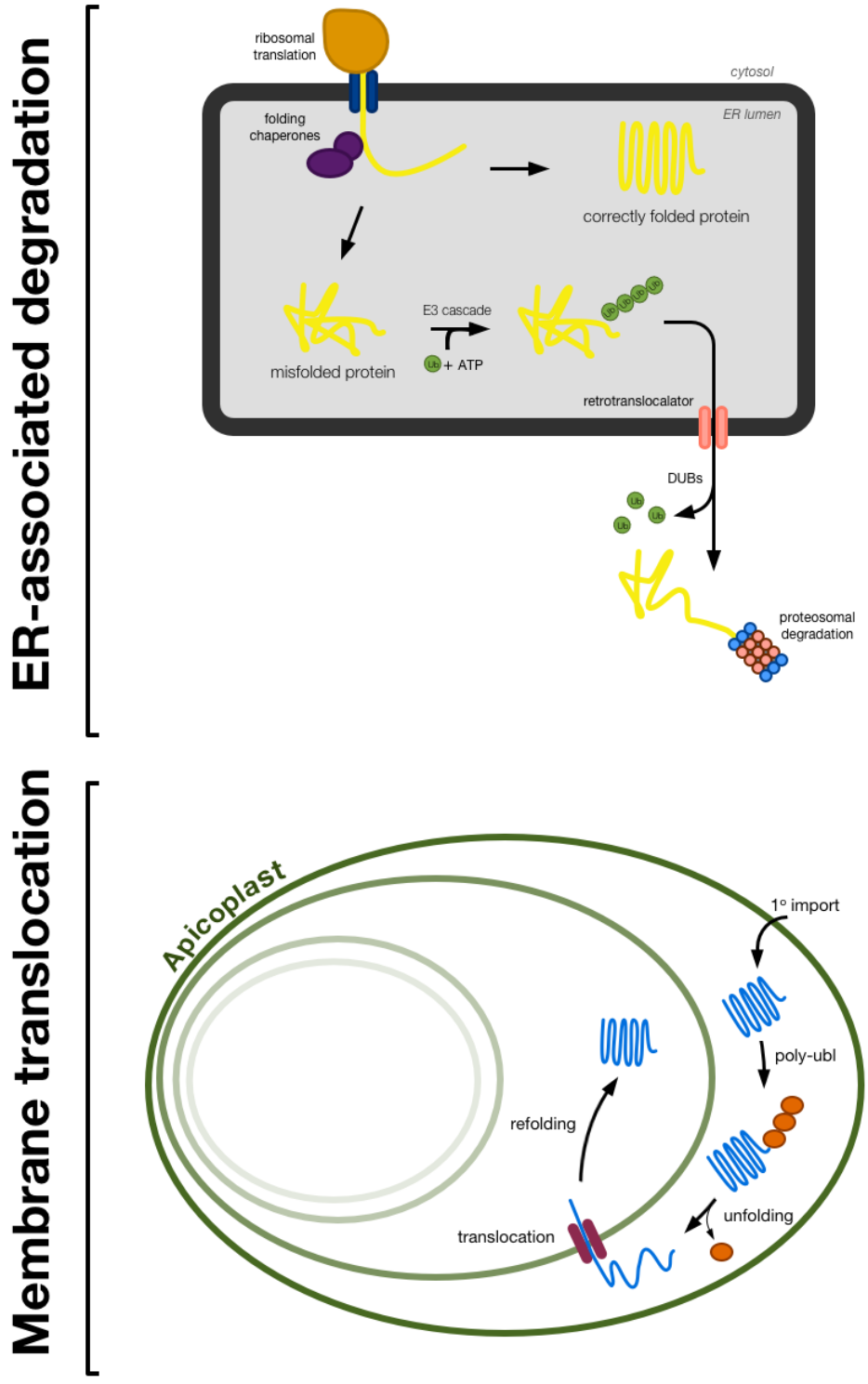


**Figure 18 Two major roles for deubiquitylation in the *Plasmodium falciparum* cell**
Ubiquitin plays many roles in the cell as it is added to and removed from substrates. Two major DUB-catalysed processes include ER-associated degradation (ERAD) and membrane translocation of proteins in the apicoplast. Unfolded or damaged material in the ER must be exported and degraded in the cytosol (top panel). Polyubiquitin marks on damaged or unfolded material are recognised by a retrotranslocator in the ER membrane which facilitates the moving of this material to the cytosol where DUBs recycle ubiquitin before the protein is degraded. Moving proteins across the second apicoplast membrane involves a similar reaction where an apicoplast-specific ubiquitin molecule is attached to a target protein. The protein is unfolded, translocated, and refolded. Before translocation, DUBs hydrolyse and recycle this plastid ubiquitin.

## 1.10 Genome editing strategies in *Plasmodium falciparum*

Merging the study of these molecular markers *in vitro* and in the field is imperative to unravel the complicated narrative of drug resistance. Molecular epidemiology work has and continues to produce highly important data about the competitive dynamics of alleles in parasite populations throughout space and time. However, if this work is not directed at the right mutations, the data being generated can be meaningless. The actual roles and impacts of the mutations must be studied *in vitro* to inform this epidemiology work. Since the adaptation of transfection techniques to *Plasmodium* in 1995, genetic experiments in *P. falciparum* have been largely confined to episomal overexpression of factors of interest or single-crossover integration of transgenes. Unfortunately, *Plasmodium* parasites do not have the endogenous machinery to facilitate RNAi, and many other genetic tools typically deployed in eukaryotic systems similarly break down [258,259]. While episomal and single-crossover experiments generated valuable insights into parasite biology, both approaches have their limitations.

Episomal overexpression necessarily competes with expression from the genomic locus. In particular, across a population of cells, expression levels can vary dramatically depending on how many copies of the plasmid a give cell retains and propagates. For certain factors, the presence these additional copies can conceivably confuse genetic regulatory mechanisms and lead to artificial phenotypes. This approach is not appropriate for studying drug resistance factors because each cell represents a mixed population, with some molecules harbouring the mutation of interest and some not. While any phenotype observed should be attributable to the mutation, it is possible mutant molecules may exert an artificial dominant negative effect. Lastly, timing of transcription can be problematic because promoters are not

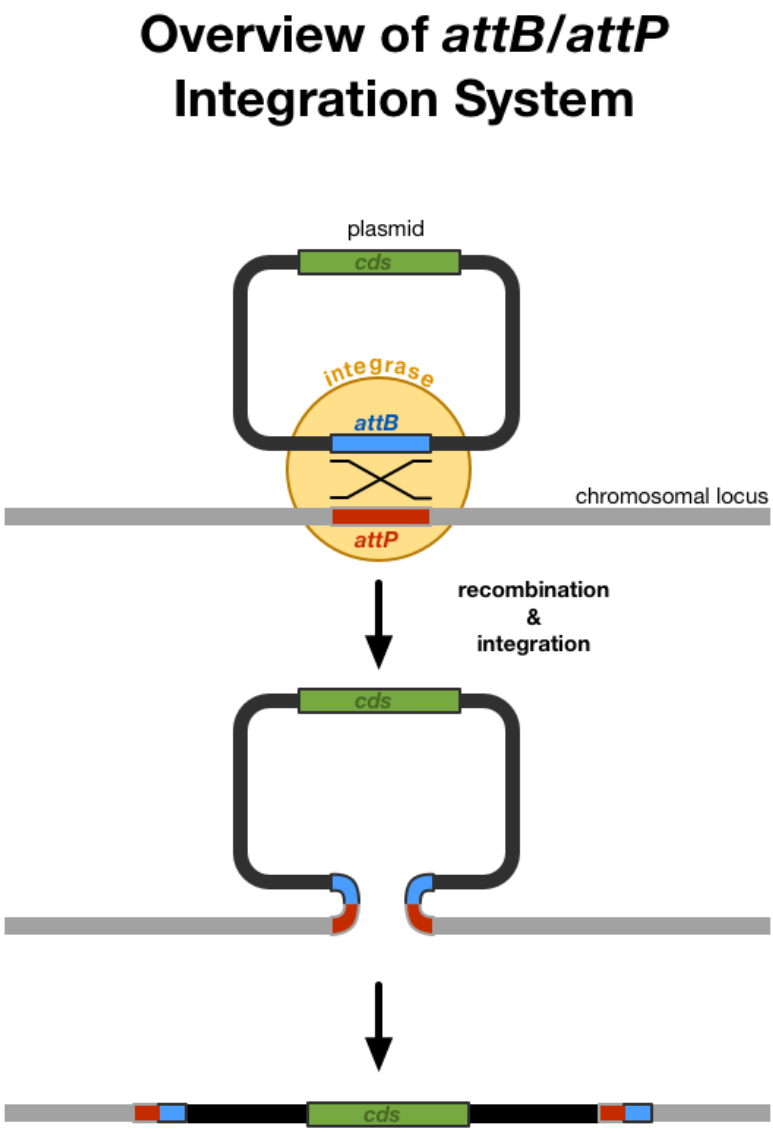


**Figure 19 Overview of the *attB/attP* integration system**
Integrating transgenes into cell genomes through the *attB/attP* recombination system requires a plasmid-derived recombination template and an integrase enzyme. The plasmid containing the transgene will insert into the cell genome during replication when the integrase enzyme directs single-crossover recombination at the *attB* and *attP* sites. *attB* is typically included on the plasmid, and *attP* is typically included in the cell genome.

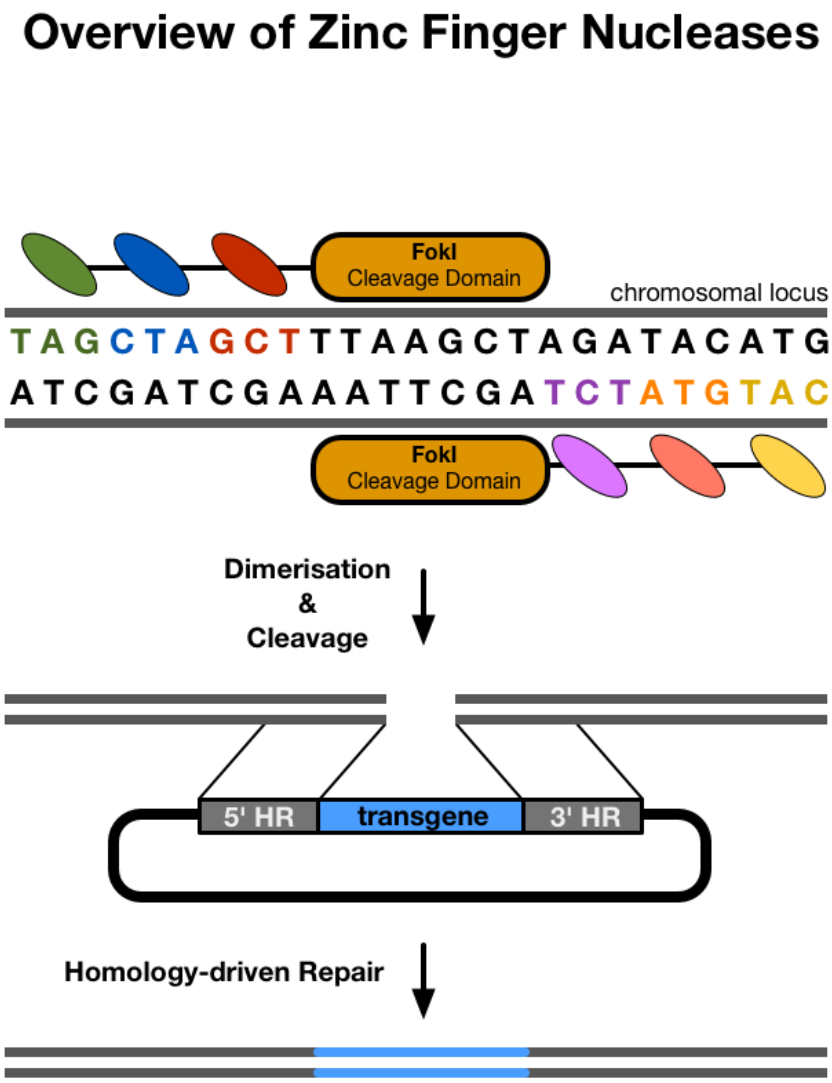


**Figure 20 Overview of Zinc Finger Nuclease-mediated Genome Editing**
Zinc finger nucleases (ZFNs) are one of several enzymes that can be programmed to introduce double strand breaks at sites in a target cell genome. ZFNs consist of several tandem zinc finger domains fused to the catalytic domain of the FokI endonuclease. Each zinc finger recognizes a single triplet DNA sequence, and thus ZFNs can be directed to nearly any locus in a genome. Specificity results from using several zinc fingers in tandem to reduce the changes of off-target cleavage. One ZFN is designed to recognise sequences upstream and downstream of the target site. The FokI domains dimerise and induce a double strand break when their respective tandem zinc fingers recongise their respective genomic sequences. A plasmid-based repair template with homology upstream and downstream of the ZFN-induced break allows the parasite to repair the chromosomal break, thus integrating the desired transgene or mutation.

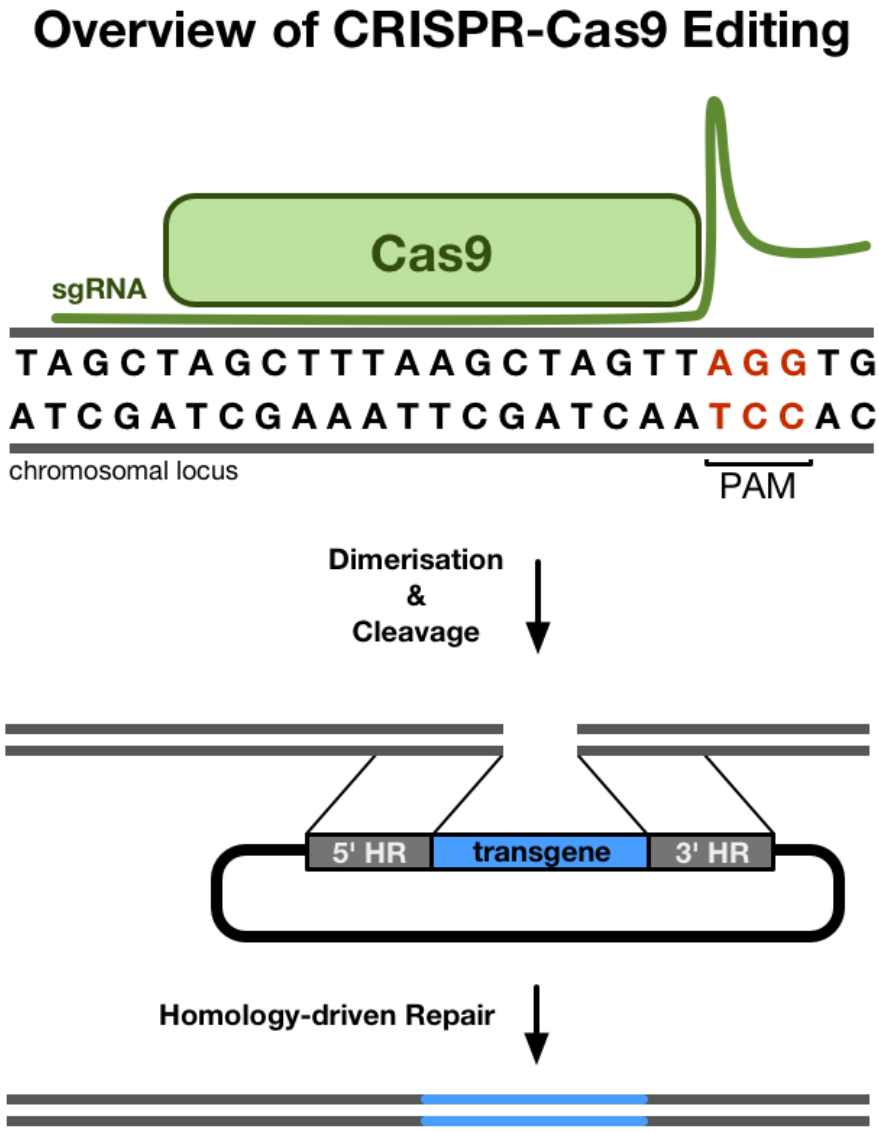


**Figure 21 Overview of Cas9-mediated genome editing**
Like ZFN-mediate editing, Cas9-mediated editing relies on a nuclease (Cas9) to induce a double strand break at a programmed location in a target genome. A plasmid-encoded small guide RNA (sgRNA), transcribed under the control of an endogenous promoter, forms a ribonucleoprotein complex with Cas9 and thus has specificity for a specific chromosomal locus. In theory, Cas9 will only induce cuts at a protospacer adjacent motif (PAM; consensus: NGG) when docked with a sgRNA and when this complex has found its chromosomal target. The induced break can be repaired with a plasmid-derived homology template as described for ZFNs.

well defined in *Plasmodium* spp. The use of validated promoters such as the *calmodulin* promoter is tempting and generally suitable for looking at protein localisation, but overexpression or expression at inappropriate times in the cell cycle can also cause issues with interpreting any phenotype observed.

Single-crossover integration was pioneered in part by David Fidock's laboratory in 2006 with the successful adaptation of the mycobacteriophage Bxb1 integrase and *attB*/*attP* recombination handles to *P. falciparum* (Fig 19)[260,261]. This system allows integration of transgenes into the genomes of strains harbouring an *attB* handle in a non-essential locus. Single-crossover integration overcomes the issues of expression variation and growth defections due to unequal segregation of plasmids across a population of cells, but these modifications have a known tendency to revert to their wild type genotype over long-term culture. Cells still express the wild type, endogenous locus, and stage-specific expression of the transgene can still be problematic. Knockout studies using single-crossover approaches aimed at disrupting the endogenous locus led to the characterisation of many genes as essential, though we now know some of these results are incorrect, and the original integration was likely unsuccessful. These limitations, as they pertain to drug resistance studies, are summarised in our previous work conducted by Gisela Henriques and meant throughput was very low, as a single modification could take months to generate.

Despite its global importance, *Plasmodium falciparum* remained a relatively intractable organism for functional genetics work until 2014 when Straimer *et al* described the adaptation of zinc finger nucleases (ZFNs) [262] (Fig 20). ZFNs are custom, sequence-specific endonucleases which dimerise and induce double-strand breaks at any genomic locus of interest. Specifically, they make use of a split

cleavage domain of FokI endonuclease, each half fused to multiple Zinc Finger Proteins, which individually recognise triplet DNA sequences on one strand of the genome. The two halves dimerise when the ZFPs recognise their target sequences on each strand, catalysing a double strand break. Interestingly, *Plasmodium* spp. lack the canonical non-homologous end joining pathway common across other taxa and therefore rely on homology directed repair to join severed or damaged chromosomes [262,263]. A custom ZFN is deployed with a DNA template that is homologous to both sides of the broken chromosome, with the desired modification sandwiched between these homology arms. ZFNs enabled a surgical-style approach to genome manipulation where one could examine the impacts of individual nucleotide changes. Immediately, the role of the K13(C580Y) variant in modulating parasite sensitivity to artemisinin was confirmed. Though they are reliable, ZFNs are highly expensive and therefore not suitable for genome-wide manipulation.

Shortly thereafter, two groups announced the adaptation of the CRISPR-Cas9 genome editing technology to *P. falciparum* (Fig 21)[263,264]. Cas9 is a bacterially-derived endonuclease that forms a complex with a short, single-stranded guide RNA molecule (sgRNA), which is homologous to a region of the genome[265]. This ribonucleoprotein is an active nuclease capable of inducing double strand breaks at, theoretically, any locus immediately upstream of a so-called protospacer adjacent motif (PAM), defined for Cas9 as any NGG trinucleotide in the genome. Different Cas nucleases have different PAM motifs[265]. Like ZFNs, a homology template can be supplied to repair the double strand break and introduce genetic elements or mutations of interest. The adaption of Cas9 editing to *Plasmodium falciparum* has led to a new dawn in functional genetic characterisation in the parasite. Cas9 has already been paired with the split-Cre recombinase system for inducible

modification of the genome and conditional knockout studies as described in other systems [266]. Currently two systems for driving sgRNA transcription exist. One, described by Ghorbal *et al*, relies on the endogenous but poorly characterised *falciparum* U6 promoter [263]. The second, described by Wagner *et al*, leverages the T7 system widely used in bacterial and protein expression work [264]. Transfected parasites express T7 polymerase, seemingly without consequence, in addition to Cas9. Currently, it is unclear if either system represents a distinct advantage. Although initially hailed as a highly-efficient system for genome editing, transgenesis with CRISPR-Cas9 has been slow because many sgRNA guides do not target the genome well. A high-throughput examination of guide activity is required to optimise a predictive activity algorithm resembling the Doench Root algorithm currently used in higher order eukaryotes [267]. While NGG sites are sparse in certain genes given the AT-richness of the parasite genome and manual guide optimisation may be needed to achieve a transgenic line, Cas9 editing is still a cheap and potentially scalable way to approach the genome

Recent work has identified another Cas-like nuclease called Cpf1 that recognises the motif TTN[268]. Though Cas9 is still the predominant RNA-guided nuclease in the field, this new PAM motif is much more common in the *P. falciparum* genome, meaning that Cpf1 may enable more accessible manipulation of the genome.

Overall, these genetic techniques present new tools to continue to interrogate *Plasmodium* biology. Currently, we now have single-crossover integration, ZFNs, Cas9, and episomal expression systems to introduce mutations, knockout and knockdown elements, and reporter tags. In this thesis, this recombineering toolbox will be used to validate the involvement of mutations in the AP-2 adaptor complex

μ-subunit (μ2) and Ubp1 ubiquitin hydrolase in the parasite drug response and interrogate the biology of these two important molecules. Eukaryotic biology is widely conserved, but there are important differences between pathogens and host cells, which both mediate the virulence of these organisms and may represent exploitable vulnerabilities.

# Chapter 2

## General Aims

The broad aim of this work is to better understand how proteins associated with drug resistance and parasite survival function in the cell and contribute to the overall phenomenon of artemisinin resistance and ACT treatment failure currently observed in patients with uncomplicated *Plasmodium falciparum* infections across the tropics. Specifically, this project aims to:

1. Examine ongoing evidence of directional selection in the *pfap2mu* and *pfubp1* genes in field isolates from East Africa using full and partial PCR-based gene amplification strategies and Sanger sequencing. If the *pfap2mu(S160N)* variant is involved in modulating parasite susceptibility to artemisinin combination therapies, I expect that the prevalence of this mutation will have increased since 2009. The samples for this analysis originate from the sample Kenyan village that we previously studied, and the local ACT formulation has not changed in the intervening years. If the haplotypes identified in *pfubp1* in 2009 are related to drug susceptibility, I would expect reduced diversity in this gene and the emergence of a dominant, alternate haplotype.
2. Validate the involvement of mutations in *pfap2mu* and *pfubp1* in determining antimalarial sensitivity via CRISPR-Cas9-mediated transgenesis in laboratory strains. Namely, the orthologues of mutations identified in a rodent model of artemisinin resistance encoding µ2(I592T), Ubp1(V3275F), and Ubp1(V3306F) are expected to modulate parasite susceptibility to artemisinin. These Ubp1 mutations may also impact parasite susceptibility to

chloroquine, as they first arose during chloroquine selection. The μ2(S160N) variant discovered in *P. falciparum* clinical infections may have effects on sensitivity to artemisinin or frontline chemotherapy partner drugs, if it is actually involved in drug sensitivity in Kenya.

3. Determine and compare the molecular and cell biology of the AP-2 adaptor protein complex and the Ubp1 deubiquitinase to those established for the human counterparts using *in vitro* approaches including protein localisation, genetic disruption, and mass spectrometry. The AP-2 complex is expected to be peripherally located in the parasite cell in association with clathrin, as in nearly all eukaryotes, and Ubp1 is expected to be localised to the nucleus, like its USP7 orthologue in higher order eukaryotes.

# Chapter 3

# Materials and Methods

## 3.1 Bacteriological Methods

### 3.1.1 Bacteriological Media

LB media was used for plasmid transformation and plasmid preparations. This media consists of 1% (w/v) bacto-tryptone, 0.5% (w/v) yeast extract, and 1.0% (w/v) NaCl in deionized water. Dissolved media was then sterilized by autoclaving for 20 minutes at 121°C and 15 psi. The sterile media was supplemented with antibiotics for selection as required by the particular plasmid transformed or cell line cultured.

Solid media (LB) for plate culture consisted of 1.0% (w/v) bacto-tryptone, 0.5% (w/v) yeast extract, 1.0% (w/v) NaCl, and 1.5% (w/v) agar in deionized water. This solution was autoclaved, cooled below 60°C, augmented with antibiotics, and poured into sterile Petri plates.

**Table 1 Antibiotics and concentrations used for cell culture**

| Antibiotic | Liquid Medium Conc. | Solid Medium Conc. |
|---|---|---|
| Ampicillin | 50μg/mL | 100μg/mL |
| Chloramphenicol | 25μg/mL | 25μg/mL |
| Kanamycin | 10μg/mL | 10μg/mL |

### 3.1.2 Bacteriological Strains

The following strains of Escherichia coli were used in this work as described.

**Table 2 *E. coli* strains used for DNA plasmid preparation**

| Strain | Source | Genotype | Antibiotic Resistance |
|---|---|---|---|
| XL-10 Gold | Agilent / reprepared as below | $Tet^r$Δ(mcrA)183, Δ(mcrCB-hsdSMR-mrr)173, endA1, supE44, thi-1, recA1, gyrA96, relA1, lac Hte [F′ proAB $lacI^qZ$ΔM15 Tn10 ($Tet^r$) Amy $Cam^r$] | Chloramphenicol |
| Stellar | Takara | F-, endA1, supE44, thi-1, recA1, rel A1, gyrA96, phoA, Φ80d, lacZΔ M15, Δ (lacZYA - argF) U169, Δ (mrr - hsdRMS - mcrBC), ΔmcrA, λ- | None |

### 3.1.3 Competent Cell Preparations

Cells were made competent by calcium chloride treatment. First, cells were transformed, restreaked, and incubated on LB plates at 37°C overnight. Then a 100 mL flask with LB media was spiked with 2.2 mL of a salt solution consisting of 0.44 M $MgCl_2$, 0.44 M $MgSO_4$, and 0.11 M KCl, inoculated with 3 colonies from the restreak plate, and grown in a 37°C shaker until 0.4-0.6 $OD_{600}$. The cell culture was then chilled on ice for 10 minutes, and the cells were harvested by centrifugation at 2000 rpm at 4°C for 7 minutes. The cell pellet was resuspended in 30 mL of prechilled FB solution (10 mM PIPES, 250 mM KCl, 15 mM $CaCl_2$). The resuspended pellet was incubated on ice for an additional 10 minutes. The cells were harvested from the calcium chloride treatment by centrifugation at 2000 rpm at 4°C for 7 minutes. The cell pellet was then resuspended in 8 mL of cold FB solution.

This resuspension was augmented with 0.5 mL of DMSO. After an additional 10 minute incubation on ice, these cells were aliquoted into sterile Eppendorf tubes, flash frozen using liquid nitrogen, and stored at -80°C.

## 3.2 DNA Methods

### 3.2.1 Custom Primer Processing

Desalted custom primers were purchased from Integrated DNA Technologies® (Coralville, IA). The lyophilized primers were centrifuged upon arrival and resuspended in TE(10,0.1) (10 mM Tris-Cl, pH 8.0, 0.1 mM EDTA) to 100 µM stock concentration. 10 µM working aliquots of primer were diluted from this stock in TE(10,0.1) and stored at -20°C. A full list of primers used in this thesis is included in Appendix V.

### 3.2.2 Phenol/Chloroform Extractions

Phenol/Chloroform extractions are a technique used to purify nucleic acid away from proteins. This purification is typically performed during a plasmid preparation to remove contaminating cellular proteins or enzymes added during the purification process such as RNaseA. Phenol/Chloroform is a 1:1 (v/v) mixture of phenol equilibrated in TE(10,0.1) and 100% chloroform. To extract a sample, 1 volume of premixed phenol/chloroform was added to the sample. The sample was then vortexed for 10-15 seconds and spun down at 13.3K rpm. The top, aqueous phase contains the extracted nucleic acids, and proteins are in the lower, organic phase. The aqueous phase is removed for further purification. This process is

repeated for a total of 2 extractions followed by 1 extraction with 500 µL of 100% chloroform to remove contaminating proteins and phenol.

### 3.2.3 Ethanol Precipitation of DNA

Ethanol precipitation is a common molecular biology technique used to concentrate DNA and perform buffer exchange or to sterilise DNA before transfection. 0.1 volumes of 3M sodium acetate pH 5.2 is added to the sample along with 2.5 volumes 100% ethanol. The solution is incubated at -20°C for 10-20 minutes and centrifuged at 13.3K rpm at 4°C for 30 minutes. The liquid is aspirated, and the pellet is resuspended in 1 ml of 75% (v/v) ethanol in water. This is incubated at -20°C for 10 minutes to draw salts out of the DNA pellet, and the DNA is reharvested by centrifugation. The liquid is again aspirated, and the DNA pellet is left to air-dry before resuspension in an appropriate volume of sterile TE(10,0.1).

### 3.2.4 Agarose Gel Electrophoresis

Agarose gel electrophoresis is one of the most ubiquitous biology laboratory techniques and is used to separate DNA fragments based on their size. Typical agarose gels were made with 1-2% (w/v) HGT agarose in 30 mL of 0.5xTBE (45 mM Tris base, 45 mM boric acid, 1.5 mM EDTA). Heating the solution for 90-120 seconds in a microwave dissolved the agarose solid. When the solution was no longer steaming, 1.5 µL of 10 µg/mL ethidium bromide was added, and the solution was mixed. The solution was then poured into a gel-casting block, well combs were inserted, and the gel was incubated at room temperature for 30-45 minutes.

To separate a sample of DNA fragments, 6x gel loading buffer (0.25% (w/v) bromophenol blue, 0.25% (w/v) xylene cyanol, 30% (w/v) glycerol) was added to the sample to a final 1x concentration. The polymerized gel was lowered into an electrophoresis box filled with 0.5 x TBE such that the running buffer covered the top of the gel. The samples were added to the lanes alongside a reference molecular weight marker. The gel was electrophoresed at 125V power for approximately 40 minutes. For the best separation, the gel agarose percentage should correspond to the size of fragments being separated. Fragments between 500 bp-1000 bp were best separated with a 1.2-1.5% gel. Smaller fragments required a higher percentage agarose gel and larger fragments were separated with a lower percentage gel.

### 3.2.5 Native Polyacrylamide Gel Electrophoresis (PAGE)

Native PAGE gels are most useful for separating DNA fragments less than 500 bp. These gels were prepared by first filling a BioRad Mini-Protean® gel casting block with stacked plates. Plates were assembled such that the back glass is separated from the front glass with two plastic spacers. The gel mixture was prepared by adding 25 mL of 30% 40:1 acrylamide, 3.75 mL 10 x TBE to 42.5 mL of deionized water. This solution was mixed and deaerated under a vacuum for 2-5 minutes, swirling occasionally. After deaeration, 300 µL of 25% (w/v) ammonium persulfate and 75µL TEMED was added to the deaerated solution. This solution was quickly taken up with a 60 mL syringe and injected through a luer valve into the filled PAGE gel casting block. This solution was added to the height of the front glass plates. Gel combs were then inserted rapidly into the plates before the gel

solution polymerizes. The casting block was incubated at room temperature for 30-60 minutes. The casting block was then disassembled, and the polymerized gels were wrapped in wet towels and stored at 4°C until use.

### 3.2.6 PCR Amplification of gene fragments

Polymerase Chain Reaction (PCR) was used to amplify gene fragments for downstream sequencing or cloning. In brief, a standard reaction consisted of either 1 x ThermoPol Reaction Buffer or 1 x $NH_4$ Buffer, 4 mM $MgCl_2$, 0.25 mM dNTPs, 0.5 µM forward and reverse primers, and 0.5 units of BioTaq polymerase in 25 µl total volume. HotFirePol master mix was used for *pfubp1* gene fragments based on optimisation performed by previous members of our laboratory, and amplicons for downstream cloning applications were generated with 1 x CloneAmp mix (Takara). These reactions were performed with 0.5 µM primers in a 25 µl reaction. In the case of nested PCR reactions, 1 µl of the Nest 1 reaction was used as a template for a 25 µl Nest 2 reaction. Thermocycling settings were optimised for each amplification but generally based on the following generic cycling and manufacturer's recommendations for elongation and denaturation temperatures:

$$3m\ at\ 95^oC \rightarrow 18-35 \times \left(30s\ at\ 95^oC \rightarrow 30s\ at\ Tm-5^oC \rightarrow \frac{1min}{1Kbp}\ 65-75^oC\right)$$

$$5m\ at\ 65-75^oC$$

Extension products were confirmed by gel electrophoresis on a 1-2 % (w/v) agarose gel. Products for cloning were extracted with the QiaQuick kit by the manufacturer's

protocol or phenol/chloroform extraction and ethanol precipitation. Custom primers were designed to have less than 60% GC content and a Tm between 50-60°C and were ordered from IDT®.

Several other polymerases were used in the production of this thesis. These polyermases were Q5 Polymerase (New England BioLabs), Pfu (made recombinantly in Prof Song Tan's laboratory at Penn State University), and PfuTurbo (Stratagene), and each polymerase was used according to the manufacturer's guidelines or methods specified here.

### 3.2.7 Cycle sequencing of double-stranded DNA

For cycle sequencing of PCR products, excess primers and dNTPs were removed from PCR reactions prior to sequencing. Briefly, 5 µl of the PCR reaction were combined with 3 units of Exonuclease I (ThermoFisher) and 1 unit of FastAP Alkaline Phosphatase (ThermoFisher) in 1 x FastAP buffer and water to 10 µl. The reaction was incubated at 37°C for 60 minutes followed by 72°C for 15 minutes. 1-5 µl of this cleaned reaction was added to a sequencing reaction containing 1 mM sequencing primer, 1 x sequencing buffer, and 0.5 µl of BigDye V3.1 in 10 µl total volume. For sequencing plasmid DNA, 50 ng of plasmid was included instead of the cleaned-up PCR reaction. The cycle sequencing reaction was thermocycled as follows:

$$1m\ at\ 96^oC \rightarrow 25 \times (30s\ at\ 96^oC \rightarrow 30s\ \ at\ 50^oC \rightarrow 4\text{m at } 60^oC)$$

This cycle sequencing reaction was EDTA/Ethanol precipitated by the manufacturer's protocol and submitted for capillary sequencing at LSHTM on a ABI 3730 platform or to Source BioScience (Cambridge, UK). Sequence data were analysed using a variety of bioinformatic tools in the Geneious version 9.1 software package.

### 3.2.8 Cloning of DNA fragments

Plasmids were assembled using a variety of cloning methods. In summary, DNA fragments were cloned either by traditional sticky-ended cloning, inFusion cloning (Clontech), or sequence-and-ligation-independent cloning (SLIC). Cloning protocols are described below. Each ligation or plasmid assembly reaction was transformed into 50 µl of XL-10 Gold ultracompetent cells (Agilent) and plated onto LB agar media supplemented with 100 µg/ml ampicillin. Colony PCR was performed to screen transformants for successful integration of the insert fragment, and screened colonies were restreaked. Selected clones were used to inoculate 5 ml LB cultures supplemented with 50 µg/ml ampicillin which were grown overnight at 37°C. Plasmids were harvested from these cultures with a Qiagen Miniprep kit and restricted mapped. Sanger sequencing was performed to confirm the sequence of the insert.

#### *3.2.8.1 Preparation of Vector and Insert DNA for Sticky-Ended Ligation*

Vector and insert DNA for sticky-ended ligation were prepared by digestion of the corresponding parent DNA sources (plasmid or PCR product) with two

restriction endonucleases. The reactions consisted of 0.5-1 µg DNA, 1 x NEB Buffer compatible with both enzymes, 0.1 mg/mL BSA, 5 mM DTT, 0.5-1.0 units of each restriction enzyme in deionized water to 30 µL total volume. The reaction was typically carried out at 37°C for 1-2 hours. All enzymes were purchased from New England Biolabs and were used according to the manufacturer's recommendations. After incubation, the reactions were analyzed by agarose gel electrophoresis.

In the event that two enzymes could not be used simultaneously in a double digest, a sequential digest was performed. In this case, the enzyme that requires a lower salt concentration was added in its corresponding buffer for 1 hour. Then, the reaction conditions were either adjusted via addition of 5 M NaCl to enable the second enzyme to become active, or the reactions were phenol/chloroform extracted, ethanol precipitated, and resuspended with the second enzyme in different buffer conditions.

#### *3.2.8.2 Preparation of Vector and Insert DNA for Blunt-Ended Ligation*

Some ligations had to be performed using blunt-ended fragments from PCR reactions. In this case, the purified PCR product had to be kinased because PCR does not attach the required 5' phosphate groups to enable ligation with a 3' hydroxyl group. The kinase reaction consisted of 1 x PNK Buffer, 5 mM ATP, 3 mM DTT, 15µL PCR product, and 5 units T4 Polynucleotide Kinase in deionized water to 30 µL. This reaction was incubated at 37°C for 15 minutes. The kinased product was then isolated by gel electrophoresis and gel extraction.

Blunt ended vectors were produced by digestion with an endonuclease such as EcoRV that produced a blunt end. The digestion was performed the same way as

the digestions for sticky-ended ligation. After the digestion was performed, 0.1 units of calf intestinal phosphatase (CIP) were added to the reaction. The reaction was then incubated at 50°C for 45 minutes. The dephosphorylated vector fragment was then purified via gel electrophoresis and gel extraction.

### *3.2.8.3 Agarose Gel Extraction of DNA*

Once vector or insert DNA was digested, separated with gel electrophoresis, and visualized with a UV transilluminator to confirm the presence of the correct fragments, the fragments were excised from the gel using a clean razor blade. These gel slices were placed into an eppendorf tube filter assembly. This assembly consisted of a 0.5 mL Eppendorf tube with a hole poked into the bottom that was covered with glass wool inserted into a 1.75 mL Eppendorf tube. The gel slice was placed into the 0.5 mL tube and spun at 7000 rpm for 3 minutes. The DNA fragment previously contained in the gel slice eluted through the filter and is collected into the 1.75 mL tube. This extraction method typically recovers between 50-70% of the material in the gel.

### *3.2.8.4 Blunt and Sticky Ended Ligations*

To ligate insert and vector fragments into a plasmid, the isolated insert and vector DNA was added at an approximately 3:1 molar ratio with 5 mM DTT, 1 x T4 Ligase Buffer, ligase and deionized water to 10 µL. For sticky ended ligations, 40 units of T4 DNA ligase were used whereas for blunt ended ligations, 750 units of T4 DNA ligase were used. The ligation reaction was incubated at room temperature for

15-30 minutes before transformation into *E. coli*. A separate ligation reaction always set up only containing the vector DNA to determine the cloning bias (ratio of colonies on vector only plate to vector and insert plate). This negative control and the cloning bias help determine the quality of the vector and insert preparations.

#### *3.2.8.5 Plasmid Transformation*

Ligation mixtures or purified plasmid DNA was transformed into *E. coli* either during subcloning or for protein expression. During subcloning, 2 µL of each ligation reaction were added to 100 µL of competent cells. When transforming purified plasmid, 0.1 ng of DNA were added to the cell mixture. In each case, the cells were then incubated on ice for 15 minutes. Following this incubation, the cells were heat shocked at 42°C for 30 seconds. 500 µL of sterile LB media were then added, and the cell suspension was then incubated in a 37°C shaker for 15 minutes. Following this incubation, 300 µL of the cell suspension were plated onto LB plates containing the appropriate antibiotics for selecting colonies with the correct plasmid.

#### *3.2.8.6 Colony PCR*

During subcloning, after transformation, several clones from the vector and insert plate were screened using colony PCR to detect whether they contained the desired insert. To perform this screening, each clone selected was resuspended in 100 µL of deionized water and restreaked onto a new LB plate containing the appropriate antibiotic. These cell suspensions were then vortex for 10-15 seconds and used as PCR templates. Primers were selected to amplify around the inserted

DNA fragment. PCR was performed using 1 µL of cell suspension in a PCR master mix containing 1 x ThermoPol buffer, 0.26 mM dNTPs, 0.5 µM forward and reverse primers, 1 unit of Pfu polymerase, and water to 20 µL. The standard thermocycling conditions are:

$$3m\ at\ 95^oC \rightarrow 25 \times \left(30s\ at\ 95^oC \rightarrow 30s\ at\ Tm - 10^oC \rightarrow \frac{1min}{1Kbp}\ 75^oC\right)$$

These PCR reactions were analysed with gel electrophoresis, and clones that produced the desired product were selected for plasmid preparation. Single clones from the restreak plates of these clones were used to inoculate flasks of 5 mL LB media with 50 µg/mL of ampicillin. These flasks were grown overnight in a 37°C shaker.

### *3.2.8.7 Site-Directed Mutagenesis*

This mutagenesis method was designed from Stratagene's QuikChange mutagenesis protocol. Custom, complementary primers were designed to have a new DNA sequence, and therefore mismatches (often swapping out codons), at the site of mutagenesis flanked by ten or more bases complementary to the template sequence. The primers are also designed to introduce or remove a restriction site around the mutagenized region to facilitate plasmid identification during downstream cloning experiments. The reaction consists of combining 5 ng template DNA, 1 x PfuTurbo reaction buffer, 0.2 mM dNTPs, 0.2 mM forward and reverse primers, and 1 unit PfuTurbo in deionized water to 25 µL. A linear amplification was then performed using the following thermocycler settings:

$$3m\ at\ 95^oC \rightarrow 18-35 \times \left(30s\ at\ 95^oC \rightarrow 30s\ at\ Tm-5^oC \rightarrow \frac{1min}{1Kbp}\ 65^oC\right)$$

$$5m\ at\ 65^oC$$

Afterwards, 2 µL of the reaction were removed and stored in a sterile Eppendorf tube. 20 units of DpnI restriction enzyme were then added to the remaining 23 µL of the reaction mix. The reaction mix was then incubated at 37°C for 1 hour. DpnI will digest methylated DNA. Because the template plasmid DNA was isolated from *E. coli* with dam methylase, the unmutated template will be methylated and cut. PCR does not methylate DNA so the mutated PCR product will not be cut. After the 1 hour incubation, 2 µL of the digested sample were transformed into *E. coli* alongside the 2 µL of undigested sample and plated onto TYE plates with ampicillin overnight. The majority of the clones screened from the digested plate should contain the desired mutation because the DpnI treatment should eliminate most of the parent plasmid.

Colony PCR primers were selected to flank the mutation site and produce a fragment less than 500 bp. In addition to screening clones from the digested plate, the parent plasmid should be included in the colony PCR experiment to provide a negative control for comparison. After thermocycling during colony PCR, 10 µL of the reaction were combined with 2 µL of 6xGLB and run on a Native PAGE gel to screen for clones that may have multiple insertions of the mutagenesis primer. This problem occurs relatively frequently during mutagenesis with Q5 and several other polymerases and is an going area of investigation. The PCR products were compared to the product amplified from the parent. Each product should be the same size.

Colonies that produced fragments larger than the parent product likely contained primer insertions.

The remaining 10 µL from the colony PCR reaction including the reaction on the parent template were digested with the appropriate restriction enzyme for the site either introduced or removed during the mutagenesis. Colonies that do not have primer insertion and produce the correct fragments after this restriction digest likely have the desired mutations and were selected for plasmid preparation, restriction mapping, and sequencing.

## 3.3 Protein and Fixed Cell Methods

### 3.3.1 Preparation of cell extracts

This protocol is for analysis of small amounts of protein (i.e. not preparative-scale immunoprecipitation). 5 ml of cell culture at 5% haematocrit and 5% parasitaemia was transferred to a 50 ml conical centrifuge tube. Infected erythryocytes were harvested by centrifugation at 800 g for 5 min at RT. Culture media was aspirated, and the cells were washed in 50 ml of sterile PBS and again centrifuged. The washed cells were washed again in 10 ml PBS and then lysed in 10 pellet volumes of 0.15% (w/v) saponin in PBS. After 5 minutes incubation at 4$^{o}$C, parasites were harvested away from lysed cell debris by centrifugation at 13K RPM for 10 minutes at 4$^{o}$C. Parasites were then washed repeatedly by centrifugation at 13K RPM for 2 minutes in sterile, cold PBS containing protease inhibitors until the wash supernatant was clear, indicating the majority of red cell debris and haemoglobin had been removed. These harvested parasites were resuspended to 50% (w/v) in PBS with inhibitors and stored on ice until further manipulation or flash frozen in liquid nitrogen.

To prepare whole cell extracts, the washed saponin-treated parasite pellet was resuspended in 4-6 volumes of cold lysis buffer. Lysis conditions vary by the protein under study and aims of the experiment but generally consist of variations on a standard lysis buffer (20 mM HEPES, 100 mM NaCl, 0.5% Triton X-100, 1 mM PMSF, 1xRoche protease inhibitors, pH 7.4) or RIPA buffer (10 mM Tris, 150 mM NaCl, 1% (v/v) Triton X-100, 0.1% (v/v) sodium deoxycholate, 0.1% (w/v) SDS, 1 mM PMSF, 2 mM EDTA, 1 x Roche protease inhibitors, pH 7.5). Parasite lysis was allowed to proceed for 30 minutes on ice, and a soluble extract was prepared by spinning this lysate at 13K RPM for 30 minutes at 4°C. If late trophozoites or schizonts were being studied, 0.5 ul of BaseMuncher (Expedeon Ltd.; San Diego, CA) was added to the lysis reaction to digest nucleic acids, which make the extraction thick and difficult to manipulate and interferes with lysis. After centrifugation, the soluble supernatant was removed into a separate tube on ice, and the insoluble pellet was washed 3 times in 1 ml cold lysis buffer to remove residual soluble factors. The insoluble pellet was then resuspended in lysis buffer to the original extraction volume and stored on ice. Equal amounts of each sample were mixed with 5xPGLB (250 mM Tris, 10% (w/v) SDS, 5 mM EDTA, 10 mM DTT, 30% glycerol, 0.05 mg/ml bromophenol blue, pH 6.8) to 1xPGLB, boiled at 95C for 1-3 minutes, centrigued to remove haemazoin, and loaded on an SDS-PAGE gel for further analysis.

### 3.3.2 SDS-PAGE Electrophoresis

One of the most common techniques for protein analysis is sodium dodecyl sulfate polyacrylamide gel electrophoresis, or SDS-PAGE. This technique uses a modification of Native DNA PAGE electrophoresis to denature proteins into their primary sequence and separate them based on size. 18% (w/v) SDS-PAGE gels were prepared by first stacking

glass gel plate assemblies into a BioRad Mini-Protean® gel-casting block in the same way as for Native PAGE gels. The separating gel solution consisted of 18% (w/v) acrylamide (30:0.5 acrylamide:bis-acrylamide), and 0.75 M Tris-Cl, pH8.8 in deionized water. This solution was deaerated under a vacuum for 5-10 minutes. Then SDS was added to 0.1% (w/v).

Polymerization was initiated by addition of 240 µL of 25% (w/v) ammonium persulfate and 60 µL of TEMED. The casting block was filled approximately 70% with this solution using a 60 mL syringe and a luer valve. Water-saturated butanol was poured over top of this separating layer. After incubation for 1 hour at room temperature, the butanol was removed and washing off with ethanol and water. A 5% (w/v) stacking gel was then mixed, poured on top of the separating gel, and incubated at room temperature once the well combs were inserted. This gel consisted of 5% (w/v) acrylamide (10:0.5 acrylamide:bis-acrylamide), 0.1 M Bis-Tris, pH 6.8, and 0.1% (w/v) SDS. This solution was prepared in the same way as the separating gel solution. After this final incubation the gels were stored like Native PAGE gels.

Samples were analyzed on these gels by first mixing the sample with an equal volume of PAGE gel loading buffer (PGLB) and boiled for 1-3 minutes to further denature the proteins. While the sample was denaturing, a pre-cast gel was fitted into a Mini-Protean II® Electrophoresis Cell, and the cell was filled with protein gel running buffer (10 mM Tris, 76 mM glycine, 0.02% (w/v) SDS). After boiling, 10 µL of sample were added to each lane along with protein molecular weight standards for size comparison. The gel was electrophoresed at a constant 20W for 10 minutes. The gel was either used for western blotting or silver staining. Additionally, 4-12% TruPAGE gels (Sigma) and 3-8% Tris Acetate gel (LifeTech) were used in this thesis, where noted.

### 3.3.3 Western Blotting

To detect protein levels with greater sensitivity than coomassie staining and identify specific factors in cell extracts or pulldowns, Western Blotting was performed. Proteins separated by SDS-PAGE were transferred to a nitrocellulose membrane (Amersham Hybond ECL®) in a Bio-Rad Turbo Blot according to manufacturer's guidelines.

Afterwards, the SDS-PAGE gel was stained with Coomassie to show that the proteins successfully transferred out of the gel, or the membrane was stained with Ponceau S and destained with TBS. The membrane was equilibrated in 1xTBS (25 mM Tris, pH 8.0, 0.15 M NaCl) for 5 minutes. The equilibrated membrane was then incubated in blocking buffer containing 5% (w/v) nonfat dry milk in 1xTBS for 30-60 minutes. The membrane was then subjected to a solution containing a dilution of primary antibody in blocking solution for 1 hour. The membrane was then washed with TBST (25 mM Tris, pH 8.0, 0.15 M NaCl, 0.1% Tween 20) for five minutes. The membrane was washed two more times with TBST to remove non-specifically or unbound antibody. The gel was then incubated in a dilution of an HRP-conjugated secondary antibody in blocking solution for 1 hour. The membrane was washed three more times with TBST. To visualize the immunostained proteins, the protein side of the membrane was covered with 1 mL of a 1:1 mixture of Pierce ECL detection solutions 1 and 2 for 5 minutes. Excess solution was poured off, and the gel was wrapped in clear plastic before exposure to X-Ray film and development.

### 3.3.4 Cryomilling and Immunoprecipitation

Because AP2μ was curiously insoluble under most mild-lysis conditions suitable for pulldowns, I turned to the novel cryomilling technique of performing near-detergent-free lysis. In this technique, parasites are harvested by saponin lysis and flash frozen in PBS.

These frozen blocks are then pulverised at very high pressure in a bead mill, generating a fine powder which can be lysed with buffer containing minimal to no detergent. This lysate is then used for immunoprecipitation as above. This technique has been used to study a variety of factors in other organisms, including endocytic factors, with excellent success. In particular, this technique is known to identify more specific interacting factors than traditional lysis and immunoprecipitation techniques, however it requires a considerable amount of material, typically more than 5 mg of total protein. This technique was performed under the guidance of Dr Martin Zoltner and Prof Mark Field at the University of Dundee. For cryomilling, lysate preparation, and immunoprecipitation, *Plasmodium falciparum* cultures were grown to approximately 8% parasitaemia in 5% haematocrit in approximately 6 L of complete medium. These infected red cells were then harvested by centrifugation when parasites were in the trophozoite stage and lysed with 0.15% (w/v) saponin in PBS at 4$^{o}$C. Trophozoites were harvested by centrifugation at 13K RPM for 5 minutes at 4$^{o}$C and washed several times with cold PBS to remove haemoglobin and red cell debris. The washed, packed parasites were resuspended to 50% density in PBS, flash frozen in liquid nitrogen, and stored at -80$^{o}$C. This process was repeated until 6-8 ml of resuspended parasites had been stored.

These frozen blocks were taken out of the tubes and placed into the ball chamber of a cryomill (Retsch). The frozen parasites were milled under 7 cycles of 3 minutes cooling and 3 minutes milling. The milled powder was then carefully removed from the ball chamber and stored in a 50 ml tube in liquid nitrogen. All steps were performed at or below -80$^{o}$C to prevent parasite material from thawing.

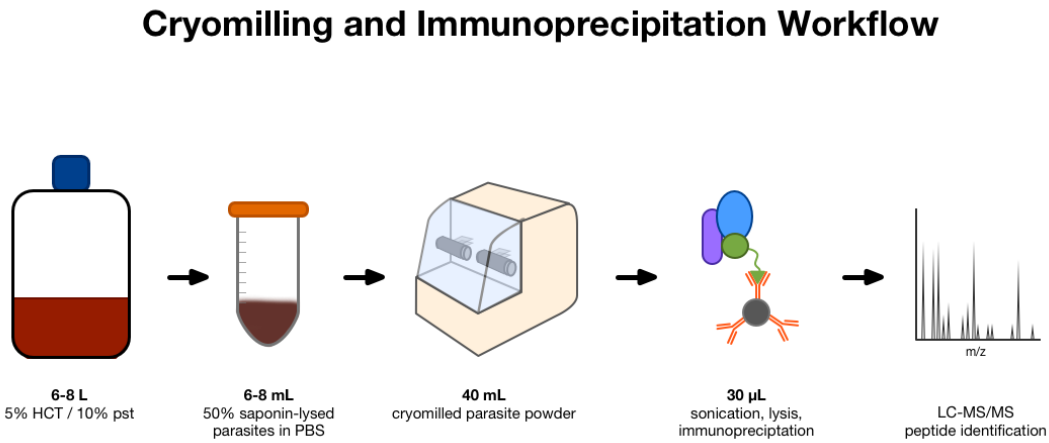


**Figure 22 Cryomilling workflow**
In preparation for cryomilling, 6-8 ml of saponin-lysed parasites (50% (w/v) in PBS) were isolated and flash frozen as small pellets in liquid nitrogen. These pellets were pulverised in a Rescht ball mill at liquid nitrogen temperatures and lysed under low-detergent conditions for immunoprecipitation and mass spectrometry. 6-8 L of cell culture typically produced 40 ml of parasite "powder", which was sufficient for 6-10 proteomics-scale pulldowns (each requiring 300 mg of ground material).

To optimise immunoprecipitation conditions, 50 mg of parasite powder was removed and mixed with 1 ml of pre-cooled test extraction buffer and resuspended by gentle pipetting on ice. The resuspension was then sonicated on ice for 4x(3 sec on/10 sec off) at 30% amplitude). The lysate was then cleared by centrifugation at 18.5K RPM for 20 minutes at 4$^{o}$C. 1 ml of the lysate was then added to 40 µl pre-equilibrated anti-HA magnetic beads (ThermoFisher) or anti-GFP magnetic DynaBeads (Field Lab) and rotated at 4$^{o}$C for 1h. The beads were then magnetised and unbound material was removed. The beads were then washed with extraction buffer 3 times to remove unbound material. The beads were then centrifuged to remove residual buffer. Bound material was then eluted by resuspending the beads with 30 µl LDS-loading buffer (Invitrogen) without reducing agent and incubating for 10 minutes at 70$^{o}$C. Eluted material was then isolated by centrifuging and magnetising the beads and removing the supernatant. Reducing agent (Invitrogen) was added to the supernatant, and the samples were incubated for 10 minutes at

70°C. Eluted material was then analysed by electrophoresis on a 4-12% gradient polyacrylamide gel and silver staining. Additionally, soluble and insoluble extract and bead flowthrough samples were examined for target protein content by western blotting.

At preparative scale, the above protocol was repeated with 300 mg of parasite powder and 240 µl, split over six tubes. Sonication was performed at 35% amplitude for a total of 12 cycles. During the final wash, the beads were combined into one tube, and bound material was eluted in 90 µl. The final eluted fraction was concentrated with a speed-vac to 30 µl and run 1 cm into a gel. The gel lane was excised and submitted to the University of Dundee Proteomics Facility for analysis.

TLCK stock (10 mM in 1 mM citric acid – unstable at higher pH)

Test extract buffers:

A. *20 mM HEPES, 100 mM NaCl, 0.1% (w/v) Brij58, 0.1 mM TLCK, protease inhibitors, pH 7.4*
B. *20 mM HEPES, 100 mM NaCl, 0.5% (w/v) CHAPS, 0.1 mM TLCK, protease inhibitors, pH 7.4*
C. *20 mM HEPES, 100 mM NaCl, 0.1% (v/v) Tween-20, 0.1 mM TLCK, protease inhibitors, pH 7.4*
D. *20 mM HEPES, 100 mM NaCl, 0.1% (v/v) Triton X-100, 0.1 mM TLCK, protease inhibitors, pH 7.4*
E. *20 mM HEPES, 250 mM NaCl, 0.1% (w/v) CHAPS, 1 mM $MgCl_2$, 10 mM $CaCl_2$, 0.1 mM TLCK, protease inhbitors, pH 7.4*

### 3.3.5 Analysis of tryptic peptides by Mass Spectrometry

Eluted immunopurified proteins were detected by tandem LC-MS/MS liquid chromatography mass spectrometry at the University of Dundee Proteomics Facility. Samples were analysed on an UltiMate 3000 RSLCnano System (Thermo Scientific) in line with a LTQ OrbiTrap Velos Pro (Thermo Scientific). Resulting spectra were mapped with MaxQuant R1.5 to the 3D7 reference proteome downloaded from PlasmoDB and MaxQuant common contaminants database. The minimum peptide length was set to 6 amino acids, and the false discovery rate was set to 0.01 as calculated against a reversed proteome.

### 3.3.6 Protein localisation by immunofluorescence

To examine the subcellular localisation of the factors discussed in this thesis, indirect immunofluorescence assays were performed. Localisation of factors of interest were examined at all stages of the asexual parasite lifecycle. Cells were first cultured to 3-5% parasitaemia under the culture conditions described above. While this is not critical, it makes observing parasites under the microscope easier and more parasites can be imaged in a single frame, though higher parasitaemias should generally be avoided because the cells may be starving or stressed in culture, which may affect the localisation of the factor or other cellular markers.

For thin-smear IFAs, once the culture was at a sufficient parasite density, blood smears were prepared on glass slides. These smears were quickly dried under cool air to avoid heat fixing the cells. Small circles (approximately 1 cm diameter) were drawn on the dried smear with a hydrophobic PAP pen for each antibody combination to be examined and allowed to dry briefly at room temperature. Cells inside each circle were fixed with 4%

paraformaldehyde in PBS for 10 minutes at room temperature in a humidified chamber. The fixative was then aspirated, and the cells were washed in PBS four times. Washing was done by pipetting PBS into the circle and aspirating after 3-5 minutes. Then cells were permeabilised with 0.1% (v/v) Triton X-100 in PBS for 10 minutes and similarly washed. Cells were then blocked for 1 hour at room temperature with 3% (w/v) BSA in PBS supplemented with 0.1% (v/v) Tween20. Primary antibodies were then added in blocking solution for 1 hour at room temperature or overnight at 4ºC. Primary antibody solution was then removed and washed off four times and replaced with secondary antibody solution in the same modified blocking buffer for 1 hour at room temperature. Secondary antibody solution was then aspirated, the cells were washed four times, and a cover slip was mounted in VectaShield with DAPI. The cover slip was then sealed to the slide with nail varnish. Importantly, each antibody stock solution was centrifuged at 13K RPM for 2 minutes at 4°C before preparing each dilution. This significantly reduced the amount of background fluorescence and floating, fluorescent debris that interfered with imaging. Slides were imaged several hours later using either an epifluorescence, confocal, or super-resolution microscope as described in the text and below.

For IFAs performed in suspension, 10-20 µl of infected erythrocytes were washed once in sterile PBS and fixed for 30 minutes in 10 volumes PBS containing 4% (w/v) formaldehyde and 0.0075% (v/v) EM-grade glutaraldehyde at 37 ºC with gentle shaking. After fixation, the cells were harvested by centrifugation at 5K RPM for 30 seconds, and fixative was replaced with 1 ml quench and permeabilisation buffer (0.1% (v/v) Triton X-100, 125 mM glycine in PBS) for 10 minutes. Blocking and antibody staining was performed as above. During the final washing step after incubation with the secondary antibody, DAPI was added to the PBS washing solution. Finally, 2-3 µl of cells resuspended to 50% density in PBS were dropped onto glass slides coated in 2% PEI. A cover slip was

applied and sealed onto the slide. These cells were imaged as described.

### 3.3.7 Fluorescent labelling of intracellular lipids

For the imaging of neutral lipids, LipidTOX Green and Nile Red stains were used. Neutral lipids are present in several structures within the cell throughout organelle and vesicular membranes as well as in lipid compartments near the digestive vacuole. These stains are unique in that they are incompatible with detergents, which disrupt the fluorescent stains at any concentration. To stain and image these lipids on their own or in conjunction with antibodies, the protocol described above was used, except the permeabilisation step was omitted and Tween20 was excluded from all buffers. Dilutions of the lipid stains were incubated on the cells after the secondary antibodies for 3 hours at room temperature and washed off with PBS. Cover slips were mounted in VectaShield with DAPI, sealed, and immediately imaged by epifluorescence microscopy. The omission of the permeabilisation step was critical because little to no signal was observed even when Tween20 was omitted from the buffers. Lipid staining could only be observed when the permeabilisation step was also omitted. Permeabilisation is optional for immunofluorescence work, though it may increase the fluorescent signal observed for low abundance proteins.

### 3.3.8 Antibodies

Below is a list of all the antibodies described in this thesis, the origin organism, and source. All antigens refer to *Plasmodium falciparum* proteins, except where noted.

**Table 3 Antibodies used in this thesis**

| Antigen | Species | Origin |
|---|---|---|
| ACP | Rabbit | Geoff McFadden Laboratory |
| AMA1 | Rabbit | Mike Blackman Laboratory |
| BiP | Rat | Tony Holder Laboratory |
| CDC48 | Rabbit | Jude Przyborski Laboratory |
| Clathrin Heavy Chain | Rabbit | Frances Brodsky Laboratory |
| ERD2 | Rabbit | Kasturi Haldar (MR4) |
| EXP2 | Mouse | Mike Blackman Laboratory |
| GAP45 | Rabbit | Anthony Holder Laboratory |
| GAP50 | Rabbit | Judith Green Laboratory |
| GFP | Rabbit | Anthony Holder Laboratory (IFA) |
| GFP | Mouse | Commercial, Sigma (Western Blot) |
| HA | Rat | Commercial, Sigma (3F10 clone) |
| K13 | Mouse | David Fidock Laboratory |
| MSP1 | Mouse | Mike Blackman Laboratory |
| Plasmepsin II | Mouse | Daniel Goldberg Laboratory (MR4) |
| Plasmepsin V | Mouse | Daniel Goldberg Laboratory (MR4) |
| Rab5A | Rabbit | Gordon Langsley Laboratory |
| Rab5B | Rabbit | Gordon Langsley Laboratory |
| Rab7 | Rabbit | Gordon Langsley Laboratory |
| Rab11A | Rabbit | Gordon Langsley Laboratory |
| RON4 | Mouse | David Baker Laboratory |

## 3.4 *In vitro* Cell Culture Methods

### 3.4.1 Cell subculturing

#### *3.4.1.1 Plasmodium falciparum cell culture*

*Plasmodium falciparum* parasites were cultured in human erythrocytes donated from the NHS Blood Bank in London, UK. The blood type was typically $AB^+$, though we receive whatever the Blood Bank has available. If whole blood is provided, cells are washed twice with RPMI 1640 (Gibco) medium to remove the Buffy coat and resuspended to 50% haematocrit in RPMI. If red blood cells are provided, the blood is washed once in RPMI and

similarly resuspended.

The culture conditions for *falciparum* cells is determined based on the parasite line. For lines that are well-adapted to suspension culture like 3D7, Dd2, and Cam3.II derivatives, parasitised red blood cells were maintained in RPMI 1640 supplemented with Albumax II, 1% (v/v) L-glutamine, and 40 µg/ml gentamycin sulphate at 4% haematocrit between 0.5% and 10% parasitaemia. For parasite lines isolated from patients and recently adapted to culture, parasitised cells were maintained in the same culture medium supplemented with 5% (v/v) heat-inactivated $AB^+$ human serum and grown at 2% haematocrit between 1% and 5% parasitaemia. All cells were maintained at 37°C in 2% $O_2$, 3% $CO_2$, 95% $N_2$ atmospheric conditions. Parasitaemia was determined by staining methanol-fixed thin blood smears on glass slides with 10% (v/v) Giemsa in PBS for 5-10 minutes and counting under a light microscope with a graticule.

**Table 4 List of compounds used in this thesis**

| Compound | Abbrev. | Origin | Application | Working Concentration |
|---|---|---|---|---|
| Compound 2 | C2 | Moon Lab | Reversible PfPKG inhibitor; parasite synchronisation | 10 µM |
| Dihydroartemisinin | DHA | MMV | Drug Susceptibility Assays | - |
| Chloroquine | CQ | MMV | Drug Susceptibility Assays | - |
| Quinine | QN | MMV | Drug Susceptibility Assays | - |
| Lumefantrine | LUM | MMV | Drug Susceptibility Assays | - |
| Piperaquine | PIP | MMV | Drug Susceptibility Assays | - |
| Mefloquine | MEF | MMV | Drug Susceptibility Assays | - |
| Brefeldin A | BFA | Conway Lab | Trafficking inhibitor; protein localisation disruption | 5 µg/ml |
| Rapamycin | RAP | Baker Lab | FKBP/FRB dimerisation induction; activation of DiCre | 10 nM |
| WR99210 | WR | MMV | Selection of transgenic parasites | 2.5 nM |
| Blasticidin-S | BSD | Sigma | Selection of | 2 µg/ml |

| | | | | |
|---|---|---|---|---|
| | | | transgenic parasites | |
| FT827 | - | Forma Therapeutics | Experimental PfUbp1 inhibitor | - |
| FT671 | - | Forma Therapeutics | Experimental PfUbp1 inhibitor | - |
| HBX19818 | HBX | MedChemExpress | Experimental PfUbp1 inhibitor | - |

All compounds used during the culture of *Plasmodium falciparum* in thesis are listed with their abbreviations which may appear in this text, as well as their source, application, and working concentration. Where no working concentration is listed, the compound was used in serial dilutions.

For subculturing cells, infected cells were harvested by centrifugation at 600g for 3 minutes with slow brake in a conical tube. The spent media was aspirated, and the culture was reseeded typically at a 1:10-1:50 dilution in fresh, uninfected blood.

Parasite strains were frozen using Glycerolyte and thawed by a 12% (w/v), 1.6% (w/v) two-step NaCl protocol as described in Methods in Malaria Research [269].

Table 4 provides a list of all compounds used in this thesis, their source, and their working concentration, where appropriate.

### *3.4.1.2 Plasmodium knowlesi cell culture*

*Plasmodium knowlesi* was cultured similarly to *Plasmodium falciparum*. Parasitised red blood cells were maintained in RPMI 1640 supplemented with Albumax II, 1% (v/v) L-glutamine, 40 µg/ml gentamycin sulphate, and 10% (v/v) horse serum at 2% haematocrit. All cells were maintained at 37°C in 2% $O_2$, 3% $CO_2$, 95% $N_2$ atmospheric conditions. To synchronise cultures, schizonts were enriched on a 55% Nycodenz cushion by centrifugation at 900 g for 10 minutes and allowed to reinvade fresh red cells for 1-3 hours. Schizonts which had not undergone egress were removed by a subsequent Nycodenz enrichment and discarded.

#### *3.4.1.3 HeLa cell culture*

In this study, the localisation of PfAP2µ and PfK13 were examined in HeLa cells. Live HeLa cells were obtained from the Polly Roy laboratory at LSHTM and cultured as adherent cells in tissue culture-treated flat-bottom flasks. Cells were maintained in DMEM supplemented with 10% (v/v) fetal bovine serum and 1xPen-Strep (100 units/ml penicillin; 0.1 mg/ml streptomycin) (Sigma). HeLa cells were passaged frequently to maintain the culture at less than 50% confluency. Cultures were maintained at 37°C in a 5% $CO_2$ atmosphere.

For passaging, growth medium was aspirated, and the cells were washed twice with PBS to remove serum, which inhibits trypsin. After two washes, the PBS was replaced with 2 ml of 0.05% Trypsin-EDTA solution (Sigma), and the culture was returned to the 37°C incubator for 2-4 minutes. The culture flask was knocked on the bench to release the cells, and culture medium containing serum was added to the cell suspension to 10 ml total volume to quench the trypsinisation. The suspension was then centrifuged at 300g for 3 minutes with slow brake at RT, and the cells were resuspended in 10 ml of fresh medium. The culture was reseeded at a 1:5 or 1:10 dilution from the stock suspension, and the remaining material was destroyed.

### 3.4.2 Parasite synchronisation

Parasite cell cultures were typically maintained as generally synchronous cultures with a 8-12 hour post-invasion window of synchrony. This was mainly accomplished by sorbitol treatment. To remove trophozoites and schizonts from ring-stage parasites in culture, infected red blood cells were harvested by centrifugation as described above. The cells were resuspended in pre-warmed 5% (w/v) D-sorbitol and incubated at 37°C for 10

minutes. Infected cells were then re-harvested by centrifugation, and the sorbitol solution was aspirated as well as any remaining liquid in the original culture flask. The infected cells were resuspended in culture medium and returned to the original flask or subcultured as appropriate. The synchronisation was confirmed by Giemsa staining.

To obtain tighter synchrony, schizonts were enriched by Percoll density-gradient centrifugation. For this method, cells were cultured up to 5-10% schizontaemia at 3% haematocrit. Parasitised cells were harvested by centrifugation and layered gently on top of 3 ml of pre-warmed 70% Percoll solution in a 15 ml conical tube. A stock of 70% Percoll was prepared by mixing 7 ml Percoll, 1 ml 10xRPMI in $dH_2O$, and 2 ml of 13.3% (w/v) sorbitol in PBS. The tube with schizont-infected cells layered onto the Percoll cushion was centrifuged at 2000g for 10 minutes at RT with slow acceleration and slow brake. Schizont-infected cells float on top of the Percoll layer and red cells that are uninfected or infected with other stages will sink below the layer. The schizont layer was gently removed by pipetting and washed with 5 ml of warmed complete media. These enriched schizonts were then allowed to invade fresh red blood cells at 20% haematocrit under gentle orbital shaking at 37$^{o}$C for 1-3 hours, after which the cells were sorbitol-synchronised to remove schizonts that had not yet egressed.

To obtain highly synchronous parasites with less than a 1 hour post-invasion (HPI) window of synchrony, 1-3 HPI parasites were obtained as described above. These cells were then treated as schizonts with Compound 2, a reversible inhibitor of PKG as described by Taylor *et al*. Compound 2 can be used to reversibly delay egress for up to 4 hours without known detriment. Parasites blocked for greater than 4 hours typically are not viable. Once more than 90% of blocked parasites in the culture were highly-segmented schizonts, the cells were harvested by centrifugation, washed with complete medium once, resuspended to 50% haematocrit in complete medium, and incubated under shaking conditions at 37°C.

Cells were then sorbitol-synchronised within 30 minutes. Alternatively, highly-segmented schizonts could be enriched by Percoll purification and incubated with fresh red cells. In practice, this additional manipulation can cool the parasites and slow their growth slightly, which promotes asynchrony and reduces the 0-30 minute ring-stage parasitaemia. Compound 2 was generously provided by the David Baker laboratory.

*Plasmodium knowlesi* can only be synchronised over a 55% (v/v) Nycodenz solution in 10 mM HEPES, pH 7.0, which behaves like Percoll. Percoll is slightly harsher, and *knowlesi* parasites do not tolerate Percoll as well as Nycodenz. After desired reinvasion has occured, infected cells can be re-treated with Nycodenz to remove schizonts that have not yet egressed. Currently, no chemical means of isolating ring-stage parasites as with sorbitol treatment exists for *Plasmodium knowlesi*, though this is under investigation.

### 3.4.3 Transfection Techniques

#### *3.4.3.1 Plasmodium falciparum transfection by ring-stage electroporation*

For transfecting *Plasmodium falciparum* cells, several techniques were used including the classical ring-stage transfection. Using the protocol for ethanol precipitation of DNA described above, 150 µg of DNA per plasmid to be transfected was precipitated in a sterile 1.5 ml eppendorf tube under under sterile, cell culture conditions. The DNA pellet was air dried in the microbiology safety cabinet for one hour at room temperature and resuspended in 15 µl of sterile TE(10, 0.1). For this method, ring-stage cultures of 5-10% parasitaemia were harvested less than 20 hours post invasion. For each transfection 400 µl of infected red cells were equilibrated in 10 volumes of pre-warmed cytomix (25 mM HEPES, 120 mM KCl, 0.15 mM $CaCl_2$, 2 mM EGTA, 5 mM $MgCl_2$, 10 mM $K_2HPO_4/KH_2PO_4$, pH 7.6) and harvested by centrifugation at 600g for 3 minutes at RT with

slow brake. 300 µl of equilibrated infected cells were combined with the resuspended, sterile DNA and added to a 2 mm transfection cuvette (BioRad) and mixed well by pipetting. The cells were then shocked in a BioRad Gene Pulser II using 0.31 kV, 950 µF, and maximum capacitance settings. The shocked cells were immediately placed into 1 ml of warm culture medium. 2-4 hours later, the transfected cells were washed once with culture medium to remove lysed cells and debris before being returned to a standard 10 ml culture. Drug selection was applied from 24 hours after transfection. Parasites typically took 3-5 weeks to recover after drug selection.

#### *3.4.3.2 Plasmodium falciparum transfection by spontaneous DNA uptake*

Another transfection technique used in this study was the spontaneous DNA uptake method. DNA was precipitated and resuspended as described above. For each transfection 500 µl of fresh uninfected red cells were equilibrated in 10 volumes of cold cytomix (25 mM HEPES, 120 mM KCl, 0.15 mM $CaCl_2$, 2 mM EGTA, 5 mM $MgCl_2$, 10 mM $K_2HPO_4/KH_2PO_4$, pH 7.6) and harvested by centrifugation at 2000g for 3 minutes at RT with slow brake. 400 µl of equilibrated cells were combined with the resuspended, sterile DNA, pipetted into a 2 mm cuvette, and incubated on ice for 15-30 minutes. Afterwards, the cells were then shocked in a BioRad Gene Pulser II using 8 square waves consisting 365V for 1 ms each, separated by 100 ms. The shocked cells washed several times with RPMI to remove cell debris and warmed in 2 ml of complete medium. 10 µl of Percoll-enriched schizonts were then added to these cells and allowed to reinvade for 3 hours with gentle orbital shaking at 37°C. 8 ml of medium was then added to the culture, and drug selection was begun 48 hours later.

Though it has not been extensively examined, this technique seems to be approximately as efficient as the ring-stage transfection. Parasites typically recover from drug selection approximately 4 weeks after transfection. Method 3.4.3.1 and 3.4.3.3 directly shock the parasite, whereas this method is comparatively gentle. This method was used to successfully transfect the HL1402 clinical isolate where the other two methods failed. This supports the general theory that clinical isolates are less robust parasites in culture and sensitive to perturbations, including electroporation, which are tolerated by standard laboratory lines.

### *3.4.3.3 Plasmodium falciparum transfection by Nucleofection*

Nucleofection on the Amaxa 4D-Nucleofector platform from Lonza differs from the other two transfection methods described above because it requires the most stringent synchronisation of the three methods. The machine is proprietary so the actual mechanism of transfection is unclear, but the system transfects 10 µg of DNA into 10 µl of enriched, highly synchronous schizonts, which are moments away from egress. This system outperforms the other two methods because transfectants are recovered two weeks after transfection rather than four weeks and it requires significantly less DNA per transfection. However, the other two methods can accommodate relatively asynchronous parasites, whereas Nucleofection requires a 30-60 minute post-invasion window of synchrony, which can take several weeks to achieve.

Briefly, parasites were synchronised tightly as described above to a 1-2 hour post-invasion window of synchrony. In the trophozoite stage, Compound 2 was applied, and highly segmented schizonts were isolated by Percoll enrichment at the end of the lifecycle. The lifecycle progression was monitored closely by Giemsa staining. After enrichment, the

schizonts were washed in pre-warmed media once and then mixed with 100 µl of Lonza P3 Primary Cell solution premixed with the proprietary transfection supplement. This was then mixed with precipitated, sterile DNA resuspended in 10 µl of sterile TE(10, 0.1) and added to a Nucleofection cuvette. The cuvette was then shocked per manufacturer recommendations. The transfection reaction was immediately transferred to 1 ml of pre-warmed 50% haematocrit culture and placed on an orbital shaker at 37°C. Transfection efficiency roughly correlates with the parasitaemia 1 hour after transfection. Parasitaemias of 1-5% typically indicate a successful transfection. Transfections producing 1 HPI parasitaemias under 1% often are successful but require 3-6 weeks to recover after drug selection. Three hours after transfection, the infected red cells were washed once and returned to a standard 10 ml culture. Drug selection was started 24 hours after transfection.

Nucleofection™ and Nucleofector™ are registered trademarks of Lonza, 2018.

#### *3.4.3.4 Plasmodium knowlesi transfection by Nucleofection*

Transfection of *Plasmodium knowlesi* schizonts was performed similarly using the Lonza Nucleofector 4D platform. Highly synchronous schizonts were enriched from infected red blood cells using a 55% (w/v) Nycodenz cushion and centrifugation. These schizonts were washed in RPMI, and 10 µl of these schizonts were resuspended in 100 µl of P3 Primary Cell solution and DNA as described above. This resuspension was added to a transfection cuvette and shocked with the same protocol as above.

Transfected schizonts were added to fresh red blood cells in warm media and allowed to reinvade overnight. These transfected cells were then selected with pyrimethamine for five days commencing the day after transfection.

### *3.4.3.5 Transient transfection of HeLa cells*

To examine the localisation of PfK13 and the µ subunit of the PfAP2 complex in HeLa cells, these genes were transiently transfected using Lipofectamine 3000. The transgenic PfAP2µ-3xHA coding sequence was PCR amplified out of genomic DNA prepared from the 3D7-AP2µ-3xHA-glmS parasite line created in this thesis and cloned into the pTriEX-3 vector (Millipore) downstream into the CMV expression cassette. The CDS of *pfk13* was similarly cloned to create a separate construct.

Briefly, cells were cultured to 50% confluency in a 25 $cm^2$ flask as described above. The cells were then trypsinised and counted using a haemocytometer. $3x10^5$ cells per well were then seeded into a 6-well plate with three 1 cm sterile round cover slips in the bottom. Once the cells had reached 70% confluency, 5 µg of DNA was precipitated and resuspended in 125 µl of DMEM, and 5 µl of P3000 reagent was added. Opti-MEM is typically used, but this reagent was not readily available and optimal transfection efficiency was not critical in these simple transient transfection and localisation experiments. According to the manufacturer's guidelines, many cell lines can be transfected without this special reagent. In a parallel tube, 3.75 µl of Lipofectamine 3000 reagent was diluted in 125 µl of DMEM. Immediately before transfection, the diluted DNA was added to the diluted Lipofectamine reagent and incubated at room temperature for 10 minutes to allow the DNA packaging reaction to occur.

Culture medium was removed from the seeded cell monolayer, and the cells were

washed with PBS. The packaged DNA solution was then added to the cell layer and incubated at 37°C for 12 hours. After 12 hours, the transfection solution was removed and replaced with HeLa cell medium. After 24 hours, the medium was removed, and the cells and cover slips were washed in place with PBS several times. PBS was then replaced with fixative solution (4% formaldehyde in PBS), and the same immunofluorescence protocol was performed as described in Section 3.3.6. 1 µl of VectaShield with DAPI was finally added to each coverslip. Coverslips were inverted and mounted onto a glass slide for imaging. µ2-HA and PfK13 were detected with the HA-specific and K13-specific antibodies listed in Section 3.3.11.

Lipofectamine™ and Lipofectamine 3000™ are registered trademarks of Life Technologies (ThermoFisher Scientific), 2018.

### 3.4.4 Cloning by Limiting Dilution

After transgenic parasites were generated by the above techniques and genotyped, they were cloned by limiting dilution. Transgenic, uncloned cultures were subcultured to 2-5% parasitaemia under standard conditions. The parasitaemia was then determined by counting a minimum of 400 red cells using a light microscope with a graticule and Giemsa staining. The cell densities of the culture and 50% haematocrit red blood cell stock were then determined with a disposable haemocytometer according to the manufacturer's protocol. A dilutant stock was prepared by diluting the red cell stock to $2x10^9$ cells/ml (2% haemtocrit) in complete media. The transgenic culture was similarly diluted. Using the dilutant stock, 10-fold serial dilutions were prepared to create a final solution with 1.25 parasites/ml in 2% haematocrit. 96-well plates were seeded with 250 µl of this final dilution

to seed 0.33 parasites/well. In this format, a successful cloning plate will have parasites in approximately one third of the wells in the plate.

One week after seeding the plate, media in each well was aspirated and replaced with media containing fresh red cells at 1% haematocrit. This was repeated 7 further days later, 14 days after seeding. At day 20, this was repeated again, and parasite growth was determined by an LDH assay as described below. At this point 12 clones were moved to 6-well plates and expanded for genotyping. Four successfully cloned, verified-transgenic parasites were further expanded and frozen. Two clones were characterised.

### 3.4.5 Drug susceptibility and parasite growth assays

#### *3.4.5.1 Standard 48-hour $EC_{50}$ determination*

For most frontline chemotherapies discussed in this thesis, a susceptibility profiles for various parasite lines were determined with standard 48h exposures to serial dilutions of the drug of interest. Briefly, ring-stage parasite cultures at 6-8 HPI synchrony were diluted to form a master stock at 0.5% parasitaemia in 4% haematocrit. Additionally, a 2x master stock of each drug of interest was prepared in complete medium. Serial two- or three-fold dilutions were made into complete medium across 8 columns of the 96-well plate, beginning in column four, with 100 µl of 2x diluted drug in each well. Columns two and three of the plate served as positive and negative growth controls, and the wells in each column were filled with 100 µl of drug-free complete medium or complete medium containing 20 µM chloroquine, respectively. 100 µl of the parasite master stock was added to each well, diluting the drug in each well to a final 1x concentration and the parasite culture to a final 2% haematocrit.

The outermost rows and columns were filled with 250 µl of sterile PBS. Over the course of a 48h incubation at 37°C, liquid in these wells commonly evaporates, which concentrates the liquid in the well in what we call the 'edge effect'. This would expose the parasites to higher concentrations of drug than intended; therefore, these wells were omitted.

The plate was then incubated for 48 hours at 37°C under standard culture atmosphere. After this incubation, the plate was frozen for 24 hours at -80°C and then thawed at 37°C to lyse the cells. The liquid in each well was resuspended, and 100 µl of each well was added to a new 96-well plate containing 100 µl/well of stain solution (1:5000 dilution of SYBR Green (Invitrogen) in PBS). The parasite material and stain solution were thoroughly by pipetting, and the plate was incubated in the dark for at least 10 minutes. SYBR Green-labelled parasite DNA was measured on a SpectraMax spectrophotometer at 480 nm excitation and 520 nm emission. Parasite proliferation and a dose response was calculated by normalising parasite proliferation between the positive and negative growth controls. $EC_{50}$ were determined using the log(inhibitor) vs growth 4 parameters non-linear regression analysis in Prism 7.0 (GraphPad). Z factors, originally described by Zhang *et al*, were also calculated as a quality control score to determine the robustness of the experiment and $EC_{50}$ estimation using the following equation [270]:

$$\boldsymbol{Z = 1 - \frac{3(\sigma^p + \sigma^n)}{\mu^p - \mu^n}}$$

where $\boldsymbol{\sigma^p/\sigma^n}$ and $\boldsymbol{\mu^p/\mu^n}$ represent the standard deviations and means of the positive and negative growth controls. A Z factor between 0.50 and 1 indicates a robust assay

and 0-0.50 indicates a poor quality assay. All assays reported in this thesis had Z scores greater than 0.7.

### *3.4.5.2 Standard 96-hour $EC_{50}$ determination*

Antibiotics like clindamycin, azithromycin, and doxycycline exert their antimalarial effects on second-generation parasites as described above in Section 1.4.5. Therefore, in order to determine parasite sensitivity to these drugs, their survival to serial dilutions of an antibiotic of interest must be examined after 96 hours rather than 48 hours. For these drugs, Method 3.3.4.1 was reproduced exactly as above except the assay plates were incubated for 96 hours rather than 48 hours.

### *3.4.5.3 Ring-stage survival assay (RSA)*

This assay was pioneered by Benoit Witkowski and first described in 2013 as the only validated method of distinguishing artemisinin susceptibility phenotypes in parasites derived from Southeast Asia. The assay involves exposing tightly synchronised parasites to a 700 nM dihydroartemisinin for 6 hours. Survival in this assay format correlates with clinical treatment failure for parasites from this region.

To perform this assay, *Plasmodium falciparum* cultures were tightly synchronised as described above to a 3 hour post invasion window of synchrony. A 2x culture stock was prepared at 0.5-1% parasitaemia in 4% haematocrit and incubated with an equal volume of 1.4 µM dihydroartemisinin freshly prepared in complete medium so that parasites were exposed to 700 nM DHA in 2% haematocrit. The assay was performed in duplicate in 48-well plates with 500 µl per well. After 6 hours, infected red cells were washed by centrifugation five times with

1 ml of complete medium in 1.5 ml Eppendorf tubes. DHA is known to adhere to plastics and extensive washing has been shown to be critical. The infected cells were resuspended in 500 µl of medium after the final wash and reseeded in an unused well. After a further 66 hours, parasite proliferation was determined by FACS by mixing one volume of parasite culture with eight volumes of freshly prepared stain solution (1:1000 SYBR Green, 1:10,000 MitoTracker Deep Red in PBS). The stained parasites were incubated at 37°C for 30 minutes in the dark, and then analysed on an LSR-II flow cytometer (BD Biosciences. Ring-stage survival was calculated as the ratio of average parasitaemia resulting from the 6h exposure to DHA or DMSO.

Multiple studies have recently demonstrated that the RSA could be modified to instead use a 3h or 4h pulse rather than a 6h pulse, while still retaining the ability to discriminate sensitive and resistant parasite RSA phenotypes. In this thesis, a 4h pulse was used except where noted because this considerably improves the ease of executing the assay as a single operator. This thesis may also use this specific notation when discussing RSA pulse-style assays: $RSA_{0\text{-}3h}^{4h}$. The subscript (e.g. 0-3h) indicates the age of the parasites when exposed to the DHA pulse, and the superscript (e.g. 4h) indicates the duration of the pulse.

#### *3.4.5.4 Lactate Dehydrogenase Assay (LDH Assay)*

The lactate dehydrogenase assay, or LDH assay, measures parasite density and therefore proliferation by detecting active parasite LDH from live cells. LDH is an enzyme that catalyses conversion of lactate to pyruvate, simultaneously reducing

$NAD^+$ (Nicotinamide adenine dinucleotide) to NADH. *P. falciparum* LDH can rapidly reduce 3-acetyl pyridine NAD (APAD), while erythrocytic LDH is only able to catalyse this reaction very slowly. In this assay cells are permeabilised in a buffer containing APAD, a fluorescent analogue of $NAD^+$ and mixed with a NBT/PES (nitro blue tetrazolium/phenazine ethosulphate) solution, which converts APADH into a coloured salt that can be detected spectrophotometrically.

Briefly, 20 µl of parasite culture was mixed with 100 µl of reaction buffer (0.1% Triton X-100, 130 mM L-Lactate, 27 mM Tris-HCl, pH 9.0) supplemented before use with 33 µM APAD (Sigma) in a 96-well plate. To each well, 25 µl of NBT/PES (2.2 mM nitro blue tetrazolium, 240 µM phenazine ethosulphate in water) was then added, and the contents of each well were mixing thoroughly by pipetting. The assay plate was then incubated at 37°C for 30 minutes. Parasite proliferation was then measured using a SpectraMax spectrophotometer set to 650 nm.

While this assay can be used to perform drug dose response experiments, in this thesis, the reagents are more expensive than SYBR Green, and the assay generally produces a smaller dynamic range between parasite-positive and -negative samples. In this thesis, the LDH assay was used to screen limiting dilution cloning plates for parasite-positive wells.

## 3.6 Microscopy Methods

This thesis involves several different microscopy modalities:

- All transgenic parasites with fluorescent tags were first screened after transfection under an EVoS inverted microscope for integration. For verifying integration and expression of these transgenes, 50 µl of standard cell culture was stained with Hoechst at 3 µg/ml for 20 minutes in the dark.

Stained cells were then washed once in PBS and resuspended to 20% haematocrit, and 10 µl of this suspension was sealed between a glass slide and 20x40 mm cover slip for imaging in on the EVoS system in a Category 3 room.

- Because the EVoS system is not suitable for colocalisation, live cell imaging and image capture was performed on a Nikon TI-3000 Eclipse inverted microscope. Cells were stained as above and immobilised on glass-bottom Ibidi µ-slides and sealed for imaging.
- The Nikon system was also used for imaging fixed, immunostained cells prepared as described in Section 3.3.8.
- All images were viewed using Fiji and Nikon Elements Advanced Research software packages. Z-stack images were background subtracted and deconvolved using the Richardson-Lucy algorithm with 8 iterations. A maximum Z projection was then performed and signal correlation analysis was performed in the Nikon software package using a standard 200x200 pixel cell window. A minimum of 35 cells were compared for comparing correlational coefficients. The majority of the images presented in this text capture cells prepared using the thin-smear IFA method. Though many prominent laboratories still use this technique for examining the localisation of factors by IFA, this technique sacrifices cell morphology in favour of experimental ease and speed. In drying the thin smears, the cells are dehydrated causing considerable loss of cell depth, making any correlation between the determined localisation of two structures possibility poorly representative of what actually happens in the cell. Additionally, correlation analysis is complicated in *P. falciparum* because the resolution limits of

conventional light microscopy (approximately 0.2 μm) makes discerning individual structures in the very small parasite cell (diameter: 1-1.5 μm) difficult without super-resolution techniques. The presented imaging data should be understood with these caveats.

- Immunoelectron Microscopy was performed by the Electron Microscopy Core Facility at the Washington University in St. Louis Children's Hospital in conjunction with the Odom-John Laboratory.

### 3.6.1 Immunoelectron Microscopy

P. falciparum were cultured at 37°C in 4 mL volumes in 6-well tissue culture dishes at 2% haematocrit until reaching 6-8% parasitaemia. Parasites were magnetically sorted from uninfected RBCs and ring stage parasites by passage through a magnetically mounted MACS LD separation column (Miltenyi Biotech, Germany). Parasites were collected by centrifugation and fixed for 1 h at 4ºC in 4% paraformaldehyde (Polysciences Inc., Warrington, PA) in 100 mM PIPES/0.5 mM MgCl2, pH 7.2. Samples were then embedded in 10% gelatin and infiltrated overnight with 2.3 M sucrose/20% polyvinyl pyrrolidone in PIPES/MgCl2 at 4ºC. Samples were trimmed, frozen in liquid nitrogen, and sectioned with a Leica Ultracut UCT7 cryo-ultramicrotome (Leica Microsystems Inc., Bannockburn, IL). 50 nm sections were blocked with 5% fetal bovine serum (FBS)/5% normal goat serum (NGS) for 30 min and subsequently incubated with primary antibody for 1 h at room temperature (anti-PDI mouse 1:100 (1D3; Enzo Life Sciences), anti-GFP rabbit 1:200 (A-11122; Life Technologies), anti-GFP mouse 1:100 (11814460001; Roche), anti-HA rabbit 1:50 (H6908; Sigma-Aldrich), anti-Rab5a rabbit 1:50 (Gordon Langsley) and anti-Rab5b rat 1:50 (Gordon Langsley)). Secondary

antibodies were added at 1:30 for 1 h at RT (12 nm Colloidal Gold AffiniPure Goat anti-Rabbit IgG (H+L)(111-205-144), 18 nm Colloidal Gold AffiniPure Goat anti-Rabbit IgG (H+L)(111-215-144), 12 nm Colloidal Gold AffiniPure Goat anti-Mouse IgG (H+L)(115-205-146), and 18 nm Colloidal Gold AffiniPure Goat anti-Mouse IgG+IgM (H+L)(115-215-068) (Jackson ImmunoResearch). Sections were then stained with 0.3% uranyl acetate/2% methyl cellulose, and viewed on a JEOL 1200 EX transmission electron microscope (JEOL USA Inc., Peabody, MA) equipped with an AMT 8 megapixel digital camera and AMT Image Capture Engine V602 software (Advanced Microscopy Techniques, Woburn, MA). All labeling experiments were conducted in parallel with controls omitting the primary antibody. These controls were consistently negative at the concentration of colloidal gold conjugated secondary antibodies used in these studies.

- - - -

# Chapter 4

# Validation of AP2 µ-subunit and Ubp1 as modulators of antimalarial sensitivity

## 4.1 Characterisations of genetic diversity in *pfap2mu* and *pfubp1* in Kenya

In 2009, our laboratory analysed parasite samples from a clinical trial in Mbita, Kenya to examine the efficacy of artemether-lumefantrine and dihydroartemisinin-piperaquine in treating uncomplicated *P. falciparum* malaria in children under the age of 10 years[205]. As part of this study, polymorphisms in *pfap2mu* and *pfubp1* were examined. These genes are new candidate markers for artemisinin and partner drug failure, first identified around the same time in an *in vivo* study of evolved resistance to artemisinin in *Plasmodium chabaudi*[207,208]. Three mutations of interest were identified in *P. chabaudi* between the two proteins, one in µ2 and two in Ubp1, and the Mbita study authors looked for evidence of selection of the orthologous mutations in these genes in clinical infections.

In this study, blood samples were taken from treated children before, during, and after treatment on days 0-3, 7, 14, 28, and 42 (Table 5, Fig 23). Whole-gene sequencing failed to identify the *falciparum* orthologue of the *P. chabaudi* mutation in *pfap2mu* encoding I592T. However, the effort did identify another non-synonymous mutation (g.479_G>A) encoding S160N that appeared to be associated with recrudescent infections and day-3 parasitaemia[205]. Additionally, the study failed to identify *falciparum* orthologues of the *P. chabaudi* mutations in *pfubp1*, which would encode V3275F and V3306F, but found an association with an alternative

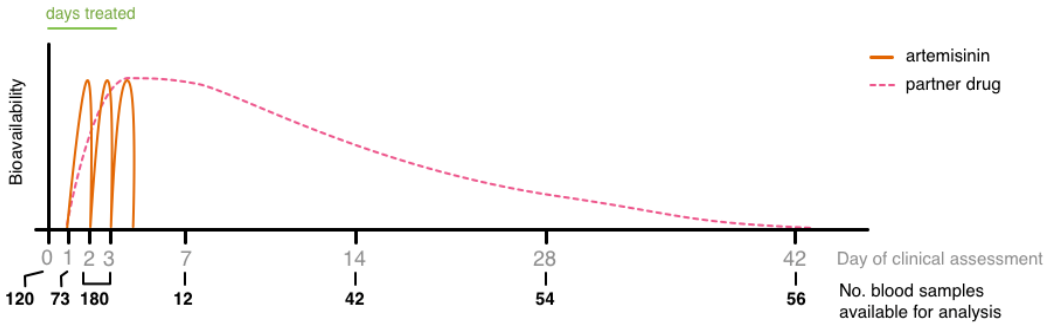


**Figure 23 Patient treatment and sampling overview for 2013 field study in Kenya**
The field study in Kenya was executed as a three-day treatment and sampling regime with multiple follow points of patient followup and sampling after treatment. Within each day of treatment, the plasma concentration of the short-acting artemisinin compound rapidly spikes and wanes (solid orange line). This rapid bioavailability helps to quickly reduce parasitaemia. The bioavailability of the longer-lasting ACT partner drug rises to its maximum of the course of treatment and is detectable in the bloodstream up to 4-6 weeks after treatment (dotted orange line). To assess clearance of parasites and antimalarial efficacy, patient blood samples were taken before treatment (day 0), during each day of treatment (days 1, 2, and 3), and at days 7, 14, 28, and 42 after treatment had commenced. The bolded numbers indicate the number of samples available to analyse at each collection date.

mutation in *pfubp1* encoding E1528D.

To follow up on this preliminary evidence of directional selection, the study authors executed another trial, this time examining artemether-lumefantrine and mefloquine-artesunate efficacy in the same village in 2013. The study protocol was similar to the 2009 study and aimed to examine these same mutations (Appendix I). However, due to funding issues out of our control, the study was stopped prematurely. Therefore, not all of the patients enrolled had blood samples drawn after the three-day regime. Additionally, many of the filter paper blood spots were lost or not returned to London by the study operators in Kenya. My work on this project commenced in the fall of 2015 and aimed to determine the prevalence of *pfap2mu* and *pfubp1* mutations in the patient samples we did receive, which included both pre- and post-treatment samples. While we sequenced every sample that we received, we omitted samples from patients who were not followed after day 28 post-treatment.

**Table 5 Patient characteristics in 2013 Mbita ACT efficacy study**

| Mbita, Kenya 2013 Study | |
|---|---|
| **Patient Characteristic** | **Total (*n* = 120)** |
| No. (%) male | 68 (52.7) |
| Wt (kg) (median [range]) | 20.75 (9-44) |
| Age (yr) (median [range]) | 7 (1-10) |
| | |
| No. (%) of patients in age groups: | |
| < 5 y.o. | 37 |
| 5-10 y.o. | 89 |
| | |
| Day 0 temperature (°C) (median, [range]) | 37.7 (35.5-39.9) |
| Day 0 haemoglobin (g/dl) (median, [range]) | 11.4 (4.5-16.1) |
| Day 0 parasitaemia (median [IQR] parsites per ul) | 27,320 (9,680-71,320) |
| | |
| No. of patients sampled, received MA (%) | 47 (39.2) |
| | |
| No. samples available per assessment day (%) of total | |
| Day 0 | 120 (100) |
| Day 1 | 73 (60.8) |
| Day 2 | 85 (70.8) |
| Day 3 | 95 (79.2) |
| Day 7 | 12 (10) |
| Day 14 | 42 (35) |
| Day 28 | 54 (45) |
| Day 42 | 56 (46.6) |

Biographical and clinical characteristics of patients enroled in the clinical study for whom pre-treatment samples were collected.

Given that our laboratory's previous preliminary transgenesis efforts indicated that the S160N variant of *pfap2mu* has some effect on artemisinin susceptibility in cell culture, I expected that the based line prevalence of this variant would be higher than that detected in the 2009 study. This would be consistent with directional selection reported by Henriques *et al*, however this study was not designed to detect evidence of a selective sweep. Although there is very little data available about the prevalence, selection, or impacts of the *pfubp1* variants described by Henrique *et al* and Borrmann *et al*, I expected the diversity of *pfubp1* haplotypes to have decreased if this region of the gene is linked to parasite fitness or drug susceptibility.

### 4.1.1 Preliminary analysis of variant *pfap2μ* alleles

According to the protocol described by Henriques *et al*, *pfap2mu*(359-1196) was amplified in a nested PCR reaction from DNA extracted from dried filter paper blood spots and sequenced by Sanger sequencing[205]. Although 311 samples were sequenced, 24 were omitted as they were from patients without day 28 followup.

Therefore, in total, 118 pre-treatment samples, 60 day 1, 59 day 2 and 3 samples, and 50 post-treatment samples were sequenced and analysed. These data were analysed using the same protocol as in the 2009 study.

The PCR amplification scheme used to examine this locus of interest lacked the sensitivity of many of the other genotyping amplifications our laboratory performs. Although extensive optimisation was attempted including varying primer sequences, thermocycling settings, and reaction composition such as divalence,

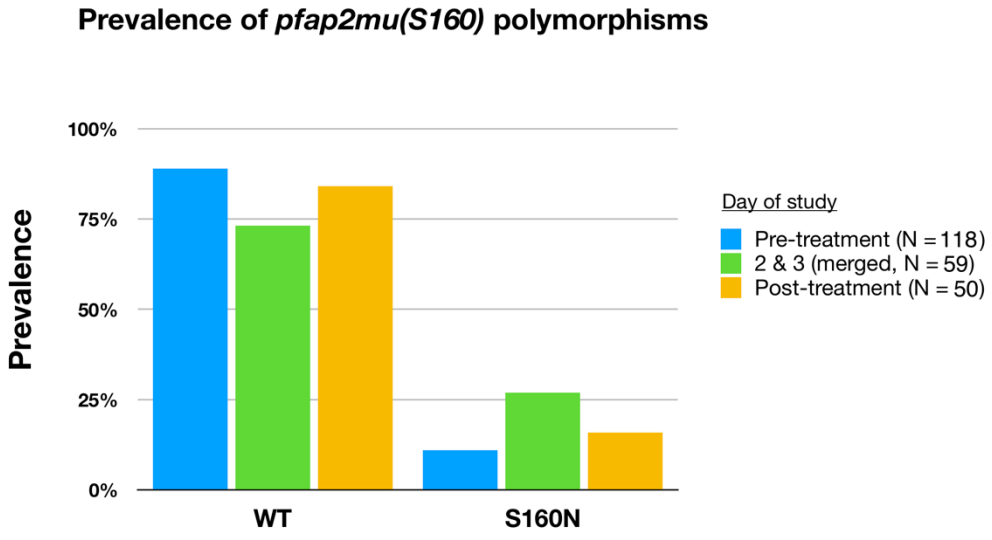


**Figure 24 Prevalence of S160N mutations in African patients**
Because of the low number of sample available to analyse and to facilitate comparison between studies, patient samples were pooled and analysed as in Henriques *et al* [205]. Thus, the prevalence of the *pfap2mu(S160N)* variant was analysed as either pre-treatment (blue; day 0), during treatment (green; days 2 and 3, merged) or post-treatment (yellow; days 7-42).

buffer composition, and primer and template concentrations, the amplification sensitivity could not be significantly improved. Unfortunately, the post-treatment, day 2 and 3 samples were most impacted by this problem because the parasitaemia, and therefore extracted parasite DNA concentration, is often very low. The investigators of the 2009 study merged the day 2 and 3 data, recording the latest sequencing result for each patient, to increase their sample size; for consistency, this operation was performed on the 2013 data set as well.

Between the two studies, the same trends hold (Fig 24, 26). When comparing all the sequenced samples from 2013 across days of treatment, there is some

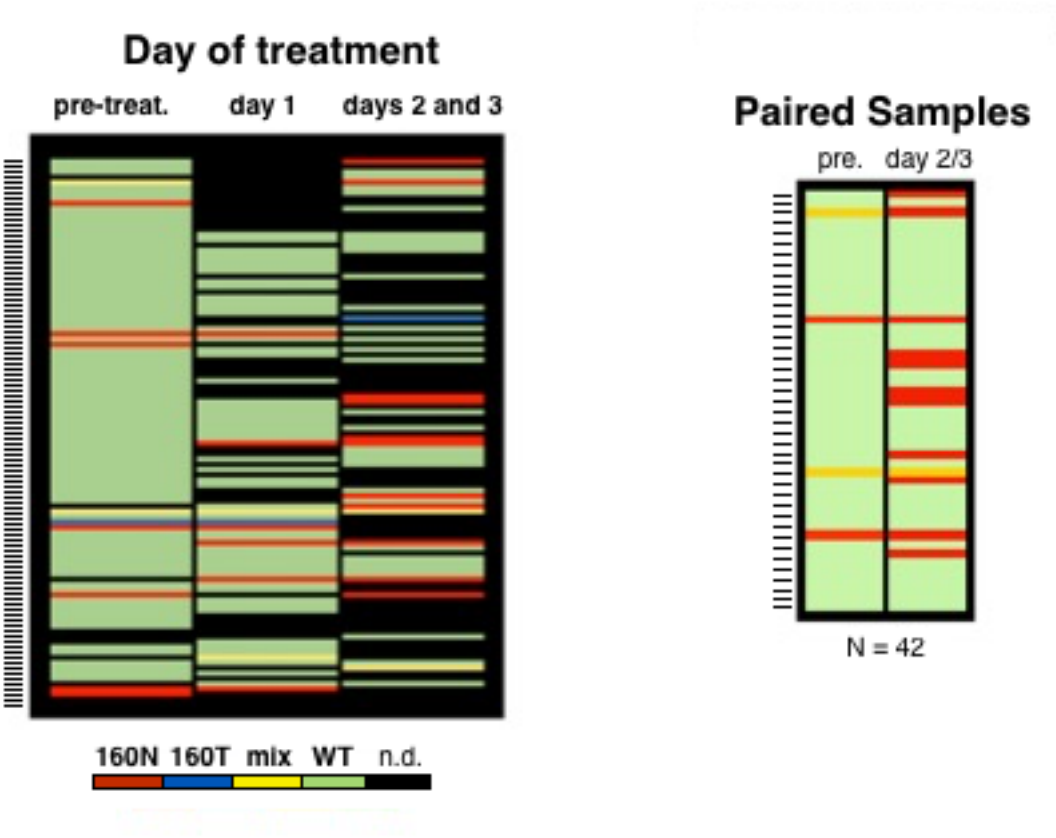


**Figure 25 Within-patient selection of *pfap2mu* variants**
Comparison of *pfap2mu* genotypes in paired blood samples taken from individual patients before, and after ACT-treatment. Each line in the heat maps represent an individual patient. Red indicates the presence of the mutant S160N allele, blue the alternate S160T allele, yellow an indeterminate mixed genotype, and green the wild type S160S allele. Black indicates no sample was available. The panel on the right examines only patients for which day 0 and day 2 or day 3 sequencing data was collected (N = 48 patients). Ticks on the left edge of each panel indicate individual patients.

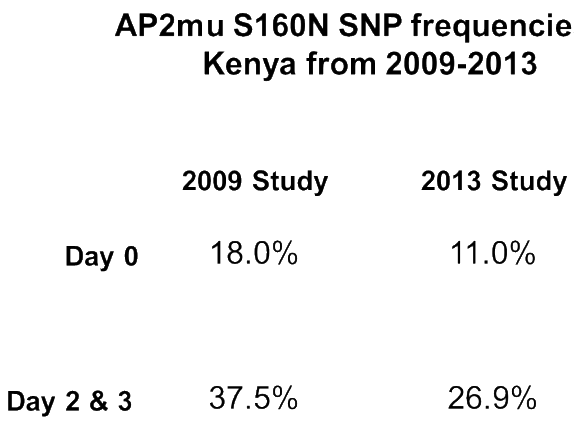


**Figure 26 Comparison of the prevalence of *pfap2mu(S160N)* between 2009 and 2013 field studies**
A comparison of the prevalence of the mutant *pfap2mu(S160N)* parasite allele detected in patient blood samples taken before and during treatment in the 2009 and 2013 studies performed in Mbita, Kenya.

evidence of positive selection for the S160N SNP. Of the pre-treatment samples, 105 (89.0%) were wild type, 13 (11.0%) possessed the S160N mutation, 2 were mixed genotype, and 2 possessed the alternate S160T allele, previously observed at similarly low frequency in 2009. At days 2 and 3, 26.9% of sequenced samples possessed the mutant allele; only one patient had parasites with the alternate S160T allele. When examined at the individual level, the trend becomes clearer (Fig 25). In patients with both pre- and post-treatment samples, 12.5% had parasites with the S160N allele before treatment, compared to 34.3% after. In this sub-analysis, infections in which both genotypes were detected before treatment resolved to single-genotype infections with the S160N mutation after treatment.

Statistical calculations performed for the original study protocol determined that 300 patients needed to be enroled and followed for the duration of the study to

detect a 20% risk difference with 90% power and type I error of 0.05. Therefore, the current sample set is too small to calculate the statistical significance of any changes identified here.

Between the two studies, the trend is similar (Fig 26). In the samples analysed, the S160N mutant *pfap2mu* allele is more prevalent in parasites detectable at day 3 of treatment. Interestingly, the prevalence of the mutation at the later days of PCR-confirmed positivity (days 20-48 after treatment) in this preliminary sample was lower than in 2009. Only 8 of 50 (15.9%) sequenced patients had the mutant allele, compared to 7 of 28 (25%) in 2009. One might expect a mutation that is under selection and tightly associated with treatment outcomes to increase in base prevalence over the four years between these studies and be present in higher prevalence in recrudescent infections. We have not looked for genomic evidence of a selective sweep, but the similar prevalence of the S160N allele determined in this work compared to the 2009 study suggests against a sweep.

### 4.1.2 Directional selection of variant *pfubp1* alleles

The evidence for selection of *pfubp1* genotypes during and after ACT treatment is more complicated. Borrmann *et al* associated Ubp1(E1528D) with artemisinin resistance *in vitro* by GWAS, however sequencing results from this locus in our 2009 study samples revealed more than 16 different haplotypes encoded within 30 bases upstream or downstream of the E1528 codon[251]. The major source of diversity in this region comes from several tandem KYD/E motifs, which seem to expand and contract as triplet motifs, shifting the reading frame by multiples of three

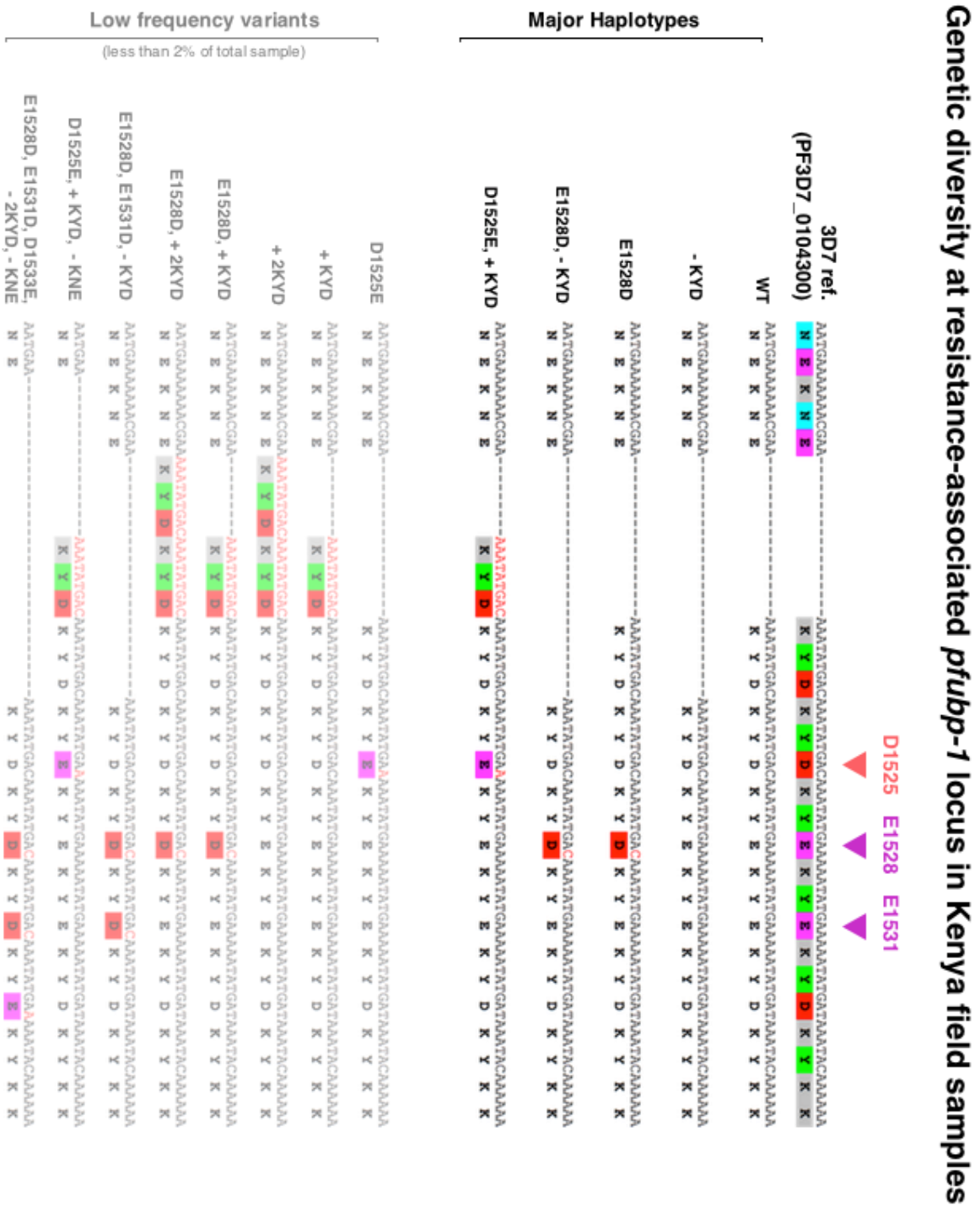


**Figure 27 Haplotype diversity identified in *pfubp1* at a resistance-associated locus**
14 different *pfubp1* haplotypes around the E1528 residue were identified in sequenced patient samples. These include polymorphisms at residues 1525, 1528, and 1531 as well as indels immediately upstream of residue 1525. Five major haplotypes (bold) and 9 low frequency haplotypes (less than 2% of total samples per haplotype; grey) were identified.

amino acids with respect to the 3D7 reference genome. Given the degeneracy of the nucleotide sequence and the similarity of the amino acid translation, it is difficult to say with certainty where these insertions and deletions occur. Thus, interpreting the prevalence of any specific Asp to Glu or Glu to Asp mutations in these KYD/E motifs is difficult, and comparing across studies is nearly impossible unless authors describe how these indels were aligned in their analysis. This analysis assumes that any insertions or deletions occur at the 5' end of the repetitive locus.

Overall, my sequencing identified 13 haplotypes involving mutations at D1525, E1528, and E1531 as well as indels around these residues (Fig 27). More than 80% of the sequenced samples harboured one of five major haplotypes. However, 8 other low frequency haplotypes, each with less than 2% prevalence in pre-treatment samples, were also identified. Because there was no evidence of selection of these minor haplotypes, they will not be discussed further in this thesis, though they may be of interest for future analyses.

When the sequences from the 2013 samples were aligned as described above to the reference CDS, there was no immediate evidence of selection at the E1528 position. Approximately 15% of samples before, during, and after treatment contained the E1528D mutation. When the haplotype of the locus was considered as a unit irrespective of indels, approximately 16% of patients harboured parasites with the DDE (D1525, E1528D, E1531) haplotype before treatment, whereas 22% of samples did after. The 2009 study did not consider haplotypes but showed 10% of sequenced pre-treatment samples harboured E1528D, as compared with 17% after treatment (day 3).

Yet when including indels in the haplotype classification, the evidence for E1528D becomes increasingly complicated. While the DDE haplotype (D1525,

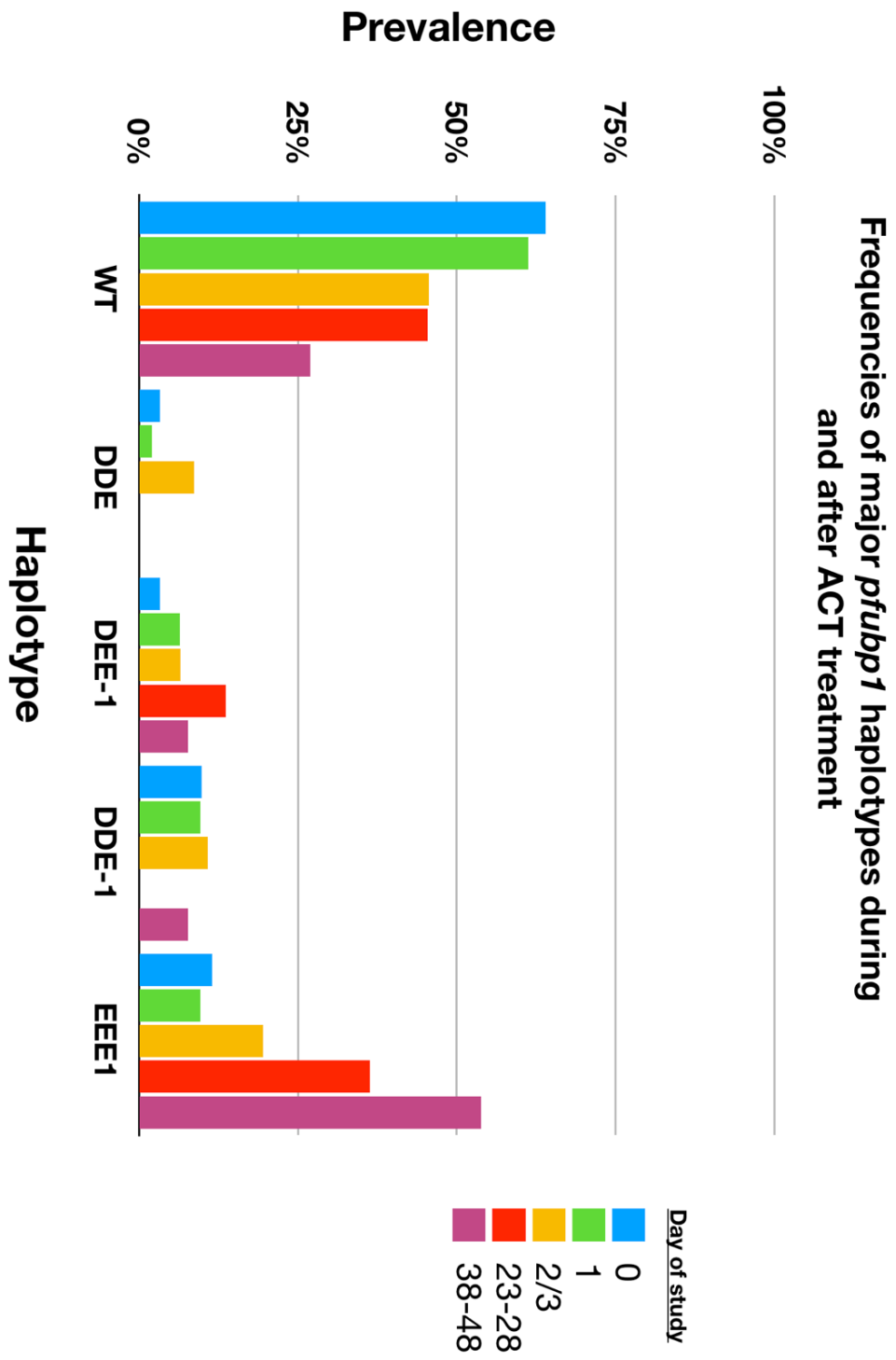


**Figure 28 Directional selection of *pfubp1* haplotypes**
The prevalence of the five major haplotypes identified around the 1528 locus was assessed before treatment (day 0), during treatment (days 1 and 2/3), and after treatment (days 23-28, days 38-48). Samples were pooled as noted for consistency of analysis and comparison with the 2009 study by Henriques *et al*[205]. Haplotypes were generated by considering residues 1525, 1528, 1531 and indels immediately upstream of 1525 as a single unit. EEE1 therefore indicates D1525E, E1528, E1531, and one KYD insertion upstream of residue 1525 (Fig 27).

E1528D, E1531, no indels) doubles in prevalence from 3.3% before treatment to 8.7% after treatment, it is not detected in any late-treatment failure (days 28-42) parasite samples, and none of the multiple other haplotypes with the E1528D mutation increase in prevalence during or after treatment. Instead, the EEE1 (D1525E, E1528, E1531, with 1 KYD insertion) haplotype seems to be selected strongly, beginning during the three days of treatment (pre-treatment: 11.48%; day 3: 19.6%) and continuing through several weeks post-treatment, peaking at 53.9% at days 28-42 after beginning the study (Fig 28). Interestingly the prevalence of the wild type 3D7 haplotype decreases from 63.9% before treatment to 45.7% after treatment and 26.9% in late treatment failure samples. It is tempting to consider these data as evidence of directional selection; however, we will not know until after the rest of the study samples are imported and analysed.

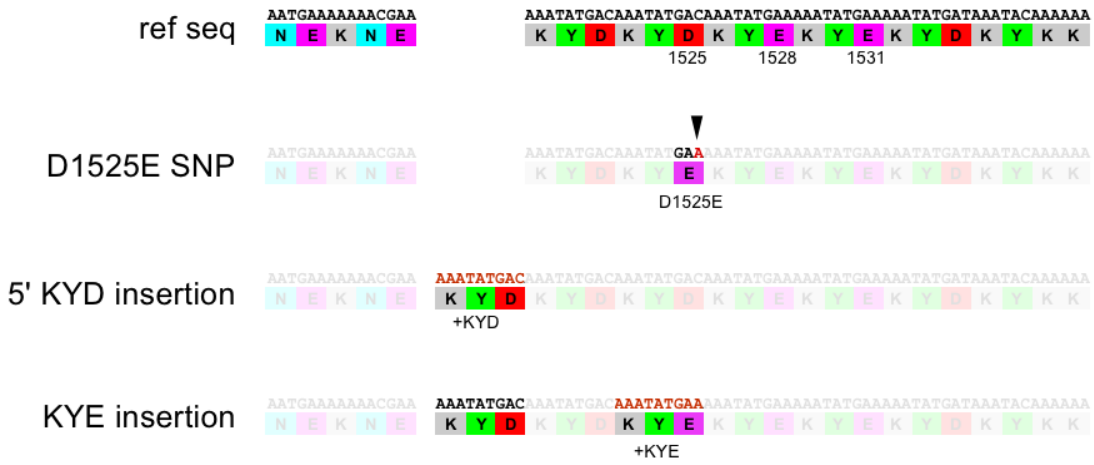


**Figure 29 Possible genetic mechanisms for observed *pfubp1* directional selection**
A schematic representing how the EEE1 haplotype could have arisen. The EEE1 haplotype is considered a D1525E and a single KYD insertion, however there is no evidence of these individual polymorphisms. Therefore, given the degeneracy of the repeats in this region, the haplotype could result from a single KYE insertion around residue 1525 (third line), which would simultaneously introduce D1525E and the single KYD "indel" upstream of this locus.

An alternative possible interpretation of this data is that rather than a discrete KYD insertion and D1525E point mutation, a KYE insertion in the middle of that region is creating the haplotype (Fig 29). This makes more intuitive sense given that there is no evidence of selection for either the D1525E or KYD insertion independently.

Unfortunately, the 2009 study was not quantitatively analysed by haplotype as discussed in this section, particularly with respect to the presence or absence of the indels. Without a full reanalysis of that data set, we can only see that 20% of the pre-treatment samples from 2009 had the EEE1 haplotype. Therefore, it is possible that a similar trend existed in 2009 but was not reported.

### 4.1.3 Whole gene sequencing reveals minimal genetic diversity in *pfubp1*

Given the importance of ubiquitin hydrolases in a wide range of pathologies and the implication of Ubp1 in antimalarial response in both rodent and human studies, I sought to probe existing genetic diversity across the entire gene. The dynamics around the 1528 locus are interesting, but the putative C-terminal catalytic domain is of particular interest. Additionally, outside of this putative catalytic domain, the protein lacks homology with other factors. Understanding which regions may be conserved or polymorphic could help map functionality onto the gene and identify other loci of interest.

To begin to characterise the genetic diversity along the rest of the *pfubp1* gene, a PCR-based strategy was designed to amplify and sequence the entire 10.5 kb coding region of the gene from randomly selected pre-treatment blood samples of patients who went on to either successfully clear their parasitaemia by day 3 or

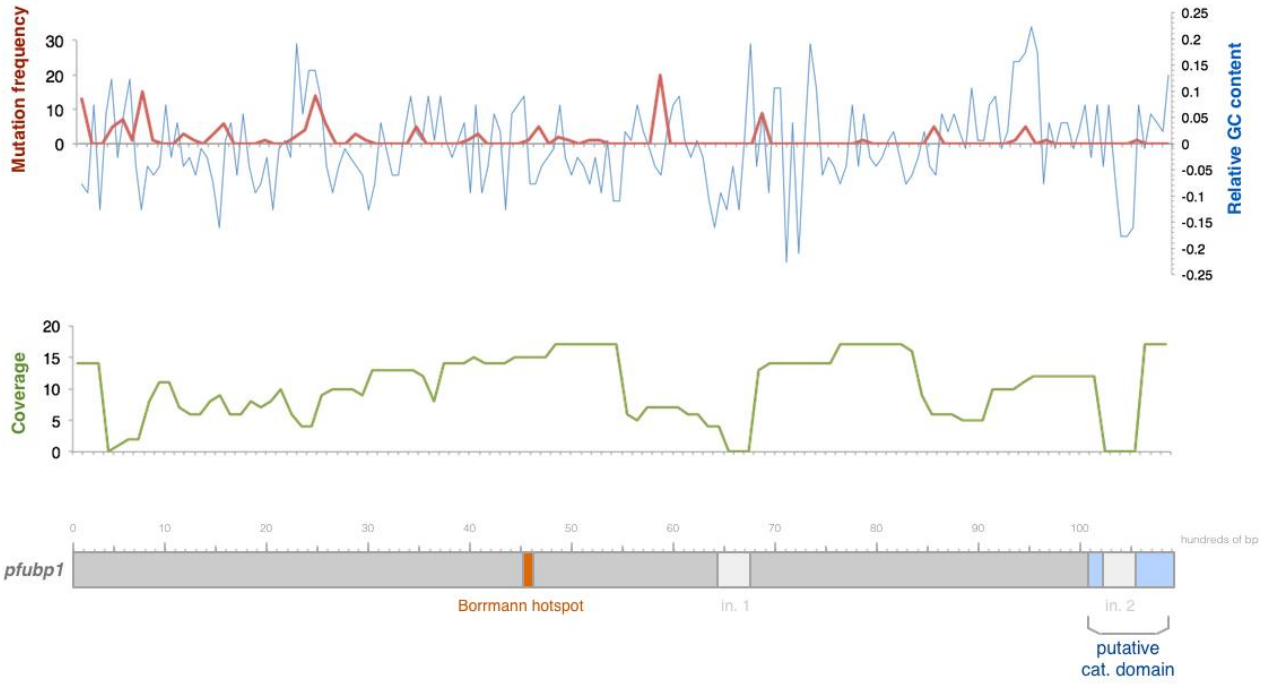


**Figure 30 Diversity topography map of *pfubp1* in selected parasite samples**
The entire *pfubp1* gene was sequenced from six samples from patients with fully cleared parasitaemia at day 3 and six samples from patients with late-day parasitaemia by PCR. The number of mutations per 100 base pairs was plotted along the length of the gene (top panel; red) alongside relative GC content per 100 base pairs (top panel; blue). The middle panel (green) depicts the sequencing coverage per 100 base pairs. A schematic of *pfubp1* is provided which depicts the splicing architecture of the gene, as well as the putative catalytic DUB domain and 1528 Borrmann hotspot[251]. In. 1 and In. 2 indicate introns 1 and 2 of the *pfubp1* gene.

experience late-day treatment failure. Six parasite *pfubp1* genes from each category were sequenced.

Given the low complexity of many regions of the gene and the low remaining amounts of DNA from the finger-prick blood spots, it was not possible to obtain high-quality reads for the entire gene from each sample. However, it was still possible to identify a number of SNPs and indels along the length of the gene that may inform future population genetics or transgenic work (Fig 30).

Interestingly, most of the gene seems generally conserved between these parasites. As expected, there are some small expansions and contractions of low-complexity, repetitive regions, but when SNP frequency is mapped against gene complexity, as measured by relative GC content, there are a few regions of higher complexity with variability. Higher complexity regions are not necessarily intrinsically functional but can be maintained if they encode important structural elements. One of these potentially interesting locations occurs approximately one quarter of the way into the gene around base 2300.

Consistent with *in silico* modelling, the C-terminal region encoding the putative catalytic domain is mostly conserved among these 12 samples (Appendix IVI)[208]. One SNP was detected in the putative catalytic domain encoding D3496N just after the 3' splice site of the second intron. At this point, it is too early to suggest which mutations could be interesting. The fact that one mutation is observed in such a small sample indicates there may be important mutation events occurring in this region of the gene. Unpublished recent work from others in our lab have identified several other mutations in this region. Work is underway to expand this topographical mapping of *pfubp1* and to sequence the C-terminal region from a large sample of patients to inform future *in vitro* transgenic and biochemical experiments.

## 4.2 Rationale for examining µ2 and Ubp1 mutations in *P. falciparum*

The mutations of interest in *pfap2mu* discussed so far in this report have been linked with artemisinin susceptibility either by statistical association with clinical treatment failure through population genetics work, computational genomics, or a rodent malaria study. There is no direct evidence for causation in *Plasmodium*

*falciparum*. Previous *in vitro* work in our laboratory attempted to probe the effects of the μ2(S160N) mutation and suggested a moderate impact on quinine sensitivity and a subtle effect on artemisinin susceptibility[206]. However, this work involved integrating a mutant copy of the gene under the control of the *calmodulin* promoter into the dispensable *cg6* locus on the Dd2, chloroquine-resistant background. This approach is problematic for several reasons.

The first issue is that the wild type protein was not disrupted in this line. Therefore, in this line, mutant and wild type copies were competing for other components of the AP2 complex, making it is impossible to know if the phenotypes observed are a blend of wild type and mutant phenotypes or artefacts of this molecular competition. Secondly, the *cam* promoter is highly active and does not reflect the stage-specific profile of the endogenous *pfap2mu* promoter. The qPCR performed in this original transgenic work suggested abnormal expression patterns of the transgene compared to the endogenous locus and a high degree of variability in the detected expression, with minimal expression in the schizont stage. AP-2 components are essential for cell survival in all organisms that have been examined, so it is unclear what effect this aberrant expression profile had on the parasite. Indeed, parasites overexpressing a wild type copy of *pfap2mu* in the *cg6* cassette showed modified sensitivity to lumefantrine. Lastly, the examination of this mutation, identified in Africa, in the Dd2 parasite of Southeast Asian origin with chloroquine resistance is also inappropriate and complicates the interpretation of these data. At the time, the Dd2-attP integration system was the state of the art. However, now we have genome editing technologies available (Section 1.11), which are vastly superior. Given the potential importance of mutations in these genes,

mutations of interest should be re-evaluated with these tools, which represent the new state of the art.

For all of these reasons, I elected to re-examine the impact of the *pfap2mu*(S160N) variant on a chloroquine-sensitive 3D7 background using the Cas9 system to install this mutation into the endogenous *pfap2mu* locus. In addition to re-examining this clinical mutation, I also examined the impacts of the mutations orthologous to those described by Hunt *et al* in *pcap2mu* and *pcubp1*, which encode PfAP2µ (I592T) and PfUbp1(V3275F) and PfUbp1(V3306F), respectively. Based on our previous data and the data presented by Hunt *et al*, I expected all of these mutations to affect parasite susceptibility to artemisinin. Additionally, the three orthologous mutations from the *P. chabaudi* study evolved in the context of multiple drug resistance, therefore these may contribute to parasite susceptibility to chloroquine. However, it is unclear from the murine drug selection regime how these mutations should be expected to modulate parasite susceptibility to these other drugs, including chloroquine.

## 4.3 Generation of *P. falciparum* strains bearing µ2 mutations using CRISPR-Cas9 editing

To validate the role of µ2 in the context of drug resistance, constructs were designed and created to install the S160N mutation, which was first identified in clinical isolates in Kenya, and the I592T mutation, which was first identified in an artemisinin-resistant *P. chabaudi* parasite.

Cas9 cleavage sites are defined by 20 nucleotides followed by the diguanine NGG protospacer adjacent motif (PAM). To design constructs to install these two mutations, PAM sites in the *pfap2mu* gene (PF3D7_1218300) were mapped using

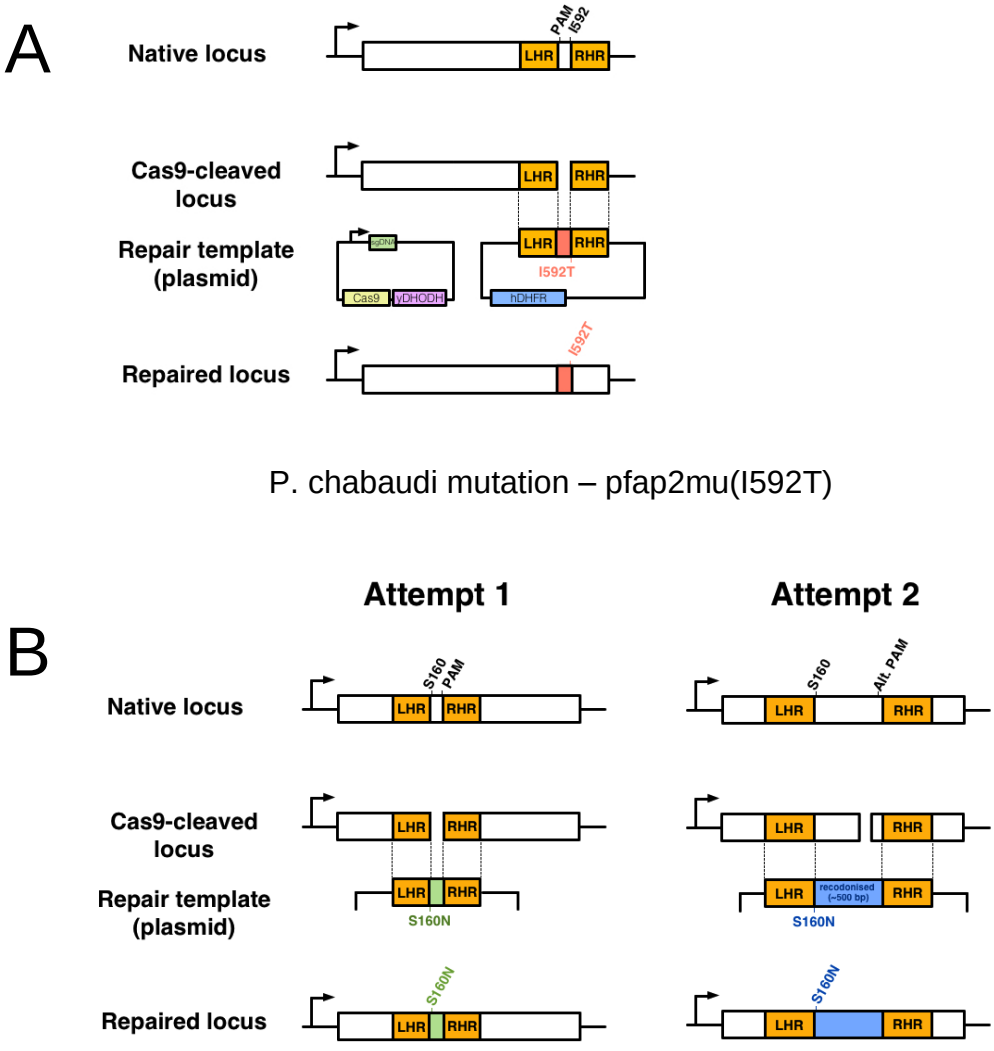


P. chabaudi mutation – pfap2mu(I592T)

P. falciparum Kenyan field mutation – pfap2mu(S160N)

**Figure 31 Schematics for manipulating *pfap2mu* by Cas9-mediated genome editing**
**A** Schematic for installing the *P. falciparum* orthologue of the *P. chabaudi pfap2mu* mutation encoding Pfμ2(I592T). A PAM site at the 3' end of the gene within 15 bp of the I592 locus was selected. A homology repair template was designed based on the pL6 system described by Ghorbal *et al* to contain approximately 300 bp homology arms (LHR, RHR) upstream and downstream of the cut site as well as the I592T alternative codon and silent mutations to destroy the PAM site[263]. **B** A similar construct was designed to install the S160N mutation (attempt 1). A second construct was designed using a downstream PAM site with greater predicted activity (attempt 2). 500 bp homology arms were designed to increase homologous repair efficiency and the region of the CDS between this PAM and the S160 locus was recodonised to prevent homologous repair from occurring before the S160N allele was installed. For recodonisation, every other codon was replaced with the second most frequently used codon for the given amino acid.

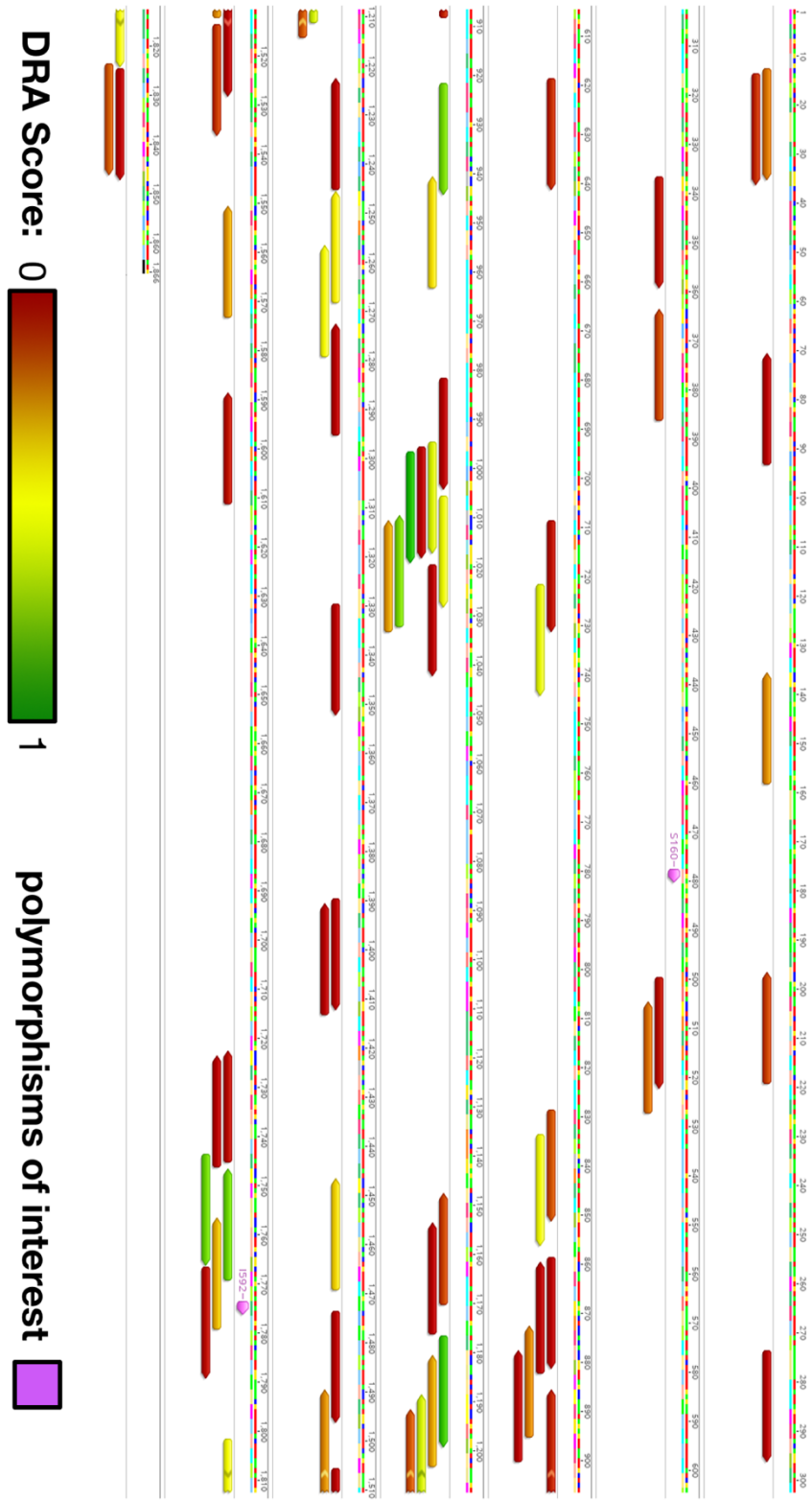


**Figure 32 Cas9 protospacer adjacent motifs in *pfap2mu***
Annotated CDS of *pfap2mu* with all Cas9 protospacer adjacent motifs (PAM) marked and coloured by predicted activity score (Doench-Root Algorithm). A sliding colour scale from red to green indicates the magnitude of the score from 0 to 1.0. PAMs were identified and scored using the CRISPR-Cas9 tool in the Geneious R8 software package. The two pink annotations mark the positions of the S160 and I592 loci.

empirical experimentation. Factors determining sgRNA activity in *Plasmodium* have the embedded CRISPR tool in the Geneious R8 software package. The Geneious PAM report has limited information, namely the position of the guide on the gene, a predicted off-target activity score, and an on-target activity score (Fig 32). The on-target score is produced by the Doench-Root Algorithm, hence the name DRA score, which was originally designed and optimised in 2014 for mammalian cells based on empirical experimentation. Factors determining sgRNA activity in *Plasmodium* have not yet been worked out, so the DRA score is one of the only available measures of possible on-target activity. Therefore, PAMs were selected that would balance maximising proximity to the locus of interest and DRA score, with preference given to proximity (Fig 32).

A homology template was designed for each mutation that would include 300-500 bp 5' and 3' arms that flank the cut site and a recodonised region that would integrate the mutation of interest and synonymous mutations to remove the PAM site. Recodonised regions including the synonymous "shield" mutations to replace the PAM and the mutations of interest were introduced with primers. The full homology template was generated by overlap PCR and cloned into the pL6 homologous repair template plasmid (Fig 31). Two complementary, single-stranded oligonucleotides containing the DNA sequence of the chosen PAMs were annealed and ligated into the sgDNA cassette in these pL6 constructs as described by Ghorbal *et al*[263].

The template repair plasmid and Cas9 expression plasmid were transfected into 3D7 parasites using the ring-stage transfection protocol described in Section 3.4.3.1. Parasites were recovered after 24 days. PCR amplification and sequencing of the genomic locus showed that the I592T SNP had been successfully installed along

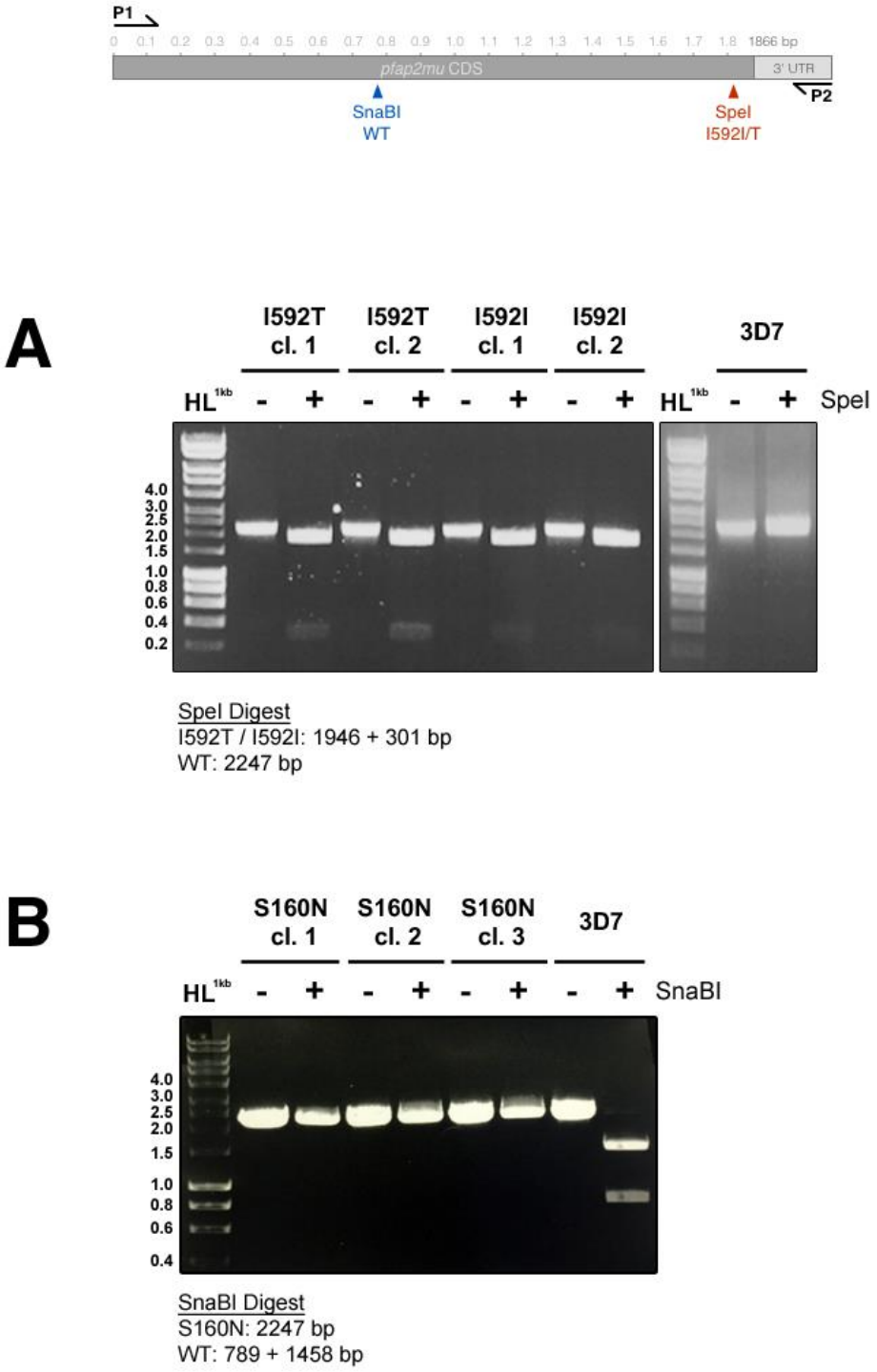


**Figure 33 PCR-RFLP mapping of transgenic parasites bearing *pfap2mu* mutations**
Successfully modified 3D7 parasites harbouring the **(A)** I592T, I592I, and **(B)** S160N mutations in *pfap2mu* were cloned by limiting dilution. The genotypes for at least two clones were confirmed by PCR-RFLP mapping and Sanger sequencing. Primers for PCR-RFLP mapping were outside the 5' and 3' homology arms of the plasmid-based homologous repair template so only the chromosomal locus would be amplified (top panel). PCR products from I592T and I592I clones were digested with SpeI, and PCR products from S160N clones were digested with SnaBI. The expected restriction fragments are annotated. SpeI site is inserted silently in the context of the mutant I592I/T transgenic allele, whereas the native SnaBI site is destroyed by the recodonised S160N transgene (top panel).

with the silent shield mutations. These parasites were then cloned by limiting dilution as described in Section 3.4.4 (Fig 33).

AP-2μ(S160N) transfectants from this first construct never recovered after drug selection. Despite several repeated transfections, no transgenic parasites have been generated using this construct, either with a wild type S160S or mutant S160N allele. Parasites that recovered from drug selection carry both plasmids suggesting this sgRNA-Cas9 ribonucleoprotein is not efficiently targeting and cleaving the desired locus (data not shown).

In the design of these constructs, I had selected a Cas9 guide RNA sequence with emphasis on maximising the proximity of the PAM site to the mutation of interest with 200-300 bp homology arms. Re-examining guide sequences annotated by Geneious, the originally selected guide near the S160N codon, which was unable to efficiently direct Cas9 to the locus, had a Doench-Root predicted activity score (DRA) of 0.11 (11%), whereas the I592T guide that successfully generated transgenic parasites had a DRA score of 0.57 (57%). Given the low predicted activity of this S160N guide, a different guide further downstream from the S160 locus with a 0.53 DRA score was selected, and a new homologous repair template to integrate this S160N mutation was designed.

Because this new PAM site was 500 bp downstream of the S160 locus, the coding sequence between the PAM site and S160 codon was silently recodonised using the next-most-frequently-used *P. falciparum* codon for each amino acid[271]. Without this recodonisation, homology-driven repair could occur immediately around the chromosomal break without integrating the S160N mutation.

To also establish the technique in our laboratory and improve transfection efficiency, this construct was transfected along with the Cas9 expression construct

into 3D7 schizonts using the Nucleofection protocol described in Section 3.4.3.3. Parasites were then selected as above, and parasites recovered after 24 days. PCR-RFLP mapping confirmed these parasites contained the S160N transgene. These parasites were also cloned by limiting dilution.

## 4.4 *In vitro* characterisation of drug sensitivity profiles of transgenic *P. falciparum* lines bearing µ2 mutations

Once independent clones for both the 3D7-µ2(I592T) and 3D7-µ2(S160N) lines had been established, their drug sensitivity profiles were characterised using 48h exposures to frontline antimalarials and the ring-stage survival assay, as described in Section 3.4.5.

When compared to the parental 3D7 parasite line, 3D7-µ2(S160N) displayed no differences in sensitivity to chloroquine, quinine, dihydroartemisinin, lumefantrine, piperaquine, or mefloquine in the standard 48h exposure assay format.

**Table 6 Nanomolar sensitivity of parasites harbouring *pfap2mu* mutations to frontline chemotherapies**

| | I592T cl 1 | I592T cl 2 | I592I cl 1 | I592I cl2 | S160N cl 1 | S160N cl 2 | 3D7 |
|---|---|---|---|---|---|---|---|
| **Chloroquine** | * 8.7 ± 0.9 | * 7.4 ± 0.3 | 11.4 ± 0.8 | 12.3 ± 0.4 | 13.5 ± 0.1 | 14.9 ± 0.4 | 13.7 ± 0.3 |
| **Quinine** | 24.8 ± 1.9 | 23.0 ± 2.3 | 23.4 ± 2.5 | 24.0 ± 2.7 | 27.7 ± 2.0 | 32.3 ± 3.3 | 31.4 ± 2.6 |
| **Dihydroartemisinin** | 3.1 ± 0.7 | 2.5 ± 0.4 | 2.8 ± 0.6 | 3.1 ± 0.7 | 2.9 ± 0.2 | 2.7 ± 0.7 | 3.4 ± 0.3 |
| **Lumefantrine** | * 20.9 ± 2.1 | * 21.8 ± 1.0 | 30.2 ± 3.0 | 31.4 ± 2.3 | 26.9 ± 2.7 | 29.6 ± 3.0 | 30.0 ± 4.0 |
| **Piperaquine** | 26.5 ± 3.0 | 22.8 ± 2.5 | 23.5 ± 3.6 | 25.9 ± 0.7 | 28.0 ± 3.1 | 29.6 ± 5.0 | 31.6 ± 4.5 |
| **Mefloquine** | 16.2 ± 1.8 | 16.0 ± 1.9 | 16.8 ± 2.4 | 17 ± 1.4 | 12.1 ± 0.5 | 12 ± 0.7 | 12.2 ± 0.2 |

The nanomolar (nM) sensitivity of parasites harbouring the I592T, I592I, and S160N *pfap2mu* variants as well as the parental 3D7 parasite was characterised to chloroquine, quinine, dihydroartemisinin, lumefantrine, piperaquine, and mefloquine using standard 48-hour exposures beginning in the ring stage. Parasite proliferation was quantitated with SYBR Green DNA stain. $EC_{50}$'s were determined using Prism v7.0 and the variable four parameter non-linear regression analysis. Significance was calculated using a one-way ANOVA with respect to the 3D7 parent. * indicates $p < 0.05$. Two clones (cl. 1; cl. 2) were analysed for each transgenic line. Mean of at least four experiments each performed in technical duplicate with standard error shown.

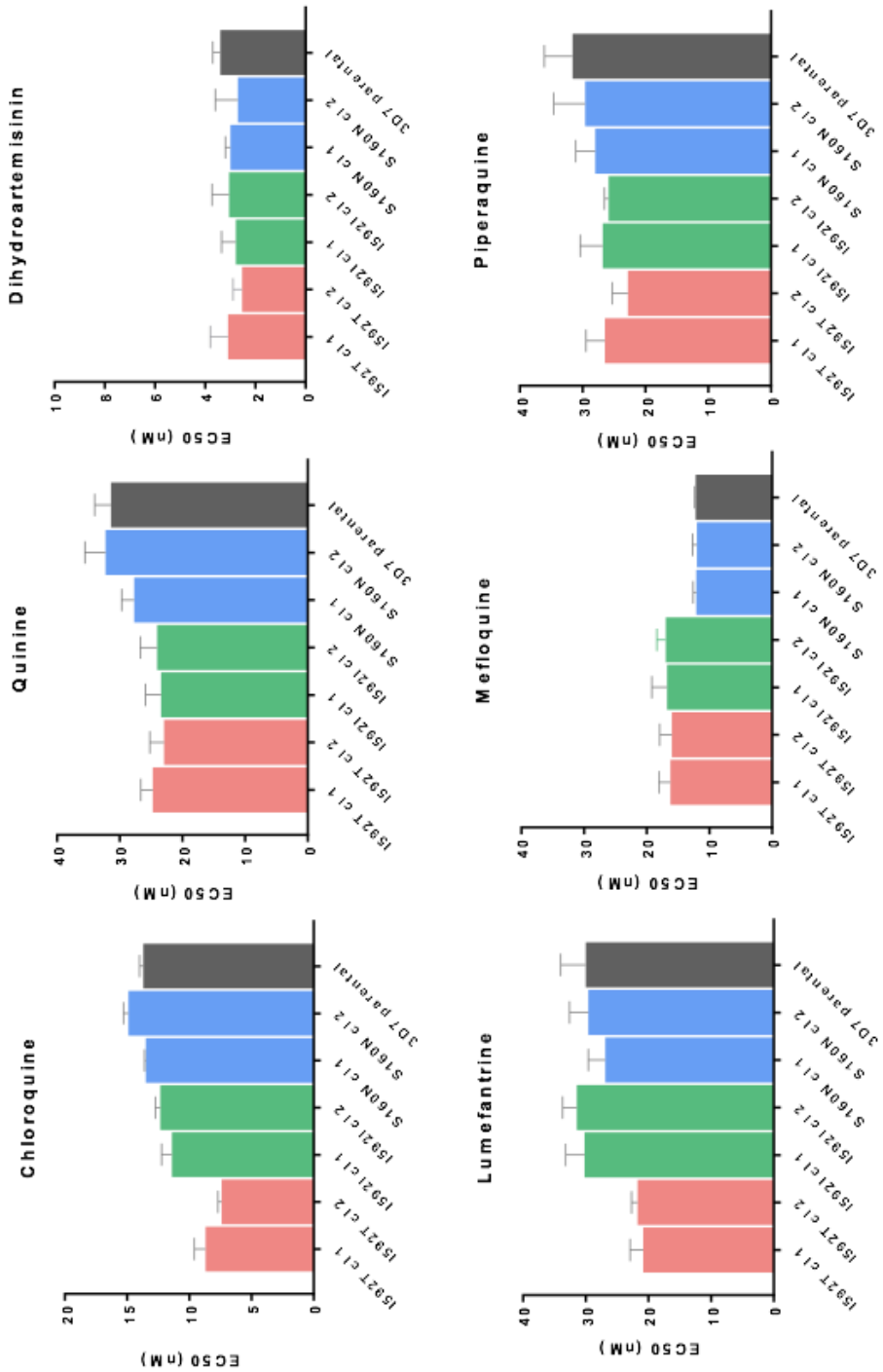


**Figure 34 Sensitivity of parasites harbouring *pfap2mu* mutations to frontline chemotherapies**
Graphical representation of the $EC_{50}$ data presented in Table 5. Displays sensitivity of transgenic parasites harbouring mutations in *pfap2mu* to 48-hour exposures to chloroquine, quinine, dihydroartemisinin, lumefantrine, piperaquine, and mefloquine beginning in the ring stage. Parasite proliferation was quantitated using the SYBR Green DNA dye as described in Section 3.4.5.1. Mean of at least four experiments each in technical duplicate with standard error shown.

This was surprising given the results of our laboratory's previous transgenic work with this mutation showing significant but small increases in dihydroartemisinin and quinine $EC_{50}$ in the same assay. The transgenic *pfap2mu* genotype was re-examined by PCR-RFLP mapping and Sanger Sequencing to rule out the possibility of a mistake in the original genotyping; however, these parasites did harbour the S160N mutation, as expected. These parasites were also fully sensitive to a 4-hour pulse of 700 nM dihydroartemisinin in the $RSA_{0\text{-}3h}^{4h}$ format validated by Yang *et al*[213]. Henriques *et al* reported that Dd2-AP2mu(S160N)$^{attB}$ was also fully susceptible to artemisinin in a 6-hour pulse format[206].

However, the sensitivity profile of the transgenic line bearing the orthologous *P. chabaudi* mutation, 3D7-μ2(I592T), displayed significant differences in sensitivity to multiple drugs. In the 48h assay format, the I592T variant displayed significantly increased sensitivity to chloroquine (clone 1: 8.7 ± 0.9 nM, clone 2: 7.4 ± 0.3 nM; 3D7: 13.7 ± 0.3 nM) and lumefantrine (clone 1: 20.9 ± 2.1 nM, clone 2: 21.8 ± 1.0 nM; 3D7: 30.0 ± 4.0 nM). There were no differences in sensitivity to quinine, dihydroartemisinin, piperaquine, or mefloquine.

As described in Section 1.6, this classic 48h drug exposure assay is inappropriate for assessing the sensitivity of parasite strains to dihydroartemisinin. This assay works well for drugs with long half-lives, but in the blood, DHA has a half-life of approximately 30 minutes. Therefore, continuously exposing parasites to artemisinin for 48 hours in a culture plate is not representative of the *in vivo* pharmacokinetics of DHA. In clinical infections, reduced susceptibility to artemisinins is known to occur exclusively in the ring stage of parasite development. In 2013, Witkowski *et al* combined these observations and designed the ring-stage survival assay ($RSA_{0\text{-}3h}^{4h}$, Section 1.6) to examine parasite susceptibility to a

physiologically-relevant concentration of and exposure to DHA[212]. Using this assay, Witkowski *et al* differentiated fast-clearing (ART-sensitive) from slow-clearing (ART-resistant) parasites in *ex vivo* cell culture, parasites that previously seemed equally sensitive to artemisinin in the classic 48h exposure assay format[212]. The RSA has since become the world standard for assessing and comparing artemisinin sensitivity.

When studied in the $RSA_{0\text{-}3h}^{4h}$, the I592T parasites displayed a significant survival phenotype, similar to what has been reported for parasites harbouring the *pfk13* mutations causing artemisinin resistance in Southeast Asia. These parasites displayed approximately 10% ring-stage survival to a 700 nM pulse of DHA. Ghorbal *et al* reported that, on the 3D7 background, the K13(C580Y) mutation causes a 13.5% survival in the $RSA_{0\text{-}3h}^{6h}$ assay format[263]. To directly compare the survival of the I592T clones with parasites bearing K13 mutations, I repeated the $RSA_{0\text{-}3h}^{4h}$ experiment with the Cam3.II-series parasites generated by the laboratory of David Fidock in parallel with the I592T clones.

The Cam3.II series consists of three parasites. The original parasite $Cam3.II^{R539T}$ is a culture-adapted clinical isolate from a patient with artemisinin-resistant parasites of Cambodian origin. This parasite was edited using Zinc Finger Nucleases to generate $Cam3.II^{REV}$, which has a wild type copy of *pfk13*, and is artemisinin-sensitive[262]. $Cam3.II^{REV}$ was then edited to install the C580Y mutation into *pfk13*, creating $Cam3.II^{C580Y}$.

In the $RSA_{0\text{-}3h}^{4h}$ format, the C580Y and R539T mutants displayed a 17.3% and 28.0% ring-stage survival phenotype; in parallel, the 3D7-μ2(I592T) parasites displayed an approximately 10% survival phenotype (cl 1: 11.2%; cl2: 9.3%). $Cam3.II^{REV}$ and 3D7 displayed an approximately 2% and 1% ring-stage survival,

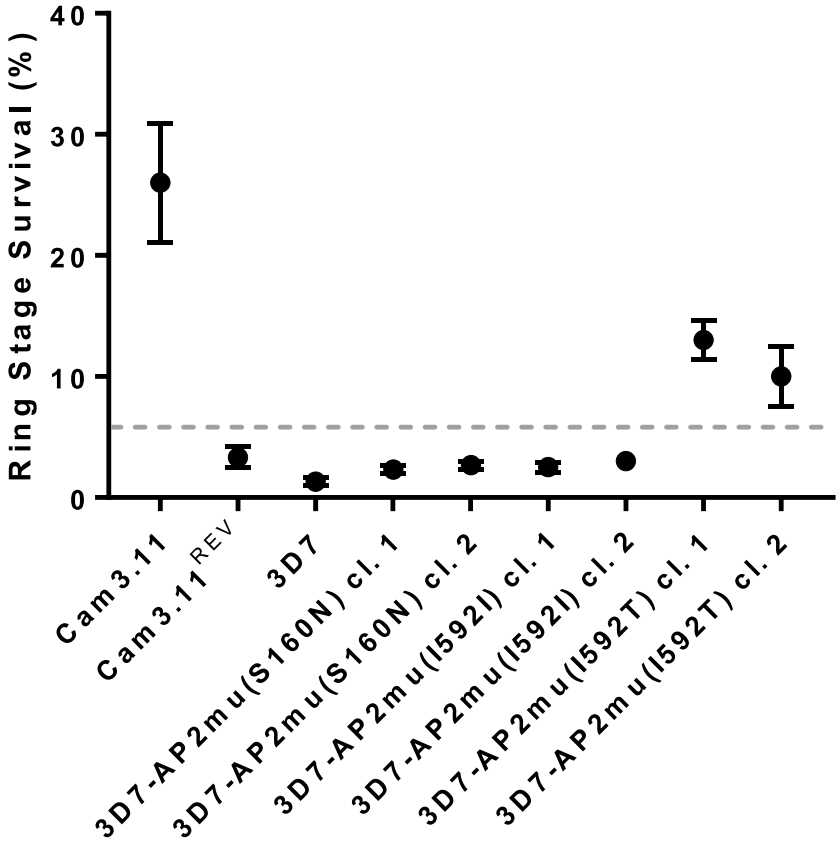


**Figure 35 Sensitivity of parasites harbouring *pfap2mu* mutations to artemisinin in a modified RSA**

Sensitivity of *pfap2mu* mutant parasites to a 700 nM pulse of dihydroartemisinin in a modified 4-hour pulsed exposure RSA. Parasites expressing µ2(I592T) have a significantly elevated ring-stage survival (cl. 1: 11.2%; cl. 2: 9.3%) with respect to parasites expressing µ2(I592I) and the parental 3D7 line (< 3% survival). Clones of µ2(S160N)-expressing parasites are equally sensitive to the parental 3D7 line. For reference, the artemisinin-resistant Cam3.II expressing $K13^{R539T}$ and $Cam3.II^{REV}$ parasites are also included. 100,000 gate-stopping events were counted in each FACS experiment. RSA survival estimates are the mean of at least 3 experiments in each performed in technical duplicate, and each technical replicate was counted twice. Standard error is shown. Survival is defined as the ratio of SYBR-positive, MitoTracker-positive events in the DHA-treated to solvent-treated samples. Hashed line indicates the cut off for statistical significance for multiple comparisons with 3D7.

respectively, which are well below the threshold for statistical significance (Fig 35). Because these data suggested the I592T mutation could cause a significant artemisinin-resistant phenotype similar to the validated *k13* mutations affecting Southeast Asia, I generated an additional parasite line bearing the wild type I592I allele with the silent shield mutations at the PAM site to ensure the changes observed were strictly due to the mutation at position 592.

The pL6-AP2μ(I592T)-sgDNA was efficiently modified with site directed mutagenesis and transfected into the 3D7 background using a ring-stage transfection. After 4 weeks, successfully integrated parasites recovered from drug selection. These independent clones were isolated by limiting dilution and genotyped with PCR-RFLP mapping and Sanger Sequencing. Two independent clones of this 3D7-AP2μ(I592I) parasite line displayed no significant differences in sensitivity to any of the chemotherapies examined in either the 48h exposure or $RSA_{0\text{-}3h}^{4h}$ assay formats as compared to 3D7, supporting that the artemisinin-resistance phenotype and potentiation of chloroquine and lumefantrine observed is solely due to the I592T mutation in μ2.

## 4.5 Generation of *P. falciparum* strains bearing Ubp1 mutations using CRISPR-Cas9 editing

To validate the role of Ubp1 in the context of drug resistance, constructs were created to install the two mutations identified in the *P. chabaudi* rodent study encoding PfUbp1(V3275F) and PfUbp1(V3306F) using the pL6 system (Fig 36). Based on the insights from generating parasites harbouring *pfap2mu* mutations, constructs were similarly designed to target *pfubp1*. A PAM site was selected to

balance proximity to the mutation site and DRA score. The region between the cut site and the PAM was recodonised to include each mutation of interest. Inadvertently, an incorrect primer was ordered which included V3306I rather than V3306F, which was not realised until after the transgenic parasites were created and sequenced. Therefore, three mutations were designed: V3275F, V3306F, and V3306I.

These constructs were transfected with pUF1-Cas9 into 3D7 using Nucleofection and selected as above. Parasites harbouring the Ubp1(V3306F) mutation are currently being generated. Successfully integrated parasites expressing Ubp1(V3306I) and Ubp1(V3275F) were obtained after three weeks. These parasites were then cloned by limiting dilution, and two clones of each construct were stored for further characterisation.

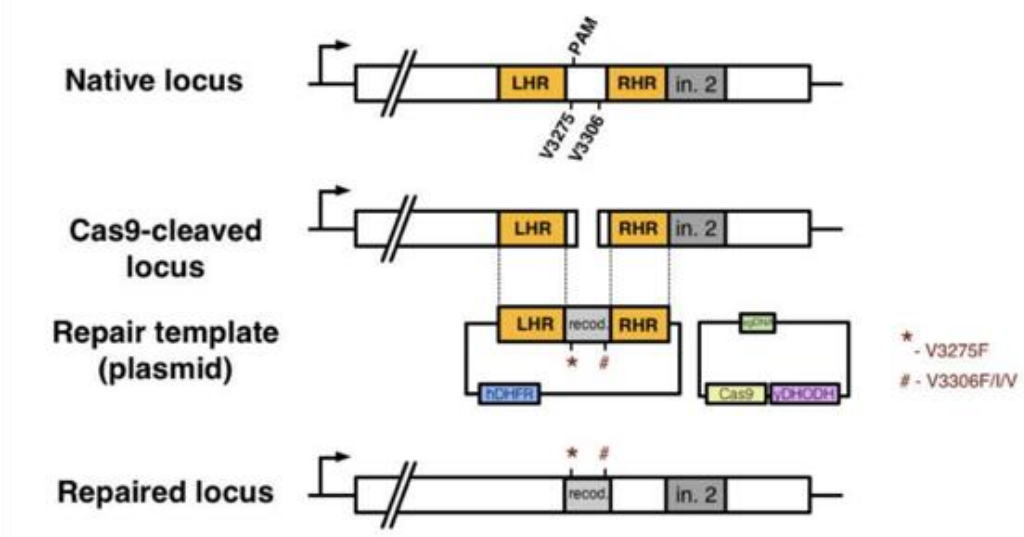


**Figure 36 Schematic for the manipulation of *pfubp1* by CRISPR-Cas9 editing**
Two constructs were designed based on the pL6 system to integrate the orthologues of the *P. chabaudi ubp1* mutations. In *P. falciparum*, these encode Ubp1(V3275F) and Ubp1(V3306F). An approximately 450 bp 5' homology region (LHR) and 250 bp 3' homology region (RHR) were designed to repair a Cas9-induced double strand break near the V3275 locus, immediately upstream of the 2nd intron.

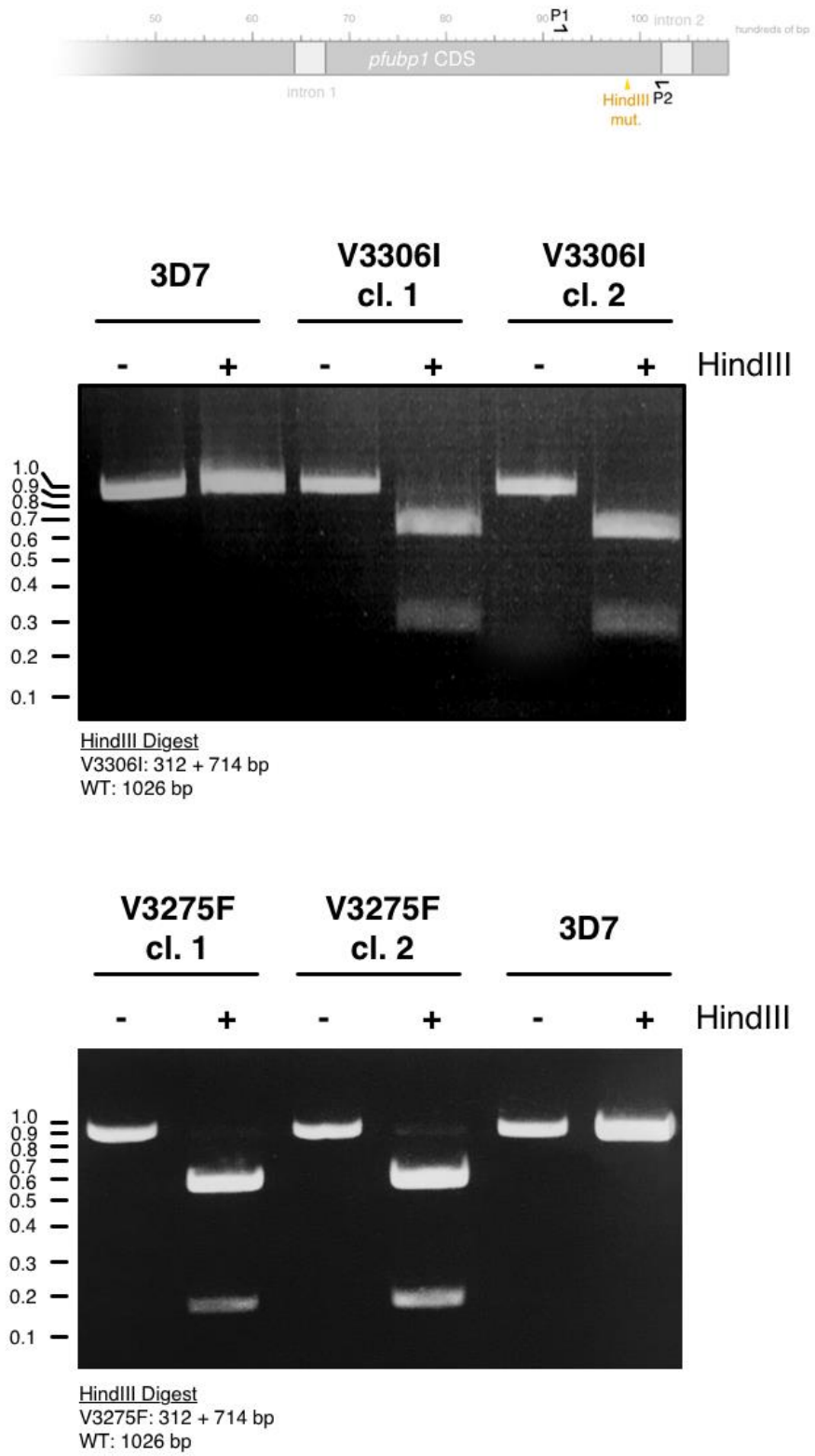


**Figure 37 PCR-RFLP mapping of transgenic parasites bearing *pfubp1* mutations**
Successfully modified 3D7 parasites harbouring the **(A)** V3306I and **(B)** V3275F mutations in *pfubp1* were cloned by limiting dilution. The genotypes for at least two clones were confirmed by PCR-RFLP mapping and Sanger sequencing. Primers for PCR-RFLP mapping were outside the 5' and 3' homology arms of the plasmid-based homologous repair template so only the chromosomal locus would be amplified. PCR products from V3306I and V3275F clones were digested with HindIII (top panel). Both transgenic mutant clones harbour a silent HindIII site (top panel). The expected restriction fragments are annotated.

## 4.6 *In vitro* characterisation of drug sensitivity profiles of transgenic *P. falciparum* lines bearing Ubp1 mutations

Two clones each of the Ubp1(V3306I) and Ubp1(V3275F) transgenic lines were characterised for their sensitivity to 48-hour exposures to standard antimalarial drugs and the ring-stage survival assay as performed for the µ2 mutants described above (Table 6).

When compared to the parental 3D7 clone, clones harbouring the Ubp1(V3306I) variant were slightly less susceptible to chloroquine (clone 1: 17.3 ± 0.5 nM; clone 2: 16.2 ± 0.8 nM; 3D7: 11.8 ± 2.0 nM), quinine (clone 1: 53.3 ± 2.5 nM; clone 2: 47.5 ± 2.8 nM; 3D7: 34.7 ± 2.3 nM), and mefloquine (clone 1: 42.3 ± 1.6 nM; clone 2: 36.9 ± 4.4 nM; 3D7: 31.5 ± 2.4 nM). However, these Ubp1(V3306I) clones were equally susceptible to piperaquine and

**Table 7 Nanomolar sensitivity of parasites harbouring *pfubp1* mutations to frontline chemotherapies**

| | V3306I cl 1 | V3306I cl 2 | V3275F cl 1 | V3275F cl 2 | 3D7 |
|---|---|---|---|---|---|
| **Chloroquine** | 17.3 ± 0.5 | 16.2 ± 0.8 | 10.8 ± 2.0 | 14.0 ± 1.9 | 11.8 ± 2.0 |
| **Quinine** | * 53.3 ± 2.5 | 47.5 ± 2.8 | 20.6 ± 6.2 | 45.2 ± 4.8 | 34.7 ± 2.3 |
| **Dihydroartemisinin** | 2.9 ± 0.4 | 2.9 ± 0.2 | 2.3 ± 0.3 | 2.2 ± 0.2 | 2.6 ± 0.1 |
| **Piperaquine** | 19.3 ± 2.5 | 16.7 ± 1.9 | 14.1 ± 0.2 | 19.7 ± 1.2 | 20.8 ± 1.2 |
| **Mefloquine** | 42.2 ± 1.6 | 36.9 ± 4.4 | 16.3 ± 1.5 | 19.7 ± 1.9 | 31.5 ± 2.4 |

The nanomolar (nM) sensitivity of parasites harbouring the V3275F and V3306I *pfubp1* variants as well as the parental 3D7 parasite was characterised to chloroquine, quinine, dihydroartemisinin, piperaquine, and mefloquine using standard 48-hour exposures beginning in the ring stage. Parasite proliferation was quantitated with SYBR Green DNA stain. $EC_{50}$'s were determined using Prism v7.0 and the variable four parameter non-linear regression analysis. Significance was calculated using a one-way ANOVA with respect to the 3D7 parent. * indicates $p < 0.05$. Two clones were analysed for each transgenic line. Mean of at least three experiments in each performed in technical duplicate with standard error shown.

dihydroartemisinin. When examined in the ring-stage survival assay, the two Ubp1(V3306I)-expressing clones were as sensitive as 3D7 to a 700 nM pulse of DHA in the early ring stage (clone 1: 4.2% survival, clone 2: 3.7% survival). Lumefantrine sensitivity is not reported in this section because $EC_{50}$'s could not be reproducibly determined. In our laboratory's hands, lumefantrine stocks are highly variable, in part because the compound has very poor solubility in aqueous media. Future work will need to characterise the sensitivity of these lines to lumefantrine.

The sensitivity of two clones of the 3D7-Ubp1(V3275F) parasites to these antimalarials was also characterised. These clones were moderately more sensitive to mefloquine than the 3D7 parental strain (clone 1: 16.9 ± 1.5 nM; clone 2: 19.7 ± 1.9 nM; 3D7: 31.5 ± 2.4 nM) and similarly sensitive to chloroquine, quinine, dihydroartemisinin, and piperaquine.

In this thesis, all RSA survival estimates determined by FACS are validated by microscopy during the first biological replicate. When the Ubp1(V3275F) clones were examined by FACS after the $RSA^{0\text{-}4h}$ experiment described in Section 4.4, they displayed a 6.7% and 7.1% ring stage survival, respectively (Fig 39A). However, by microscopy 72 hours after the DHA pulse, the parasitaemia of the DHA-treated cultures was higher than that determined by FACS with a substantial proportion of cells looking 8-12 development hours younger (Fig39B). MitoTracker Deep Red does not stain ring-stage parasites well because their mitochondria are so small (Fig 39B). Small populations of ring-stage parasites straddle the gate separating live and pyknotic parasites (SYBR-positive/MitoTracker-negative events). Therefore, to reconcile this difference in parasitaemia count, the reversible PKG inhibitor Compound 2, which blocks egress, was applied to DMSO- and DHA-treated cultures, and parasitaemia was re-examined by FACS the next day (96 HPI)[272].

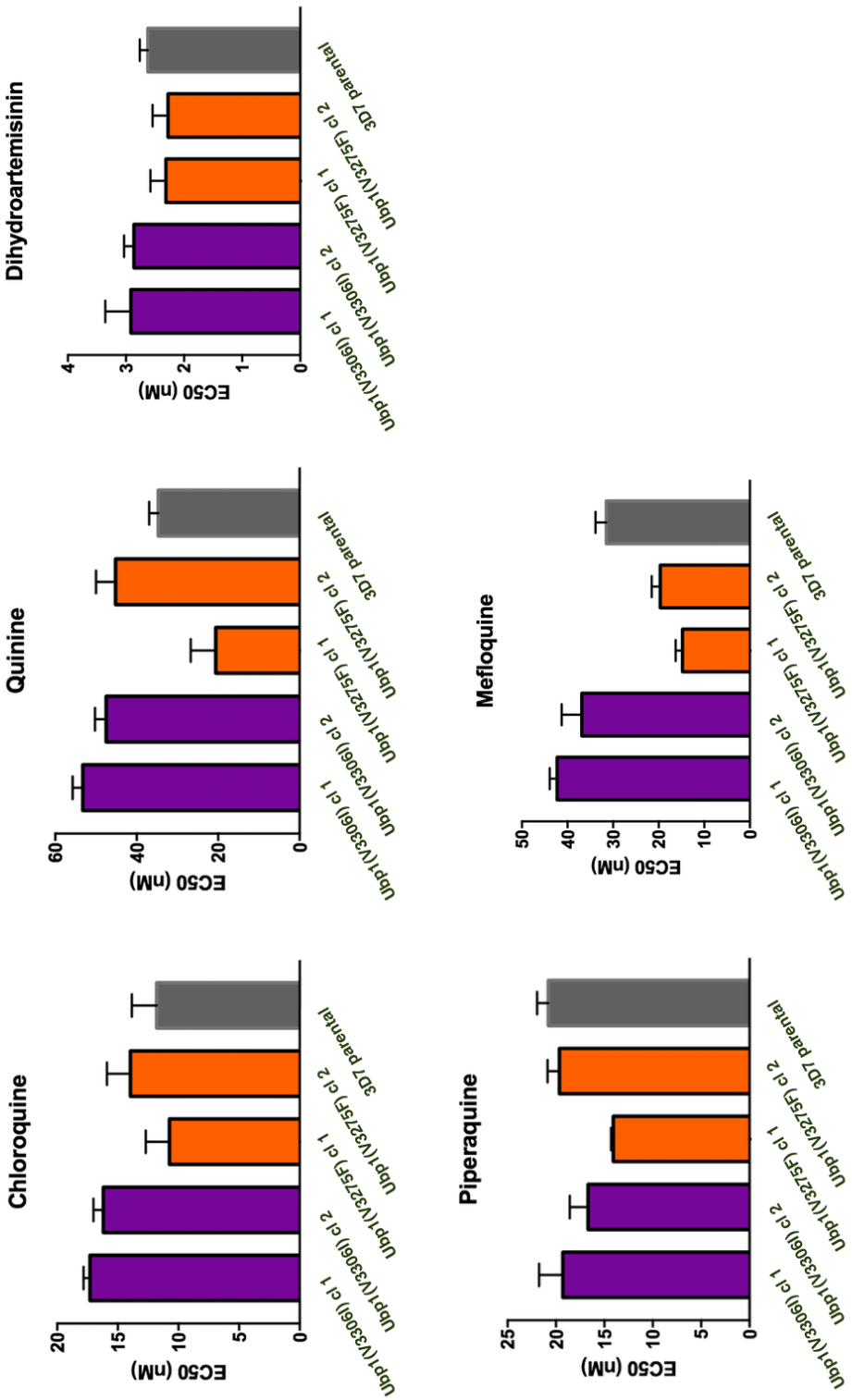


**Figure 38 Sensitivity of parasites harbouring *pfubp1* mutations to frontline chemotherapies**
Graphical representation of the $EC_{50}$ data presented in Table 6. Displays sensitivity of transgenic parasites harbouring mutations in *pfubp1* to 48-hour exposures to chloroquine, quinine, dihydroartemisinin, piperaquine, and mefloquine beginning in the ring stage. Parasite proliferation was quantitated using the SYBR Green DNA dye as described in Section 3.4.5.1. Mean of three experiments in technical duplicate with standard error shown.

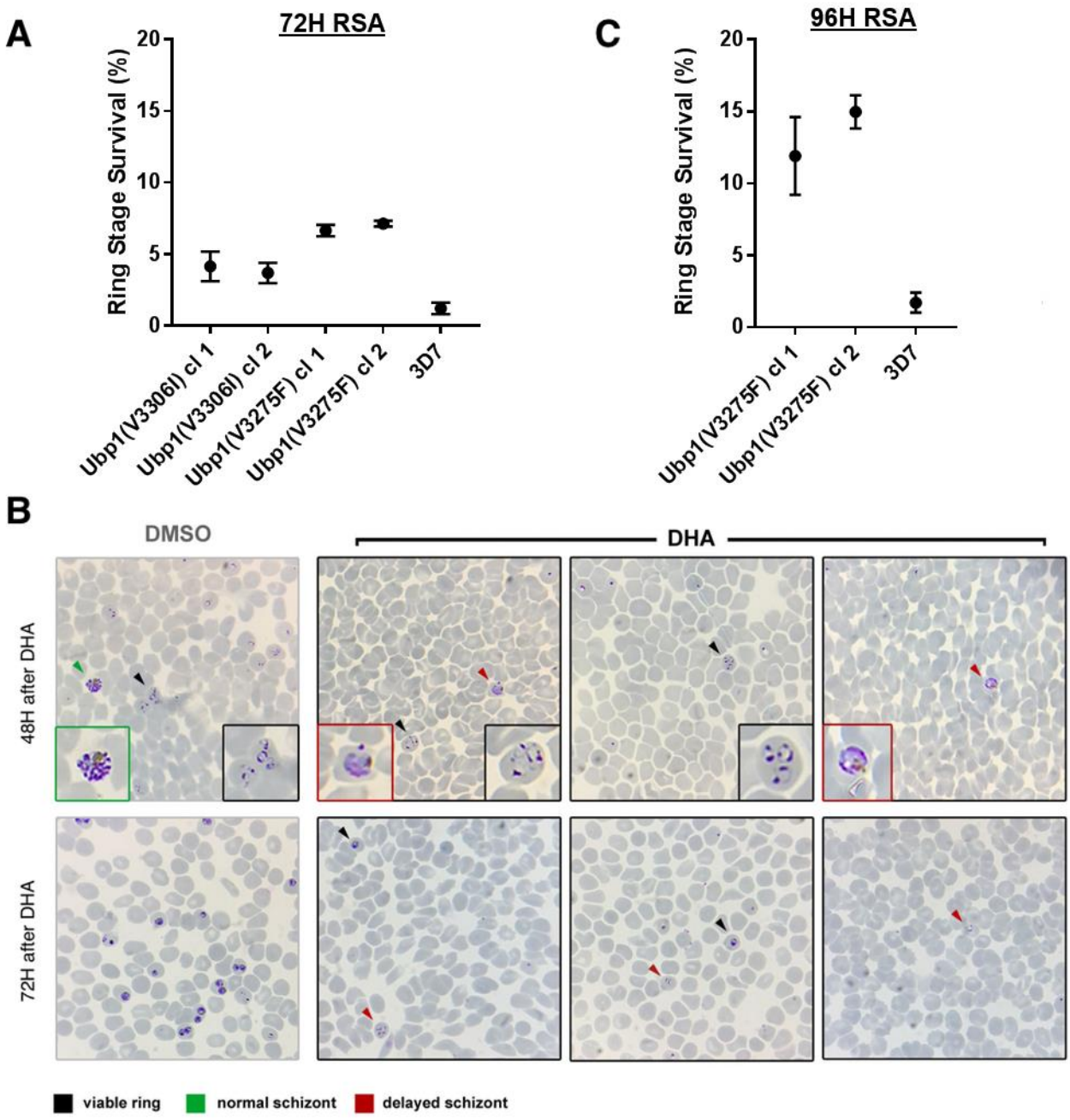


**Figure 39 Sensitivity of parasites harbouring *pfubp1* mutations to artemisinin in the RSA**
Sensitivity of *pfubp1*-mutant parasites to a 700 nM pulse of dihydroartemisinin in a modified 4-hour pulsed exposure RSA. Clones of Ubp1(V3306I)-expressing parasites are equally sensitive to the parental 3D7 line. **B** Giemsa staining of cells 48 and 72 hours after the DHA pulse reveals a developmental delay induced by DHA exposure (red boxes and arrows) in a subpopulation of cells. **C** Parasites expressing Ubp1(V3275F) have a significantly elevated ring-stage survival (cl. 1: 11.9%; cl. 2: 16.1%) with respect to parental 3D7 parasites when observed 96 hours post-invasion. 100,000 gate-stopping events were counted in each FACS experiment. RSA survival estimates are the mean of at least 3 experiments in each performed in technical duplicate, and each technical replicate was counted twice. Standard error is shown. Survival is defined as the ratio of SYBR-positive, MitoTracker-positive events in the DHA-treated to solvent-treated samples.

Without compound 2, some of these parasites would undergo egress and invasion over the additional 24-hour incubation, which would artificially increase the recounted parasitaemia. When examined at 96 hours post-invasion by FACS, the Ubp1(V3275F) clones displayed a 11.9% and 14.8% ring-stage survival, respectively (Fig 39C). The parasitaemia of DMSO-treated cells as determined by FACS did not significantly change between the two time points. All parasite lines examined in the RSA are tightly synchronised before the DHA pulse, therefore this phenomenon is indicative of a DHA-induced developmental delay in a sub-population of DHA-treated cells. When observed by Giemsa stain, there is an approximately 8-12 hour difference between these two populations of cells. Interestingly, the $K13^{R539T}$ parasites display a similar developmental split (data not shown).

## 4.7 Discussion

The data presented in this chapter are the first evidence that SNPs in genes other than *pfkelch13* can reduce parasite susceptibility to artemisinin. Specifically, mutations in *pfap2mu* and *pfubp1*, first identified in two evolved artemisinin-resistant *Plasmodium chabaudi* clones, confer similar, though less intense, ring-stage survival phenotypes as compared to *pfkelch13*-mutant parasites. Data from a recent genome-wide knockout study in *P. falciparum* suggests both proteins are required for asexual replication, though their cellular roles have not yet been resolved[273].

Without functional or structural data, anticipating the impacts of the resistance-causing mutations described above is difficult. However, homology modeling of PfAP2μ based on available structures of the mammalian AP2m1 (*pfap2mu* sequence homologue), presented in Appendix I, reveals that the I592T

mutation in PfAP2μ may disrupt van der Waals interactions between layered beta sheets in the core μ2 fold. Destabilised μ2 and its role in artemisinin resistance is explored in Chapter 6. The same modeling predicts that the S160 residue is located on an unstructured loop that does not make contacts with the other AP2 complex subunits. There is no evidence that S160 is phosphorylated in *P. falciparum*. Therefore, it may be less surprising that the S160N mutation does not modulate parasite susceptibility to frontline chemotherapies.

Additionally, homology modeling of PfUbp1 based on mammalian USP7 (*pfubp1* sequence homologue) reveals similar insights into potential functional consequences of the mutations studied in this Chapter. Specifically, V3275 is predicted to reside near the catalytic triad, three spatially grouped residues essential for DUB catalysis, whereas V3306 is predicted to reside in the ubiquitin binding pocket. The spatial accommodation of V3275F may alter the catalytic activity of the DUB domain by disrupting the orientation of the catalytic triad. Though there may be redundancy in the DUB network in the cell, Ubp1 is believed to be essential, and therefore it is surprising that parasites expressing Ubp1(V3275F) grow normally (data not shown). Experiments validating the ability of native Ubp1 to interact with ubiquitin are presented in Chapter 7, but a future biochemical characterisation of Ubp1's DUB domain and its essentiality in the cell will be instructive.

Unlike V3275 and the catalytic domain, many residues interact with ubiquitin in the binding pocket, which may offset steric consequences of mutation at V3306. This may explain why the V3306I mutation has no apparent phenotypic consequence. I have recently generated parasites expressing Ubp1(V3306F) and am currently characterising their drug sensitivity profile.

Importantly, none of the mutations identified in the *P. chabaudi* study and linked here with artemisinin susceptibility have been identified in patient isolates, and the *pfap2mu(S160N)* variant detected in these clinical samples does not seem to have significant impacts on antimalarial sensitivity in the drug-sensitive 3D7 background. Although the field data presented here suggest the S160N mutation is more prevalent after ACT treatment and in patients who fail ACT treatment, a larger sample set is necessary to have the statistical power to test these associations. Additionally, recent unpublished surveillance data show the S160N mutation arose in southwest Kenya before ACTs were introduced in the 1990s, supporting a different role for this mutation than in determining parasite susceptibility to ACTs. Further transgenic work may be required to examine the consequences of the S160N variant as well as variants of *pfubp1* near codon 1528 detected in this thesis in other representative parasite backgrounds, particularly recently culture-adapted clinical isolates. This work has been started and a protocol for transfecting these isolates is established in Appendix II.

# Chapter 5

# Functional characterisation of role of AP-2 adaptor complex and µ-subunit in *Plasmodium falciparum*

## 5.1 Generation of transgenic *P. falciparum* parasites expressing epitope-tagged µ2

Understanding the underlying biology of µ2 and the AP-2 complex has increased importance given the data presented above showing that a mutation in the µ subunit of AP-2 complex can modulate parasite susceptibility to artemisinin. Therefore, to probe the biology of this factor, the construct used to install the µ2(I592T) mutation into 3D7 background parasites was modified to instead install a triple hemagglutinin (3xHA) epitope tag onto the C-terminus of the protein with a short, flexible linker to expose the tag beyond the globular domain of µ2 (Fig 40A). The PAM site used for the I592T mutation is in close proximity to the 3' end of the coding sequence and therefore was suitable for integrating this modification. Additionally, it is reasonable to assume this guide and homology arm combination targets and modifies the desired locus well because no wild type parasites could be detected in the bulk I592T transgenic culture by PCR-RFLP mapping (not shown).

In addition to the epitope tag at the 3' end of the CDS, the inducible *glmS* ribozyme was installed into the 3' UTR immediately after the stop codon. The *glmS* ribozyme was first identified in the *glmS* gene in *Bacillus subtilis* in 2004 by Winkler *et al* and was first used in *Plasmodium falciparum* by Prommana *et al* in

2013[274,275]. The ribozyme is an inducible element that, upon binding glucosamine (GlcN), rapidly forms a hairpin structure that self-cleaves. Thus, transcribed mRNA with the ribozyme in this configuration will have the 3' UTR removed prior to translation. mRNAs which lack a 3' UTR are degraded. The ribozyme is not activated in the absence of GlcN and seems to be well tolerated by the parasite, and the degree of activation can be controlled by the amount of GlcN added to the culture medium, yielding a titratable, inducible mRNA-level protein knockdown[275]. The magnitude of the knockdown seems to vary based on the protein targeted but generally seems to be greater than 50%.

As stated, the pL6-AP2µ(I592T)-sgDNA construct was modified to include the 3xHA-*glmS* elements and was transfected with pUF1-Cas9 into 3D7 using the spontaneous DNA uptake method and selected for a week using daily changes of 2.5 nM WR99210 and 1.5 µM DSM-1. After 19 days, parasites were detected by Giemsa smear. These transgenic parasites were then cloned by limiting dilution (Section 3.4.4). The genotypes of two of these clones were verified by PCR screening and Sanger Sequencing (Fig 40B). Additionally, anti-HA western blot confirmed the presence of the tagged fusion protein (Fig 40B). Two clones were selected randomly for further characterisation. The localisation of µ2 was equivalent in both clones, and therefore the data presented hereinafter corresponds to clone 1.

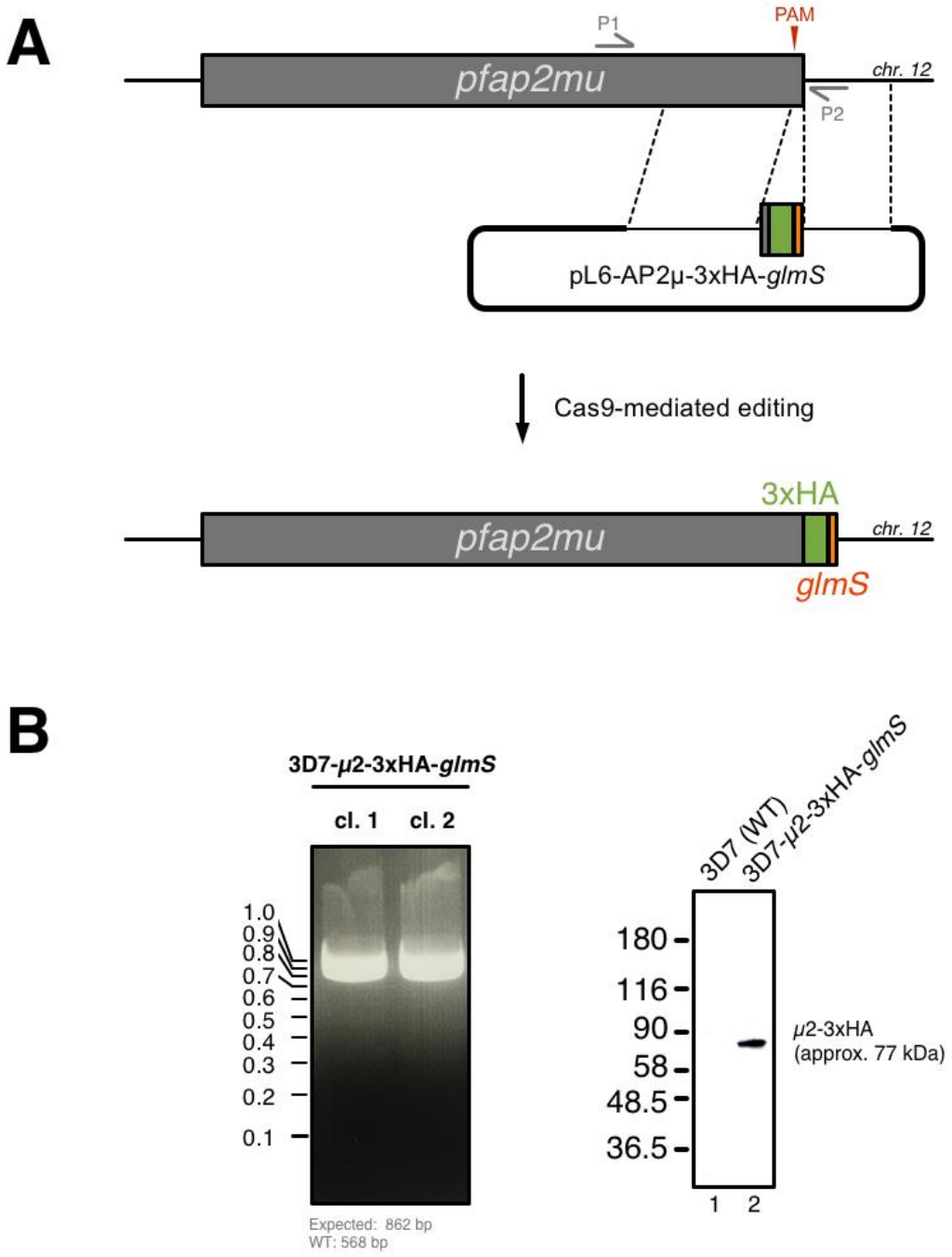


**Figure 40 Schematic for tagging of *pfap2mu* with the HA epitope and *glmS* ribozyme**
**A** Because the I592 locus is proximal to the stop codon, the pL6 construct used to introduce the I592T mutation was modified to introduce a triple hemagglutinin (HA) epitope tag into the CDS and the *glmS* ribozyme into the 3' UTR immediately after the stop codon. The homology regions were the same as used for the I592T manipulation. The *glmS* ribozyme sequence was ordered as a synthetic gBlock from IDT. **B** The genotypes of two clones was confirmed by PCR screening using primers P1 and P2 which are depicted in panel A (expected µ2-3xHA-*glmS*: 862 bp, WT 3D7: 568 bp). Anti-HA (rat, Sigma 3F10 clone, 1:5000) western blot was performed on saponin-lysed parasites from mixed stage cultures of clone 1 and wild type parasites to confirm the expression of the tagged fusion protein.

## 5.2 Examination of localisation of µ2

Given there is partial sequence homology of *P. falciparum* µ2 and human AP2m1, which mediates endocytosis, and endocytosis, at least of haemoglobin, is essential for intraerythrocytic parasite development (Section 1.7), I speculated that µ2 would be localised to the parasite periphery in the blood stage form. However, when examined by indirect immunofluorescence, I found the localisation of µ2 different from what has been observed for µ2 immunostaining in nearly all other organisms (Fig 41)[233,276–281]. First examining asynchronous cultures, rather than at the periphery, µ2 is localised to a cytoplasmic focus in ring stages that multiplies during development to provide µ2-labelled compartments or structures to each daughter merozoite. To further probe this stage-specific localisation, parasites were tightly synchronised, and slides were prepared for immunofluorescence at 6-hour windows throughout the asexual lifecycle. These studies showed that µ2 stains a focus throughout the ring and trophozoite stages before multiplying and segregating late in development during schizogony (Fig 41). In ring stage parasites, µ2 also faintly stains a perinuclear ring, (Fig 41, first panel). Interestingly, in developing trophozoites, the µ2-defined foci seem to label a conspicuous compartment proximal to the digestive vacuole (Fig 41, fourth and fifth panels). In merozoites, µ2 seems apically oriented, between the nucleus and apical complex (Fig 41, last panel). These data show that µ2 is most abundant in schizonts, which is consistent with

**Figure 41 Localisation of µ2 during asexual development**
The localisation of µ2-3xHA was characterised by indirect immunofluorescence using anti-HA (rat, Sigma 3F10 clone; 1:150) and anti-rat-488 (Invitrogen; 1:150). Transgenic 3D7-µ2-3xHA parasites were tightly synchronised to a 2 hour post-invasion window of synchrony. Thin smears were prepared every 6 hours, fixed, and stained as described in Section 3.3.7. Images were acquired on a Nikon TI-3000 inverted microscope, and post-acquisition background subtraction and deconvolution was performed using the Nikon Elements AR Analysis software package. Representative single cell windows were cropped to 200x200 pixels. Figure on next page.

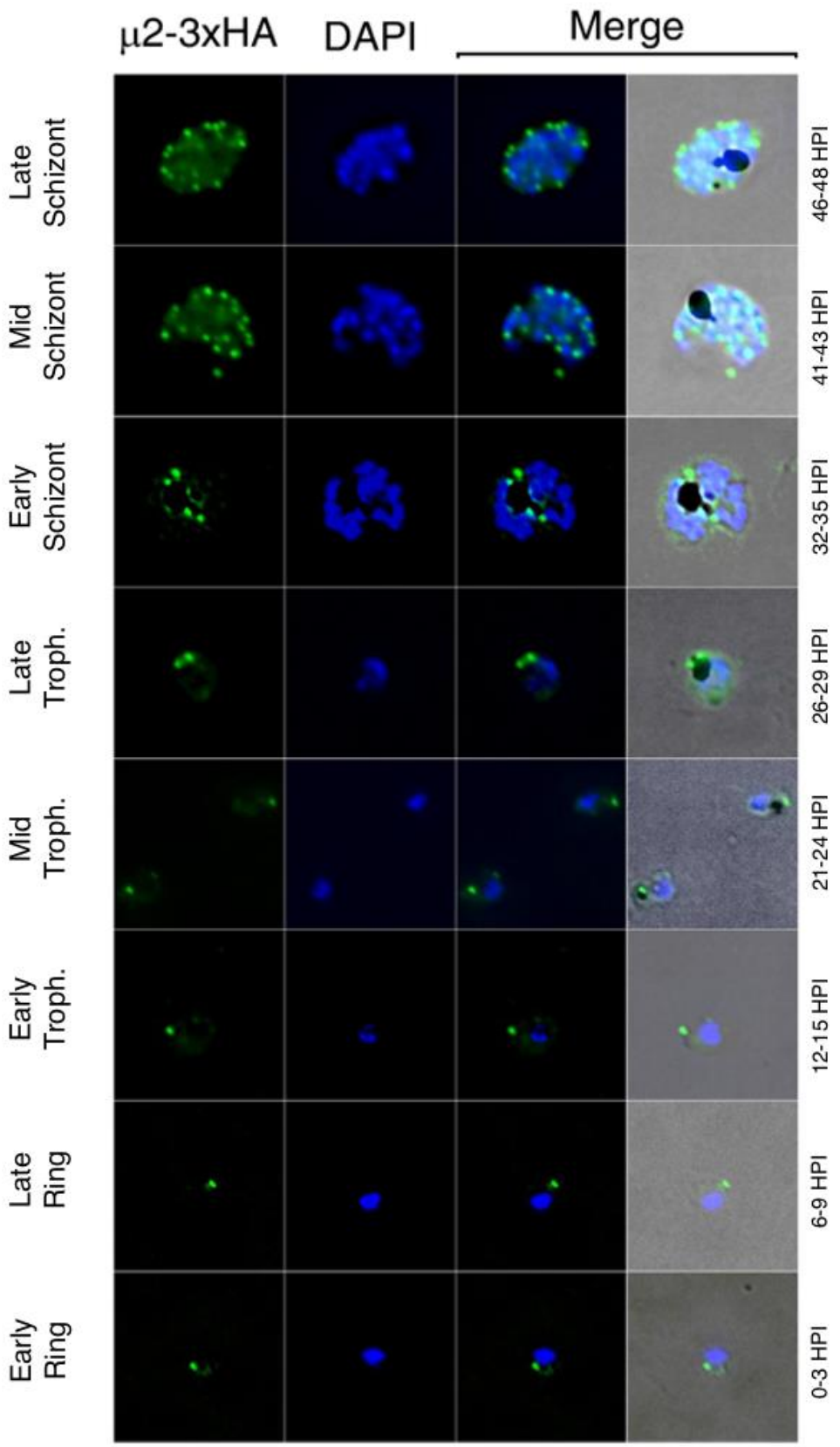
μ2-3xHA
DAPI
Merge
Late Schizont
Mid Schizont
Early Schizont
Late Troph.
Mid Troph.
Early Troph.
Late Ring
Early Ring
46-48 HPI
41-43 HPI
32-35 HPI
26-29 HPI
21-24 HPI
12-15 HPI
6-9 HPI
0-3 HPI

transcriptomic data showing the expression of *pfap2mu* increasing during schizogony, and µ2 is carried into the nascent ring via the merozoites. It is important for the interpretation of these data to note that these components of vesicular traffic only assemble and are visible at "membranes of origin", wherever the vesicle departs. In other eukaryotes, AP-2 and clathrin and their associated chaperone factors mediate cargo recognition, coat assembly, and membrane invagination and scission processes, before loading the vesicle onto the acto-myosin highway[224]. Just before the vesicle begins to move, these factors all disassemble[282]. Therefore, when observing trafficking components in live or fixed cells, one will never observe these trafficking initiation factors at the vesicle destination. In *Plasmodium falciparum*, µ2 clearly stains an intracellular compartment rather than the plasma membrane, suggesting a different cellular role for AP-2 in *P. falciparum* than what is understood to occur in all other taxa.

Additionally, though the localisation of the mutant µ2(I592T) was not examined in this study, the localisation of µ2 did not appreciably change after a ring-stage pulse with 700 nM or 5 nM DHA when examined either immediately after the pulse or 24 hours later (not shown).

## 5.3 Localisation of µ2 with markers of subcellular organelles

To better understand where µ2 is localised in the cell, correlation studies were undertaken. Specifically, I looked at markers of the endoplasmic reticulum, *cis*-Golgi apparatus, apicoplast, mitochondria, rhoptries, and microneme due to the perinuclear localisation of µ2 in ring stages, and punctate, near-DV localisation

throughout trophozoite development, and apical orientation in schizonts (Fig 42, 43). Pearson's Correlation Coefficients for co-stained images of ring and schizont stages are presented in Figure 45.

The µ2 structure with faint perinuclear extension in ring stages described in the previous section locates adjacent to and partly overlapping with both ERD2, a marker of the *cis*-Golgi and BiP, a luminal HSP70 ER-stress chaperone (Fig 42, top left panel), though these species do not colocalise. In trophozoites, µ2 staining again partially overlaps with ER staining, though there are many BiP-labelled structures not labelled with µ2 (Fig 42, first row, bottom left panel).

Given the near-DV staining, I speculated that the punctate structures were the apicoplast or mitochondria. The apicoplast is located near the DV in a conspicuous cytoplasmic focus, segregates into merozoites late in development, and is Apicomplexan-specific, which could explain the seemingly diverged localisation of Pfµ2. On the surface, an apicoplast or mitochondrial localisation would seem inconsistent with trafficking biology since the adaptins do not travel with the vesicle to the cargo destination, and these compartments are not known to export cargo molecules, though the biology of these organelles are still under investigation. In some images of parasites stained with antibodies against ACP, µ2 did overlap with some ACP-labelled apicoplast structures. However, this staining was poorly reproducible, and µ2 was clearly distinct from staining with an antibody against the apicoplast-localised AAA-type ATPase CDC48, which is involved in protein import into the apicoplast. (Fig 44, top panels), as well as MitoTracker staining, which highlights the mitochondrial lumen.

In schizonts, immunostaining against structures other than the apical complex organelles is particularly difficult because of the small size of the individual

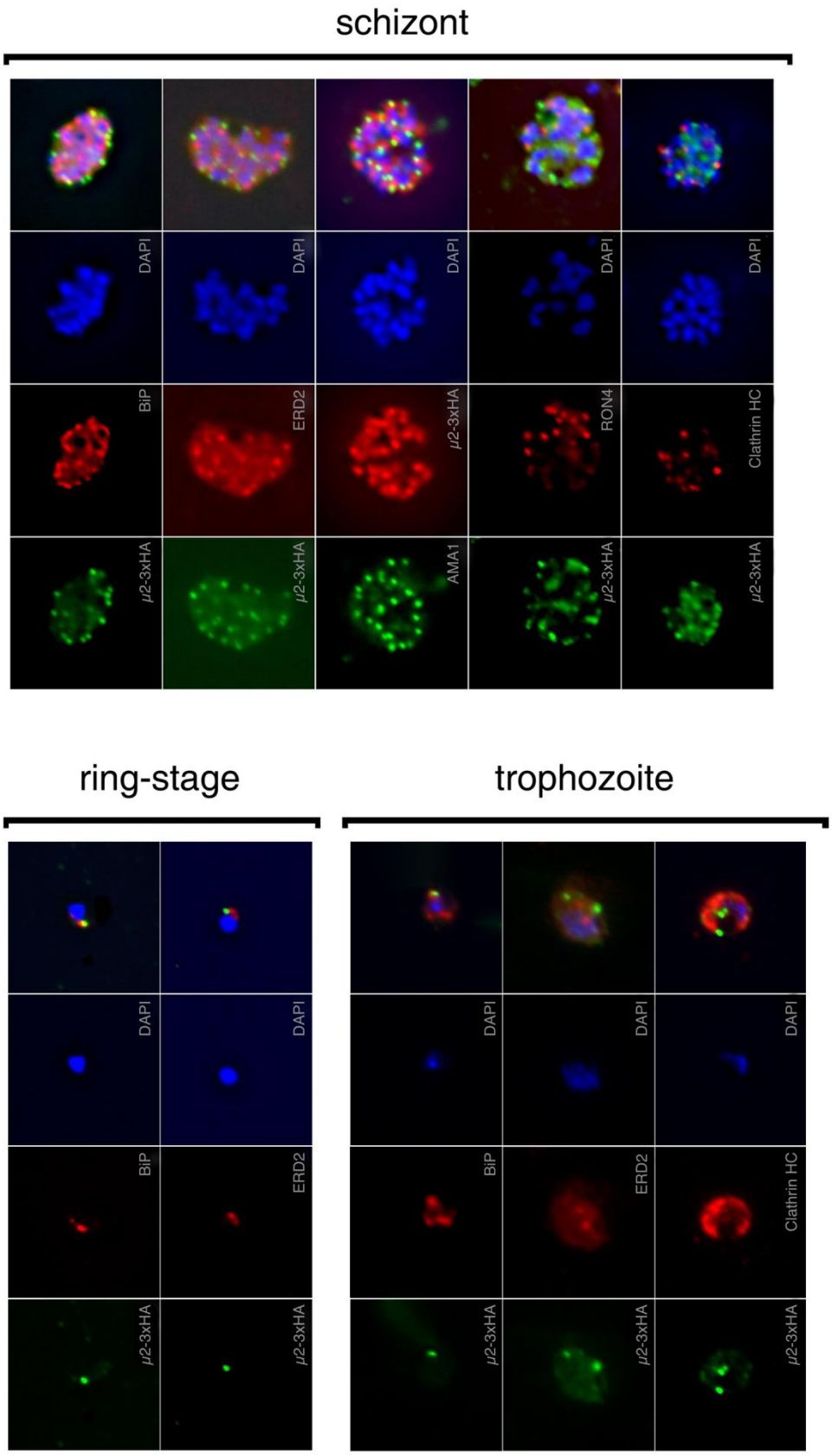


**Figure 42 Localisation of µ2 with clathrin and factors of the early secretory pathway**
Thin smears of parasites expressing µ2-3xHA were made in ring, trophozoite, and schizont stages, and the localisation of µ2 was examined with respect to the ER (anti-BiP), *cis*-Golgi (anti-ERD2), and clathrin heavy chain (anti-CHC) by indirect immunofluorescence.

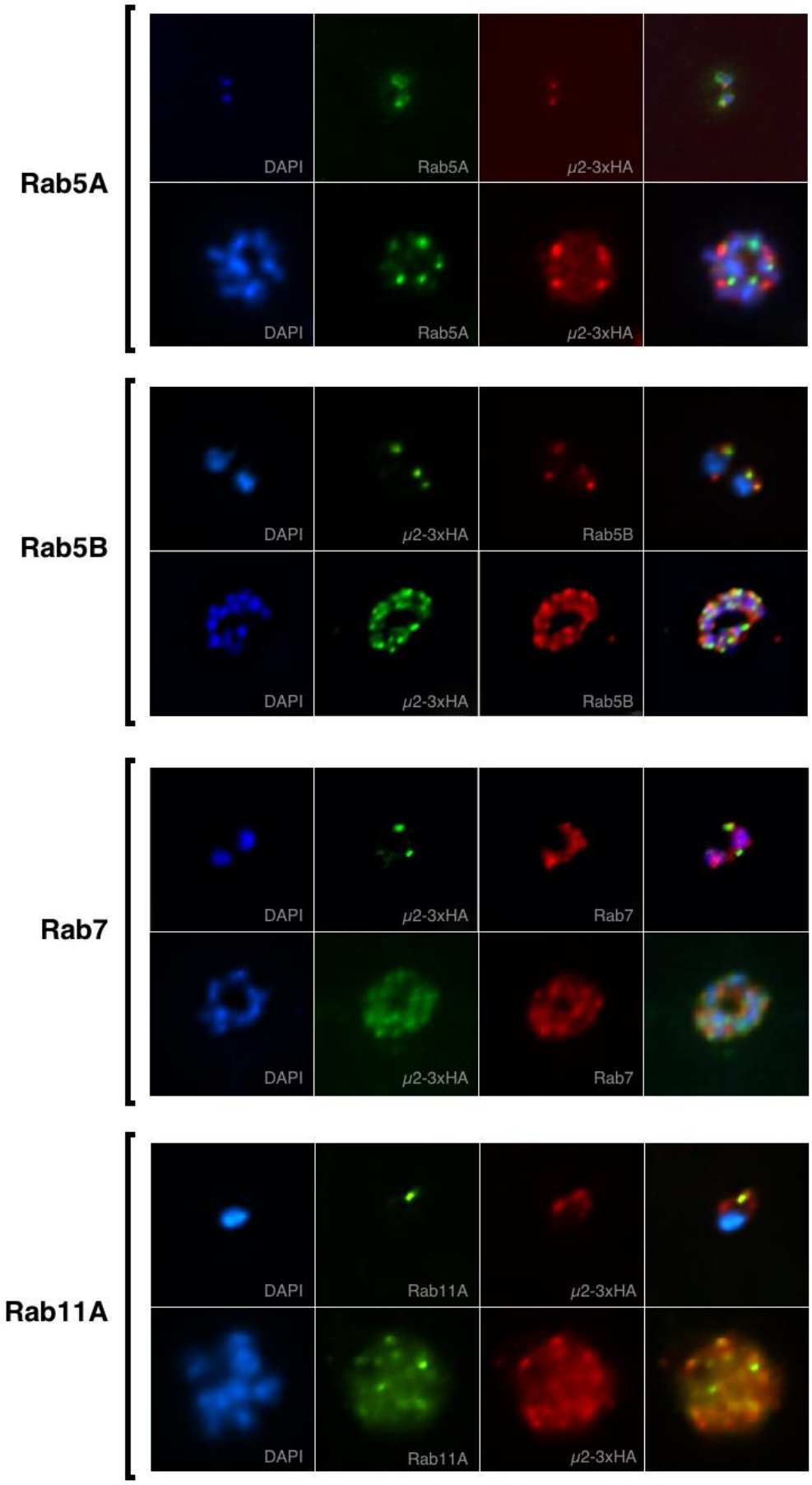
Rab5A
DAPI
Rab5A
μ2-3xHA
DAPI
Rab5A
μ2-3xHA
Rab5B
DAPI
μ2-3xHA
Rab5B
DAPI
μ2-3xHA
Rab5B
Rab7
DAPI
μ2-3xHA
Rab7
DAPI
μ2-3xHA
Rab7
Rab11A
DAPI
Rab11A
μ2-3xHA
DAPI
Rab11A
μ2-3xHA

**Figure 43 Examination of localisation of µ2 and several RabGTPases**
The localisation of µ2 with respect to several RabGTPase family members was examined by indirect immunofluorescence in trophozoites and schizonts. Rab5A, Rab5B, Rab7, and Rab11A were examined. Rab5A may be involved in haemoglobin uptake; Rab5B is implicated in targeting vesicles to the food vacuole and plasma membrane, Rab7 to post-Golgi endosomes, and Rab11A to the IMC. All anti-Rab antibodies were used at 1:150 dilution and were provided courtesy of Prof Gordon Langsley. (Figure on previous page)

merozoite, the number of merozoites in the segregating schizont, and the limits of this light microscopy resolution. The ER, *cis*-Golgi, apicoplast, and mitochondria all segregate into merozoites late in schizogony, but the staining of these structures does not correlate with µ2 staining (Figs 42,44, 45).

Given that the observed localisation pattern for µ2 does not correspond to any common macrostructures in the cell, correlation with known trafficking molecules was probed. Specifically, Rab GTPases are key effectors of vesicular traffic and are found on the cytoplasmic surfaces of vesicles and organelles[283]. Rab-specific tethers found on target membrane surfaces interact with these Rab GTPases, which mediate vesicular docking in their GTP-bound state[283]. In *Plasmodium,* Rabs are less well characterised, but they are still known to mediate specific compartment-to-compartment traffic and can thus provide insight into the trafficking routes in which AP-2 may participate in the cell.

In *P. falciparum,* there are 11 Rab family membranes annotated in the genome[284]. Several publications have provided insight into how individual Rabs function, however broadly these molecules lack extensive characterisations. Using published antibody reagents, localisation of µ2 with respect to Rab5A, Rab5B, Rab7, and Rab11A was probed. Rab5C was also probed, but the antibody stained nearly the entire cell in my hands. Though distinct Rab-specific spots were observed and an image most representative of the punctate localisation is shown in Figure 43, many images taken with these Rab antibodies contained high background fluorescence in

the cell that artificially inflated the Pearson's correlation coefficient, therefore this PCC value was not calculated for these costained cells. Any correlation between µ2 and Rab-specific spots is discussed qualitatively here, and further work is necessary to improve the resolution of this analysis.

Of all Rabs examined, punctate spots of maximum Rab5B and Rab11A intensity were localised very near those for µ2, particularly in trophozoites and schizonts (Fig 43). In other organisms, the Rab5 family are markers of the early endosome, the target of AP-2 mediated endocytosis[285]. One study in *P. falciparum* localised Rab5A by EM to vesicular structures consistent in size with small haemoglobin-containing vesicles and showed an overexpressed constitutively-active mutant form of Rab5A disrupted haemoglobin uptake and digestive vacuole integrity[191]. The cellular role of Rab5B is less clear with one study showing it is involved in traffic to the digestive vacuole and another suggesting it may be involved in targeting proteins to the parasite periphery and food vacuole via the secretory pathway[286,287]. Rab7 seems to be involved in cargo sorting at the *trans*-Golgi and mediates vesicular traffic to cytosolic endosomes[288]. Rab11A has been implicated in the biogenesis of the IMC and therefore has a potential role in late secretory traffic[289]. That µ2 may be spatially nearby both Rab5B and Rab11A suggests a potential role for the AP-2 complex in targeting towards the cell periphery. Interestingly, a recent study showed that AP-2 in human neuronal cells is also capable of mediating retrograde traffic from the endosomal system back towards the plasma membrane, which may be more consistent with these observations than a canonical endocytic role for AP-2[290].

Surprisingly, µ2 staining does not correlate with structures labelled with an antibody against *P. falciparum* clathrin heavy chain (Fig 42,45). AP-2 is one of

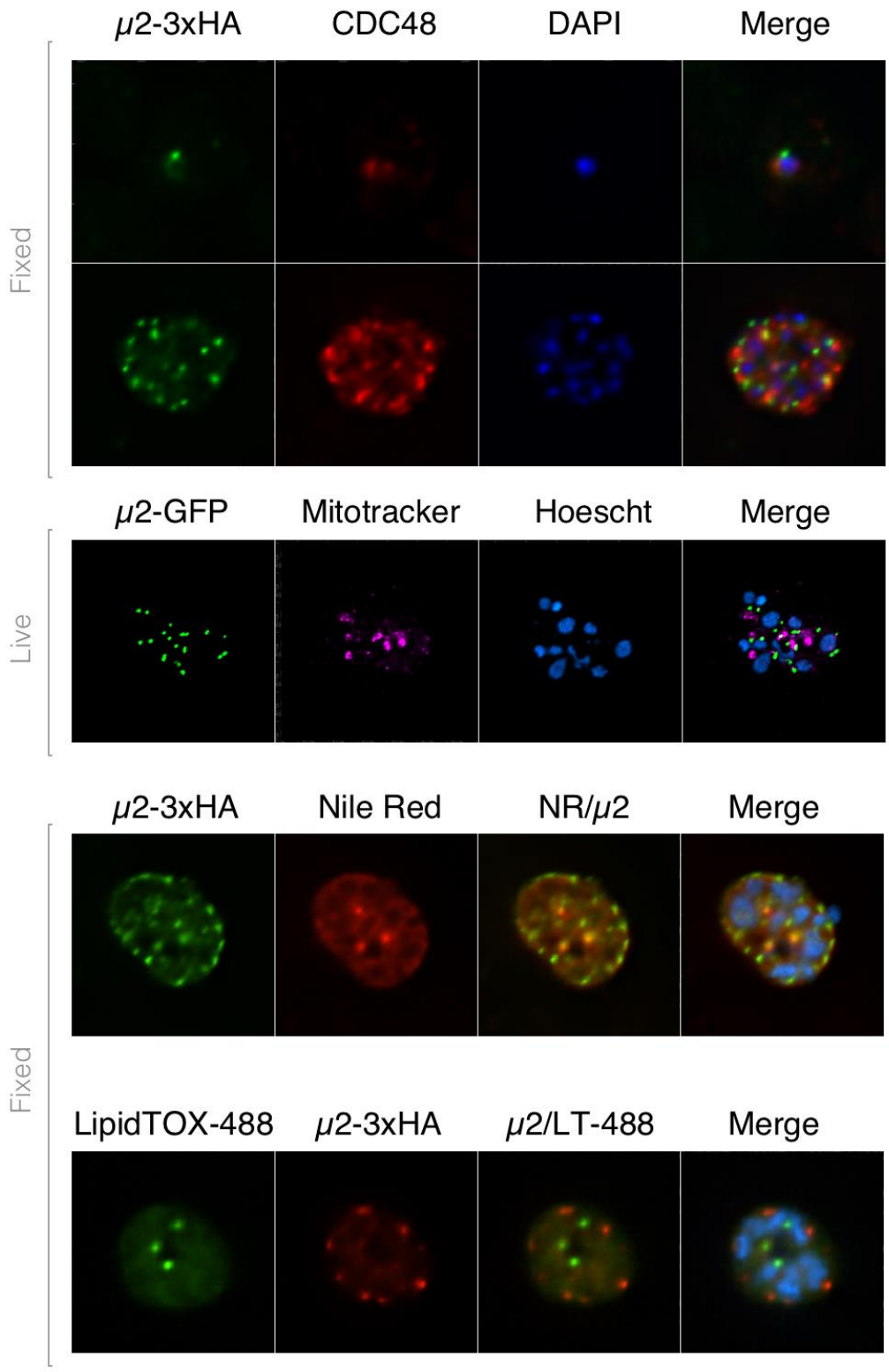


**Figure 44 Localisation of µ2 with respect to subcellular markers and lipids**
Localisation of µ2-3xHA with respect to various subcellular lipid-rich compartments was examined using indirect immunofluorescence (CDC48, Nile Red, LipidTOX-488) and live-cell imaging (MitoTracker). CDC48 (top panel) and MitoTracker (second panel) stain the apicoplast and mitochondria respectively. Though µ2 is in close apposition to the apicoplast, no correlation was observed. Nile Red and LipidTOX are lipid stains. Nile Red emits red light when interacting with polar lipids; LipidTOX stains neutral lipid deposits. µ2 correlates partially with Nile Red and not with LipidTOX, suggesting an association with membranes comprised of polar lipids. All antibodies used are described in Table 3.

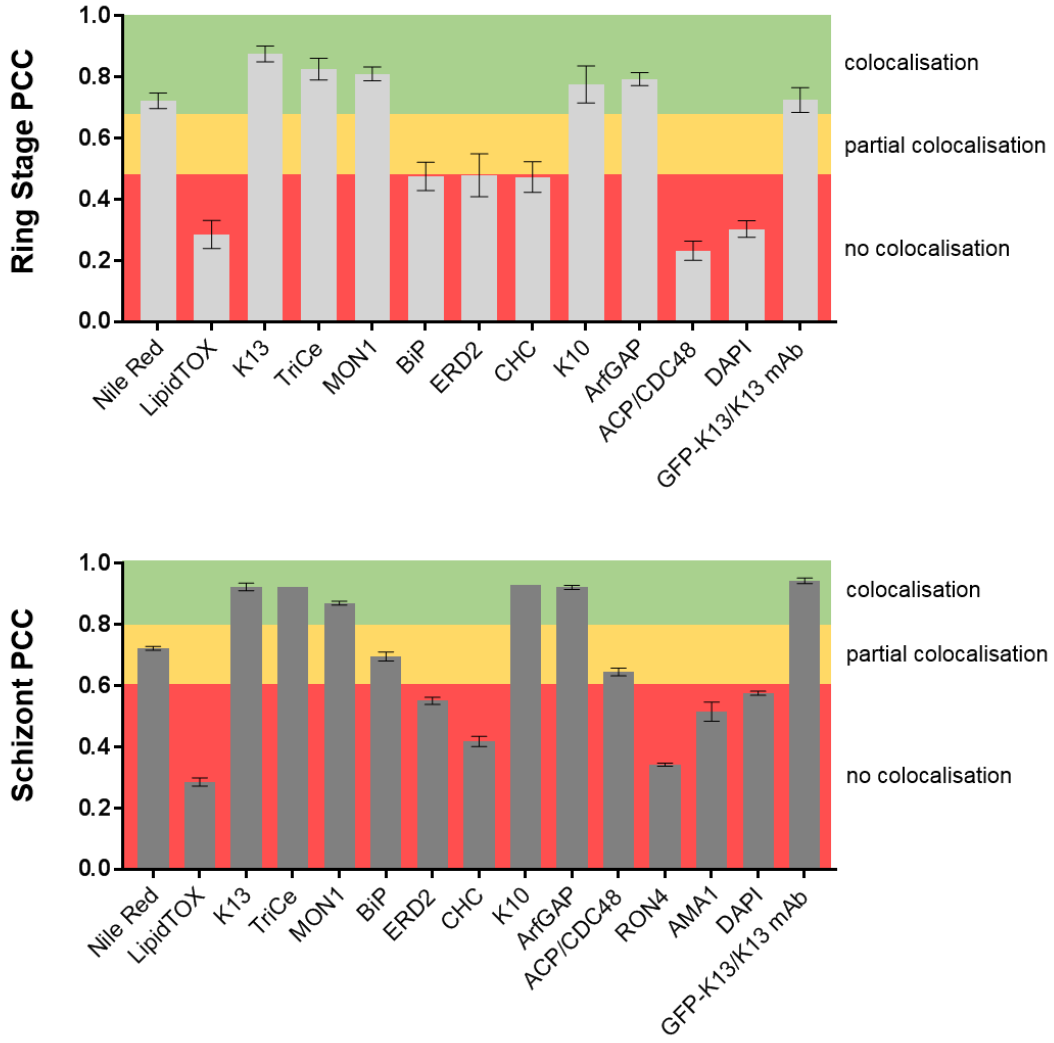


**Figure 45 Analysis of colocalisation of µ2 with subcellular markers**
Understanding that no two molecules can spatially colocalise, the correlation of fluorescent signal between µ2 and various subcellular markers was quantified using the Pearson's Correlation Coefficient (PCC) as described in Section 3.6 in the ring and schizont stages. Colocalisation with DAPI is considered a negative control and colocalisation of anti-GFP and anti-K13 signal in a parasite expressing a GFP-K13 fusion was considered a positive control. These two thresholds were used to characterise ranges of PCC values that are used to define the terms colocalisation, partial colocalisation, and no colocalisation in this thesis. The PCC metric of colocalisation is more robust on larger than smaller fluorescent objects (i.e. schizonts compared with ring stages). Therefore, the threshold for colocalisation and partial colocalisation was decreased by 0.1 units in ring stages to accommodate this and capture the positive colocalisation control. Mean PCC and standard error is shown of at least 35 cells. K10 and TRiC do not have standard error shown because less than 35 images were available for analysis.

the canonical clathrin adaptor complexes in eukaryotes, and they function together in nearly all cell types studied. A brief characterisation of clathrin heavy chain is provided in Appendix VI. To the best of our knowledge, this is the first description of clathrin in the parasite, and as discussed in greater detail in Appendix VI, clathrin heavy chain labels punctate structures at the periphery and in cytosol, consistent with what has been reported in higher order eukaryotes.

Lastly, I examine whether the near-DV structures labelled by µ2 corresponded to neutral lipid bodies. Two studies have shown these structures are involved in haem crystallisation but the details of this process remain under investigation[291,292]. Using two lipid-specific stains, LipidTOX Green and Nile Red, neutral lipids were labelled (Fig 44, bottom panels). LipidTOX stains neutral, non-polar lipids and is known to highlight conspicuous compartments closely apposed to the DV. The emission wavelength of Nile Red fluorescence depends on the polarity of the lipid environment. In neutral, polar lipids (membrane phospholipids), Nile Red is intensely red (emission maximum: 640 nm), whereas in neutral, non-polar lipids (storage lipids), Nile Red emission is blue shifted and emits yellow light (emission maximum: 590 nm). µ2 signal correlates well with Nile Red when viewed under excitation and emission parameters for red fluorescent proteins (excitation: 590 nm; emission: 620 nm), indicating a presence in phospholipid-rich bodies or surfaces, whereas µ2 does not overlap with the DV-apposed, lipid-enclosed sites of haemoglobin degradation labelled with LipidTOX Green. The Alexa-488 emission spectrum corresponding to µ2 overlaps partially with the yellow light emission by Nile Red in neutral, non-polar lipid environments. However, the lack of overlap of µ2 (when detected with an Alexa-594-conjugated secondary antibody) and LipidTOX-488, which has no spectral overlap with Alexa-594, suggests that

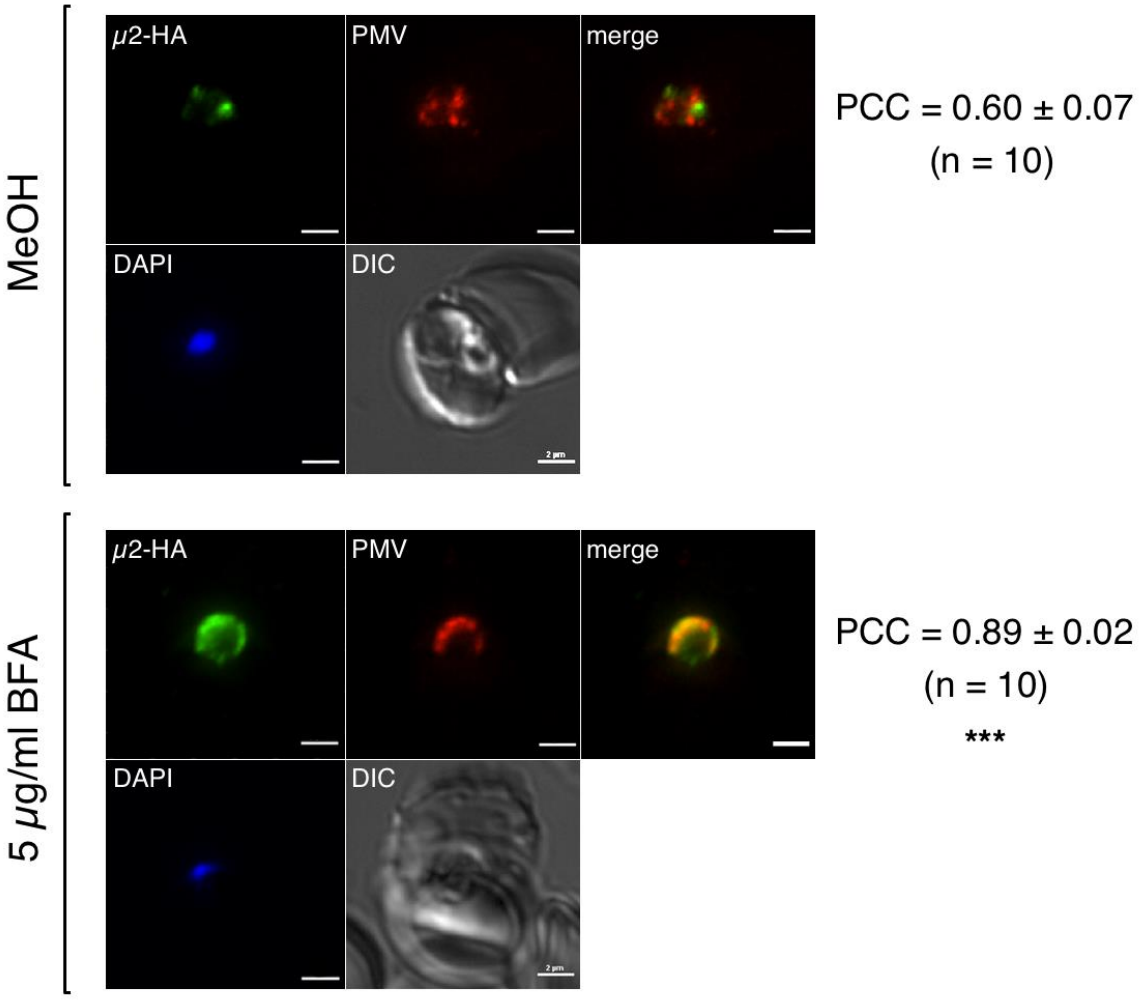


**Figure 46 Effects of Brefeldin A exposure on µ2 localisation**
The effect of Brefeldin A on µ2 localisation was examined by treating ring stage parasites expressing µ2-3xHA with 5 µg/ml BFA for 16 hours. Parasitised red cells were fixed and stained in suspension and imaged. Mean and standard error are shown for the Pearson's Colocalisation Coefficient (PCC) for the overlap between the µ2-HA and PMV signal intensities across ten cells. By a t-test of independent means, PCC are significantly different (P = 0.005).

the correlation observed with µ2 and Nile Red is indicative of a localisation of µ2 to phospholipid-rich membranes, which is also consistent with adaptor protein complex biology[224].

While performing these localisation studies, I examined whether the fungal metabolite Brefeldin A effected localisation of µ2. BFA is canonically used to investigate trafficking factors and blocks ER-exit traffic by blocking exchange of ARF-bound GDP for GTP[293]. Over time, any protein that is trafficked down the

secretory pathway accumulates in or at the ER[288,294]. To examine the effects of BFA exposure on µ2 localisation, ring stage parasites were treated with 5 µg/ml BFA or equivalent methanol solvent for 16 hours. The localisation of µ2 with respect to the ER-resident protein plasmepsin V was examined by indirect immunofluorescence. These slides revealed significant evidence of relocalisation of µ2 to a perinuclear ring from its normal punctate cytoplasmic localisation. In BFA-treated cells, µ2 staining is perinuclear and correlates well with PMV (BFA: PCC = 0.89 ± 0.02; MeOH vehicle: PCC = 0.60 ± 0.07), consistent with a localisation along the secretory pathway (Fig 46). However, BFA is cytotoxic and it is unclear whether this "relocalisation" is a result of a true secretory location of µ2 or an artefact of the cells dying. Neither µ2 nor any other AP-2 component has an ER signal sequence, though this relocalisation could occur if µ2 is peripherally associated with membranes. Though BFA relocalisation experiments can be difficult to interpret, these results are still supportive of a localisation of µ2 near the ER or in the secretory system.

## 5.4 Examination of µ2 localisation by immuno-electron microscopy

To provide greater resolution, µ2 localisation was probed by immunoelectron microscopy and immunocolocalisation on thin sections with gold-conjugated antibodies in collaboration with Dr Rachel Edwards and Prof Audrey Odom John at Washington University, St Louis.

Because ring stages are so small and difficult to capture on thin sections, localisation was examined in trophozoites and schizonts. In trophozoites, 18-nm gold particles corresponding to µ2 were consistently observed in the endoplasmic reticulum and vesicular structures in the cytosol (Fig 47, 48). In a few images, µ2 was detected at the plasma membrane; however, this localisation was seen

infrequently (<4% of all images, Table 8) and is inconsistent with the fluorescence data presented in the previous section. Additionally, µ2 was not detected on membranes forming cytostomes or any budding structures from the plasma membrane.

In *Plasmodium* parasites, the endoplasmic reticulum extends throughout the cytoplasm in long tubular structures. In a given section, it is unclear if vesicle-like structures in the cytoplasm are actually detached and free vesicles or if they are simply cross-sections of these ER extensions. To examine this, co-staining was performed with a commercial antibody against protein disulfide isomerase (PDI), an ER-resident folding chaperone (Fig 47), which was detected using a secondary antibody conjugated to 12-nm gold particles. While we cannot rule out the possibility that some of these structures are free µ2-labeled vesicles, these co-stained

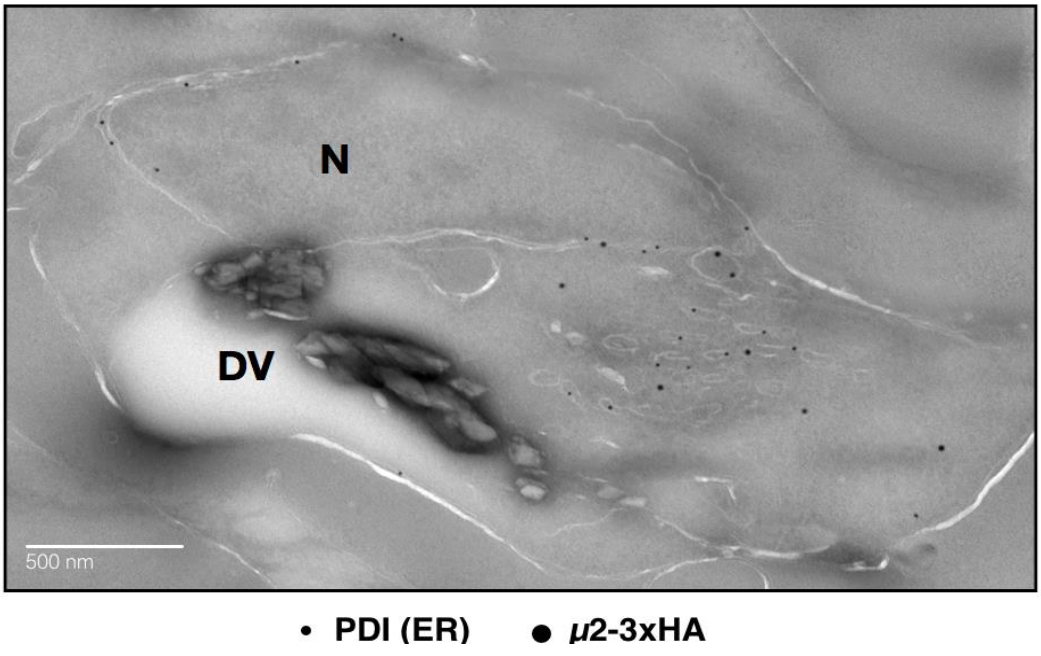


**Figure 47 Localisation of µ2-3xHA by immunoelectron microscopy**
A representative image of µ2-3xHA by immunoelectron microscopy. Localisation was examined in trophozoites. Sections were stained with anti-HA and anti-PDI (protein disulfide isomerase; luminal ER marker) to visualise µ2 in relation to the ER. A secondary antibody conjugated to 12 nm gold particles was used to label bound anti-PDI antibody, and an 18 nm gold particle-conjugated secondary antibody was used to detect anti-HA antibody. Immunoelectron microscopy in Figs 47-49 was performed by the Electron Microscopy Core Facility at Washington University, St. Louis, USA in conjunction with Dr Rachel Edwards and Prof Audrey Odom-John.

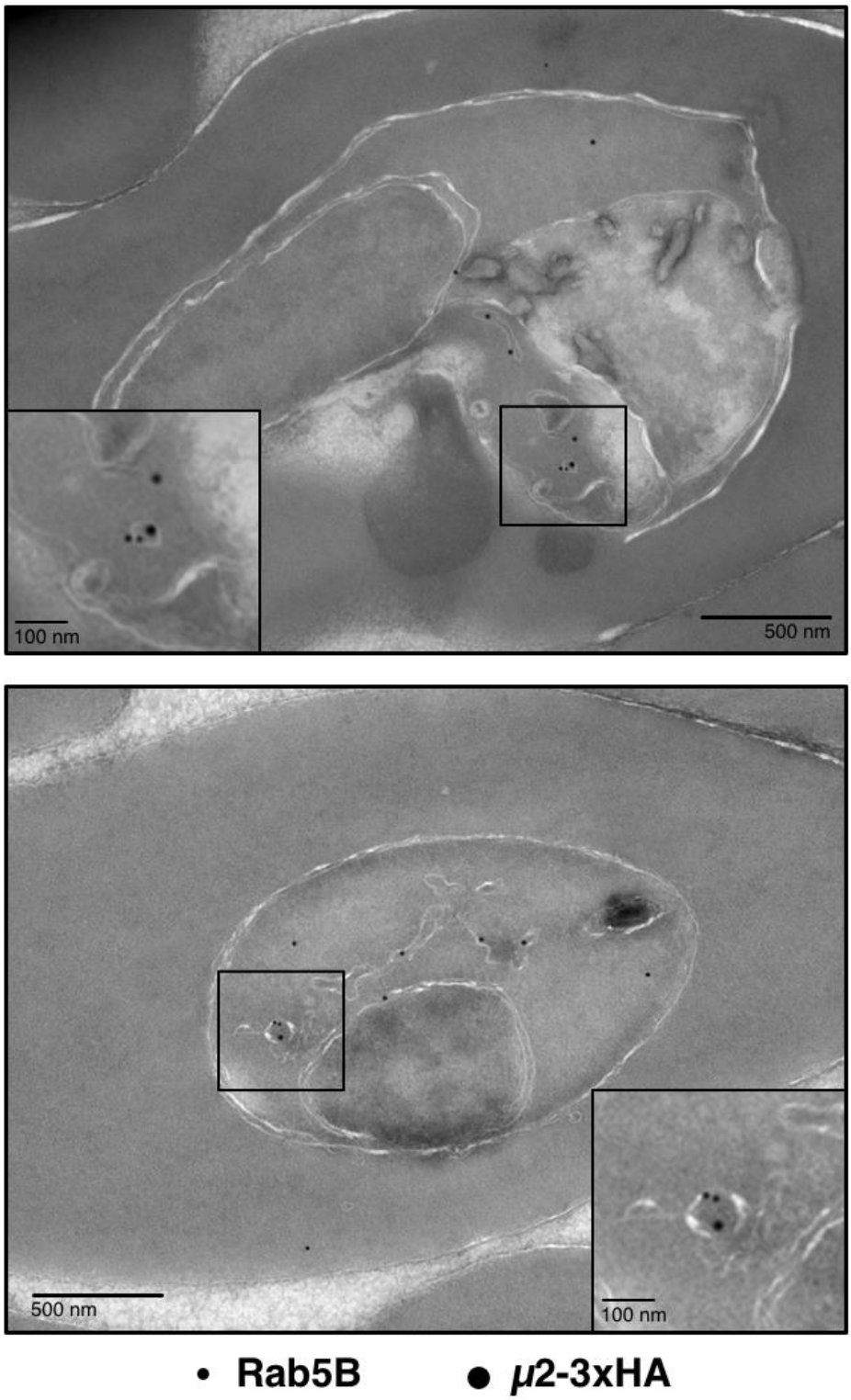


**Figure 48 Colocalisation of Rab5B and µ2 by immunoelectron microscopy**
Two representative images of µ2-3xHA colocalisation by immunoelectron microscopy with Rab5B. Cryo-preserved thin sections were probed with anti-HA and anti-Rab5B. µ2-3xHA (18 nm gold particles) localisation is consistent with that reported above, and Rab5B staining (12 nm gold particles), though few spots are detected, labels vesicle-like structures in the cytosol. µ2 label colocalises with Rab5B in cytosolic vesicles.

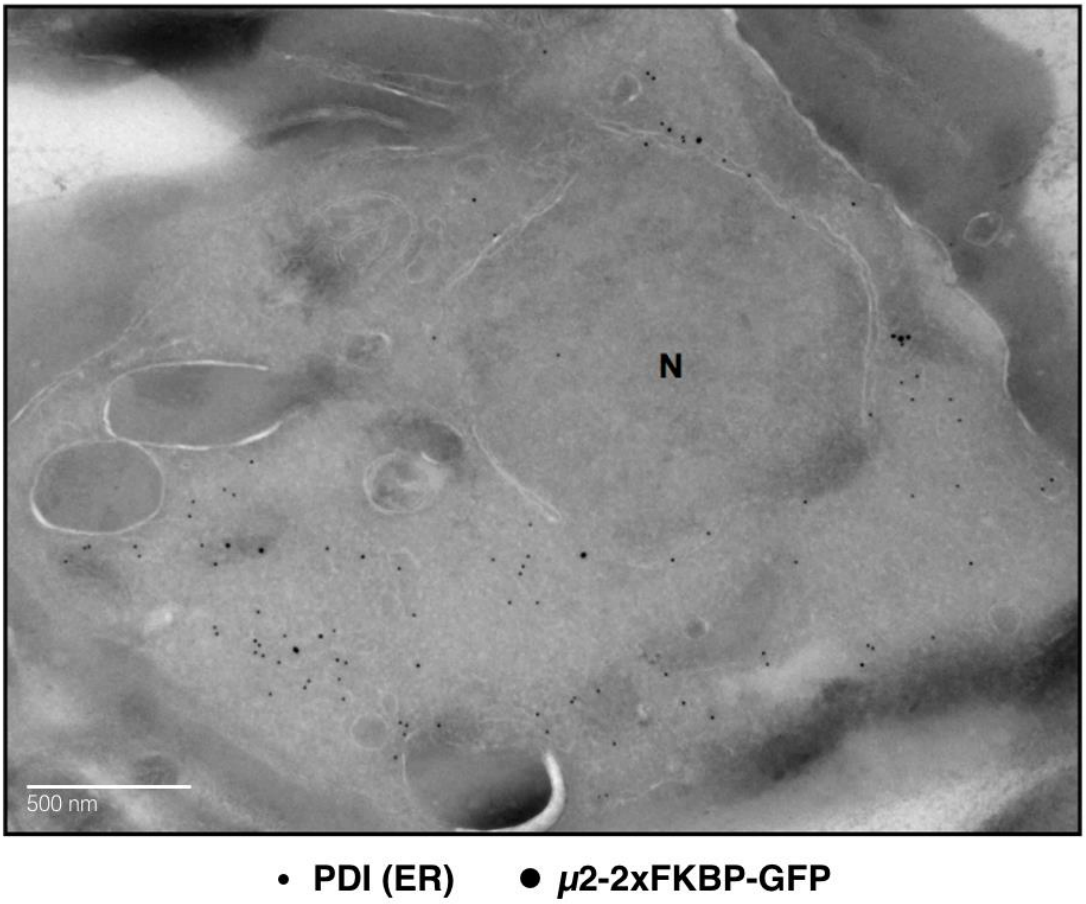


**Figure 49 Localisation of µ2-2xFKBP-GFP by immunoelectron microscopy**
A representative image of µ2-2xFKBP-GFP localisation by immunoelectron microscopy. To corroborate the localisation of µ2-3xHA observed by immunoelectron microscopy, the localisation of µ2-2xFKBP-GFP in trophozoites was also examined. Cryo-preserved thin sections were probed with anti-GFP and anti-PDI. The localisation of µ2-2xFKBP-GFP is consistent with the localisation observed for µ2-3xHA by IEM. µ2-2xFKBP-GFP (18 nm gold particles) colocalises with ER structures demarcated by anti-PDI staining (12 nm gold particles) and some vesicle-like structures in the cytosol.

images suggest that the majority of the structures in the cytoplasm are cross-sections of tubular ER extensions. Indeed, these vesicle-like structures are consistent with vesicular tubular clusters present in higher order eukaryotes, which define ER-to-Golgi trafficking departure sites[295].

Additionally, an antibody against Rab5B was used to probe the correlation reported in the previous section (Fig 48). These images resolved that a subset of cytoplasmic vesicle-like structures may co-label with µ2 and Rab5B. Without a

**Table 8 Analysis of localisation of m2 by immunoelectron microscopy**

| | μ2-3xHA | μ2-GFP |
|---|---|---|
| **Structure** | **Localisation** | **Localisation** |
| Nuclear Lamina/ER | 73.8% | 85.2% |
| DV | 5.8% | 4.3% |
| Tubular ER extension/Golgi | 93.6% | 87.6% |
| Periphery | 4.2% | 3.9% |
| Vesicles | 37.9% | 30.0% |
| Cytoplasmic (non-membranous) | 7.6% | 8.0% |

The localisation of gold particles detecting anti-HA and anti-GFP antibodies bound to μ2-3xHA or μ2-2xFKBP-GFP molecules in fixed thin sections of trophozoites expressing these fusion proteins was quantitated. In each section, the location of each spot was assigned to one of the categories listed which correspond to structures that were clearly visible and well described in the literature or co-labelled with an antibody (i.e. anti-PDI for Tubular ER extension/Golgi). Percentages indicate the number of images where the indicated structure was labelled for μ2, if it was visible. (i.e. 5.8% of images in which the DV was visible had anti-HA/GFP gold label). (All images available were analysed. N = 66 for HA-tagged μ2; N = 72 for μ2-GFP)

triple-labelled section, it is still impossible to say if these structures exist still within the ER or if they are free vesicles. However, their more circular structure seems different from the elongated, tubular structures labelled by PDI in previous images (comparing Figs 47 and 48).

While these immunoelectron micrographs support that μ2 is located at an ER interface and in cytoplasmic vesicles, they contained relatively few spots and provided little clarity on the identity of clear, singular punctate structures observed by immunofluorescence. The linear triple HA tag was initially selected to label μ2 because it is spatially small and would be unlikely to disrupt protein function. However, because it is so small, the tag may not be well exposed in thin sections, depending on the conformation of the C-terminal linker and tag when the cells are fixed and sectioned. Therefore, to try to capture more molecules per image, the 3xHA tag was swapped for a much larger 2xFKBP-GFP tag. Parasites expressing

µ2-2xFKBP-GFP were previously created by the laboratory of Prof Tobias Spielmann at the Bernhard-Nocht-Institut für Tropenmedizin in Hamburg, Germany using the selection-linked integration technique his laboratory recently pioneered. Using a polyclonal anti-GFP antibody, µ2 localisation was probed in thin sections of trophozoites prepared from this line. As expected, the same localisation pattern was broadly observed (Fig 49, Table 8).

Overall, these localisation experiments do not provide clear evidence of exactly where the AP-2 complex is in the cell. By epifluorescence, punctate structures labelled by µ2 partially correlate with the ER and known regulators of secretory traffic; by immunoelectron microscopy, µ2 clustering seems to consistent with vesicular tubular clusters. This localisation does not seem to be an artefact of the fixation method because the same punctate structures are observed when cells are fixed for immunostaining in acetone/methanol and formaldehyde either in solution or on a slide. Additionally, the µ2 localisation pattern visualised by both indirect immunofluorescence and immunoelectron microscopy was consistent between two different antibodies detecting the 3xHA and 2xFKBP-GFP tagged molecules. Overall, these experiments suggest a non-canonical role for µ2 in *Plasmodium falciparum* that warrants further functional characterisation.

## 5.5 µ2 is required for asexual growth

In other organisms, the adaptor protein complexes are necessary for cell survival[296,297]. Therefore, given the potential divergence in µ2 function from canonical pathways discovered in this study, the essentiality of µ2 for asexual

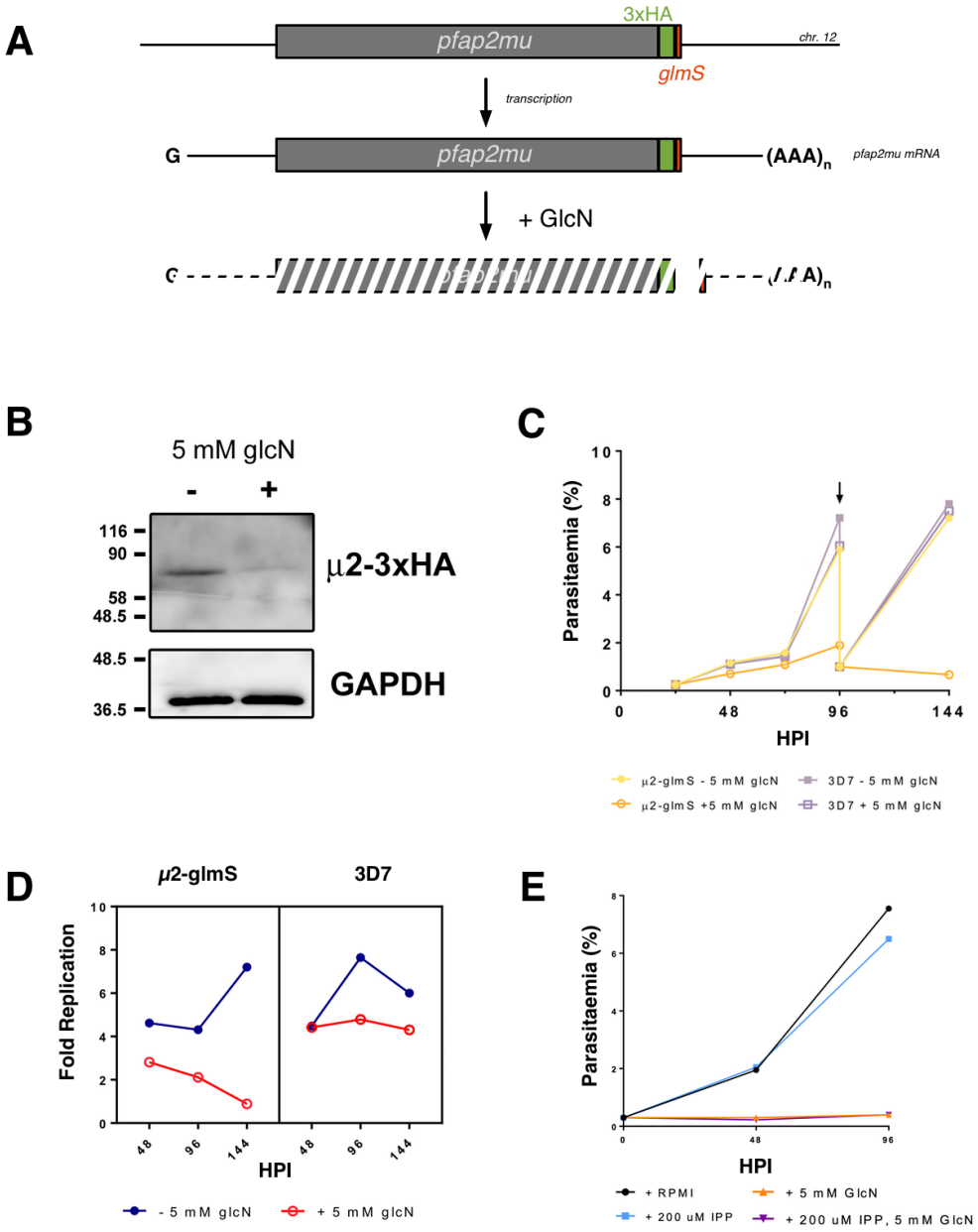


**Figure 50 Inducible knockdown of *pfap2mu* with the *glmS* ribozyme**
**A** Schematic of the integrated µ2-3xHA-*glmS* chromosomal locus and mechanism of *glmS*-mediated knockdown. In the presence of 5 mM glucosamine (glcN), the *glmS* ribozyme self-cleaves; thus, the ribozyme removes the 3' UTR from a newly-transcribed mRNA molecule, targeting it for degradation before translation. **B** Analysis of *pfap2mu* mRNA knockdown on levels of µ2-3xHA protein after two development cycles when growth fully arrests. Schizont-infected red blood cells were saponin lysed, and soluble proteins were extracted with RIPA buffer and analysed by SDS-PAGE electrophoresis and western blotting (anti-HA; and anti-GAPDH, loading control). **C** Glucosamine-induced *pfap2mu* knockdown is lethal. The growth of µ2-*glmS*-expressing parasites, determined by FACS with SYBR-Green/MitoTracker Deep Red, is significantly disrupted after two cycles in the presence of 5 mM glucosamine whereas control parasites are not. Arrow indicates that all cultures were diluted to 1% parasitaemia to prevent overgrowth over an additional development cycle. **D** Analysis of growth in (B) by determination of fold replication after each invasion cycle in control and glucosamine-treated parasites. **E** Addition of 200 µM isopentenyl pyrophosphate (IPP) does not rescue *glmS*-mediated *pfap2mu* knockdown, indicating µ2 is not involved in traffic to the apicoplast.

parasite survival was explored using the inducible *glmS* ribozyme embedded into the 3' UTR directly after the stop codon in the 3D7-µ2-3xHA-*glmS* line (Fig 50A).

To initiate the mRNA knockdown, 5 mM glucosamine (GlcN) or solvent control vehicle (deionised water) was added to early ring stage parasites in 6-well plates. Parasite medium with glucosamine or water control was refreshed daily. Glucosamine treatment induced a substantial knockdown of µ2-3xHA levels over two asexual cycles (Fig 50B). Parasite proliferation was then assessed by FACS with SYBR-Green and MitoTracker Deep Red as described in Section 3.4.5.3.

After one cycle, a 50% reduction in parasite replication was observed. However, after a second cycle in the presence of glucosamine, no further replication was observed. This delayed death phenotype was consistent across two independent clones. By knocking down *pfap2mu* mRNA in schizonts, the parasites in the next cycle are non-viable (not shown). Interestingly, no obvious, single-stage developmental stalling or death phenotype was observed by Giemsa stain during the knockdown. In some cases, some parasites seemed to die as late trophozoites, and in others, it seemed like some rings failed to develop properly after invasion.

Though these ribozyme knockdown experiments showed that µ2 is required for intraerythrocytic parasite survival, the *glmS* system only produced a transient protein knockdown rather than a complete and irreversible genetic knockout. Further, in aqueous solution, the *glmS* activator, glucosamine, is light sensitive and unstable. Though in this study and others, glucosamine was refreshed in the culture medium each day and produced a protein-level knockdown, it is not known if mRNA levels recover between doses of glucosamine as the molecule degrades. Thus, interpreting the consequences of *glmS*-knockdown of a constitutive factor like µ2 is complicated.

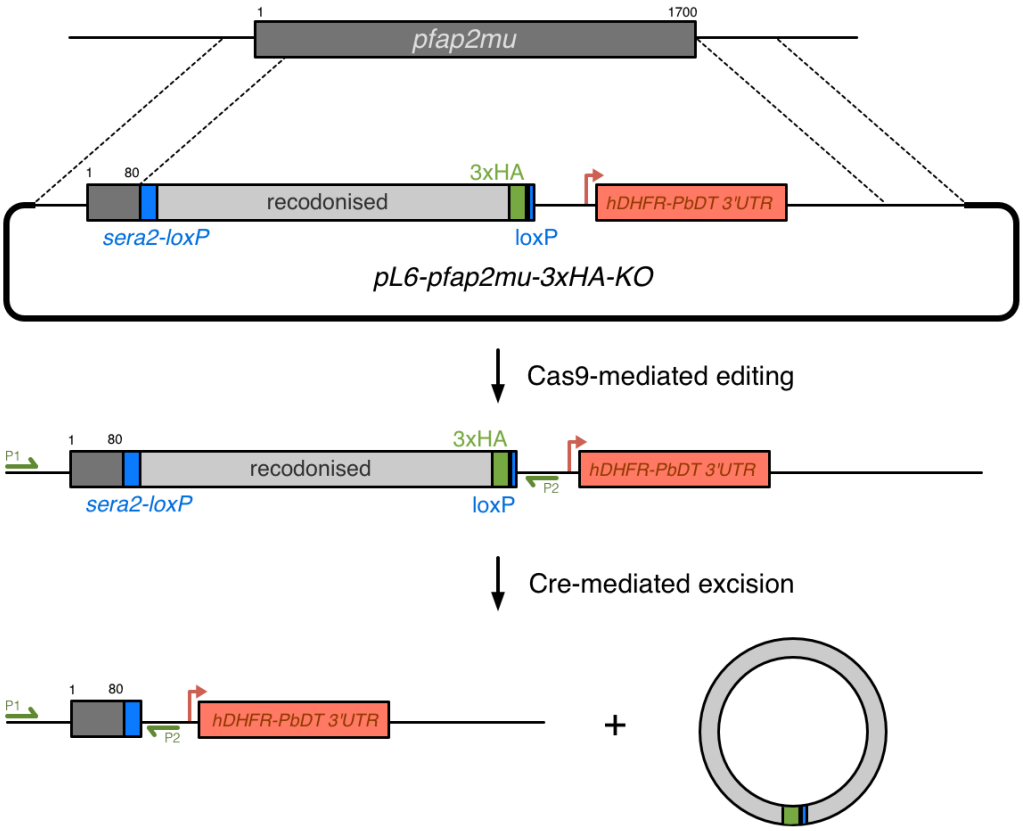


**Figure 51 Inducible knockout of *pfap2mu* by Cre recombinase**
Schematic for the inducible chromosomal deletion of *pfap2mu* with Cre recombinase. The pL6 construct used to integrate the 3xHA-*glmS* elements into *pfap2mu* was modified to install a synthetic, loxP-containing intron into the *pfap2mu* CDS near the 5' end of the gene, 1.5 kbp of recodonised CDS, and a 3xHA tag and downstream loxP site into the 3' UTR immediately after the stop codon. Additionally, a DHFR-expressing cassette was also integrated under the control of the *hsp86* promoter. These elements were efficiently integrated into the genome by Cas9 editing. The addition of rapamycin will induce the dimerisation of constitutively-expressed split-Cre recombinase, which will excise the loxP-flanked region (*"floxed"*), deleting the majority of the *pfap2mu-3xHA* CDS. Dimerisable-Cre ("DiCre")-expressing 3D7 parasites were obtained from Prof Michael Blackman. P1 and P2 indicate the annealing location of PCR primers used to examine the efficiency of the Cre-mediated knockout. P1 lies upstream of the 5' homology region encoded on the pL6 knockout plasmid construct, and thus should only amplify the transgenic locus from successfully modified parasites.

The dimerisable Cre recombinase (DiCre) system is an alternative inducible approach and can be used to permanently excise regions of a chromosome. Cre recombinase binds to *loxP* recognition sequences and loops out any sequence that is flanked with two *loxP* elements ("*floxed*"). By splitting the Cre enzyme into two halves, each fused to a rapamycin-inducible dimerisation domain, an irreversibly dimerised, active Cre recombinase is formed by the addition of rapamycin[298,299].

This system has been used to generate irreversible, inducible genetic knockouts of factors of interest in *Plasmodium* and other organisms[300,301]. Unlike the ribozyme, which reduces expression in each parasite, genetic excision is an all-or-nothing process. Though some parasites in the population may not excise the *floxed* region, this proportion of cells is expected to be very small, and all other cells will display a complete knockout phenotype.

Given the advantages of this system, a construct was designed to integrate *loxP* elements into the µ2 CDS and 3' UTR, respectively. *Pfap2mu* does not have an endogenous intron within which to embed the 5' *loxP*, therefore, the *pfsera2* intron with a *loxP* site was engineered into the CDS[266]. Even if *pfap2mu* encoded an intron in the 5' region of the gene, branch points in *Plasmodium* introns have not been well characterised, and inserting the *loxP* element blindly into any endogenous intron could block proper splicing. In 2011, Zhang *et al* described the consensus splice site sequence requirements around *Plasmodium* introns, and using these guidelines, the *sera2-loxP* "artificial intron" has been introduced into other genes without apparent consequence[266,302]. Using the same Cas9 guide RNA construct used to integrate theI592T mutation and 3xHA-*glmS* element, a homology template encoding a *floxed*, 3xHA-tagged CDS and a cassette to drive genomic expression of the human DHFR selectable marker was integrated into the endogenous *pfap2mu* locus (Fig 51).

This inducible knockout construct was co-transfected with pUF1-Cas9 into a 3D7-based *P. falciparum* parasite line provided by Prof Michael Blackman that constitutively expresses a split, FKBP/FRB-tagged Cre recombinase, which dimerises and activates in the presence of rapamycin. Parasites were selected with WR99210 and DSM-1, and drug resistant parasites were observed in culture after two weeks. This line was only recently generated and because wild type, unmodified parasites were not detected in culture by PCR, this line was not cloned so a characterisation of the consequences of *pfap2mu* knockout could be provided for this thesis. Cloning of this line by limiting dilution is underway.

These cells were seeded at 1% parasitaemia and treated with 10 nM rapamycin for 1 hour in early ring stages. After 24 hours, >99% of the *floxed*

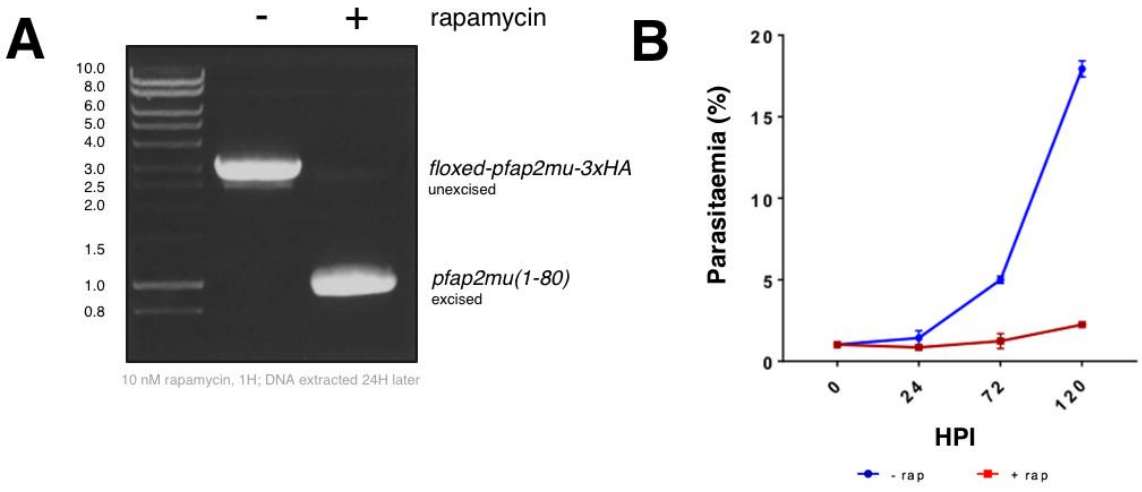


**Figure 52 Cre-mediated *pfap2mu* knockout blocks parasite development**
**A** Cre-mediated knockout was induced by adding 10 nM rapamycin to an early-ring stage culture for 1 hour. After 1 hour, rapamycin was extensively washed off. Genomic DNA was extracted from excised and unexcised cultures 24 hours after addition of rapamycin. The transgenic locus was amplified using primers P1 and P2 (Fig 52), which selectively amplify the transgenic locus. **B** Analysis of growth by FACS with SYBR-Green/MitoTracker Deep Red. Rapamycin-induced excision of *pfap2mu* disrupts parasite growth within 1 development cycle.

*pfap2mu* region had been excised (Fig 52A). Parasite development was monitored by Giemsa staining and FACS every 24 hours. Parasite development proceeds normally until schizogony, when there is an obvious defect in merozoite formation and segmentation (Fig 53, middle panel). Rather than segmenting normally into distinct daughter merozoites within the parasitophorous vacuole, *pfap2mu*$^{-}$ schizonts contain merozoites that seem to stay linked as beads on a string (Fig 53, middle panel). Additionally, these defective schizonts occupy approximately 50% less volume within the erythrocyte compared to wild type schizonts (Fig 53, left panel).

Even though merozoite formation does not proceed normally, the parasitophorous vacuole seems to rupture, and the defective merozoites stay connected within the red blood cell, even with an additional 12 hours of incubation on an orbital shaker (Fig 53, right panel). By FACS, *pfap2mu*$^{-}$ parasites do not

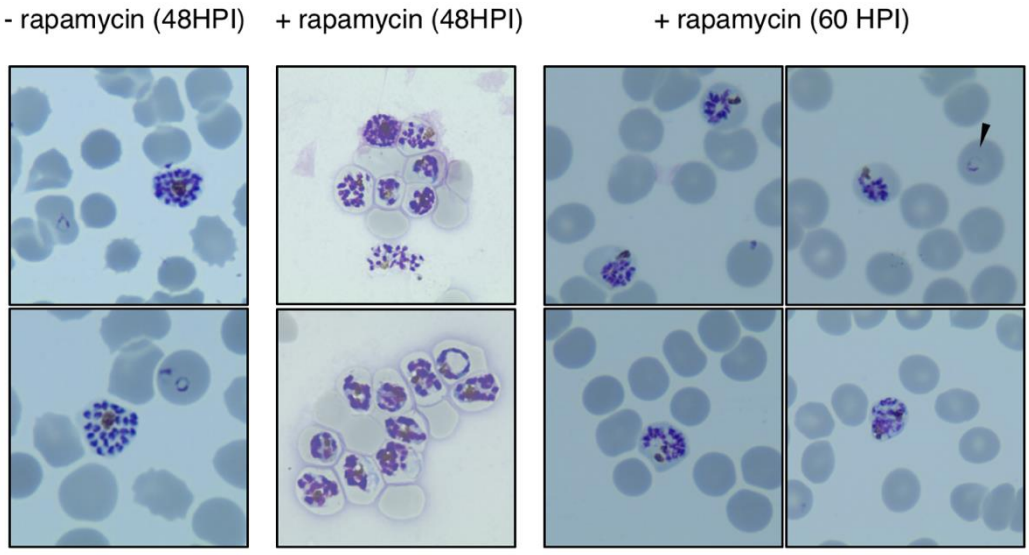


**Figure 53 Examination of the effects of *pfap2mu* knockout by Giemsa staining**
48 hours after the addition of rapamycin, parasites lacking *pfap2mu* display an abnormal schizont phenotype. Solvent-treated parasites (left) are well segmented and occupy the entire volume of the infected red cell; some parasites have undergone egress and invasion. Rapamycin-treated parasites (middle) have not properly segmented and few parasites have undergone egress and invasion. These cells were imaged 12 hours later and still had not segmented properly or egressed (right). *pfap2mu*$^{-}$ merozoites do not fill the red cell volume and seem linked together by an unknown structure. Some cells have undergone egress and invasion, though these may not have successfully excised *pfap2mu* or may not have integrated the knockout transgene (this is an uncloned parasite line).

proliferate (Fig 52B). When rapamycin is added in the ring stage, even up to 24 hours post-invasion, parasites mostly do not complete development and proliferate. Though some new rings are observed and parasitaemia does gradually recover, this is expected because this parasite line was not cloned. Therefore, this residual population is likely consists of either unintegrated or unexcised parasites, which recrudesce with time following a single treatment with rapamycin.

## 5.6 Effect of *pfap2mu* knockout on cell development

These data show that µ2 is required for parasite development and revealed a visible defect in schizont maturation resulting from *pfap2mu* knockout. To better characterise the nature of this developmental requirement, the DNA content of each cell and the integrity of several organelles were examined. Synchronous early ring stage 3D7-µ2-*floxed*-HA parasites were treated with 10 nM rapamycin or equivalent DMSO for 1 hour and incubated at 37ºC. Media was refreshed 24 hours after rapamycin treatment. When parasites reached the late trophozoite stage, 10 µM Compound 2 (reversible protein kinase G inhibitor; Table 4) was added to prevent wild type cells from initiating egress. Cells were closely monitored by Giemsa staining until approximately 75% of wild type cells were well segmented; cells were kept in this Compound 2 block for less than 2 hours.

To examine whether *pfap2mu*$^{-}$ cells display a defect in nuclear replication, 100 µl of rap- or DMSO-treated egress-blocked culture was mixed with an equal volume of 1:5000 SYBR Green in PBS and analysed by flow cytometry. Overlaid histograms plotting the SYBR-Green signal detected across all gate-stopping events indicates there is no significant difference in DNA content between WT and KO

schizonts, suggesting DNA replication occurs normally, and the defective schizonts have the same DNA content as wild type schizonts (Fig 54).

Thin smears were also prepared from these DMSO- or rapamycin-treated cultures in order to probe the localisation and integrity of key markers of subcellular structures by indirect immunofluorescence. Specifically, the localisation of plasmepsin V (ER), ERD2 (*cis*-Golgi), GAP45 (IMC, soluble), GAP50 (IMC, transmembrane), MSP1 (plasma membrane), EXP2 (PV), CDC48 (apicoplast), AMA1 (micronemes), and RON4 (rhoptries) was examined (Fig 55). Between knockout and wild type cells, the ER and *cis*-Golgi appeared equivalent in morphology and distribution.

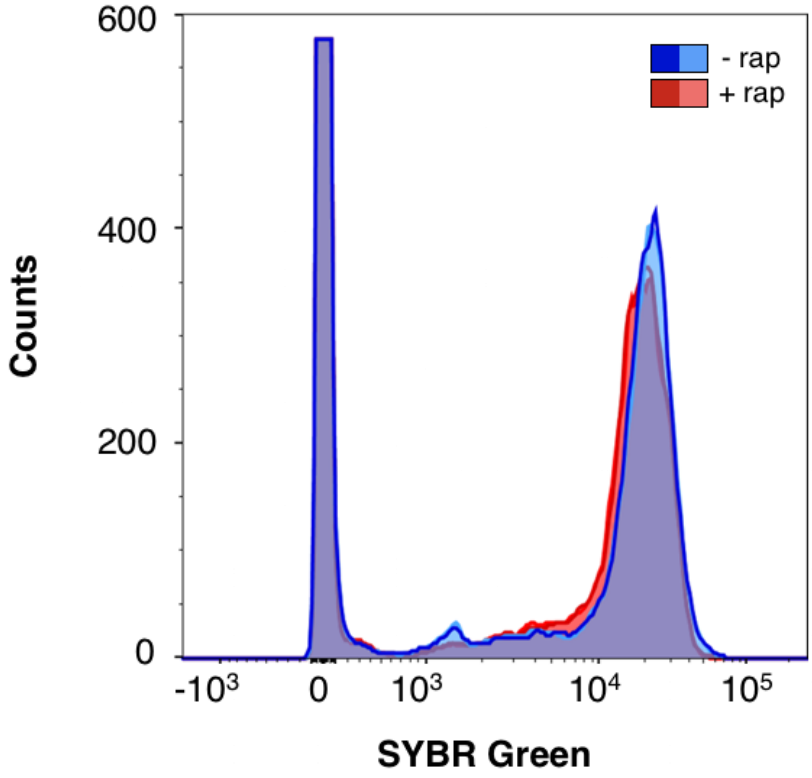


**Figure 54 Comparison of DNA content in *pfap2mu* KO and WT parasites**
Compound 2-blocked *pfap2mu* knockout (red traces) and wild type (blue traces) schizonts were stained with SYBR Green (1:10,000; Molecular Probes) and analysed by FACS (LSR-II, BD Bioscience). Wild type and knockout samples were analysed twice, and each FACS analysis corresponds to 100,000 gate-stopping events. Cell population around 0 SYBR Green absorbance units corresponds to uninfected red cells. Overlays were created using FlowJo version X, showing technical replicates.

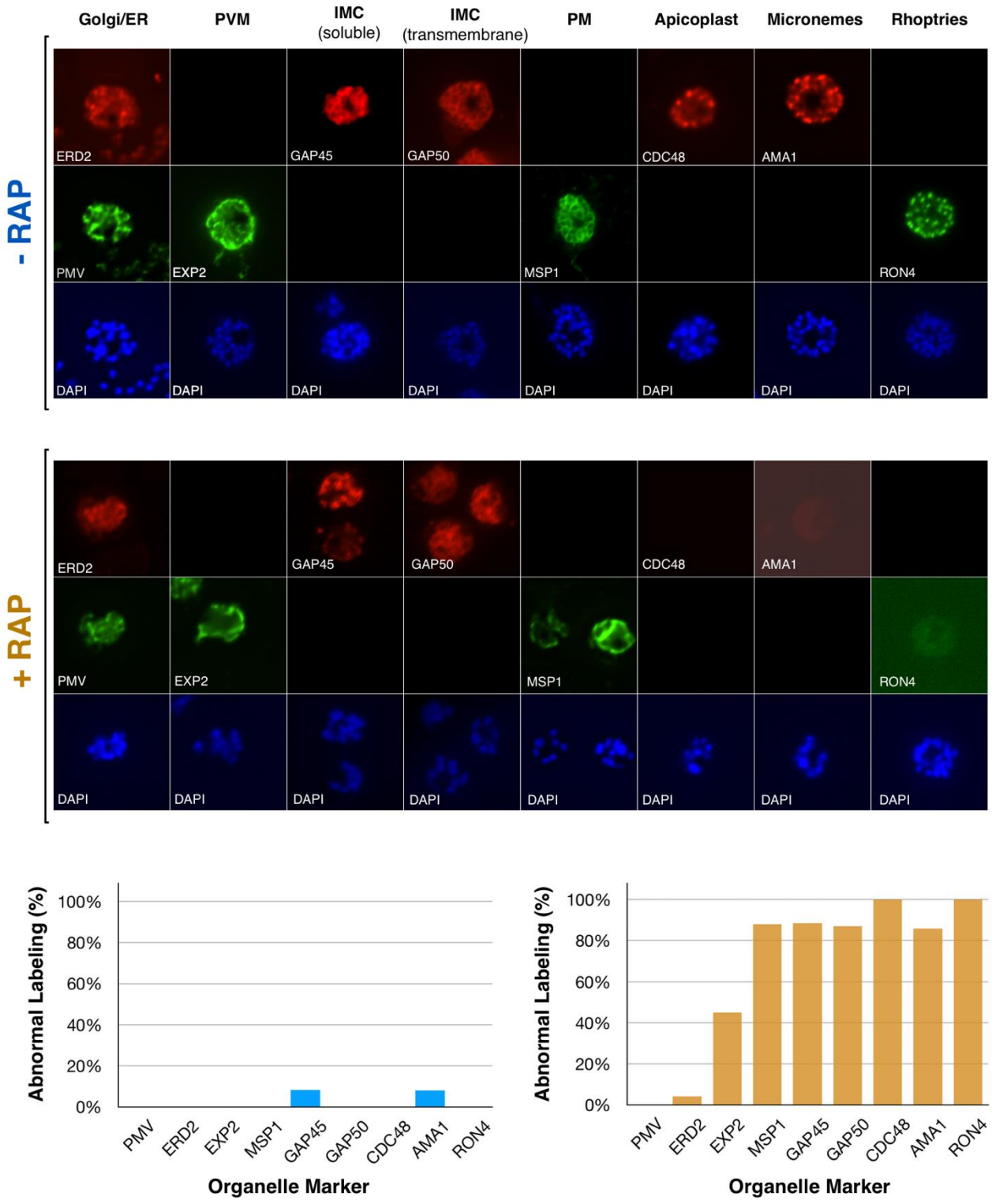


**Figure 55 Effects of *pfap2mu* knockout on organelle biogenesis**
The effects of *pfap2mu* knockout on organelle biogenesis and integrity was analysed in DMSO- (top panel) or rapamycin-treated (bottom panel) fixed, compound 2-blocked schizonts by indirect immunofluorescence. Antibodies against plasmepsin V (ER), ERD2 (*cis*-Golgi), EXP2 (PVM), GAP45 and GAP50 (IMC), MSP1 (plasma membrane), CDC48 (apicoplast), AMA1 (micronemes), and RON4 (rhoptries) were used. For each marker, at least 70 cells were examined. Abnormal labelling refers to the organisation, abundance, and apposition of the organelle marker with respect to the parasite nuclei relative to the localisation observed in wild type parasites (top panel). Cells were imaged on a Nikon TI-3000 inverted microscope, and image analysis was performed in Nikon AR Analysis software.

Interestingly, MSP1, GAP45, GAP50, and to a lesser extent, EXP2, are mislocalised in schizonts lacking µ2. In comparison to the bright staining demarking the parasitophorous vacuole membrane in wild type cells, EXP2 staining is more diffuse and less contiguous. Most cells seem to have an intact PVM, but the integrity of the membrane seems compromised in many cells (WT: 100% correct localisation; KO: 55% correct localisation). MSP1 staining reveals a defect in membrane organisation in the developing daughter merozoites. While some nuclei in a given schizont seem to be fully encircled with MSP1 staining, most nuclei are still bundled within a single parasite plasma membrane, with MSP1 staining encircling the schizont rather than the individual merozoites. GAP45 localisation is similarly affected. In wild type cells, the GAP45-stained inner membrane complex encircles each merozoite. However, in *pfap2mu*$^{-}$ cells, GAP45 staining is abnormal, staining discontinuous structures localised near each DAPI-stained nucleus. These spots resemble GAP45 staining in early IMC development, as described by Ridzuan *et al*[303]. As with MSP1 staining, some merozoites are encircled by GAP45 staining, but within a single schizont, the majority of merozoites display the abnormal staining. GAP50, a transmembrane component of the IMC, is similarly mislocalised to diffuse structures that are clearly different from the perinuclear staining characteristic of late segmented schizonts. Surprisingly, the apicoplast marker CDC48, microneme marker AMA1, and rhoptry marker RON4, are completely absent from schizonts lacking µ2, whereas these all stain the expected punctate structures in DMSO-treated cells.

It is possible that µ2-knockout parasites arrest before the IMC forms, membranes segment, and rhoptries and micronemes form. However, because wild type and µ2-knockout schizonts have similar total DNA content and the nuclei seem

to have segmented by Giemsa staining, it seems unlikely that these knockout cells arrest long before these developmental checkpoints. Additionally, the apicoplast is present throughout the cell cycle, so that CDC48 is also not detected indicates that µ2 deletion causes a significant defect in the secretory system. AMA1, RON4, and CDC48 were also probed by western blot in wild type and knockout cells confirming they are mislocalised and undetectable rather than degraded (Fig 56).

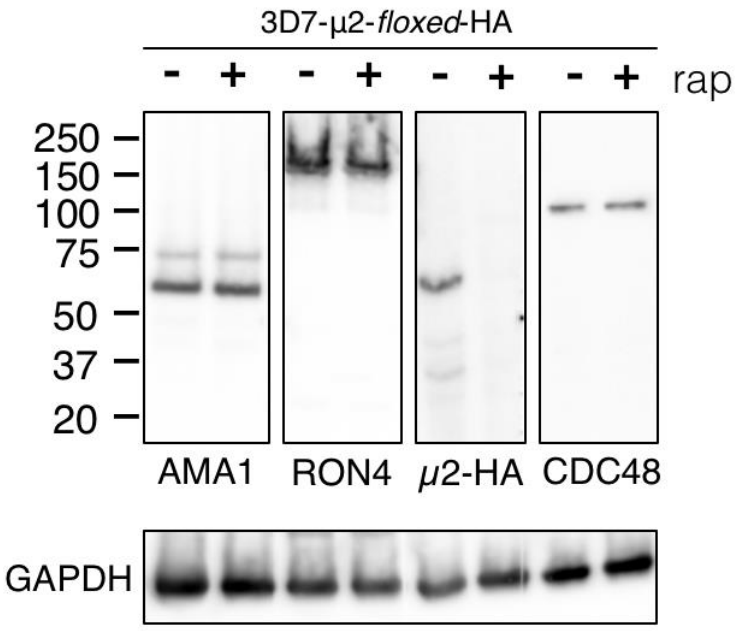


**Figure 56 Effect of µ2 knockout on protein levels of secretory markers**
The effect of µ2 knockout on markers of secretory organelles (AMA, 1:10,000, micronemes; RON4, 1:10,000, rhoptries; CDC48, 1:5000, apicoplast) was examined by western blot. µ2 knockout was also confirmed by anti-HA blotting (1:5000). Equal amounts of rap- or DMSO-treated late-stage schizonts were lysed in 5 volumes of 20 mM Tris, 150 mM NaCl, 0.5% Triton X-100, pH 7.5 with protease inhibitors. Soluble extracts were separated on a 4-12% TruPAGE gel (Sigma).

These data show that μ2 affects the integrity of several membrane-bound organelles and support a role for the AP-2 complex in the early secretory pathway.

## 5.7 Immunoprecipitation of μ2 and examination of interacting partners

Because these data show that *pfap2mu* encodes a non-canonical AP-2μ subunit located near the endoplasmic reticulum that can mediate significant levels of ring-stage artemisinin resistance and is required for asexual maturation, I sought to identify what factors might interact with AP2μ. As previously described, *P. falciparum* does not encode a recognisable AP-2β subunit. A similar streamlining occurs in *Dictyostelium* in which the β1 swaps into the AP-2 complex[236]. I speculated the same occurred in *Plasmodium* and aimed clarify this via immunoprecipitation and mass spectrometry. Additionally, a IP-MS characterisation would provide clarification on the lack of fluorescent correlation with clathrin.

Traditionally, immunoprecipitations, or pulldowns, are performed by isolating parasites from red cells by saponin lysis and then lysing the parasites in buffer containing 0.5%-1% (v/v) detergent. The soluble lysate material is then passed over antibody-conjugated beads to remove the tagged factor of interest and interacting partners. However initial solubilisation experiments showed that μ2 was insoluble under common extraction conditions (not shown). μ2 could be efficiently solubilised in RIPA, however this harsh condition is typically unsuitable for identifying protein interacting partners, and introducing crosslinking reagents to capture interactions can result in a high number of non-specific hits.

Recently, Prof Mark Field at the University of Dundee has pioneered the adaptation of cryomilling to lysing *Trypanosoma bruceii* parasites for IP-MS

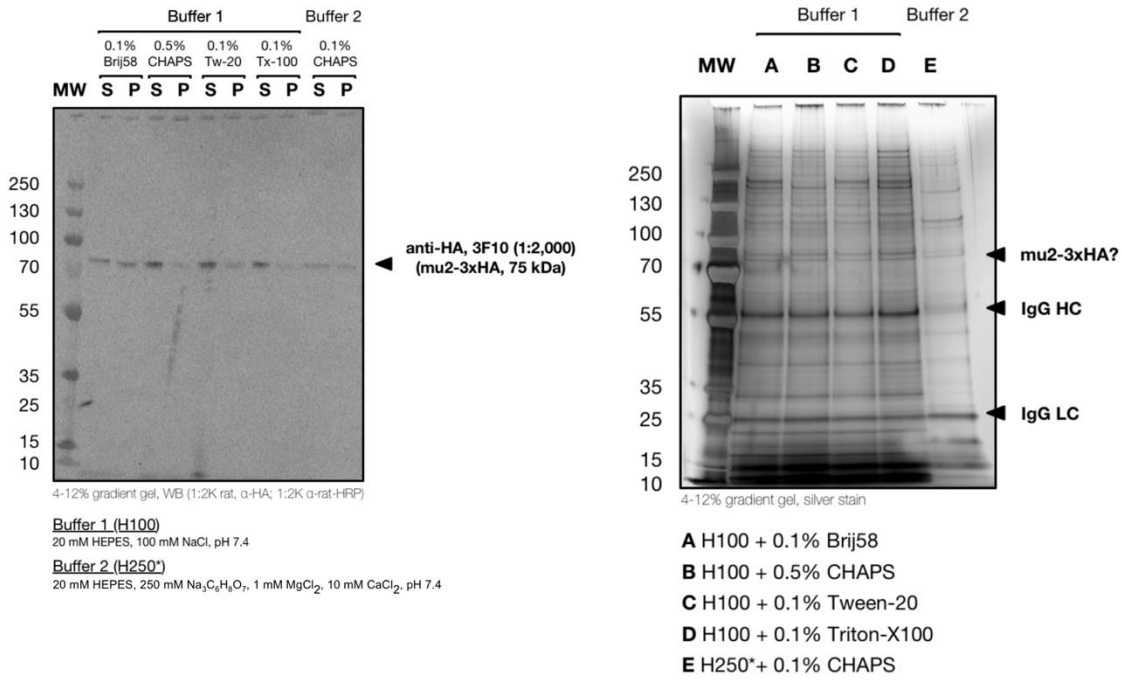


**Figure 57 Examination of several µ2 extraction and pulldown conditions**
After trophozoite-stage saponin-lysed parasites were cryo-milled, the solubility of µ2-3xHA and pulled-down interacting factors were examined under five different extraction conditions. Two basic buffer conditions were utilised, one consisting of 20 mM HEPES, 100 mM NaCl, pH 7.4 and the other 20 mM HEPES, 250 mM NaCitrate, 1 mM $MgCl_2$, 10 mM $CaCl_2$, pH 7.4. The first buffer was supplemented with either 0.1% (w/v) Brij-58, 0.5% (w/v) CHAPS, 0.1% (w/v) Tween-20, or 0.1% (w/v) Triton X-100, and the second buffer was supplemented with 0.1% (w/v) CHAPS. All buffers were supplemented with EDTA-free protease inhibitors, including PMSF and TLCK. Solubility of µ2-3xHA was examined in each condition by Western Blot (left), and pulled-down partners were examined by silver stain (right). S and P refer to soluble and insoluble fractions.

pipelines. Cryomilling is a new technique by which parasites released from red cells by saponin lysis are rapidly frozen in liquid nitrogen. These pellets are then ground into a fine powder in a bead mill also at liquid nitrogen temperatures. This powder can be lysed with 90-95% less detergent than standard lysis conditions. This procedure preserves labile protein-protein interactions that could be lost in traditional pulldown conditions.

Developing trophozoites between 24 and 36 hours post-invasion were harvested and saponin lysed. Approximately 3 ml of saponin-lysed, pelleted

parasites were resuspended with an equal volume of PBS, frozen in liquid nitrogen, and milled as described in Section 3.3.4. Several extraction buffer conditions were examined for their ability to solubilise µ2-3xHA. Four of these buffers were based on a standard 20 mM HEPES, 100 mM NaCl, pH 7.4 buffer and included either 0.1% (v/v) Brij-58, 0.5% (v/v) CHAPS, 0.1% (v/v) Tween-20, or 0.1% (v/v) Triton X-100 and EDTA-free protease inhibitors (Roche). Additionally, a fifth extraction condition was included, which had previously been designed and optimised for clathrin heavy chain pulldowns from *Trypanosoma spp*. This extraction buffer consisted of 20 mM HEPES, 250 mM sodium citrate, 1 mM $MgCl_2$, 10 mM $CaCl_2$, 0.1% (v/v) CHAPS, pH 7.4 and EDTA-free protease inhibitors. Most of these conditions solubilised µ2-3xHA well, and the four H100 (HEPES + 100 mM NaCl) buffers seemed to pull down similar factors by silver stain with the exception of several high-molecular weight proteins around 250 kDa (Fig 57). The H100 + CHAPS pulldown seemed to contain considerably less of an approximately 240 kDa protein, whereas it did retain an approximately 230 kDa protein. While the Brij-58 and Tween-20 extraction conditions contained both of these fragments, they seemed to isolate more of the larger protein. The Triton-based condition seemed to contain approximately equal amounts of both proteins. Interestingly, the *T. brucei*-optimised extraction condition seemed to pull down the fewest interacting factors, though this may be due to underloading. Since the four H100 buffers extracted similar proteins, H100 + Triton was selected for proteomic-scale IP's because it isolated roughly equal amounts of the high molecular weight fragments that seemed differentially isolated in the other conditions (Fig 57, right panel, lane D). The H20*/0.1% CHAPS buffer was also selected because it is optimised for *T. brucei* clathrin heavy chain and appeared to pull out different size proteins.

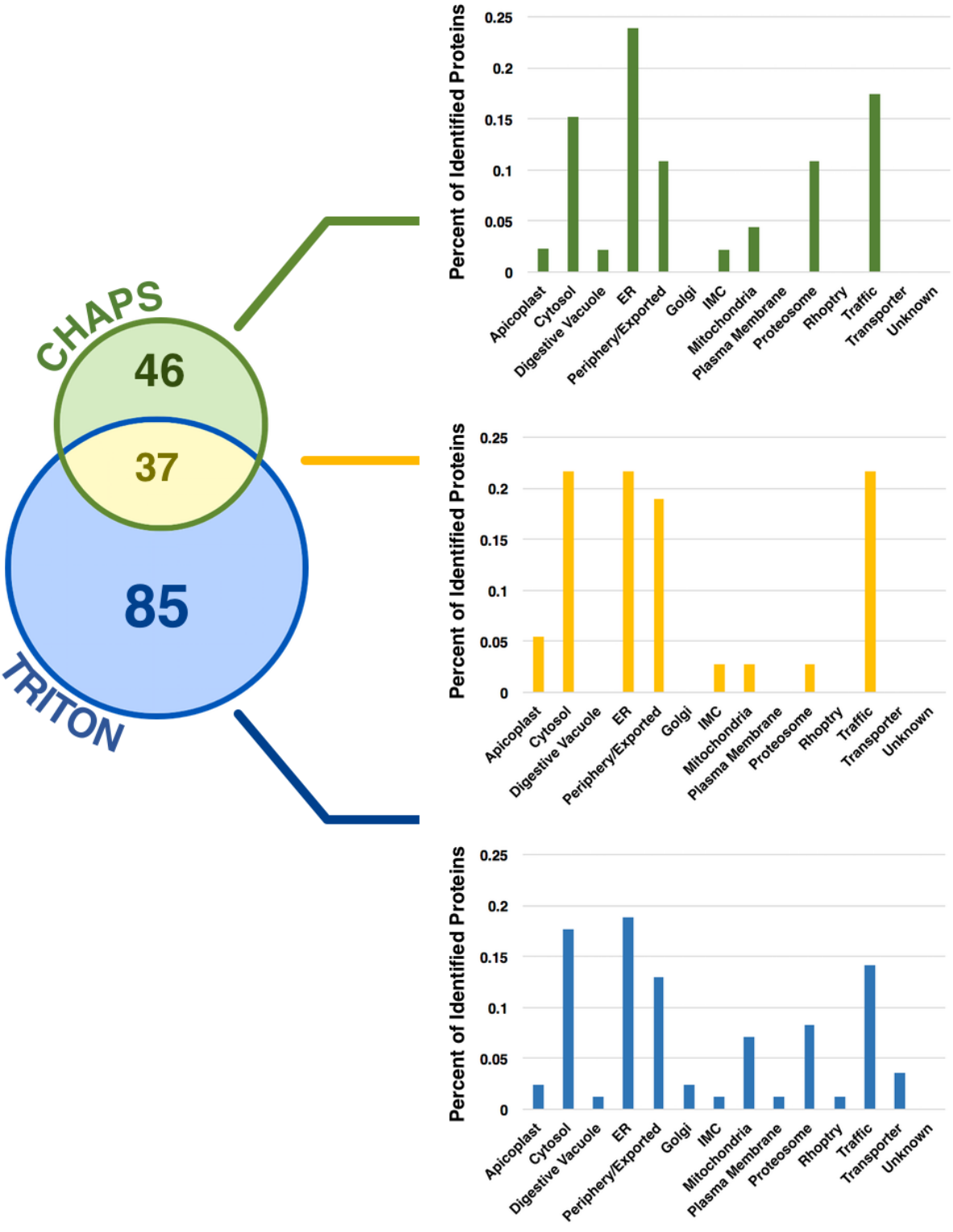


**Figure 58 Immunoprecipitation and mass spectrometry reveals potential µ2-interacting factors** Proteins identified from immunoprecipitation and mass spectrometry experiments in both triton- and CHAPS-based extraction conditions were annotated with a putative localisation by the information and annotations available in the Malaria Parasite Molecular Pathways (MPMP) resource embedded in PlasmoDB. 37 factors were shared between the triton and CHAPS datasets, with 85 and 46 unique factors remaining in those datasets, respectively. Overall, proteins putatively involved in cytosolic, ER, peripheral/export, and traffic-related functions account for more than 80% of the µ2 interactome.

The proteomics-scale anti-HA pulldowns were performed as described in Section 3.3.4, and bound protein was eluted and detected by LC-MS/MS at the University of Dundee. Control pulldowns were performed by incubating µ2-3xHA lysate with Rabbit anti-Ig beads (same Fc as anti-HA beads with a different antigen binding domain) and wild-type trophozoite lysate with the same anti-HA beads.

These experiments were performed under the guidance of Martin Zoltner in Prof Mark Field's laboratory. Pulldowns and mass spectrometry were performed in duplicate. Peptides were mapped to the 3D7 reference proteome using MASCOT, and contaminants were filtered using MaxQuant and Perseus.

Identified proteins were filtered such that only factors with greater than or equal to 2-fold enrichment over the control and identified from at least two peptides in both replicates were considered. Putative localisations or pathways for each factor were annotated based on entries in the Malaria Parasite Molecular Pathways (MPMP) database embedded in PlasmoDB.

Broadly, the identified interacting factors from each extraction condition support the localisation of µ2 determined above and a role for µ2 and the AP-2 complex in secretory traffic (Fig 58). Both conditions extracted factors that map to components or functions of many organelles in the cell including cytosolic metabolism, translation, and regulation proteins, ER folding and stress response factors, peripheral and export-related proteins, and intracellular transport factors, but cytosolic, ER, and export factors are most enriched. Additionally, a few mitochondrial, apicoplast, DV, and IMC factors were also identified (Table 7). Interestingly, a large number of ribosomal and ribosome-related proteins were identified in both conditions that seemed to be enriched above the background identified in control pulldowns. Because there are so many ribosomal subunits and

ribosome-associated proteins, these were largely excluded from the analysis presented in this section simply because they obscure the potential importance of other interacting partners. Additionally, it is very important to note that only two biological replicates have been performed so far, and these ribosomal factors are common "sticky" protein contaminants identified in LC-MS/MS experiments. Additional replicates and controls are currently underway, but the data from these experiments were not yet available for analysis in time for this thesis. Therefore, for these reasons, though ribosomal factors may be important interactors requiring further investigation, for the purposes of this thesis, they will be, for now, not considered further.

With these factors excluded, the CHAPS-based extraction condition revealed 122 enriched interacting factors, and the triton-based extraction identified 83 factors. 37 proteins were shared between both datasets (Table 9). Approximately 80% of the overlapped proteome corresponds to cytosolic, ER, peripheral/exported, and trafficking factors. The unique datasets are similarly enriched for these four groups, though proteasome-related factors were also identified as approximately 8-10% of the interacting factors. Broadly, these data support a localisation of μ2 near the ER and suggest interactions with machinery involved in intracellular traffic and protein turnover.

Specifically, these data confirm the hypothesis that the core AP-2 complex is comprised of α2, β1, μ2, and σ2. This is consistent with invertebrate biology where a single gene often encodes β1 and β2. These factors were enriched between both the triton and CHAPS extraction conditions, and μ2 was the most abundant protein in either dataset. No other adaptor protein complex subunits were significantly enriched. Interestingly, the only other trafficking factors found in both datasets were

**Table 9 Highly enriched µ2 interacting factors identified by LC-MS/MS in both CHAPS- and Triton-based extraction conditions**

| PFID | Name | Location | CHAPS Enrichment | Triton Enrichment |
|---|---|---|---|---|
| PF3D7_0816600 | chaperone protein ClpB1 | Apicoplast | 1.98E+09 | 1.72E+09 |
| PF3D7_0907400 | ATP-dependent protease ATPase subunit ClpY | Apicoplast | 1.78E+09 | 7.45E+08 |
| PF3D7_1132000 | ubiquitin-like protein, putative | Cytosol | 1.19E+10 | 1.23E+09 |
| PF3D7_1235600 | serine hydroxymethyltransferase | Cytosol | 3.17E+09 | 2.62E+09 |
| PF3D7_1225800 | ubiquitin-activating enzyme E1 | Cytosol | 3.16E+09 | 2.15E+09 |
| PF3D7_1022600 | **kelch protein K10** | **Cytosol** | **2.49E+09** | **9.97E+10** |
| PF3D7_1037100 | pyruvate kinase 2 | Cytosol | 1.07E+09 | 9.16E+08 |
| PF3D7_1434300 | Hsp70/Hsp90 organizing protein | Cytosol | 1.04E+09 | 2.65E+09 |
| PF3D7_0624000 | hexokinase | Cytosol | 7.99E+00 | 1.01E+01 |
| PF3D7_0308200 | T-complex protein 1 subunit eta | ER | 4.20E+10 | 4.46E+09 |
| PF3D7_1450100 | signal recognition particle subunit SRP54 | ER | 2.90E+10 | 1.87E+09 |
| PF3D7_1136400 | signal recognition particle subunit SRP72, putative | ER | 1.20E+10 | 1.41E+10 |
| PF3D7_1216300 | signal recognition particle subunit SRP19 | ER | 1.14E+10 | 8.06E+09 |
| PF3D7_0311300 | phosphatidylinositol 3- and 4-kinase, putative | ER | 5.14E+09 | 1.12E+09 |
| PF3D7_0110600 | phosphatidylinositol-4-phosphate 5-kinase | ER | 3.61E+09 | 1.62E+09 |
| PF3D7_1368200 | ABC transporter E family member 1, putative | ER | 2.65E+01 | 9.60E+00 |
| PF3D7_1136800 | DnaJ protein, putative | ER | 1.26E+01 | 9.11E+08 |
| PF3D7_1460600 | inner membrane complex sub-compartment protein 3 | IMC | 1.42E+09 | 7.88E+08 |
| PF3D7_1027300 | peroxiredoxin | Mitochondria | 1.30E+03 | 9.96E+01 |
| PF3D7_0532100 | early transcribed membrane protein 5 | Periphery/Exported | 1.61E+10 | 3.58E+09 |
| PF3D7_1149000 | antigen 332, DBL-like protein | Periphery/Exported | 1.20E+10 | 1.28E+09 |
| PF3D7_1228600 | merozoite surface protein 9 | Periphery/Exported | 8.67E+09 | 4.90E+09 |
| PF3D7_0402000 | Plasmodium exported protein (PHISTa), unknown function | Periphery/Exported | 1.90E+09 | 2.04E+10 |
| PF3D7_0730900 | EMP1-Trafficking protein | Periphery/Exported | 1.84E+09 | 5.52E+08 |
| PF3D7_1436300 | translocon component PTEX150 | Periphery/Exported | 1.02E+09 | 1.48E+09 |
| PF3D7_1129100 | parasitophorous vacuolar protein 1 | Periphery/Exported | 6.57E+01 | 2.28E+01 |
| PF3D7_1328100 | proteasome subunit beta type-7, putative | Proteasome | 3.51E+09 | 1.76E+09 |
| PF3D7_1218300 | **AP-2 complex subunit mu, putative** | **Traffic** | **4.35E+11** | **1.67E+11** |
| PF3D7_0217300 | **AP-2 complex subunit sigma, putative** | **Traffic** | **7.54E+10** | **1.04E+10** |
| PF3D7_1244600 | **ADP-ribosylation factor GTPase-activating protein** | **Traffic** | **3.62E+10** | **3.10E+09** |
| PF3D7_0304200 | EH domain-containing protein | Traffic | 1.16E+09 | 3.77E+09 |
| PF3D7_1352800 | **vacuolar fusion protein MON1, putative** | **Traffic** | **9.76E+08** | **3.97E+09** |
| PF3D7_1340700 | ras-related protein Rab-11B | Traffic | 6.52E+08 | 1.96E+09 |
| PF3D7_0617100 | **AP-2 complex subunit alpha, putative** | **Traffic** | **1.65E+03** | **5.62E+02** |
| PF3D7_0528100 | **AP-1 complex subunit beta, putative** | **Traffic** | **1.84E+02** | **5.98E+00** |
| PF3D7_0932200 | profilin | unknown | 1.64E+09 | 1.23E+09 |

List of proteins identified in µ2-3xHA pulldowns performed in CHAPS- and Triton-based extraction conditions. Cellular extracts, pulldowns, and interactomes were prepared as described in Sections 3.3.4 and 3.3.5. Pulldowns using the same cellular extracts (containing µ2-3xHA) were performed using magnetic anti-rabbit IgG beads of the same species (donkey) as the anti-HA beads used to isolate µ2-3xHA. Enrichment is calculated as the ratio of the abundance of a given protein in the anti-HA pulldown to the abundance in the control pulldown, which was performed in parallel. Proteins were assigned to a putative location by their annotation in the Malaria Parasite Molecular Pathways database (MPMP) in PlasmoDB. Enriched proteins (> 2 peptides, >2-fold enrichment) identified in both extraction conditions are listed. Bold black script indicates identified adaptor protein subunits; red bold script indicates factors that were selected for *in vitro* validation. Enrichment is averaged from two replicate pulldowns.

ADP Ribosylation Factor GTPase Activating Protein (ArfGAP), MON1, Rab11B, and an EH-domain containing protein. ArfGAP and MON1 are both regulators of the second messengers GTP and GDP. ArfGAP is a GTPase-activating protein, which leads to the hydrolysis of GTP to GDP; MON1 is part of a guanine nucleotide exchange factor complex (GEF), which exchanges hydrolysed GDP for GTP[216,304]. In higher order eukaryotes, these two factors function as regulators of intracellular traffic[304,305]. Rab11B has been shown to be required for IMC biogenesis in *Toxoplasma gondii* and regulates secretory traffic downstream of the ER[306]. The EH domain-containing protein identified here shares homology with EHD4, which is an effector of AP-2 in humans[223]. Several exported factors including the major virulence factor EMP1 and components of the signal recognition particle (SRP) are enriched between both extraction conditions, hinting at the possibility that μ2 could be involved in the transportation of proteins destined for the cell periphery from a sub-region of the ER.

Surprisingly, a kelch-domain containing protein, Kelch protein 10 (hereinafter referred to as K10), were significantly enriched across both datasets. K10 is similar to K13 in that both proteins have a kelch-type β-propeller domain. However, the K10 propeller seems to contain 5 blades and be located at the N-terminus whereas the K13 contains a 6-bladed C-terminal propeller. Additionally, K10 does not appear to contain a BTB/ POZ domain. Though *pfkelch10* mutations have not been linked directly to artemisinin resistance as with K13, K10 variants have been epistatically associated with artemisinin resistance in a GWAS study[307]. K10 shares some homology with KLHDC4 in humans, which has been linked to poor cancer outcomes, though is also functionally uncharacterised[308]. K13 has been proposed to be a regulator of parasite phosphatidylinositol-3-kinase (PfPI3K),

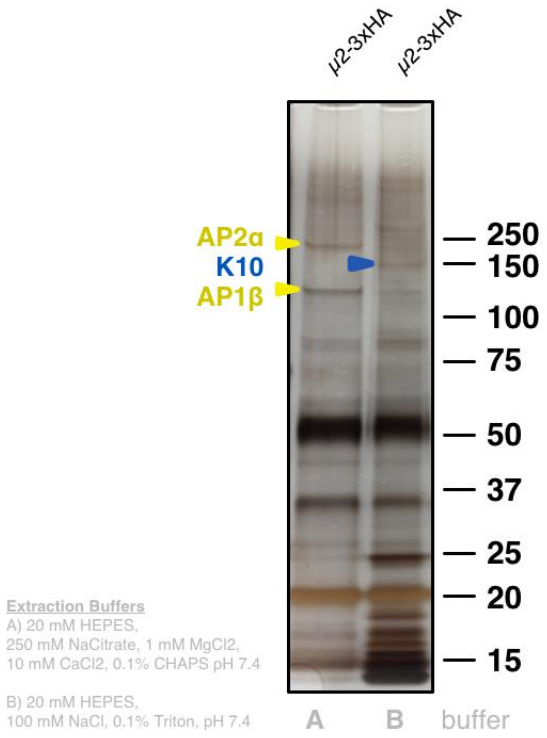


**Figure 59 Analysis of high-molecular weight μ2 interacting proteins by mass spectrometry**
To more specifically probe whether clathrin heavy chain is present in the μ2-3xHA interactome, several high molecular weight fragments around the approximate expected size of clathrin heavy chain were excised from a silver stained gel of μ2-3xHA pulldowns performed in each buffer condition used for proteomics. These gel slices were submitted to the proteomics facility at the University of Dundee for peptide identification. No clathrin was detected in any of the slices submitted. The highest abundance proteins detected in these slices were AP2α, AP1β, and K10, as annotated, further supporting their interaction with μ2. These experiments were performed in collaboration with Dr Martin Zoltner and Prof Mark Field at the University of Dundee.

however, PfPI3K was not found in either dataset. Instead, phosphatidylinositol-3-and-4-kinase and phosphatidylinositol-4-phosphate-5-kinase are identified here, but their significance is unclear.

Conspicuously, the μ2 interactome is lacking clathrin heavy chain and clathrin light chain. Both genes are annotated in the *Plasmodium falciparum* genome, and eukaryotic dogma says that the AP-2 complex associates with clathrin.

While it is important to note that peptides mapping to clathrin heavy chain are detected in both replicates of both extraction conditions, there was no evidence

of enrichment in the μ2 samples compared to the controls. Though this supports conclusions from my localisation data, this observation was still unexpected. To further clarify whether μ2 interacts with clathrin, several high molecular weight fragments around the expected size of clathrin heavy chain (255.1 kDa) were excised from a silver-stained gel of pulldowns performed in both extraction buffer conditions and sent for peptide identification by mass spectrometry. Peptides identified from slices of the same regions of a gel of a control pulldown performed in each buffer condition using the IgG agarose beads were used to subtract contaminants from the anti-HA gel slices. No clathrin was detected in any of the fragments. However, these slices did re-identify AP2α, AP1β, and K10 as highly enriched interactors in both conditions (Fig 59).

The full lists of the factors uniquely enriched in each extraction buffer can be found in Appendix I. As stated above, these interactors cluster similar to the common interactors between the datasets, with 80% of identified factors putatively involved in ER-, periphery- and export-, cytosol-, and trafficking-related processes. Largely, these factors suggest the same story as the overlapped interactomes and reveal more proteins related to ER and Golgi quality control, sorting, and export. Given the functional similarity between the two datasets, as additional replicates are available for analysis, it is possible that some of these unique factors may be common to both extraction conditions. In lieu of additional experiments, that the two extraction and pulldown conditions used in this study are so different (in ionic strength, detergent, and divalence), should give some additional confidence in the 35 proteins identified between the two conditions. However, several factors were further explored in cultured parasites to provide empirical support for this list of proteins that may interact with μ2.

## 5.8 Validation of μ2 interacting factors identified by IP-MS

Mass spectrometry is known for generating long lists of potential interacting factors. While one may be generally safe in assuming some of the expected and most enriched hits probably interact with the tagged handle protein of interest, steps should be taken to empirically validate the interactions of some of these expected factors as well as some of the more interesting or unexpected factors.

From the list of 35 μ2 interactors identified in the previous section, several factors were selected for tagging and *in vivo* validation. The criteria for selection were that, if possible, the factors would have been tagged before to show that they can be tagged without disrupting their function. Additionally, these factors should be amenable to overexpression and have relevance to understanding the mechanism or localisation of μ2.

Given the intense interest in mechanisms of artemisinin resistance, K10 was immediately selected. K10 was one of the most enriched and highest confidence hits but has not been previously characterised. TCP-1 ring complex subunit epsilon (TRiCε) was selected because this is a known ER-associating factor. Lastly, MON1 and ADP-ribosylation factor, GTPase-activating Protein (ArfGAP) are competing GTP exchange factors that were recently shown to have a punctate localisation by immunofluorescence that resembles that of K13 and μ2[192]. ArfGAP and MON1 in higher order eukaryotes are known regulators of vesicular traffic in the cell[304,305].

The CDS for each protein was cloned into the pDC2-cam-BSD *Plasmodium* expression vector in frame with a short, flexible linker and GFP (Fig 60A). In the case of β1, the CDS was amplified from cDNA to remove introns and, based on studies in other organisms indicating C-terminal GFP is not tolerated, was cloned downstream of an N-terminal GFP and linker. K13 was also N-terminally tagged

because the β-propeller kelch domain comprises the C-terminus, and tagging this domain would likely interfere with its folding and function. Additionally, Birnbaum *et al* recently described the localisation of an N-terminally tagged K13[192].

These constructs were transfected by Nucleofection into 3D7-μ2-3xHA-glmS schizonts and selected with 2.0 μg/ml blasticidin-S until parasites were observed by Giemsa stain. In all of these episomal transfections, blasticidin-resistant transgenic parasites were obtained within 5-8 days. Interaction of these factors with μ2 was validated by immunofluorescence and co-immunoprecipitation (Fig 60). Pearson's Correlational Coefficients for each marker are presented in Fig 45.

As previously reported by Birnbaum *et al*, ArfGAP-GFP and MON1-GFP displayed a punctate cytoplasmic localisation[192]. In rings, these structures are located near the nucleus and are localised near the digestive vacuole in the developing trophozoite, ultimately segmenting into a single structure per merozoite. As examined in ring stages and schizonts, μ2-3xHA signal correlates well with both ArfGAP-GFP and MON1-GFP signal. There are some ArfGAP and MON1 spots that do not overlap with μ2, namely in rings, however all μ2-3xHA-labeled structures overlap with MON1 and ArfGAP signal, within the limits of resolution of this technique. The μ2 interacting factors identified in Section 5.7 may not exclusively interact with μ2, therefore it is not expected that they would exclusively localise near μ2. The same was true of TRiCε, a cytosolic chaperone complex. The signal observed for most of the labelled TRiCε–GFP structures correlates with μ2-3xHA structures, and all μ2-3xHA structures overlap with TRiCε–GFP structures. Correlation between μ2-3xHA and K10-GFP localisation was similar. To the best of my knowledge, the localisation of K10 has never been reported, and therefore this finding provides the first evidence that K10 may also be located in the cytosol and

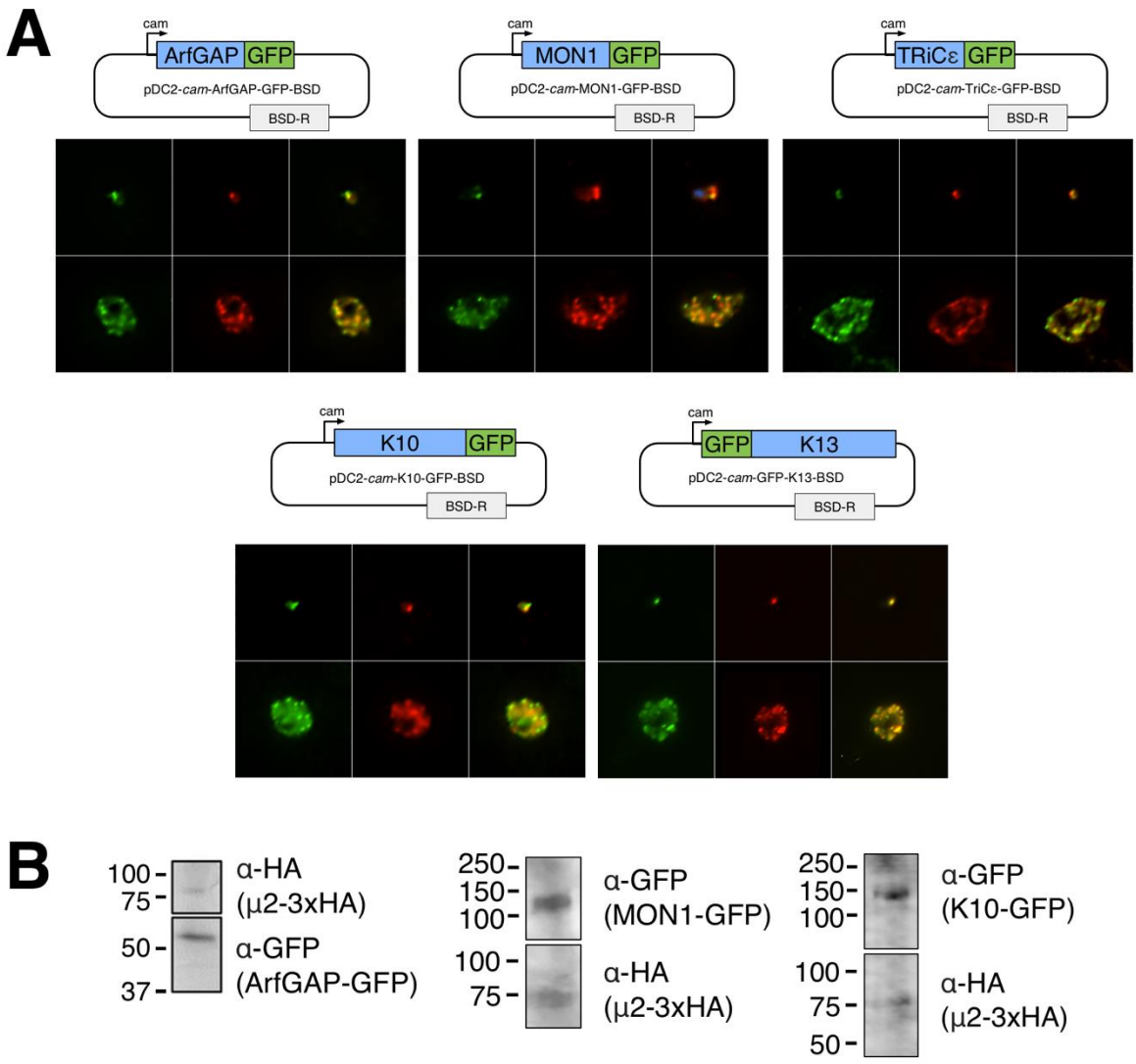


**Figure 60 Validation of selected µ2 interacting factors**
To validate the µ2 interactome determined in Section 5.7, several factors were episomally overexpressed as fusion proteins with GFP. Specifically, ADP ribosylation factor GTPase-activating protein (ArfGAP), vacuolar fusion protein MON1, T complex protein 1 subunit epsilon (TRiCε), Kelch 10 (K10), and Kelch 13 (K13) were selected. **A** The CDS for each factor was cloned in frame with either N-terminal or C-terminal GFP, as shown. These constructs were transfected into 3D7-µ2-3xHA-*glmS* parasites and selected with 2 µg/ml BSD. Colocalisation of each factor with µ2-HA was examined in formaldehyde-fixed schizonts and ring stages by indirect immunofluorescence using anti-HA (rat, 1:150, 3F10; anti-rat-488, goat, 1:150, Invitrogen) and anti-GFP (rabbit, 1:500, A. Holder Lab; anti-rabbit-594, goat, 1:150, Invitrogen) antibodies. **B** ArfGAP-GFP, MON1-GFP, and K10-GFP were also pulled down using magnetic anti-GFP beads (M. Field laboratory) in H100+0.1% Triton X-100 buffer (Section 5.7) from cryo-milled parasites (Section 3.3.4). Eluted fractions were run on a 4-12% TEA-Tricine TruPAGE gel (Sigma) and analysed by western blot for the presence of GFP-tagged and HA-tagged species.

near the ER. The localisation of episomally-expressed GFP-K13 was also punctate and cytoplasmic, as found by Birnbaum *et al*, and showed strong correlation with µ2 throughout life stages.

To better understand whether these factors interact with µ2 beyond simple colocalisation, co-immunoprecipitations were performed using anti-GFP magnetic beads. For these experiments, only ArfGAP-GFP, MON1-GFP, and K10-GFP were analysed. Parasites expressing µ2-3xHA with episomes expressing the GFP fusions of interest were harvested by saponin lysis and flash frozen in liquid nitrogen as 50% (w/v) in PBS. These parasite pellets were ground into a powder at liquid nitrogen temperatures and lysed in buffer consisting of 20 mM HEPES, 100 mM NaCl, 0.1% (v/v) Triton X-100, pH 7.4 supplemented with protease inhibitors (Roche). The lysate was cleared by centrifugation and incubated with magnetic anti-GFP beads (Mark Field laboratory) for 1 hour. The beads were washed several times with lysis buffer, and bound material was eluted using gel loading buffer. The eluted material was separated by SDS-PAGE electrophoresis and probed for the presence of the GFP-tagged interacting partner and µ2-HA by western blot (Fig 60B). These co-immunoprecipitation experiments revealed that ArfGAP, MON1, and K10 all interact with µ2, providing empirical support for the mass spectrometry-determined µ2 interactome. Experiments are underway to validate the interaction of TRiCε with µ2. Additionally, experiments to validate the colocalisation and interaction of AP-1β with µ2 are also planned.

Given the similarity in the ART-R phenotype mediated by µ2 mutation (Section 4.4), I also probed the localisation of µ2 with respect to K13. Using the same episomal approach as above, I introduced an N-terminally GFP-tagged K13 into the µ2-3xHA tagged parasite line and examined the localisation of µ2 and K13

by IFA. The localisation of K13 reported by Birnbaum *et al* is very similar to what I have observed for µ2 (cytoplasmic, near the DV), and in my hands, the localisation of these species correlate well, within the limits of resolution of widefield light microscopy (Fig 60A, 45). We are currently investigating this localisation further and how it may relate to the function of µ2 and both proteins' involvements in artemisinin resistance.

## 5.9 Discussion

These results suggest a possible repurposing of traditional trafficking machinery in *Plasmodium*. Rather than participating in receptor-mediated endocytosis from the plasma membrane to the early endosome compartment, AP-2 seems to play a role in the early secretory pathway near the ER. By immunofluorescence, µ2 labels a punctate sub-compartment near the ER throughout most of the asexual cycle. This structure either replicates or somehow segregates into the daughter merozoites so that each merozoite and new parasite inherits a single focus. When examined with immunoelectron microscopy, µ2 mainly decorates distal surfaces of the ER that resemble the vesicular tubular clusters of mammalian cells. Due to the limits of resolution of light microscopy, the punctate structures observed by IFA and tubular structures identified by IEM are probably the same. By super-resolution structured illumination microscopy, each previously observed single focus may contain several smaller foci. Either way, these data show that AP-2 is not primarily located at the plasma membrane, in contrast to other eukaryotes. To the best of our knowledge this is the first description of such a divergence in the adaptor protein complexes. AP-1 has been shown to traffic from the Golgi to the apical secretory organelles including the rhoptries in *Toxoplasma* and potentially also in

*Plasmodium*. While other eukaryotes obviously do not have these organelles, and in that respect Apicomplexan AP-1 may broadly have a novel function, AP-1 still mediates a *trans*-Golgi to vesicular body transport route.

Recently, AP-2 has been described as mediating retrograde traffic from endosomes to the plasma membrane in human neuronal cells[290]. At the time, this finding again was dramatic because AP-2 canonically mediates anterograde traffic from the plasma membrane to the early endosome. It was recognised that recycling of transmembrane receptors from the endosome to the plasma membrane occurs, but this process was thought to proceed via a different route.

The observations in this chapter may be consistent with retrograde secretory traffic as µ2 co-purifies with several ER- and export-related elements. Interestingly, µ2 partially colocalises with Rab5B and Rab11A by IFA. By immunoelectron microscopy, µ2-3xHA and Rab5B co-label vesicular structures in the cytosol. Both of these Rab GTPases have been shown to mediate traffic towards the cell periphery, with Rab5B directing to the plasma membrane and Rab11A to the IMC. Consistent with this, knocking out µ2 seems to cause defects in peripheral membrane organisation in segmenting schizonts including of the parasite plasma membrane and the IMC.

The lack of µ2 at the plasma membrane may be possible because the malaria parasite has adapted to obligate intracellular life inside the parasitophorous vacuole. The parasite is known to perform a massive endocytic event in the ring stage to ingest a large volume of haemoglobin from the host cell, and small endocytic events occur throughout the life cycle via cytostomes[191]. Because AP-2 classicly engages with specific cargo by facilitating receptor-mediated endocytosis in higher order eukaryotes, for AP-2 to be involved in these endocytic processes seems inconsistent.

Further, it is not clear how receptor-mediated endocytosis could occur in the context of a double membrane system. Importantly, the immunoelectron microscopy performed in this study did identify cytostomes, and μ2 was not detected anywhere along these structures.

IP-MS characterisation of μ2/AP-2-interacting factors provided further support for this localisation and potential function of AP-2 in the cell. Specifically, these data support the hypothesis that AP-2 actually exists as a hybrid AP-1/2 complex, necessary because one of the canonical large subunits of the AP-2 complex is missing from the *P. falciparum* genome. Bioinformatic analysis of the conserved proteins of unknown function with similar abundance to the α2 subunit did not reveal a β2 subunit (not shown).

Without a detailed characterisation of the *cis*-Golgi and some of the trafficking factors that interact with the AP-2 complex, it is difficult to state from these data exactly to which compartment AP-2 directs cargo. From these data, the most plausible possibilities include to the plasma membrane as a direct export mechanism or to the IMC, but all secretory pathway destinations should still be carefully considered. Given the enrichment of nearly the entire signal recognition particle and ribosome (ribosomal subunits were omitted from the discussion in Section 5.7, but nevertheless may still be important), it is tempting to speculate a model of μ2-mediated cargo aggregation by which the AP-2 complex assembles near the SRP, which cotranslationally imports nascent polypeptides into the ER. Though speculative, bioinformatic analysis of the identified enriched peripheral and exported proteins did not reveal conserved N-terminal or C-terminal sequences that might be consistent with the YXXΦ or dileucine motifs characteristic of μ2 cargo recognition elements. Identifying cargo molecules will be difficult but will provide important

insight into these observations and shed further light on how the secretory pathway functions in *Plasmodium falciparum*.

Interestingly, when expressed in human cells (Appendix IV), PfAP2µ seems to be localised to the cell periphery, consistent with its canonical localisation and function. Given how much is known about how the human AP-2 complex functions, this orthologous expression system may provide a valuable path to probing PfAP2µ biology and the functional impacts of clinically relevant mutations. Overall these data suggest that though key processes in *Plasmodium* may be diverged from eukaryotic dogma, the underlying molecules may be functionally similar. Though *Plasmodium* biology may seem very strange and different, the parasite may have co-opted conserved systems to suit its obligate intracellular needs.

# Chapter 6

# Modulation of *in vitro Plasmodium falciparum* artemisinin sensitivity by physiochemical perturbation

## 6.1 Rationale for pursuing physiochemical perturbation experiments

To date, published studies and informal conversations indicate that we as a field are trying to understand artemisinin resistance by comparing artemisinin resistant, $K13^{mut}$ parasites to artemisinin sensitive, $K13^{wt}$ parasites using multi-omic tools[193]. However, over the course of this thesis, I began to wonder whether this approach is appropriate. Artemisinin is unlike any antimalarial that has been used in the field because it does not seem to disrupt a single enzyme or target a specific pathway. Additionally, stably acquiring resistance takes the parasite an impressively long time, and any resistance achieved is partial. $K13^{R539T}$ is the most potent of the known K13 mutations, conferring 20-30% survival in the RSA (Section 4.4). Yet even these parasites are 70-80% sensitive to artemisinin in the ring-stage *in vitro*. In contrast, chloroquine resistant parasites are totally insensitive to therapeutic doses of chloroquine, and *in vitro* $EC_{50}$ estimates of sensitivity to chloroquine in these parasites can be multiples of the $EC_{50}$'s of sensitive parasite strains. Therefore, "artemisinin-resistant" parasites still mostly sensitive to artemisinin. The one multi-omic investigation of $K13^{mut}$ parasites that has so far been published supports this idea because the authors identified only subtle differences at the proteomic,

transcriptomic, and metabolomes levels, compared to wild type cells[193]. Instead of trying to back into an understanding of artemisinin resistant via K13 mutations or poly-omic investigations, I wondered whether we might find ways of reversibly rendering sensitive parasites less sensitive to artemisinin and thereby explore the cellular modulations required for artemisinin resistance.

### 6.1.1 A primed stress response may underlie artemisinin resistance

The data presented thus far in this thesis show that a genetic change in the μ2 trafficking factor can generate significant levels of artemisinin resistance *in vitro*. Subsequent molecular characterisation of this factor revealed an unexpected interaction with the artemisinin resistance factor K13 and suggested a role for both proteins in secretory traffic.

Recent work has shown that ring-stage translational dormancy is the basis of K13-mediated artemisinin resistance[202]. As described in Section 1.5.3.1, this dormancy is marked by a signalling cascade initiated by BiP in the ER that triggers phosphorylation of cytosolic eIF2α[202]. BiP, also known as GRP78, is a soluble ER-resident HSP chaperone that is capable of responding to ER stress[202,311]. Under normal cellular conditions, BiP/GRP78 interacts with newly synthesised and translocated proteins in the ER lumen and is one of several chaperones that mediates proper folding. When proteins abnormally accumulate in the ER, BiP alternatively activates ER membrane kinases, which activate the unfolded protein response and reduce translational activity until the ER stress subsides. Therefore, given that artemisinin triggers the UPR, and the drug accumulates in the ER of other eukaryotic

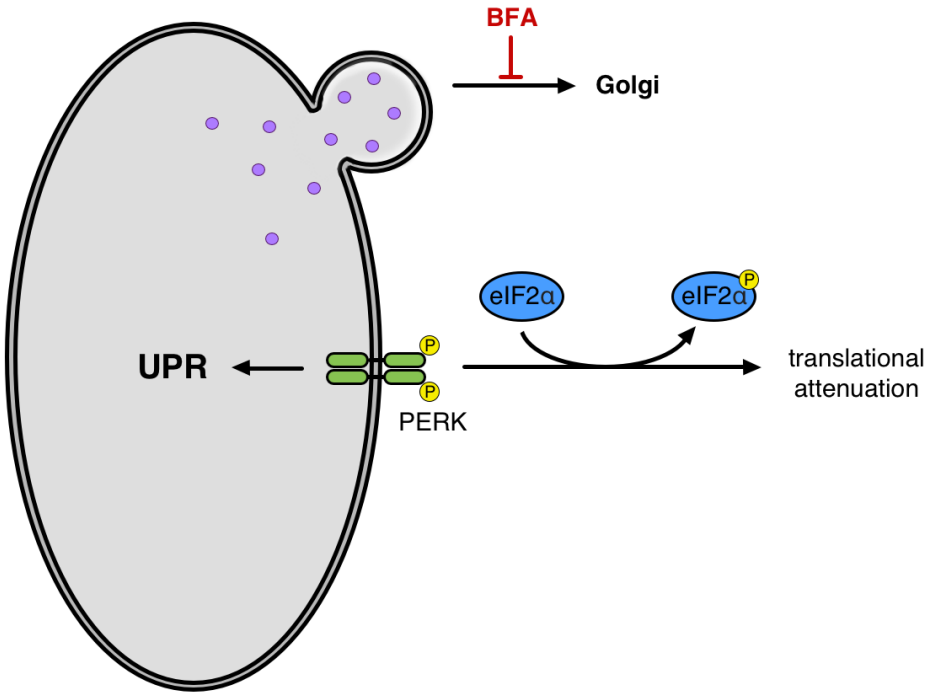


**Figure 61 Chemical manipulation of ER protein dynamics and artemisinin sensitivity**
The impacts of Brefeldin A (BFA), known to disrupt trafficking and protein dynamics at the ER, was examined for its ability to disrupt artemisinin sensitivity. Brefeldin A is a fungal metabolite that blocks ER-to-Golgi traffic, leading to a buildup of secretory material in the ER. In other eukaryotic systems, BFA has been used to induce and study the unfolded protein response and disrupt ER protein dynamics, which canonical induces phosphorylation of cytosolic eIF2α by a PERK-dependent mechanism. eIF2α-P interacts with ribosomes to globally reduce translational initiation.

cells, it is possible that "artemisinin resistance" is really just a primed ER-based stress response[202,312]. Since K13 mutations mediate ring-stage artemisinin resistance via an ER-based, BiP-dependent translational dormancy, and as described in Chapter 5, the wild type molecule is clearly located near the ER and interacts with trafficking partners, it follows that K13 mutations may induce an ER-based stress response rooted in a dysregulation of secretory traffic. In yeast, deletion of ER-to-Golgi

trafficking factors confers hypersensitivity to artemisinin, suggesting the cell cannot simultaneously cope with artemisinin-induced damage and a near-lethal accumulation of material in the ER[313]. However, a modulation of this ER traffic resulting in low-level accumulation of material in the ER may result in a primed stress response capable of inducing a short period of dormancy, mitigating oxidative stress caused by artemisinin.

In this line of thinking, I wondered whether I could reversibly trigger an ER stress response in drug-sensitive parasites that would phenocopy these artemisinin-resistant parasites. To this end, I investigated the effects of short exposures to brefeldin A, transient changes in environmental temperature, chemical ablation of the apicoplast, and reversible depletion of μ2 on parasite susceptibility to artemisinin and latency as detected by survival in the RSA and cytosolic eIF2α phosphorylation in the drug-sensitive 3D7 line. The 3D7 line was isolated and culture adapted in the 1970s and has never been exposed to artemisinins in the field and should therefore have no adaptive response to artemisinins. The studies and analysis presented in this chapter both predated and were informed by the publication of the recent Zhang *et al* study showing that eIF2α phosphorylation and translational dormancy underpins ring-stage artemisinin resistance[202].

## 6.2 Effect of Brefeldin A on artemisinin sensitivity

The data presented in Chapter 5 suggest that traffic is involved in artemisinin resistance. To therefore establish whether interfering with this process can protect cells from artemisinin, the effects of Brefeldin A treatment on RSA survival was examined.

As described in the previous chapter, Brefeldin A (BFA) is a fungal metabolite that rapidly and reversibly blocks ER-to-Golgi traffic in eukaryotic cells. This blockade ultimately causes the fusion of the Golgi and the ER as Golgi-destined vesicles cannot exit the ER.

The build-up of secretory proteins in the ER leads to the upregulation of protein turnover machinery and a reduction in global protein synthesis until ER stress can be mitigated or the cell dies. Recent efforts to study the programmed cellular response to ER stress in various mammalian pathologies leveraged the mechanism of BFA to interfere with protein homeostasis in the ER. In these studies, Brefeldin A treatment induces phosphorylation of eIF2α–Ser51[314,315]. Thapsigargin is typically used to induce and study the UPR in eukaryotic cells. However, a recent study has shown that thapsigargin does not stimulate the same calcium-release pathway in *Plasmodium* as in higher order cells, and molecular docking suggests PfSERCA, the orthologue of the human target (hSERCA), is incapable of interacting with the molecule[316]. Therefore, only Brefeldin A was used.

To probe the effects of Brefeldin A on artemisinin sensitivity, 2-hour-post-invasion ring stage parasites were treated with 5 μg/ml BFA or equivalent methanol control for 1 hour (Fig 62A). At hour 3 post-invasion, an equal volume of 1.4 μM DHA or DMSO equivalent was added to the cells (final concentration 0.7 μM DHA, 2.5 μg/ml BFA), and the cells were incubated for a further 4 hours. Thereafter, both drugs were extensively washed off, and cells were returned to culture. Parasite survival was determined by FACS with SYBR Green and MitoTracker Deep Red. As anticipated, pre-treatment of early ring-stage parasites with Brefeldin A provided substantial protection from artemisinin. Approximately 50% of parasites treated with BFA survived the RSA artemisinin pulse, compared with less than 3% of untreated

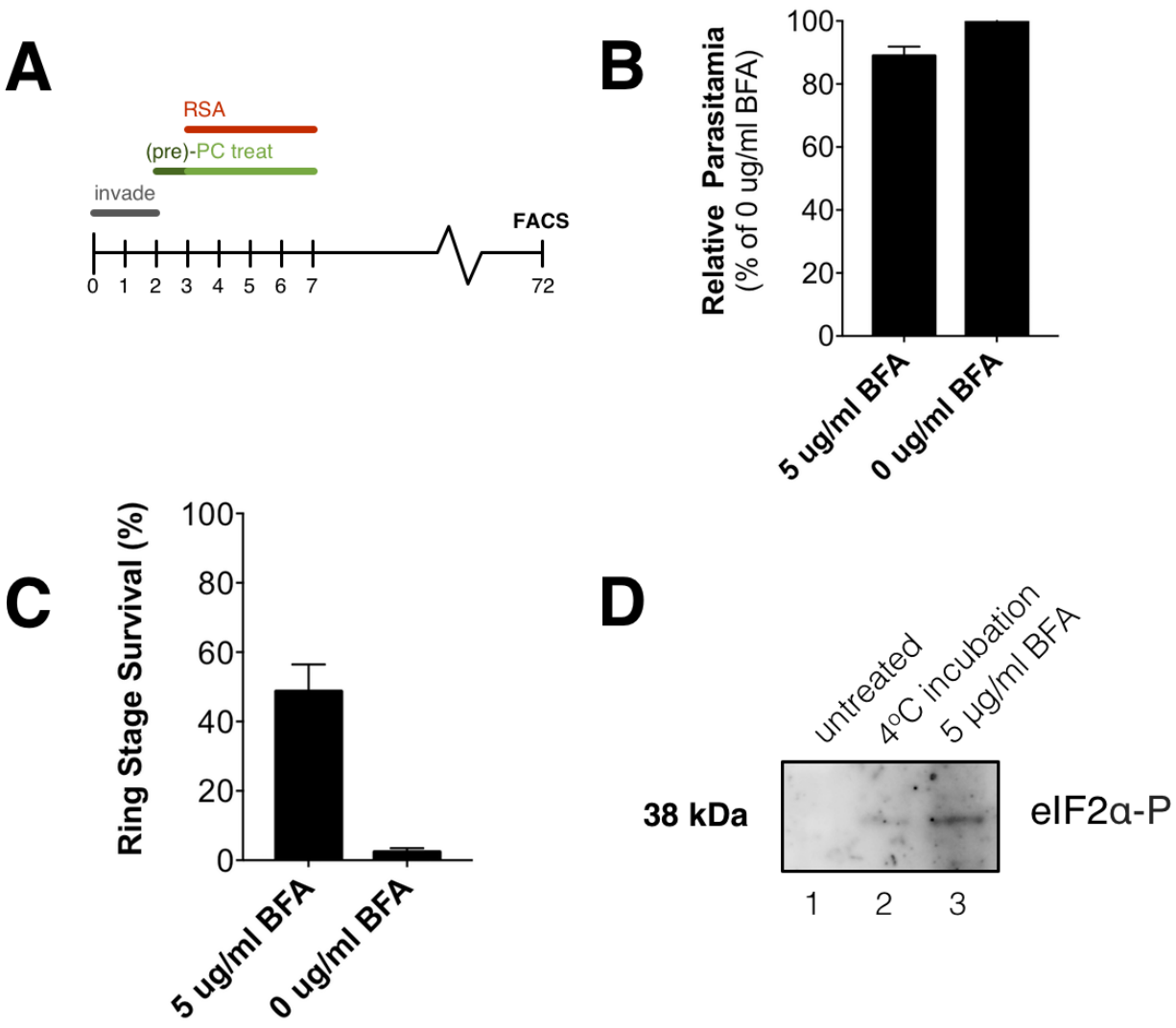


**Figure 62 Effects of Brefeldin A on artemisinin sensitivity**
**A** Schematic of the pulsed physiochemical (PC) treatment/RSA experiments. PC treatment was pre-performed from hours 2-3 post-invasion, and the RSA was administered from hours 3-7 post-invasion. **B** Pulsed exposure to 5 µg/ml Brefeldin A (BFA) has little effect on parasite proliferation in the absence of DHA. **C** Pulse exposure to 5 µg/ml Brefeldin A provides significant protection from artemisinin-mediated cytotoxicity. Mean of at least 3 experiments each performed in technical duplicate. Each technical replicate was counted by FACS twice and contains 100,000 gate-stopping events. **D** Western blot of eIF2α–P in PC-treated or control cells. Anti-eIF2α–P (rabbit, 1:1000; Cell Signalling) was generously provided by Prof Sibylle Mittnacht at UCL. Equal amounts of protein (15 µg) as determined by Bradford Assay were loaded in each lane.

cells. Further, eIF2α is phosphorylated in BFA-treated cells, supporting the notion that BFA exposure provokes a cell stress response.

## 6.3 Effect of pulse temperature on artemisinin sensitivity

I then wondered if a similar ER stress/ART-R response could be more broadly triggered by varying the culture temperature during the RSA. In practice, we can slow down parasite growth as a synchronisation technique by leaving culture flasks at room temperature for several hours or in the refrigerator for short periods of time. Especially when performed in the ring stage, this environmental perturbation has minimal effect on parasite development other than just slowing the cell cycle. One can even leave ring-stage cultures at 4°C overnight and still resume growing the cultures nearly normally the next day. As I made this observation by mistake while performing the above experiments, I wondered whether a similar induced ring-stage dormancy is involved and could also provoke a cytoprotective response. Indeed, in stroke patients, rapidly cooling the patient provides protection from oxidative damage, and in neuronal cell culture models, mild hypothermia has been shown to activate the unfolded protein response and induce cytoprotective dormancy[317–321]. Cooling has also been used to study trafficking dynamics as mild hypothermia slows down intracellular vesicular traffic[322]. If in *Plasmodium*, hypothermia treatment only causes parasite development to slow down, this would theoretically extend the ring stage, which is hyper-sensitive to artemisinin, and no wild type parasites would survive the RSA. However, if hypothermia slows down trafficking and induces a protective ER stress response, these cells should be less susceptible to artemisinin.

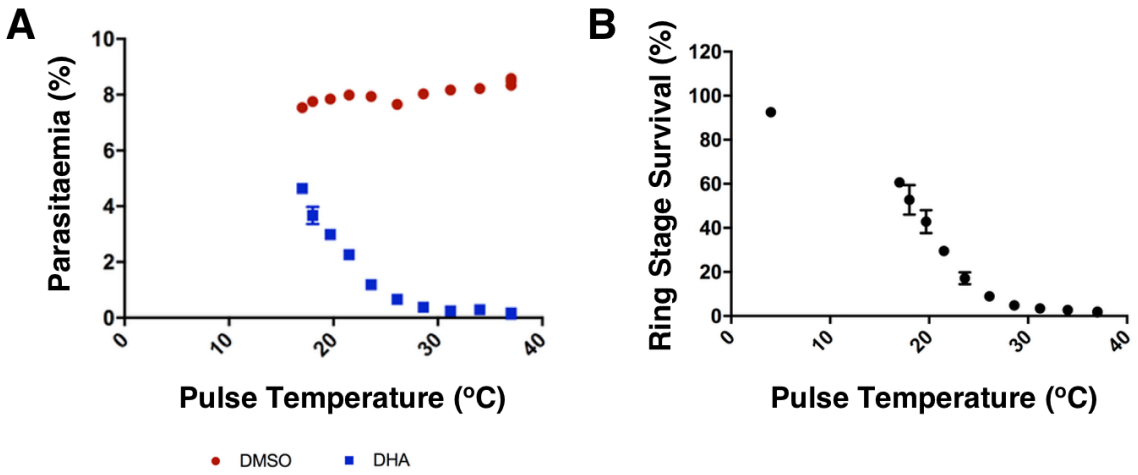


**Figure 63 Effects of pulse temperature on artemisinin sensitivity**
Temperature pulse experiments were carried out exactly as for Brefeldin A exposures. From hours 2-3 post-invasion, cultures were cooled to the stated temperature; DHA or solvent was added at hour 3, and the RSA pulse was performed at the stated temperature. **A** Transient cooling has little effect on parasitaemia after reinvasion in the absence of DHA (red circles), whereas this cooling dramatically effects parasite susceptibility to artemisinin (blue squares). **B** Ring stage survival estimates with respect to pulse temperature. These experiments were carried out in the same format described in Figure 62A. Mean of at least 3 experiments each performed in technical duplicate. Each technical replicate was counted by FACS twice and contains 100,000 gate-stopping events.

As a proof of principle experiment, I left a synchronous ring-stage culture (2 HPI) on the bench in a 17°C (RT) water bath for 1 hour and then incubated these parasites with either 700 nM DHA or solvent similarly for a further 4 hours. The parasites were washed extensively with pre-warmed media and returned to culture. More than 50% of cells survived the DHA treatment without significant consequence to development or reinvasion due to the reduced temperature as compared by Giemsa smear or FACS.

To probe the relationship between temperature and artemisinin resistance, I performed a temperature titration by pre-incubating parasites for 1 hour and performing the RSA at a series of temperatures from 17C-37°C. Cells were also

incubated at 4°C in the refrigerator. These experiments showed a sigmoidal relationship between temperature and RSA survival, where mild hypothermic pre-treatment (24-28°C) provides significant artemisinin resistance (> 5% survival). Cells incubated at 4°C for 2 hours were examined for their eIF2α phosphostatus and, as expected, contained phosphorylated eIF2α (Fig 62D).

Although total phosphorylated eIF2α was lower than in the BFA-treated cells despite these cells displaying a greater RSA survival, some of the survival may be due to broad slowing of enzymatic and chemical processes. Hypothermia is likely to also attenuate the rate of protein synthesis and the rate of activation of artemisinin. Artemisinin stability in aqueous solution is temperature dependent[323]; therefore, it is reasonable to expect that the thermodynamic spontaneity of activation is similarly temperature dependent *in vivo*. However, the presence of eIF2α–P indicates that at least some of the decreased susceptibility to artemisinin comes from an induced ER stress response, possibly caused by attenuated activity of chaperones and protein folding leading to an accumulation of misfolded and mis-trafficked proteins in the ER.

## 6.4 Effect of chemical ablation of the apicoplast on artemisinin sensitivity

The results described above and Zhang's results establish a compelling relationship between the cell stress response and artemisinin sensitivity in the early ring-stage parasite. Specifically, the profound antagonistic effects of brefeldin A exposure on artemisinin cytotoxicity shows manipulation of secretory traffic can induce this response and provide protection from artemisinin. However, longer

exposures to brefeldin A are lethal and therefore this induced state cannot be maintained. I wondered if there was a way of non-lethally maintaining disrupted secretory traffic. To the best of my knowledge, nearly all secretory trafficking routes are essential. However, apicoplast traffic can be successfully knocked out by genetic or chemical means and complemented.

The apicoplast, evolutionarily descended from the chloroplast, is a relic organelle that participates in 4 core biosynthetic processes: haem, iron-sulphur cluster, fatty acid, and isoprenoid biosynthesis. In the blood stage, isoprenoid biosynthesis is the only apicoplast pathway that is required for parasite survival[82]. Though many of the genes involved in these four processes are encoded by the nuclear genome, the apicoplast contains its own organellar genome and performs some *de novo* protein synthesis using prokaryotic-like ribosomes. Because of the unique prokaryotic nature of the organelle, the apicoplast is a target for antimalarial chemotherapy. In particular, as described in Section 1.4.5, certain antibiotics including doxycycline and azithromycin exert their antimalarial properties by inhibiting apicoplast-resident prokaryotic ribosomes. Antibiotic-treated parasites cannot replicate the apicoplast during schizogony and therefore cannot supply essential isoprenoids to the daughter parasite. In 2011, Yeh *et al* showed that supplementing parasite growth medium with isopentyl pyrophosphate (IPP), the biosynthetic product of the apicoplast isoprenoid pathway, allows antibiotic-treated parasites to survive and propagate over multiple development cycles[82]. Interestingly, Yeh *et al* showed that proteins destined for the apicoplast are mislocalised in IPP-treated, apicoplast-null parasites[82]. Although these parasites propagate normally, I wondered whether this disrupted secretory traffic would be enough to induce a sub-lethal ER stress response that would provide ring-stage protection from artemisinin.

To this end, I first planned to chemically ablate the apicoplast in the validated artemisinin-sensitive/artemisinin-resistant isogenic parasite pair Cam3.II$^{REV}$ and Cam3.II. While I expected that apicoplast removal would provide protection from artemisinin, the inclusion of Cam3.II would reveal any unexpected hypersensitivity caused by this manipulation. As described in Chapter 4, Cam3.II was isolated from a patient in Cambodia and harbours K13$^{R539T}$. Cam3.II$^{REV}$ was genetically edited to overwrite the K13 mutation and install the wild type locus. As described by Yeh *et al*, these cells were synchronised and exposed for 48 hours to 2 µM doxycycline[82]. After 48 hours, 200 µM IPP was added to the culture medium. After 96 hours, doxycycline was removed. To confirm successful apicoplast ablation and complementation, a subculture of these cells was cultured for a cycle in the absence of IPP. These experiments were performed in tandem with 3D7. Unexpectedly, the Cam3.II parasite continued to proliferate normally in the absence of IPP, whereas 3D7 DOX-treated cells died without IPP. After titrating the sensitivity of the Cam3.II parasites to doxycycline using a standard 96-hour dose response, it was clear that these parasites are highly resistant to doxycycline and azithromycin (Cam3.II $EC_{50} \approx 3.2$ µM; Cam3.II$^{REV}$ $EC_{50} \approx 2.8$ µM; 3D7 $EC_{50} \approx 0.5$ µM; Fig 64). To the best of our knowledge, this is the first demonstration of bloodstage antibiotic resistance in Southeast Asian parasites. We are currently examining whether these parasites harbour mutations in apicoplast-encoded ribosomes that would explain this result. However, validated genetic markers for doxycycline resistance are lacking.

Because the Cam3.II parasites are resistant to doxycycline and azithromycin, further experiments were only conducted with the 3D7 strain. A dose response experiment with 3D7 and doxycycline in the presence of IPP confirmed that 200 µM

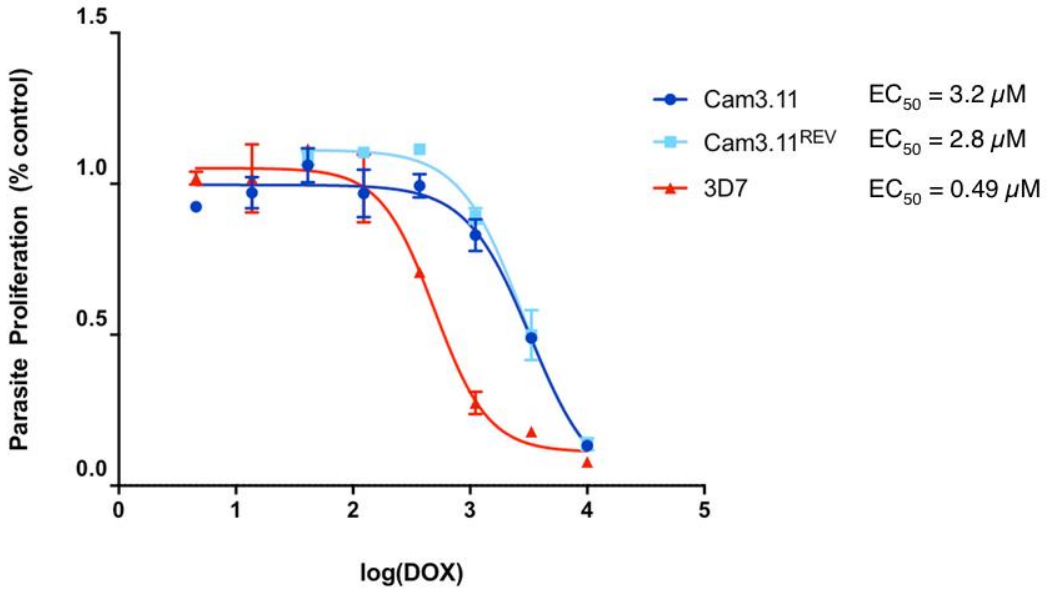


**Figure 64 Sensitivity of ART-R and ART-S parasites and to 96h exposure to doxycycline**
Cambodian parasites harbouring $K13^{R539T}$ (Cam3.II) and $K13^{WT}$ ($Cam3.II^{REV}$) alleles and 3D7 were examined for their sensitivity to doxycycline. The primary mechanism of doxycycline cytotoxicity kills parasites after two cycles, therefore parasite proliferation was examined after 96 hours of exposure to the drug rather than the standard 48 hours. Total DNA content was examined by cell lysis and SYBR Green staining as previously described. Cam3.II parasites are dramatically less sensitive to doxycycline than 3D7.

IPP compensates for the loss of the organelle.

To examine the effects of apicoplast ablation on artemisinin sensitivity, 3D7 parasites were tightly synchronised and then cultured for 96 hours in the presence of 2 µM doxycycline and 200 µM IPP to remove the apicoplast. At 96 hours post-invasion, apicoplast-null parasites were pulsed with 700 nM DHA for 4 hours and cultured for a further 65 hours (Fig 65A). IPP was refreshed daily. Parasite proliferation was examined by FACS. Though IPP-supplemented parasites cultured in parallel continued to proliferate normally, apicoplast-null schizonts did not reinvade or proliferate well after Percoll treatment. With this in mind, it seems that a substantial proportion of these cells survive the RSA pulse with DHA, although solvent-treated RSA control parasites only displayed a 2-fold expansion after 72 hours rather than the normal 5-6-fold expansion observed during normal

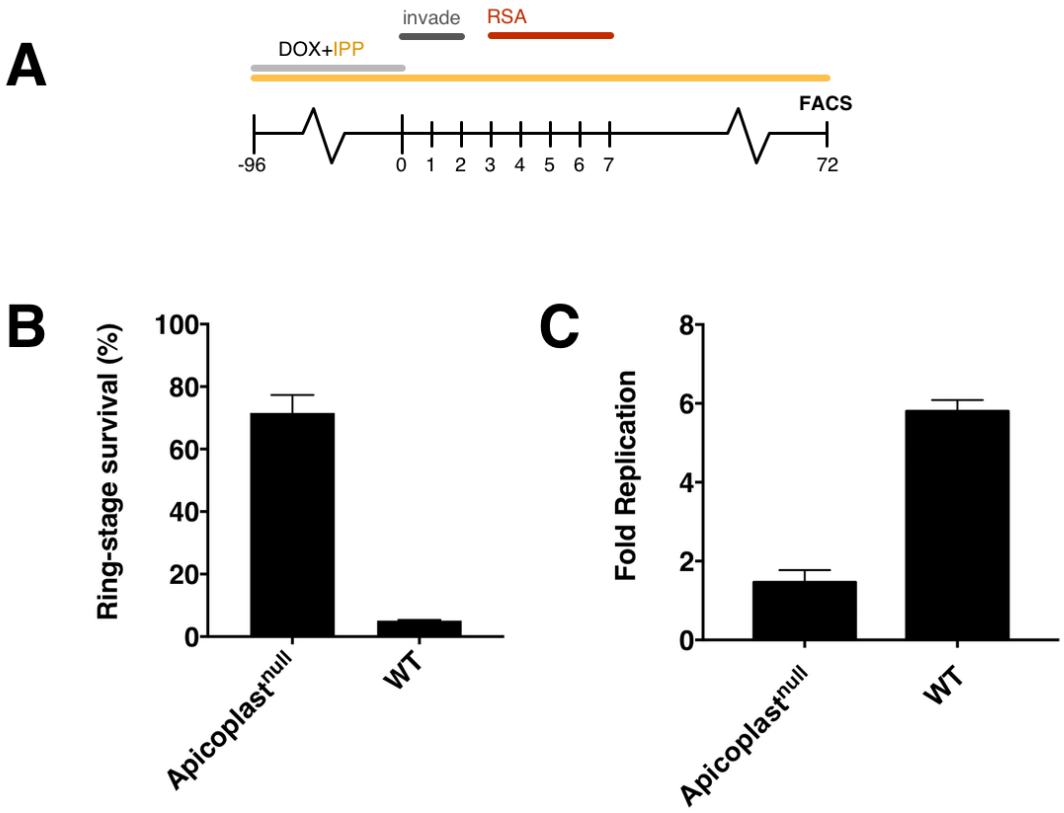


**Figure 65 Effects of chemical ablation of the apicoplast on ring-stage artemisinin sensitivity**
**A** 3D7 background parasites were treated with 2 µM doxycycline and 200 µM isopentenyl pyrophosphate (IPP) for 96 hours. After 96 hours, early ring stage parasites were synchronised and exposed to 700 nM DHA or solvent for 4 hours in the RSA protocol described above. **B** Ring stage survival was determined 65 hours later by FACS with SYBR-Green/MitoTracker Deep Red. Mean and SEM are reported of at least 3 experiments each performed in technical duplicate. Each technical replicate was counted by FACS twice and contains 100,000 gate-stopping events (left). **C** Fold replication was also enumerated between DMSO-treated cells with and without an apicoplast and refers to the ratio parasitaemia before and after the RSA (right).

culture. Given that IPP is exceedingly expensive, sufficient culture volumes could not be grown in order to probe eIF2α-P status in DOX/IPP-treated parasites. Electron micrographs of parasites lacking an apicoplast show that the parasite cytoplasm is clogged with apicoplast-targeted vesicles. Presumably there is a dynamic equilibrium which eventually causes material destined for the apicoplast to back up along the secretory pathway, which may induce a cell stress response, and generate DHA resistance.

Because the apicoplast produces haem by an endogenous biosynthetic pathway, and haem is believed to be the activator of artemisinin in the cell (Section 1.5.3.1), I wondered whether these results could be explained as a consequence of knocking out this endogenous haem biosynthetic pathway, since the amount of haemoglobin per cell volume in ring stages is exceedingly low (Section 1.5.3.1). However, parasites lacking two enzymes in the endogenous haem biosynthetic pathway, 5-aminolevulinic acid synthase and ferrochelatase, were equally sensitive to DHA as compared to wild type progenitors in the RSA (Fig 66).

Even though these experiments are difficult to interpret alone, the results presented in this section are consistent with the results presented above showing that disrupting secretory traffic can provide protection from artemisinin in early ring-stage parasites. Interestingly, during the production of this thesis, a study examining the effects of transient plastid-derived biosynthetic precursors on recovery from

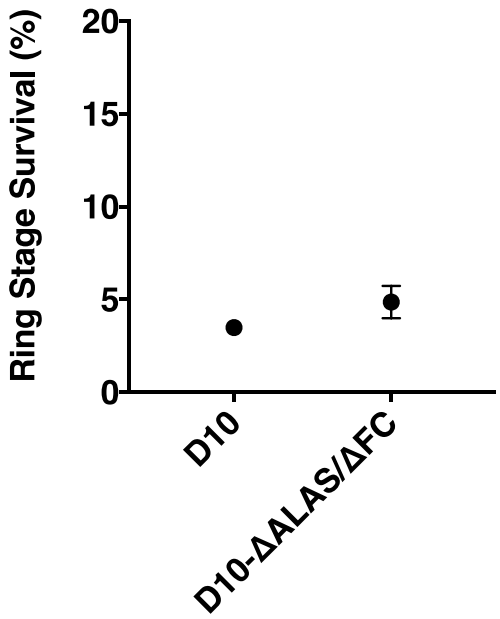


**Figure 66 Effect of haem biosynthetic knockout on ring-stage sensitivity to artemisinin**
Parasites lacking 5-aminolevulinic acid synthase (ALAS) and ferrochelatase (FC) were obtained from Prof Akhil Vaidya and Dr Hangjun Ke at Drexel University (Philadelphia, USA). These cells were synchronised and examined for their susceptibility to a ring-stage pulse of DHA in the RSA in parallel with wild type D10 parental parasites. RSA was quantified by FACS as previously described. Mean and SEM are presented of at least three experiments, each performed in technical duplicate.

artemisinin-induced dormancy reported that DOX/IPP-treated parasites recrudesce significantly faster than wild type parasites possessing an apicoplast, consistent with these results[203].

## 6.5 Effect of μ2 knockdown on artemisinin sensitivity

The results described above and Zhang's results establish a compelling relationship between the ER stress response and artemisinin sensitivity in early ring-stage parasites[202]. As described in the Section 6.1, the results described in Chapter 5 show that K13 is somehow involved in AP-2-dependent traffic. It is therefore tempting to logically link the phenomena of mutant trafficking factors causing resistance and physiochemically disrupted ER dynamics causing resistance into a model of how artemisinin resistance occurs. However, I wanted to find genetic support for this link.

Without knowing what the AP-2 complex is trafficking, it is difficult to directly monitor the rates of this traffic in artemisinin-resistant and -sensitive parasites. Additionally, because μ2 knockout parasites are not viable, it is impossible to perform the RSA on ring stage parasites devoid of μ2. Therefore, to investigate whether defective AP-2 traffic causes artemisinin resistance, I aimed to created a parasite in which the abundance of μ2 could be transiently manipulated. To this end, I planned to introduce a regulable copy of *pfap2mu* into my inducible DiCre *pfap2mu* knockout parasite line. Specifically, I planned to knock out the chromosomal *pfap2mu* locus and grow the parasites on an episome expressing a titratable μ2-GFP-DDD under the control of the *cam* promoter.

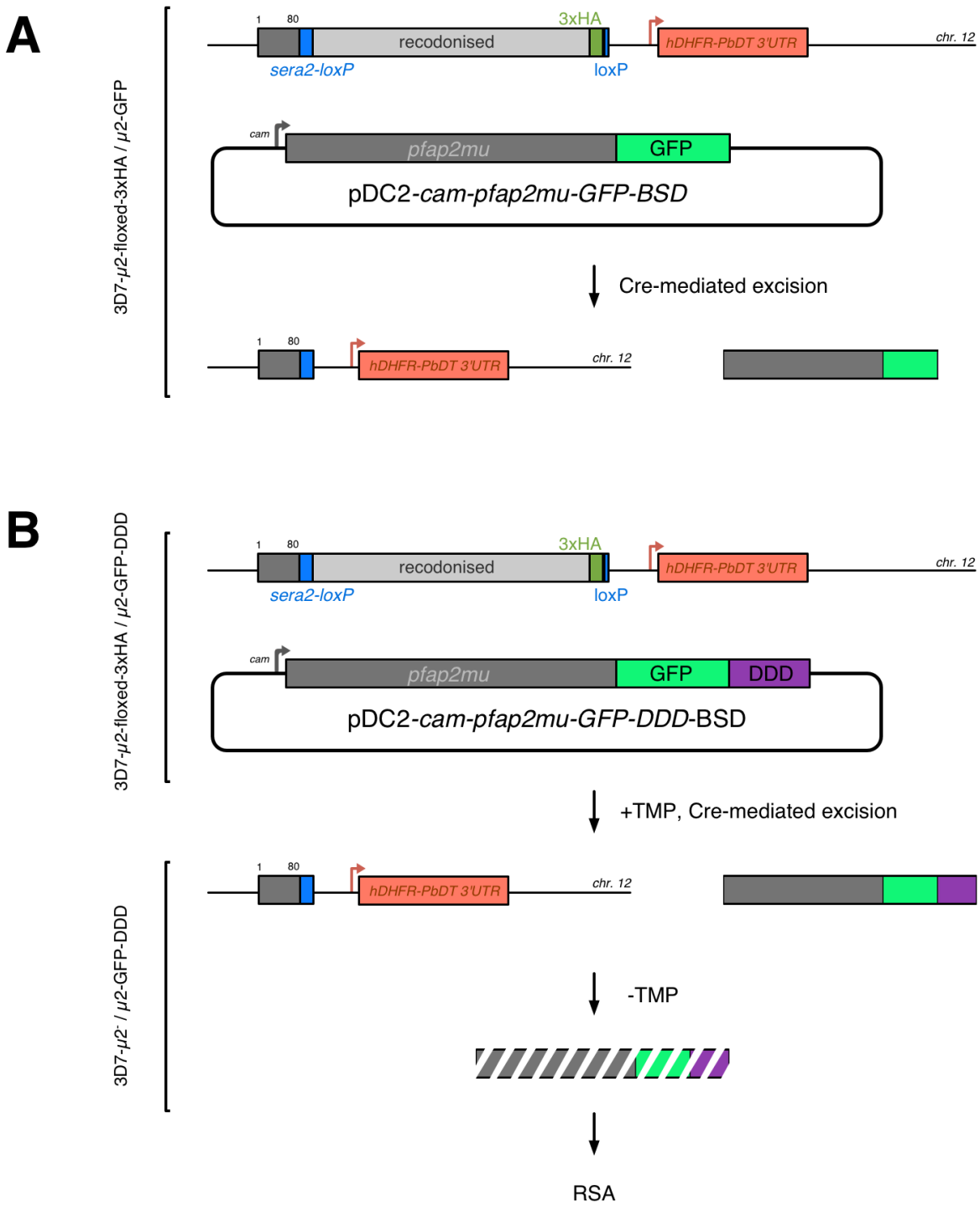


**Figure 67 Schematic of µ2 complementation and transient regulation**
**A** Schematic of complementation of DiCre-mediated µ2 knockout with episomally-expressed µ2-GFP. **B** Schematic of modification of pDC2-cam-*pfap2mu-GFP*-BSD construct to introduce the DHFR degradation domain (DDD) onto the C-terminus of episomally-expressed µ2, enabling transient protein-level knockdown of µ2 once the endogenous *pfap2mu* CDS has been excised by Cre recombinase. Trimethoprim (TMP) stabilises the DDD tag and can be washed out of culture medium to induce rapid degradation of the µ2-GFP-DDD fusion protein.

Principally, the DHFR destabilisation domain (DDD) is a trimethoprim (TMP)-sensitive protein unfolder. In the absence of TMP, the DDD element is destabilised and is marked for degradation. Thus, any protein fused to the DDD element can be stabilised or degraded by adding or removing TMP from the cell culture. In previous studies, the DDD element has been shown to cause degradation of a target factor within minutes[324].

The previously described (Section 5.5) 3D7-µ2-*floxed*-HA parasite line is aptly suited for these experiments because TMP is a DHFR substrate analogue and is mildly toxic to parasites. Therefore, to use the DDD system, the parasites must express an additional copy of DHFR, which my µ2 knockout parasite line does. Additionally, by fusing µ2 to GFP, I can independently monitor the levels of both the endogenously-expressed, HA-tagged µ2 and the episomal, regulable µ2-GFP. Lastly, because the *cam* promoter is constitutively active, whereas the endogenous *pfap2mu* promoter has a stage-specific transcriptional profile, functional µ2-GFP-DDD could be transiently knocked down and restored by removing or adding TMP to the culture. If the endogenous promoter were used, the cells may not retranslate sufficient amounts of µ2 until much later in the cell cycle, by which time the cells may have died. Thus, the *cam* promoter would allow me to examine the consequences of transiently depleting µ2 at various times in the cell cycle.

This scheme depends entirely on the assumption that episomally-expressed µ2-GFP can complement an endogenous *pfap2mu* knockout. To investigate this, a episomal construct expressing µ2-GFP under the control of the *cam* promoter was created based on the pDC2-expression system. This construct was transfected into 3D7-µ2-*floxed*-3xHA schizonts by Nucleofection and selected continuously.

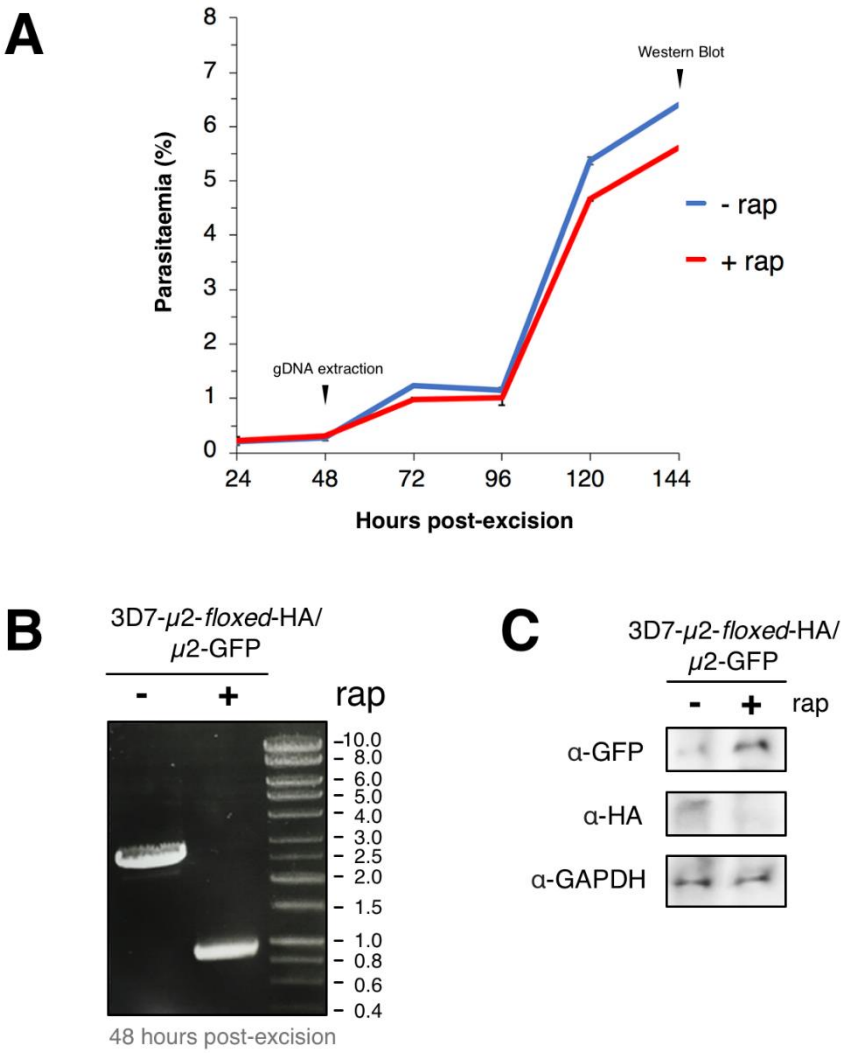


**Figure 68 Episomally-expressed *pfap2mu-GFP* can complement an endogenous *pfap2mu* knockout**

**A** Growth of 3D7-µ2-*floxed*-HA/µ2-GFP parasites treated with rapamycin or equivalent DMSO was monitored with SYBR Green/MitoTracker Deep Red FACS over multiple life cycles. Rapamycin was added in trophozoites; at 24 hours post-excision, parasites cultures were in the ring stage. Genomic DNA was extracted 48 hours post-excision to examine the efficiency of excision (**B**), and cultures were lysed at 144 hours post-excision for a Western Blot to examine the presence of endogenous µ2-HA and episomal µ2-GFP (**C**).

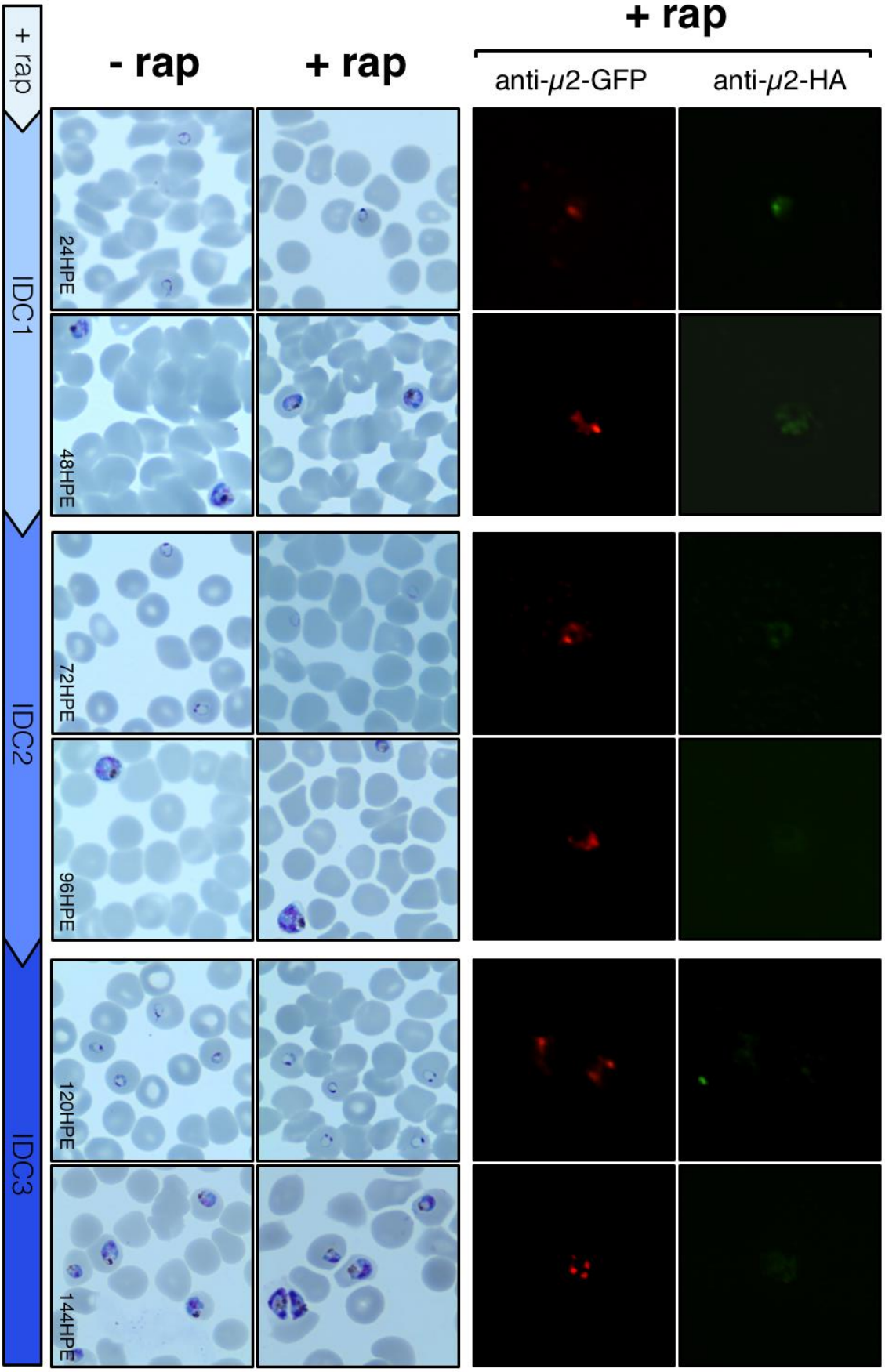
+ rap
IDC1
IDC2
IDC3
- rap
+ rap
+ rap
anti-μ2-GFP
anti-μ2-HA
24HPE
48HPE
72HPE
96HPE
120HPE
144HPE

**Figure 69 Cells proliferate normally when complemented with episomal µ2-GFP**
At 24 hour intervals after rapamycin-induced excision of the endogenous *pfap2mu* locus, thin smears were prepared for Giemsa staining and indirect immunofluorescence to examine the cell morphology, presence of endogenous µ2-HA, and localisation of episomally-expressed µ2-GFP in rapamycin- and solvent-treated parasites. Cell development appears unaffected by episomal complementation of an endogenous *pfap2mu* knockout, and endogenous µ2-HA signal decays in a single intraerythrocytic development cycle (IDC). (Figure on previous page).

Once these cells were stably growing, the culture was split, and 10 nM rapamycin or equivalent DMSO solvent was added to trophozoites for 1 hour. After 1 hour, the cells were extensively washed and returned to culture. Parasite growth was monitored daily with SYBR-Green/MitoTracker-Deep Red FACS for several asexual cycles. Before the knockout was induced, thin smears stained for both the endogenous and episomal µ2 showed the two molecules colocalised well, confirming the episomally expressed µ2 is in the expected location in the cell. Throughout this growth experiment, thin smears were prepared at several points to examine cell morphology by Giemsa staining and the half-life of endogenous µ2-3xHA. Both cultures were maintained on 2 µg/ml blasticidin-S.

Over multiple cycles, *pfapmu*$^{-}$ cells complemented with episomal µ2-GFP expressed by the *cam* promoter grew as well as the WT cells, indicating these knockout parasites could be successfully grown on an episome for multiple cycles (Fig 68,69). Morphologically, cells with and without endogenous µ2 appeared equivalent with no gross deformations (Fig 69). Genomic DNA was extracted 48 hours after treatment with rapamycin, and PCR amplification of the *floxed* µ2-HA locus confirmed nearly complete excision. µ2-3xHA signal disappeared within the same cycle as the excision and was not re-detected later. Western blot analysis 144 hours after rapamycin treatment confirmed the absence of µ2-HA and presence of µ2-GFP.

Because these proof of concept experiments validate this experimental approach and indicate *cam*-expressed episomal µ2 complements an endogenous knockout, a construct expressing the planned µ2-GFP-DDD was transfected into 3D7-µ2-*floxed*-HA schizonts by Nucleofection. Transgenic parasites were continuously selected with 2 µg/ml blasticidin-S and recovered within 1 week.

These cells were then cultured on 10 µM TMP for 2 cycles to stabilise episomally-expressed µ2. The endogenous *pfap2mu* was then knocked out with rapamycin as previously described. To explore the role of functional µ2 in ring-stage sensitivity to artemisinin, reinvading parasites were washed into medium containing 0, 1, 5, or 10 µM TMP. Parasites were incubated in this medium for 3 hours, synchronised, and then exposed to 700 nM DHA or DMSO equivalent also in the presence of this TMP titration from hours 3-7 post-invasion. After the $RSA^{4h}$ was performed, and at hour 7, the cells were extensively washed, and all cells treated ith TMP were washed into medium containing 10 µM TMP. Medium containing TMP was refreshed daily and cell proliferation was examined by FACS.

As expected, parasites not treated with rapamycin that retained the endogenous *pfap2mu* gene were completely sensitive to DHA. However, µ2-GFP-DDD-knockdown ring stage cells lacking chromosomal *pfap2mju* were much less sensitive to artemisinin. In the presence of 5 µM or 1 µM TMP, 50.2% and 68.4% of cells were resistant to the ring-stage pulse of artemisinin. Cells could not be propagated when transiently cultured without TMP indicating that the parasite cell is sensitive to the level of µ2, even in the ring stage. Interestingly, cells treated with 10 µM TMP still displayed a 14.8% ring-stage survival to artemisinin. This could indicate µ2-GFP-DDD is still unstable, even in the presence of TMP, or that the DDD element partially disrupts the normal function of µ2, generating a stress response.

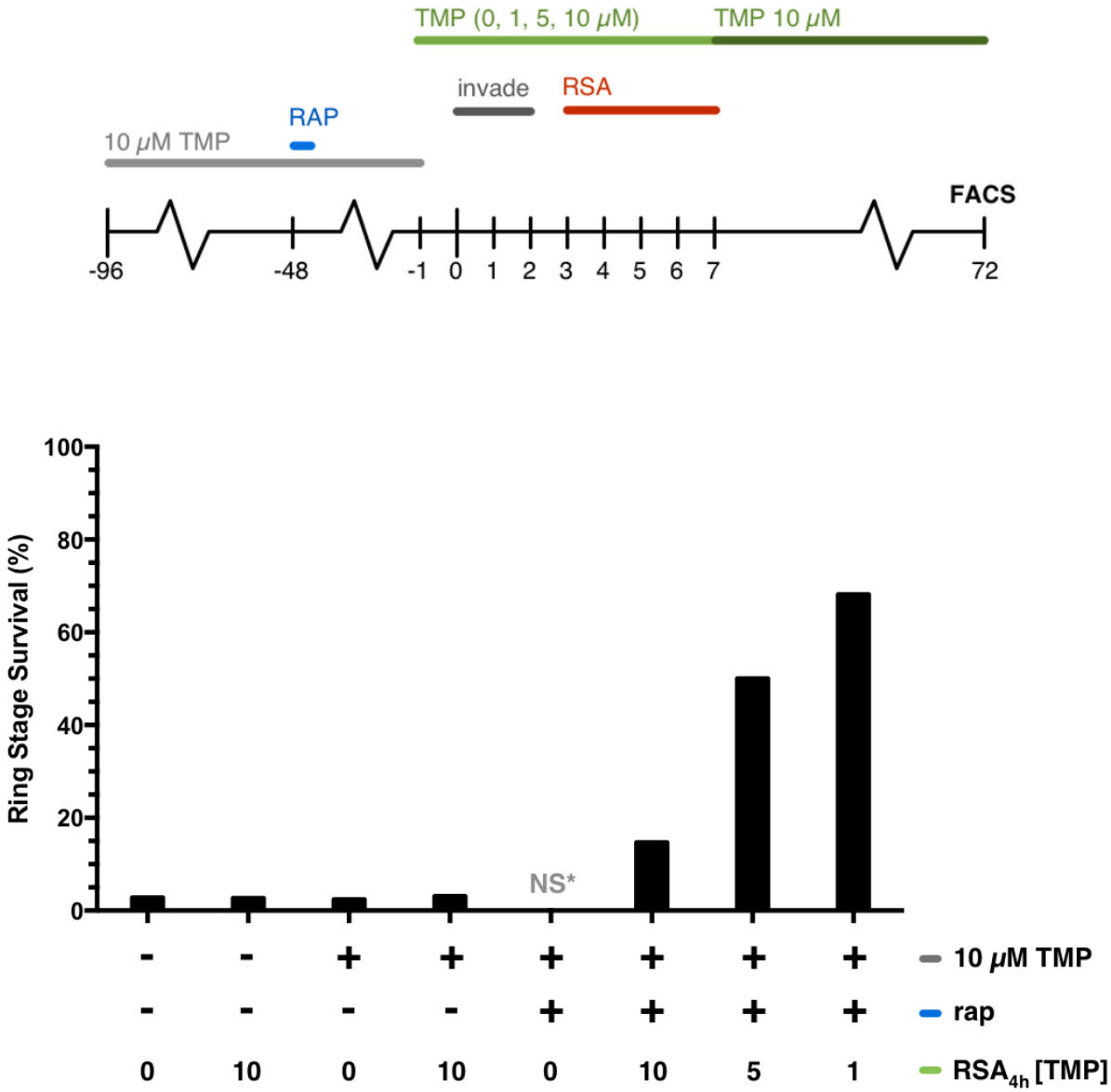


**Figure 70 Effects of transient µ2 knockdown on ring-stage artemisinin sensitivity**
(Top panel) 3D7 background parasites were treated with 10 µM trimethoprim (TMP) or DMSO, refreshed daily, for two lifecycles (grey). These cells were then treated with 10 nM rapamycin or DMSO for 1 hour in the ring stage (blue). From the end of this second cycle (T = -1 HPI), these cells were then washed into 0, 1, 5, or 10 µM trimethoprim for 4 hours while they were synchronised to regulate the amount of µ2-GFP-DDD in the cell. These synchronised parasites were then exposed to 700 nM DHA or solvent for 4 hours in the RSA protocol described above. Cells treated with any concentration of TMP during the RSA were then incubated with 10 µM TMP for a further 65 hours. (Bottom panel) Ring stage survival was determined by FACS with SYBR-Green/MitoTracker Deep Red. Mean survival from one experiment performed in technical duplicate. Each technical replicate was counted by FACS twice and contains 100,000 gate-stopping events. *NS indicates no survival.

While more experiments are certainly required to clarify and probe this result, such as IFA and western blots to confirm the transient knockdown of μ2-GFP-DDD and examine the magnitude of the knockdown in relation to the artemisinin resistance phenotype, these data are consistent with my previous data suggesting that transient manipulation of secretory traffic protects the parasite cell from artemisinin. Interestingly, these data also suggest that simply triggering the proteasome in the cytosol is not sufficient for ring-stage artemisinin resistance. In this experiment, cells expressing μ2-GFP-DDD in the absence of TMP should be constitutively degrading this destabilised protein. However, these cells (Fig 70, first column) are fully sensitive to artemisinin. Thus, because we know μ2 is in the cytosol rather than in the ER lumen, it follows that the disruption of μ2-GFP-DDD may induce a ER-like stress response, that protects cells from artemisinin like the experiments described by Zhang *et al*[202].

## 6.6 A model of artemisinin resistance in *P. falciparum*

Taken together, these data suggest that artemisinin resistance centres around the ER. BFA is commonly used in mammalian culture systems to stimulate the ER stress response, also known as the unfolded protein response. Though *Plasmodium* species do not have many of the classic components of the UPR, they do have eIF2α, a stress-sensitive translation repression factor. The data shown here show that BFA antagonises the action of artemisinin in early ring-stage parasites and leads to eIF2α phosphorylation. Because this phosphorylation process is one of the few recognisable elements of the UPR in *Plasmodium*, we can conclude that BFA treatment induces a UPR stress response. These data are consistent with the findings

of Zhang *et al* indicating activation of this pathway underpins artemisinin resistance[202].

The manipulations discussed in this chapter provide important logical connections to understanding how variants of K13 and µ2 may reduce parasite susceptibility to artemisinin. The data presented in Chapter 5 strongly support that µ2 is localised along the early secretory pathway, that K13 and µ2 interact, and that knocking out µ2 causes a lethal defect in parasite maturation by disrupting the integrity and biogenesis of multiple secretory organelles. Previous data shows that K13 is also required for asexual survival[192]. Therefore, µ2 and K13 both play important roles in parasite development.

It is known that mutations in K13 cause ring-stage artemisinin resistance, and the data presented in Chapter 4 shows that a mutation in µ2 causes a similar phenotype. Molecular modelling suggests that resistance-causing mutations in K13, which occur in the β-propeller, may disrupt disulfide bond formation and propeller integrity (unpublished data), and the resistance-causing µ2(I592T) mutation possibly disrupts the folding of the µ2 core domain (Appendix II). Supporting this, reversibly disrupting µ2 in early ring stages induces artemisinin resistance in otherwise sensitive cells (Section 6.5). Therefore, these data all suggest that ring-stage artemisinin resistance arises when ER/secretory protein dynamics are disrupted in the young, developing parasite. eIF2α–P is a hallmark of disrupted ER dynamics and cell stress, and both $K13^{C580Y}$ and ring-stage BFA treatment induce this regulatory phosphorylation.

Tentatively, I would like to suggest a model for ring-stage artemisinin action and resistance (Fig 71). Activated artemisinin seems to cause disseminated oxidative damage in the cell. In response to this generalised, systemic stress, the cell must

respond by upregulating and activating protein turnover machinery. Therefore, to survive artemisinin-induced stress, parasites need to either 1) avoid or reduce activation of artemisinin or 2) enhance or pre-activate their stress response mechanisms. Since the parasite absolutely requires haemoglobin, it is unlikely that this process can be majorly manipulated to achieve resistance. It is known that resistant parasites upregulate genes associated with the stress response and protein turnover. However, the molecular basis for this is unclear. In other words, why are these factors upregulated in artemisinin-resistant cells under normal, drug-free conditions?

My suggestion is that these parasites, whether they harbour K13 or μ2 mutations, are treated with BFA, lack apicoplasts, or have reduced levels of μ2, all display defects in secretory traffic. Intracellular traffic exists as a delicate equilibrium between the origin and destination, and as molecules accumulate in one compartment or another, the literal traffic on the intracellular highways backs up. In response to this stress, the cell responds by upregulating turnover machinery. When these cells encounter artemisinin, they are better suited to respond to artemisinin-induced damage and propagate to the next cycle.

If these cells have enhanced stress responses, why does artemisinin resistance only occur in the ring stage? Multiple studies suggest that haemoglobin metabolism activates artemisinin, and the amount of haemoglobin per cell volume in ring stage parasites is exceptionally low (Section 1.5.3.1). Additionally, data presented in Section 6.4 show that endogenous haem biosynthesis is not responsible for ring-stage activation of artemisinin. My suggestion is that though the concentration of DHA may be the same in exposed ring and trophozoite or schizont stages, the proportion of activated DHA may be quite low in ring stages when there is

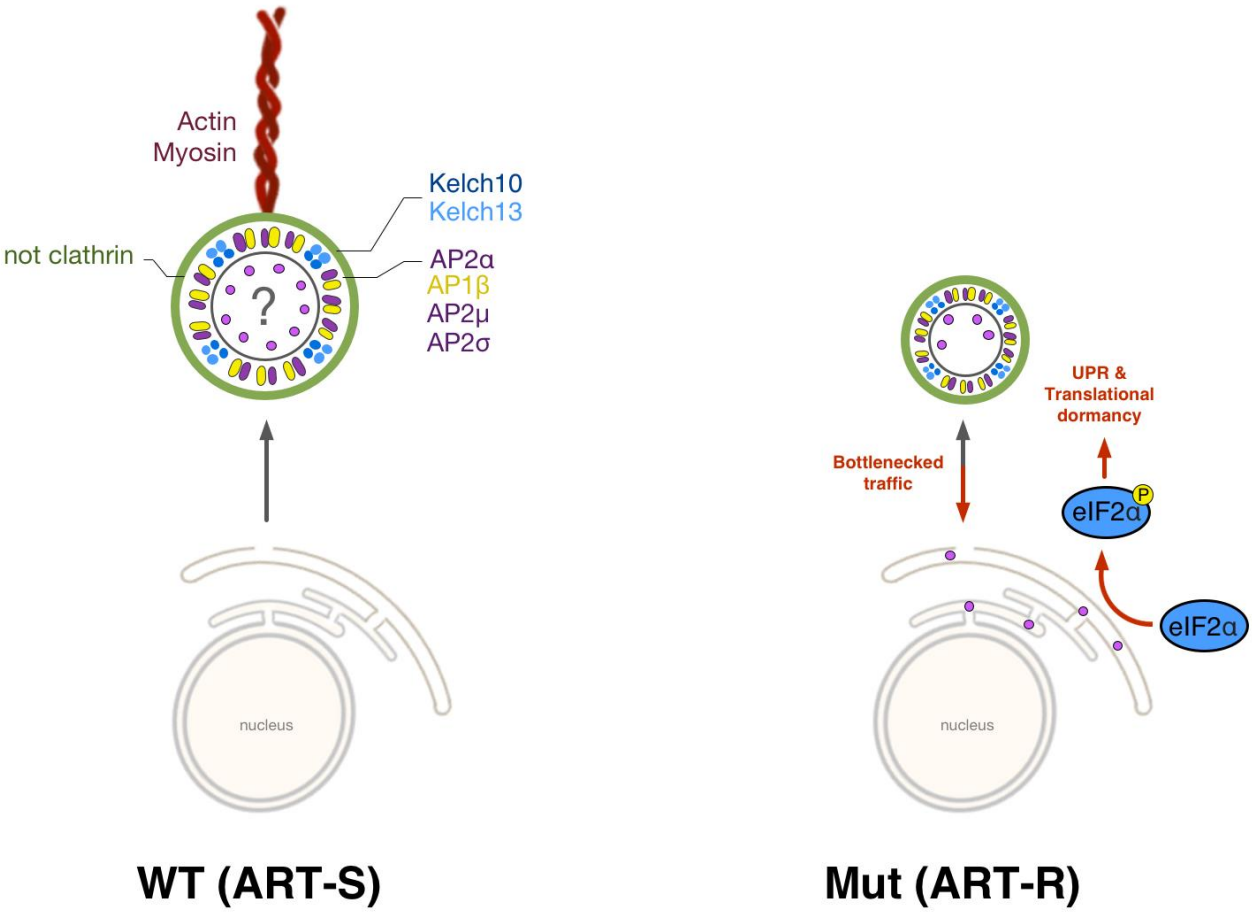


**Figure 71 A model for ring-stage artemisinin resistance**
A model for ring-stage artemisinin resistance based on the data presented in Chapters 5 and 6. Under normal conditions, AP-2 and K13 interact and localise along the early secretory pathway. μ2 and K13 are both essential molecules, supporting the importance of this trafficking route. Disruptions to the underlying pathway either by genetic mutation or physiochemical modulation induce a stress response that provides protection from artemisinin. The diagram presented is not intended to imply direct molecular interaction because the annotated molecules may interact via unknown scaffolds, but are designed to label potentially important molecules. Additionally, it is unknown exactly from where the AP-2 complex traffics, however it is likely to be somewhere in the early secretory pathway near the ER. The small AP-2 structure (right) is meant to depict disrupted traffic.

comparably little haem and haemazoin. Therefore, the hurdle may be quite low for ring stages to achieve resistance, and the parasite cell may tolerate manipulations to these essential pathways in early ring stages when metabolism is starting, whereas the comparable manipulations in the much-more-active trophozoites would be lethal.

Perhaps the most concerning deduction from this model is that, while K13 mutations dominate in Southeast Asia, potentially any mutation that disrupts ring-stage secretory traffic in a non-lethal way may reduce parasite susceptibility to artemisinin.

# Chapter 7

# Exploration of the cellular role of the *Plasmodium falciparum* Ubp1 ubiquitin hydrolase and its potential as a drug target

## 7.1 Deubiquitination in *Plasmodium falciparum*

Deubiquitination, as discussed in Chapter 1, is a dynamic post-translational modification process that contributes to nearly every signalling pathway in the eukaryotic cell. For every ubiquitin ligation reaction, there is a downstream deubiquitination step catalysed by a ubiquitin hydrolase, also known as a deubiquitinase, that recycles ubiquitin monomers back into a free ubiquitin pool[240]. In *Plasmodium falciparum*, 30 different deubiquitinases (DUBs) have been annotated in the genome[195]. Of these 30, only one has been characterised. This enzyme, PfUCHL3, was interrogated structurally and biochemically by Artavanis-Tsakovas *et al*[250]. Interestingly, this group showed this enzyme did not bear structural similarity to the mammalian orthologue, and also unlike its orthologues, is capable of removing Nedd8, a ubiquitin-like protein, from neddylated substrates. Her work also provides experimental evidence that some of the other putative DUBs interact with ubiquitin and potentially also Nedd8[249].

Because the work described in Chapter 4 shows that Ubp1, one of the 30 putative *P. falciparum* DUBs, can modulate parasite susceptibility to frontline chemotherapy, including artemisinin, I also sought to explore the role of Ubp1 using

cellular and molecular approaches. DUBs represent promising drug targets in cancer cells, and they may be similarly exploitable in the malaria parasite.

## 7.2 Generation of transgenic *P. falciparum* expressing Ubp1-GFP

To determine where Ubp1 is located in the cell and begin to understand its function, I designed a CRISPR-Cas9-based scheme to tag Ubp1 at the genomic locus. Transcriptomic evidence suggests that the entire ~3200 bp mRNA is transcribed and spliced, but it is possible that the protein is post-translationally processed to release a smaller, catalytically active domain. In order to detect the putative active DUB, I aimed to GFP or HA tag the C-terminal catalytic domain.

The structure of the chromosomal copy of *pfubp1* is comprised of three exons and two introns. The putative catalytic domain spans exons 2 and 3, and exon 3 is only 341 bp. Based on my experience selecting sgRNAs for Cas9-modification of *pfap2mu*, I selected a guide sequence at the 5' end of exon 3 with a DRA (predicted guide activity) score of greater than 50%. A 500 bp region immediately upstream of intron 2 was selected as the 5' homology arm, exon 3 was recodonised and fused to a short poly(Gly-Ser) linker and GFP, and 500 bp of the 3' UTR was selected as the 3' homology arm. This donor template was also modified to swap the endogenous intron 2 with the synthetic *sera2*-LoxP intron sequence and insert a second LoxP site immediately after the stop codon to mediate DiCre conditional excision of the putative catalytic domain (Fig 72A). An HA tag was also included in frame between the lox elements, which could be used to examine the efficiency of Cre-mediated excision on a protein level. The donor construct with and without the DiCre elements

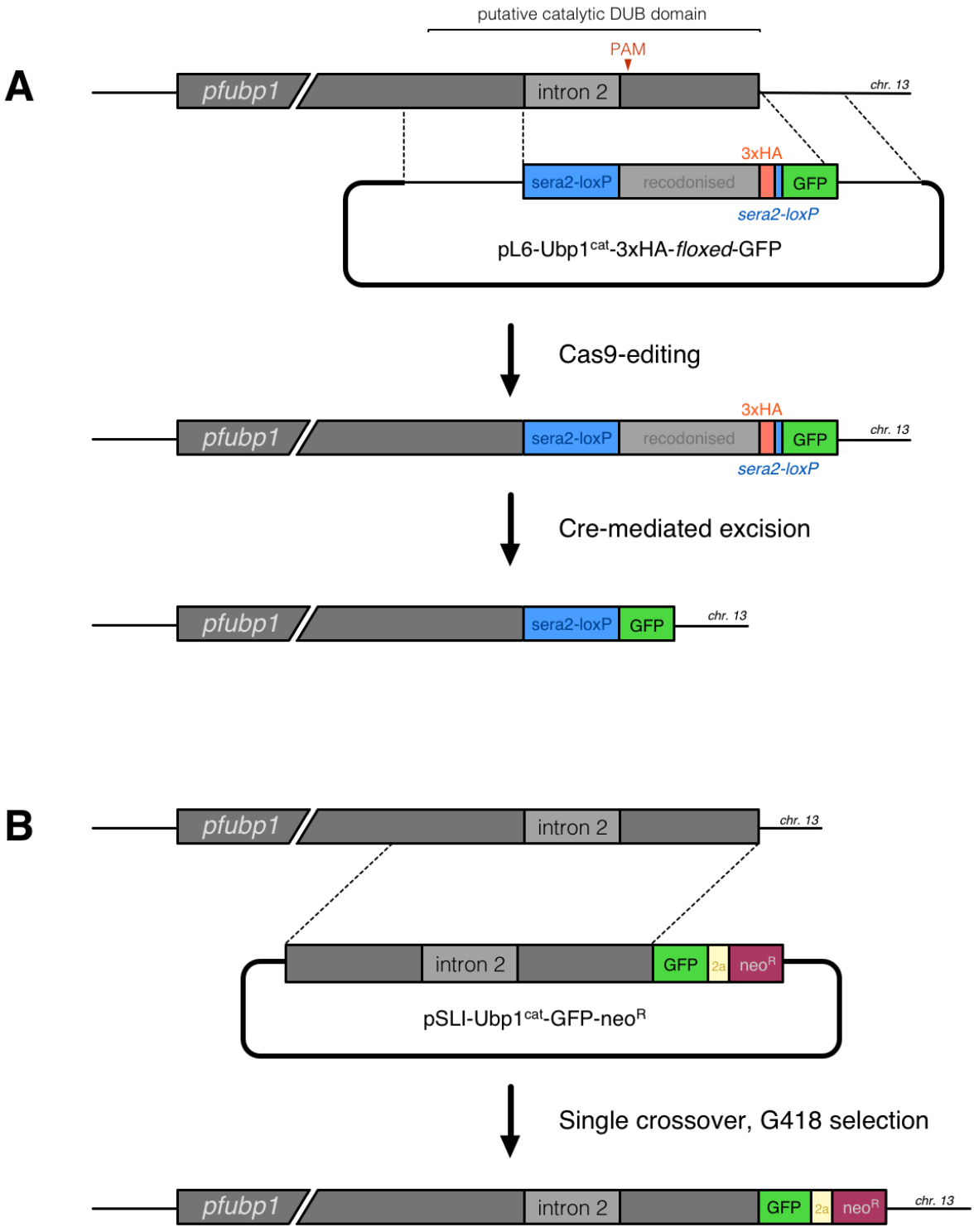


**Figure 72 Schematic of the tagging of PfUbp1**
**A** A pL6-based Cas9 donor repair template was designed to integrate loxP sites to flank the putative Ubp1 catalytic domain (*flox*), swap the endogenous intron 2 with the synthetic loxP-containing *sera2* intron, and install tandem HA and GFP tags via a selected PAM site downstream of intron 2. After rapamycin-inducible Cre-mediated excision, the coding sequence for the HA-tagged putative catalytic domain would be excised, while leaving the GFP CDS in frame. This tagging scheme failed.
**B** A second tagging scheme using the selection-linked integration (SLI) approach. The 3' 1.5 kbp of the genomic *pfubp1* sequence, including intron 2, was cloned in frame with a GFP-T2a-NeoR coding sequence. G418-treating parasites harbouring this pSLI episome selects for parasites that successfully integrated the desired transgene by single-crossover recombination.

along with pUF1-Cas9 were transfected into 3D7 and a 3D7-based DiCre-expressing parasite line by Nucleofection, as described in Section 3.4.3.3.

Transfected parasites were selected with WR99210 and DSM-1 as described. After three weeks, parasites recovered in both transfections but were unmodified. A second transfection with the tagging-only donor template and pUF1-Cas9 was also unsuccessful. Like the original µ2(S160N) attempts, these failures indicate a problem with the transgenesis strategy. This could be due to poor targeting of the sgRNA-Cas9 complex to the genome or a broader problem with the tagging scheme, for example if Ubp1 does not tolerate C-terminal tags.

Rather than selecting another guide sequence, I switched to the selection-linked integration (SLI) method of transgenesis[192]. This technique involves fusing the protein of interest to an aminoglycoside phosphotransferase (NeoR), which provides resistance to neomycin (G418), with a self-cleaving T2a peptide (Fig 72B). In this setup, a single homology arm of approximately 1-1.5 kbp is cloned upstream of an affinity or fluorescent tag and the T2a-NeoR element. Transfected parasites are first selected for those containing the SLI donor plasmid, and then they are selected with G418 for parasites which have successfully integrated the plasmid by single-crossover recombination. These cells express the tagged protein of interest and the neomycin resistance factor.

Using this method, the 3' 1.5 kbp of the genomic *pfubp1* sequence was cloned into Prof Tobias Spielmann's pSLI-GFP-NeoR vector[192]. This construct was transfected into purified 3D7 schizonts by Nucleofection. Transfected parasites were selected with 2.5 nM WR99210 for 17 days until recovered parasites were growing stably. At this point, these parasites were seeded at 3% parasitaemia in 2%

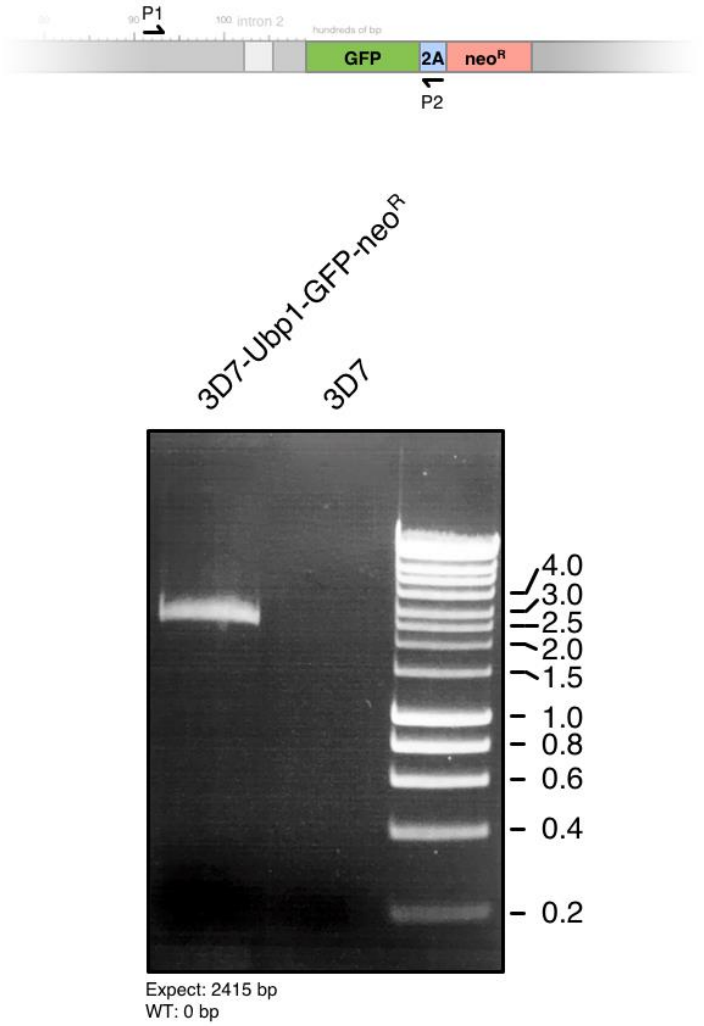


**Figure 73 PCR confirmation of PfUbp1 tagging construct integration**
After G418 selection, genomic DNA was extracted from G418-resistant parasites, and successful integration of the pSLI-Ubp1$^{cat}$-GFP-neo$^{R}$ tagging construct into the 3D7 genome was confirmed by PCR. A forward primer annealing upstream of the single-crossover integration homology arm and reverse primer annealing in the *neo$^{R}$* gene CDS were used to specifically amplify the expected, modified *pfubp1-GFP-neo$^{R}$* chromosomal locus (2415 bp fragment). Wild type 3D7 genomic DNA was amplified in a parallel to confirm the specificity of the primers for the transgenic locus.

haematocrit in two wells of a 6-well plate and treated with 0.4 µM G418 for 48 hours. The drug was washed off, and successfully integrated parasites expressing Ubp1-GFP-NeoR were obtained one week later. Integration was confirmed by PCR and IFA (Fig 73 and 74).

## 7.3 Localisation of Ubp1

I had hoped to be able to observe Ubp1 localisation by live microscopy. However, the GFP signal observed was too faint to reproducibly characterise across any stage of the asexual lifecycle. Thin smears were prepared in ring, trophozoite, and schizont stage, and Ubp1-GFP localisation was probed by indirect immunofluorescence with an anti-GFP antibody produced by Ellen Knuepfer and Prof Anthony Holder. Interestingly, the localisation of Ubp1 resembled beads on a necklace around the nucleus, particularly in ring-stage parasites where Ubp1 stains punctate structures in a tight perinuclear ring (Fig 74). As the parasite matures through the trophozoite stage, Ubp1 staining becomes more diffuse and less intense. The few spots observed in mid-trophozoites are in close apposition to the nucleus. In schizonts, Ubp1 staining seems punctate, with each merozoite inheriting a single Ubp1-labeled structure. These localisation experiments are consistent with transcriptomic data showing Ubp1 is expressed in ring stages, lowly expressed in trophozoites, and more highly expressed in schizonts.

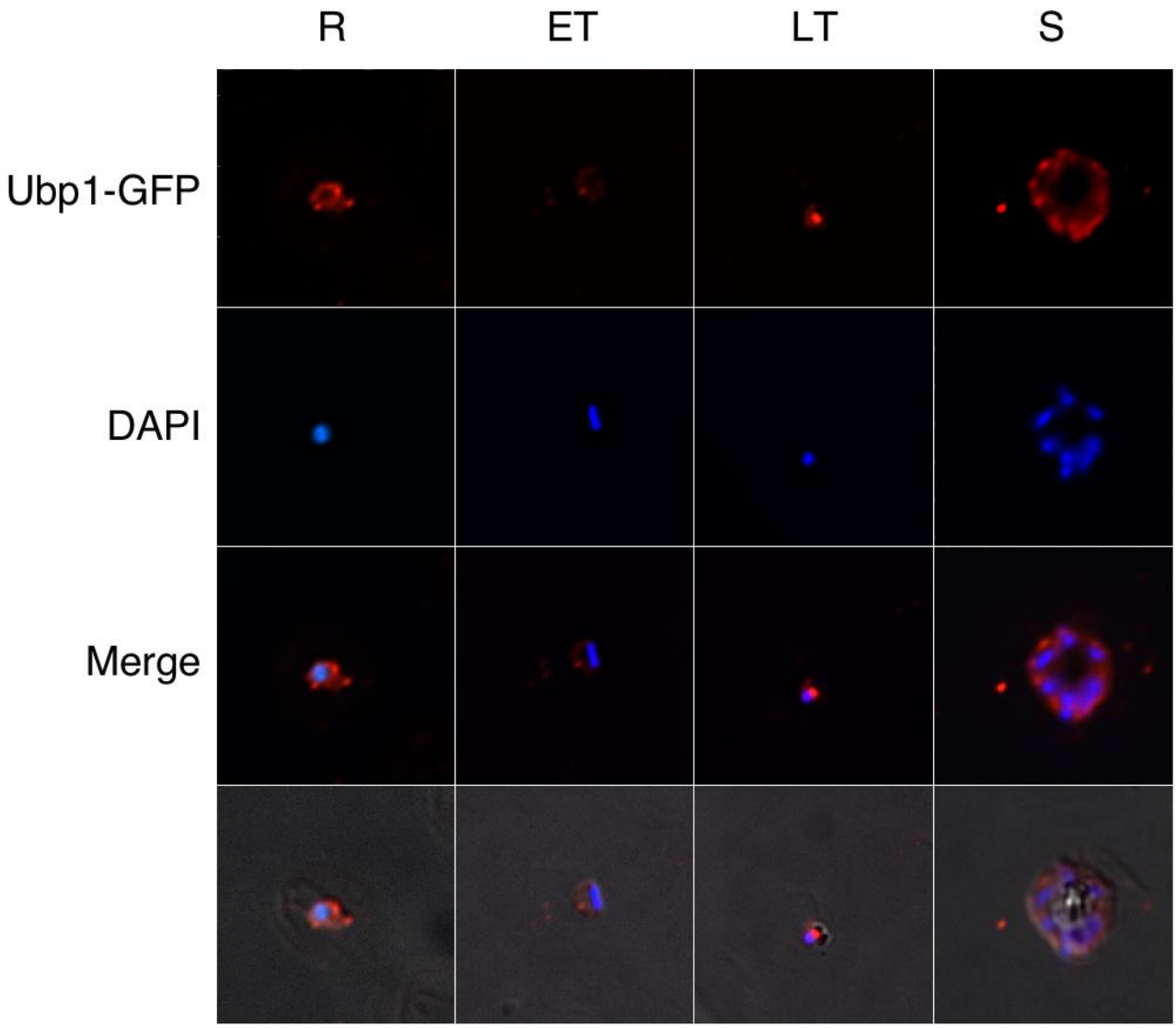


**Figure 74 Localisation of Ubp1-GFP throughout the asexual lifecycle**
The localisation of Ubp1-GFP was examined throughout the asexual lifecycle by IFA in formaldehyde-fixed thin smears using anti-GFP (rabbit, 1:500; Holder laboratory) and anti-rabbit-594 (1:150, Invitrogen). Ubp1-GFP staining appears perinuclear in ring-stages, ring-like but hardly above background in early trophozoites, developing into a large punctate spot that segments into daughter merozoites in schizonts.

## 7.4 Interaction of Ubp1 with ubiquitin

Ubp1 is functionally annotated as a putative deubiquitinase. As stated above, a previous study showed that some DUBs may also catalyse the hydrolysis of ubiquitin-like modifiers, including Nedd8[249]. Though the C-terminus of the protein shares sequence homology with known DUBs and while molecular threading algorithms suggest a similar folding is possible, it is unknown whether *P. falciparum* Ubp1 can interact with ubiquitin. Additionally, it is unknown whether the entire annotated gene encodes a single DUB. Therefore, to first probe the size of mature Ubp1, whole cell lysates were prepared from mixed stage cultures and analysed by western blot. However, using both 4-12% TEA-Tricine gels (Sigma) and 3-8% Tris-Acetate gels (Invitrogen) and extracts prepared in RIPA buffer, no Ubp1-GFP could be consistently detected by anti-GFP western blot, even though clear signal could be detected by IFA and correct integration was confirmed by PCR. 3D7-Ubp1-GFP lysates were also passed over anti-GFP beads to enrich any GFP-tagged species. However, eluted fractions from these test pulldowns also did not reveal any GFP-positive species by western blot.

Because transfer efficiency of high molecular weight proteins from polyacrylamide to nitrocellulose is known to be relatively poor (Ubp1 is expected to be ~416 kDa), the presence of a GFP-tagged species was probed by dot blot. To do this, 2 µl of RIPA-extracted mixed-stage soluble lysate was dotted onto nitrocellulose, dried, and probed against GFP. Compared to approximately equal amounts (5 µg total lysate) of either unmodified 3D7 or 3D7-MON1-GFP lysates (GFP control, created in Section 5.7), there was a very faint GFP-positive signal in

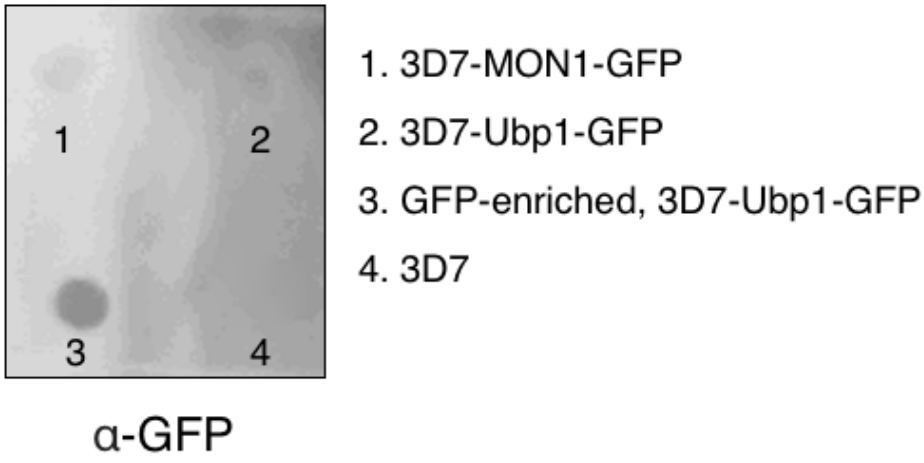


**Figure 75 Dot blot of soluble extracts from Ubp1-GFP-expressing parasites**
Because Ubp1-GFP could not be resolved and detected by SDS-PAGE electrophoresis and western blotting, a dot blot was performed. 2 µl of cell extract was dotted onto a nitrocellulose membrane and probed with anti-GFP (mouse, Sigma; 1:5000) and anti-mouse-HRP (BioRad, 1:5000). Dot 1: positive control, 3D7-MON1-GFP RIPA lysate; dot 2: 3D7-Upb1-GFP RIPA lysate; dot 3: elution of anti-GFP pulldown on RIPA-extracted Ubp1-GFP lysate; dot 4: wild type 3D7 control.

the 3D7-Ubp1-GFP cell extract. The pulldown experiment was repeated in RIPA buffer, and the eluted fraction (without bromophenol blue) is clearly enriched for the GFP-tagged molecule (Fig 75). Because there is no size resolution with a dot blot, it is impossible to say that the GFP species detected here is definitively Ubp1-GFP. However, because by PCR the SLI construct was successfully integrated, and by IFA there is a conspicuous localisation pattern, it is likely that the signals detected here correspond to Ubp1-GFP.

To examine whether Ubp1 is capable of interacting with ubiquitin, a labelling experiment involving Ub-HA-VME, a synthetic ubiquitin analogue, was performed. Ub-HA-VME is a reagent commonly used to study DUBs. It consists of a ubiquitin monomer with an N-terminal HA epitope tag and C-terminal vinyl sulfone (VS) group. As described in Section 1.9, ubiquitin is typically conjugated to a target substrate via an isopeptide linkage between an ε-$NH_3$ of a lysine side chain and

Gly76 of ubiquitin. The isopeptide bond is hydrolysed by DUBs. In Ub-HA-VME, the vinyl methylether group replaces Gly76 and forms an irreversible thioether with the sulfhydryl group of reactive cysteines in target proteins that is immune to DUB-mediated hydrolysis.

Whole cell lysates were again prepared with RIPA buffer supplemented with 1 mM PMSF. These lysates were incubated with 1 µM Ub-HA-VME, a synthetic ubiquitin analogue, for 90 minutes at room temperature before being diluted with an equal volume of RIPA supplemented with 2x protease inhibitors. This reaction solution was then incubated with anti-GFP beads overnight at 4$^{o}$C. After overnight incubation, the anti-GFP beads were washed, and bound material was eluted and analysed by dot blot. As expected, blotting against the activity-based probe with anti-HA antibodies produced a clear HA-positive signal in the eluted protein fraction. These simple labelling experiments suggest that native Ubp1 is capable of interacting with ubiquitin *in vitro* (Fig 77).

## 7.5 Exploration of experimental hUSP7 inhibitors in *P. falciparum*

Ubp1 is functionally annotated as a putative deubiquitinase. As stated above, a previous study showed that some DUBs may also catalyse the hydrolysis of ubiquitin-like modifiers, including Nedd8. Though the C-terminus of the protein shares some sequence homology with known DUBs and molecular threading algorithms show a USP7-like conformation is possible, it is unknown whether Ubp1 is either a functional DUB or can be similarly targeted with known DUB inhibitors.

To begin to probe some of these questions surrounding druggability of deubiquitinases in *Plasmodium falciparum*, three recently described hUSP7

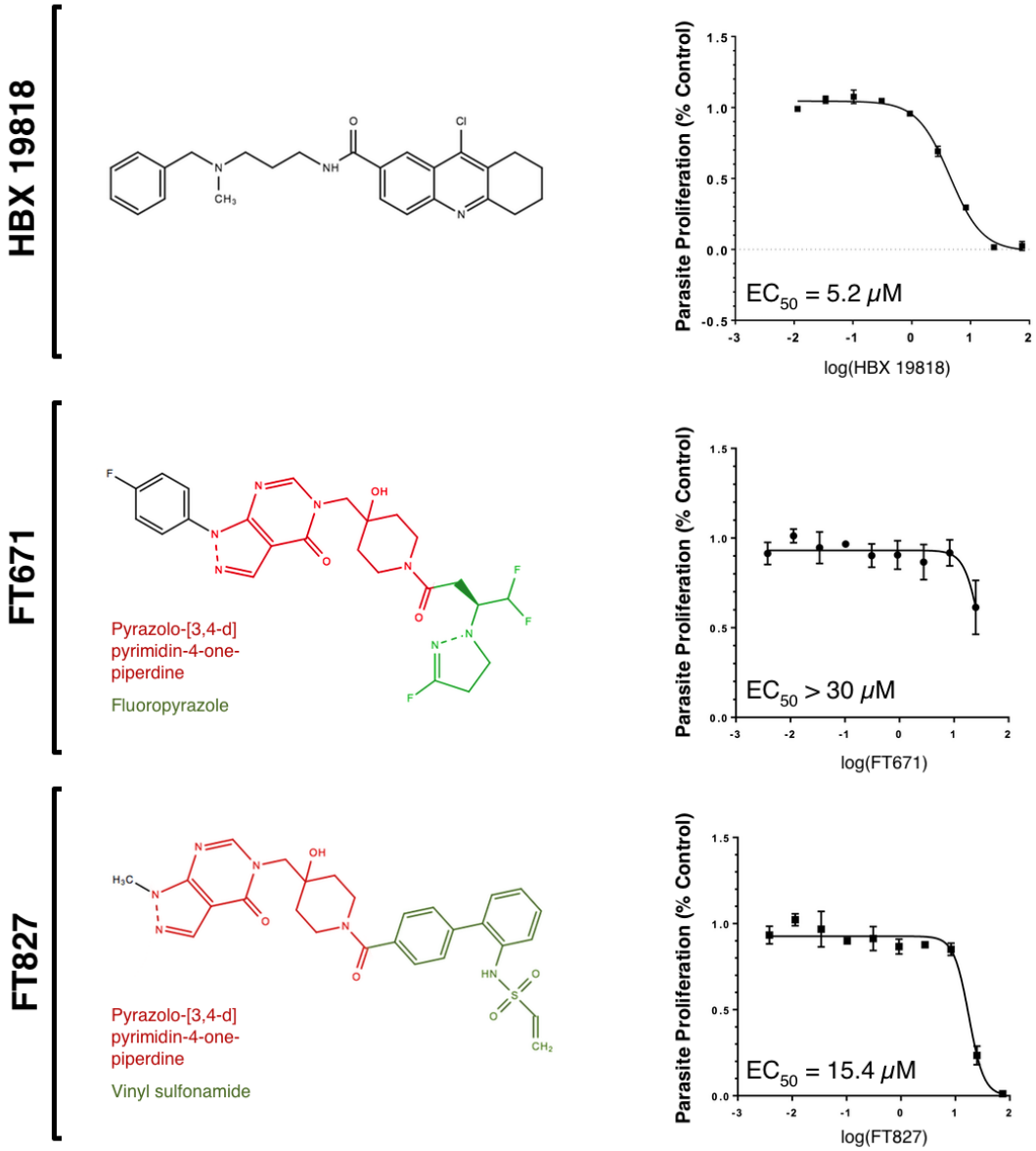


**Figure 76 Molecular structures and antimalarial activity of three hUSP7 inhibitors**
Three known inhibitors of hUSP7 were probed for their antimalarial activity against the 3D7 strain using standard 48-hour exposures to serial dilutions of compound. $EC_{50}$ estimates are a mean of at least 2 biological replicates, each performed in technical duplicate. $EC_{50}$ estimates were calculated using Prism 7.0 as described elsewhere in this thesis.

inhibitors were examined for their anti-plasmodial effects: HBX 19818, FT671, and FT827 (Fig 76). HBX 19818 is a hetero-tricyclic ring that was identified through a high-throughput library screen at Hybrigenics Pharma, which covalently inactivates the active cysteine of hUSP7 both *in vitro* and *in vivo* with an $IC_{50}$ of approximately 20-30 µM[325]. Though HBX 19818 was thought to be highly specific for hUSP7, this compound has since been shown to also exert off-target effects against other DUBs.

FT671 and FT827 were discovered by Turnbull *et al* in a 2017 collaboration between the University of Oxford and Forma Therapeutics[326]. FT671 and FT827 build on extensive research into hUSP7 inhibitors as anti-cancer drugs since the discovery of HBX 19818.

FT671 and FT827 are related compounds based on a pyrazolo-piperidine scaffold but have important chemical differences and functionality. FT671 reversibly inhibits hUSP7 through a fluoropyrazole group that interacts with sidechains in the catalytic pocket of USP7, preventing a conformational shift required for hUSP7 to accept ubiquitin. FT827 uses a vinyl-sulfonamide group to irreversibly target the active cysteine of hUSP7 by a similar mechanism as the vinyl sulfone group of the Ub-ABP described in Section 7.4. Importantly, FT671 binds hUSP7 with a $K_D$ of < 100 nM whereas FT827 targets hUSP7 with a $K_D$ of approximately 8 µM. Despite this difference in affinity for the molecule, both FT compounds display highly-specific activity against hUSP7 *in vitro* and *in vivo*, even up to 50 µM.

The sensitivity of the 3D7 *Plasmodium falciparum* strain to these compounds was determined using standard 48-hour drug exposures and SYBR-Green quantitation as described in Section 3.4.5.1. To HBX 19818 and FT827, 3D7 displayed $EC_{50}$'s of 5.2 µM and 15.4 µM, respectively. FT671 is ineffective against 3D7 at concentrations under 25 µM. Interestingly, for HBX, this $EC_{50}$ is well below

the reported $K_D$ and $IC_{50}$ reported for hUSP7 and HEK293 cells by Reverdy, whereas for FT827, the $EC_{50}$ determined here is similar to the $K_D$ reported for hUSP7 by Turnbull[325,326]. On the other hand, *P. falciparum* is more than 500 times less sensitive than human cells to FT671.

## 7.6 *In vitro* validation of experimental hUSP7 inhibitors in *P. falciparum*

These sensitivity data suggest important differences in structure and function between the *Plasmodium falciparum* and human DUBs, particularly as highlighted by the FT-series compounds. Importantly, the results of the previous section do not clarify whether these USP8 inhibitors are active against Ubp1. As stated above, FT671 is a reversible binding pocket blocker for the human USP7; it does not interact with or inactivate the catalytic cysteine. Instead, FT671 prevents a conformational shift in the catalytic domain required for USP7 to accept and hydrolyse ubiquitin chains. The fact that FT671 does not appreciably kill *Plasmodium falciparum* at concentrations below 30 μM yet disables the human enzyme at low nanomolar concentrations is consistent with important differences existing in the three-dimensional DUB fold between the two enzymes, even though molecular modelling suggests a similar tertiary structure is possible for PfUbp1 (Appendix II). FT827 attacks and covalently modifies the active cysteine of USP7 and does not dock in the same way with the USP7 fold as FT671[326].

To probe the ability of these two compounds to disrupt Ubp1's interaction with ubiquitin, simple delabeling experiments were performed (Fig 77). HBX was not taken forward to these experiments because this compound is known to have pleiotropic effects in other systems and no libraries were generated around this compound, while the FT series have several libraries available for lead optimisation.

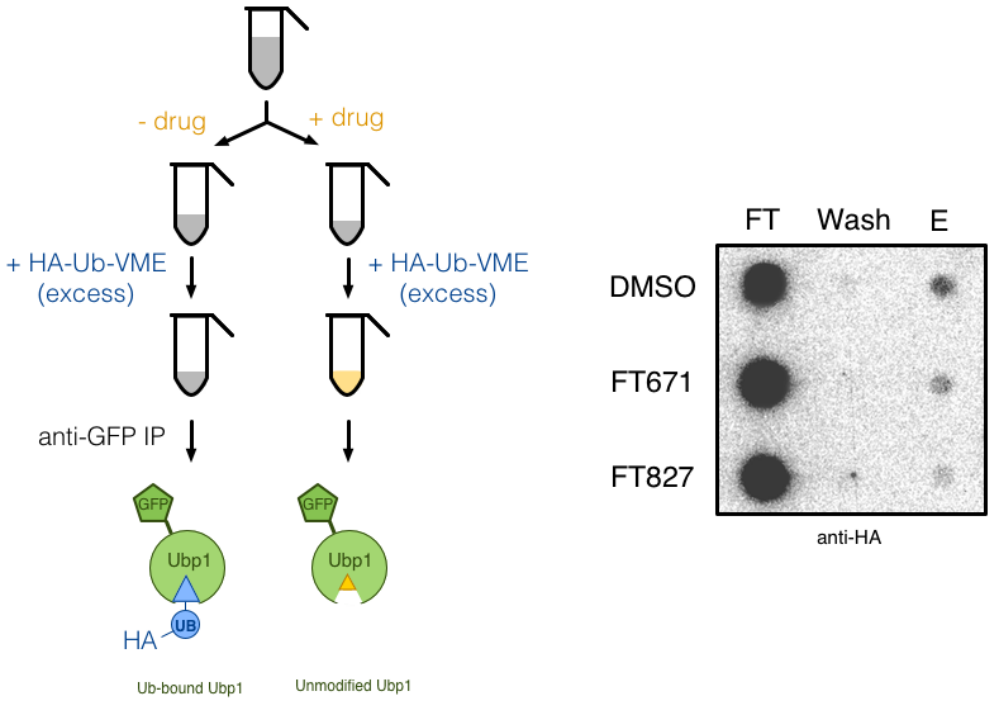


**Figure 77 *In vitro* chemical Ubp1-ubiquitin delabelling assay**
Schematic of Ubp1 delabelling assays. 3D7-Ubp1-GFP lysates were prepared in RIPA buffer and incubated with 30 µM FT671, 30 µM FT827, or solvent. These lysates were then treated with HA-Ub-VME and pulled down on anti-GFP beads. Bound material was eluted and examined for the presence of HA-Ub-VME by dot blot (right). Densitometric analysis of HA signal in FT671 and FT827 elution fractions with respect to the DMSO control reveals 53.6 ± 6.3% and 83.1 ± 5.2% reduction in labelling due to 30 µM FT671 and FT827 respectively.

Briefly, RIPA-lysed cells were incubated for 45 minutes with either 30 µM FT827 or FT671 or equivalent solvent at room temperature. After this incubation, excess Ub-HA-VME was added to both drug-treated and untreated samples for a further 60 minutes at room temperature. Then, an equal volume of RIPA buffer with 2x protease inhibitors was added to quench labelling and prevent further degradation of proteins in solution. Anti-GFP beads were then added to both reactions and incubated overnight at 4°C. These beads were washed extensively and eluted, and

bound material was analysed by anti-HA dot blot. Interestingly, both drugs block HA-Ub-VME labelling of Ubp1. As expected, FT827 dramatically reduces the amount of HA-Ub-VME bound to Ubp1, though FT671 may still be capable of partially inhibiting Ubp1 (FT671: 53.6 ± 6.3%, FT827: 83.1 ± 5.2% reduction in labelling). FT671 is a reversible inhibitor of USP7 and therefore will also compete with ubiquitin for Ubp1 binding, which may also contribute to its lower potency against *P. falciparum* since there are likely differences in the conformation of the active site of Ubp1.

## 7.7 Discussion

The data described in this chapter provide preliminary insights into the cell and molecular biology of the Ubp1 putative deubiquitinase. Interestingly, prior to this work, Ubp1 was believed to be a putative homologue of the human USP7 deubiquitinase. USP7 is located in the nucleus in human cells, where it regulates the turnover of the Mdm2 tumour suppresor[327]. In contrast to this expected nuclear localisation, PfUbp1 is localised to a near-nuclear location in the cell, which may be the ER. Although I could not resolve Ubp1-GFP on a western blot, potentially due to its annotated size (> 400 kDa), I did detect and successfully enrich what is likely Ubp1-GFP using an anti-GFP pulldown. Using a ubiquitin activity based probe, I also show that this GFP-tagged species interacts with ubiquitin, providing further support that native Ubp1 is a functional deubiquitinase. Further colocalisation and EM experiments will provide a clearer localisation of Ubp1, and *in vitro* deubiquitinase experiments using recombinant and native Ubp1 will be necessary to formally demonstrate DUB activity.

Because of their essential functions in cellular regulation, DUBs, and USP7 in particular, are attractive drug targets for broad human pathologies. Several known USP7 inhibitors were explored for their anti-plasmodial activity in this chapter, and two covalent inhibitors, HBX 19818 and FT827, display low micromolar potency against the 3D7 *Plasmodium falciparum* strain. HBX 19818 is promiscuous in human cells, but FT827 has been shown to specifically target USP7 even at concentrations as high as 50 µM. *In vitro* delabeling experiments using a ubiquitin activity-based probe (HA-Ub-VME) suggest that FT827 is capable of blocking ubiquitin interaction with Ubp1, which presents Ubp1 as a new target that could be considered for antimalarial drug development. It is important to note that the experiments described in Section 7.6 do not prove the antiplasmodial effects of FT827, demonstrated in Section 7.5, are on-target. They show that Ubp1 can be targeted by FT827, but additional DUBs may still be inhibited by FT827.

Screening drug-DUB interactions via these delabeling experiments is very low throughput and labour intensive, but previous efforts have shown that ubiquitin activity-based probes can be used for high-throughput mass spectrometry-based drug discovery and simultaneously reveal DUB specificity of the compounds screened. FT827 will never be a viable antimalarial because it was designed for human cancers and invariably will therefore have a poor selective index. However, many FT827-like molecules have been synthesised and screened for anti-cancer and cytotoxic effects. The compounds which have been binned as ineffective against human cancer cell lines yet are non-toxic to non-cancerous cells could be screened for their antimalarial properties using the techniques outlined in this chapter and mass-spectrometry based approaches.

# Chapter 8

# Discussion

This thesis set out to address four major questions under the theme of understanding antimalarial drug resistance. Though detailed discussions of the work presented in each chapter are included in each chapter, several points of summary are provided here with respect to the general aims outlined in Chapter 2.

Specifically, this thesis asked:

1. **To what extent is there continued evidence of directional selection of *pfap2mu* and *pfubp1* variants in patient samples from Western Kenya?**

   The results presented in Chapter 4 suggest that there may be ongoing selection of the *pfap2mu(S160N)* variant allele. Similar selection was observed in the samples analysed from this study and those from our previous study conducted in the same town in Western Kenya. Specifically, the prevalence of the S160N allele approximately tripled between pre-treatment and post-treatment samples when considering samples from the same patient. However, the prevalence of this mutation several weeks after treatment was nearly back to baseline 16%. It is important to note that the patient sample collection protocol in this study was deeply flawed, and over half of the study samples remain in Africa. Therefore, the prevalence of this variant allele may change as the analysis

of these samples is completed in the future. However, the preliminary data suggest the *pfap2mu(S160N)* variant is selected during ACT treatment. It is unclear why this mutation has not increased in prevalence in this study site over the four years between the two studies if it is actually associated with treatment failure since ACT therapies have been the frontline treatment option over this time. Additionally, ACT efficacy remains high in this area.

Analysis of selection of *pfubp1* variants is more complicated due to the dramatic sequence diversity at the resistance-associated "Borrmann hotspot" near Ubp1(E1528). Sequencing of this region revealed 16 different haplotypes in parasite samples from this same clinical trial. Interestingly, when the E1528D mutation identified by Borrmann *et al* was considered independent of this surrounding diversity there was some evidence of selection, with the prevalence of the mutation approximately doubling between pre- and post-treatment samples[251]. However, when the entire haplotype of this region was considered as a unit, the selection landscape reveals a different haplotype with more than half of recrudescent parasites having a single variant haplotype encoding D1525E and a three-amino-acid insertion. Previous studies have not considered this whole region as a single haplotype and instead have focused on single residues. Reanalysis of previous data should be conducted to examine whether a similar trend has been previously identified and not reported.

**2. To what extent do mutations in *pfap2mu* and *pfubp1* contribute to reduced susceptibility to frontline antimalarial chemotherapies in laboratory strains and culture-adapted clinical parasite isolates.**

To validate the involvement of *pfap2mu* and *pfubp1* variants in sensitivity to frontline chemotherapies, variants in these genes were installed in the 3D7

genome by CRISPR-Cas9 editing. Specifically, the S160N mutation identified from patients in Kenya and the I592T mutation identified from an artemisinin-resistant *Plasmodium chabaudi* clone were installed into *pfap2mu,* and the V3306I and V3275F mutations identified in the same *Plasmodium chabaudi* study were installed into *pfubp1*. These parasites displayed minor changes in their sensitivity to chloroquine, quinine, dihydroartemisinin, lumefantrine, mefloquine, and piperaquine by standard 48-hour drug exposure assays. However, by the ring-stage survival assay, parasites expressing the mutant µ2(I592T) and Ubp1(V3275F) displayed reduced ring-stage susceptibility to artemisinin. The resistance phenotype displayed by these parasites is moderate, yet significant, as it is above the 5% RSA survival cut-off assigned by WHO, validating the involvement of these proteins in determining parasite sensitivity to artemisinin. These are the first data showing that SNPs in genes other than *pfkelch13* may cause ring-stage artemisinin resistance.

This thesis also produced the first transfection and Cas9-mediated transgenesis of a recently culture-adapted African clinical parasite isolate. This thesis establishes a protocol for transfecting these poor-growing, relatively fragile parasite lines. Though the *pfap2mu(S160N)* mutation has been successfully installed into an African isolate, we have not yet been able to successfully clone these parasites, which has delayed the characterisation of this important line. Though this variant had no effect on parasite susceptibility to frontline chemotherapies in the 3D7 background, characterising the effects of this mutation in an African isolate is still important.

**3. Given there are well defined orthologues of PfAP2µ and PfUbp1 in mammalian cells by sequence similarity, how similar are the localisations and functions of *P. falciparum* proteins to their counterparts?**

To examine the localisation and function of µ2 and Ubp1 in the parasite cell, both proteins were tagged by genome editing. By immunofluorescence and immunoelectron microscopy, µ2 seems to be located in the early secretory pathway near the ER. This is surprisingly diverged from the canonical eukaryotic function of the AP-2 complex in receptor-mediated endocytosis. Knocking out µ2 causes broad defects in the biogenesis of several membrane-bound organelles including the micronemes, rhoptries, and apicoplast, which further supports a role for µ2 in early secretory traffic. A µ2 interactome generated by immunoprecipitation and mass spectrometry shows that the core AP-2 complex consists of three canonical AP-2 subunits and AP-1β. This AP complex hybridisation is common in invertebrates and has been previously noted in *Dictyostelium*. A µ2 interactome generated through immunoprecipitation and mass spectrometry identified several trafficking factors and supports a role in early secretory traffic near the ER. The identification of Rab11B suggests that AP-2 traffic may aimed towards the plasma membrane or IMC.

Additionally, the µ2 interactome contains several artemisinin resistance-associated factors including K13 and another kelch domain-containing factor called K10. Co-immunoprecipitation experiments revealed that these factors interact with µ2. This non-canonical localisation and association with K13 also seems to exist in *Plasmodium knowlesi*, supporting a repurposing of traditional endocytic machinery in *Plasmodium spp.*, which may be a consequence of adaptation to an obligate intracellular life.

During the course of this exploration into the biology of µ2, I also began an initial characterisation of clathrin heavy chain. Clathrin heavy chain is localised to vesicles throughout the cytoplasm and the cell periphery. Additionally, as expected, many components of key late secretory organelles pulldown with clathrin, suggesting that clathrin-coated vesicles deliver essential cargo throughout the cell.

Ubp1 is also located in the cytosol and may be associated with the ER, given its perinuclear localisation in early ring stages. The data presented in Chapter 7 reveal Ubp1 is capable of interacting with ubiquitin and may be a drug target using experimental hUSP7 inhibitors. However, USP7 is localised in the nucleus of human cells, indicating a functionally different role for Ubp1 than what has been determined for USP7, though this is not unexpected as the sequence similarity between the two factors is limited.

**4. To date, none of the resistance-causing *pfkelch13* mutations have been detected in parasites from African patients. Do the results of these studies provide any insight into how artemisinin resistance occurs at the cellular level or could occur in Africa?**

Overall, the results of Chapters 5 and 6 provide compelling evidence for a model of artemisinin resistance centred around the ER and protein homeostasis. The AP-2 complex associates with K13 in the cell, and mutations in both confer varying degrees of protection from artemisinin to ring stage parasites. Given that AP-2 is localised to the early secretory pathway, it follows that dysfunction may disrupt or slow down secretory traffic. Experiments described at length in Chapter 6 provide support for this theory and show that physically and chemically disrupting protein dynamics confers high levels of artemisinin

resistance to ring stage parasites. Building off of this, transient degradation of µ2 in the ring stage also confers a cytoprotective effect. Overall, these data imply that K13-mediated artemisinin resistance may result from a dysfunctional intracellular trafficking system that induces a low-level stress response in the absence of artemisinin. By pre-activating or priming this stress response, cells are better equipped to mitigate the disseminated oxidative damage caused by artemisinin. My theory both explains and is supported by transcriptomic, proteomic, and *in vitro* biochemical data implicating an enhanced, ring-stage stress response in artemisinin resistance.

Recently, Bhattacharjee *et al* proposed a trafficking-related mechanism for artemisinin resistance, though they focus mostly on protein export and PfEMP1 as causative effectors of K13[200]. Though protein export machinery is implicated in the mechanism of the AP-2 complex in *P. falciparum*, neither PI3K nor PI3P interacting proteins (also implicated by Bhattacharjee *et al* and Mbengue *et al*) were detected[196,200]. Some of the work presented by Bhattacharjee in support of their model, particularly regarding the involvement of PI3P as a causative molecule, ignores clear criticisms pointed out by Boddey *et al*, which represents the work of six separate laboratories[201]. Therefore, the model presented by Bhattacharjee *et al*, though generally related to my model by implicating intracellular traffic, demands further support and explanation, complicating the interpretation of their results.

Ultimately, this thesis provides little insight into how and whether artemisinin resistance will occur in African parasites. That a single mutation in *pfap2mu*, a gene that has been shown to be under some directional selection in East Africa, can confer significant levels of artemisinin resistance is rightly

concerning. However, this mutation has never been detected in circulating parasites anywhere in the world. One of the more concerning conclusions from this thesis is that mutations in potentially many proteins involved in protein homeostasis may confer resistance to artemisinin, if the presented model is correct. However, there are good arguments for why the high transmission setting across many parts of Africa may complicate the evolution of artemisinin resistant strains, but these are the subject of another thesis.

# Chapter 9

# Future Directions

The work outlined in this thesis provide proof-of-principle and justification for pursuing many further lines of work. Four of these additional projects are described here:

1. **Explore the impact of genetic background on the effects of mutations in *pfap2mu* on parasite susceptibility to frontline chemotherapies.**

   In this thesis, the *pfap2mu(S160N)* variant does not alter parasite susceptibility to the frontline chemotherapies examined. However, in Henriques *et al*, Dd2 parasites (CQ-resistant background) expressing an additional copy of the mutant gene displayed decreased susceptibility to quinine and DHA[206]. This could be caused by the overexpression of μ2, a dominant negative effect of the additional, mutant copy, or a consequence of different metabolism caused by a mutant PfCRT. Dd2(S160N) parasites should be created by Cas9-mediated editing and examined for their drug sensitivity, and additional copies of *pfap2mu* could be integrated into wild type backgrounds to explore the consequences of overexpression.

2. **Further characterise the cellular effects of µ2 knockout.**

This thesis shows that inducible *pfap2mu* knockout disrupts several membrane-bound compartments, including the micronemes, rhoptries, and apicoplast, as well as the IMC and plasma membrane. This knockout should be further characterised by electron microscopy to understand the cross-sectional morphology of these cells, which may provide greater insight into the role of µ2. Additionally, the regulable µ2-DDD described in Chapter 6 may be a valuable genetic tool for looking at the effects of manipulating µ2 levels in the cell. The construct described here can be integrated into an attB site as is, and a cloned, single-copy integrant would be required for these experiments. Additionally, this parasite line might allow the identification of AP-2 cargo molecules with TMT-labelling and whole-cell proteomics. Proteins that are differentially abundant shortly after a protein-level µ2 knockdown might represent important cargo molecules. Understanding these cargo molecules may provide further insight into the artemisinin resistance phenotype induced by µ2 knockdown and µ2 mutation.

3. **Explore the viability of parasite DUBs as antimalarial drug targets.**

Chapter 7 turns an important page in understanding the biology of deubiquitinating enzymes in the parasite. These enzymes are

becoming important anti-cancer drug targets and could represent viable antimalarial targets. Specifically, the HA-Ub-VME reagent described here and widely utilised to study mammalian ubiquitin biology is a powerful molecular tool and can be used for high throughput mass spectrometry-based drug screening. Forma Therapeutics has designed several libraries of compounds around the pyrazolo-piperadine scaffold that produced FT671 and FT827. These libraries have already been screened against human cells, resulting in a sub-library of negatively screened compounds which might target the malarial DUBs. Simple cytotoxicity assays can be performed in very high throughput to identify compounds for further characterisation using ABPs and mass spectrometry. Forma have already stated their interest in pursuing this work.

**4. Characterise role of clathrin in the malaria parasite**

This thesis provides a very preliminary characterisation of clathrin heavy chain in *Plasmodium falciparum*. Clathrin heavy chain clearly is involved in transporting cargo to many important compartments in the cell, and a full characterisation of the molecule will provide valuable insights into parasite cell biology. The techniques described and used in Chapter 5 should be deployed in these studies.

## References


1. Poinar, G. Plasmodium dominicana n. sp. (Plasmodiidae: Haemospororida) from Tertiary Dominican amber. *Syst. Parasitol.* **61,** 47–52 (2005).
2. Neghina, R., Neghina, A. M., Marincu, I. & Iacobiciu, I. Malaria, a journey in time: in search of the lost myths and forgotten stories. *Am. J. Med. Sci.* **340,** 492–8 (2010).
3. World Health Organization. *World Malaria Report. World Health Organization* (2017). doi:10.1071/EC12504
4. Ta, T. H., Hisam, S., Lanza, M., Jiram, A. I., Ismail, N. & Rubio, J. M. First case of a naturally acquired human infection with Plasmodium cynomolgi. *Malar. J.* **13,** 68 (2014).
5. Contacos, P. G., Coatney, G. R., Orihel, T. C., Collins, W. E., Chin, W. & Jeter, M. H. Transmission of Plasmodium schwetzi from the chimpanzee to man by mosquito bite. *Am. J. Trop. Med. Hyg.* **19,** 190–5 (1970).
6. Coatney, G. R., Chin, W., Contacos, P. G. & King, H. K. Plasmodium inui, a quartan-type malaria parasite of Old World monkeys transmissible to man. *J. Parasitol.* **52,** 660–3 (1966).
7. Brasil, P., Zalis, M. G., de Pina-Costa, A., Siqueira, A. M., Júnior, C. B., Silva, S., Areas, A. L. L., Pelajo-Machado, M., de Alvarenga, D. A. M., da Silva Santelli, A. C. F., Albuquerque, H. G., Cravo, P., Santos de Abreu, F. V., Peterka, C. L., Zanini, G. M., Suárez Mutis, M. C., Pissinatti, A., Lourenço-de-Oliveira, R., de Brito, C. F. A., *et al.* Outbreak of human malaria caused by Plasmodium simium in the Atlantic Forest in Rio de Janeiro: a molecular epidemiological investigation. *Lancet. Glob. Heal.* **5,** e1038–e1046 (2017).
8. Sutherland, C. J., Tanomsing, N., Nolder, D., Oguike, M., Jennison, C., Pukrittayakamee, S., Dolecek, C., Hien, T. T., do Rosário, V. E., Arez, A. P., Pinto, J., Michon, P., Escalante, A. A., Nosten, F., Burke, M., Lee, R., Blaze, M., Otto, T. D., Barnwell, J. W., *et al.* Two Nonrecombining Sympatric Forms of the Human Malaria Parasite *Plasmodium ovale* Occur Globally. *J. Infect. Dis.* **201,** 1544–1550 (2010).
9. Betson, M., Sousa-Figueiredo, J. C., Atuhaire, A., Arinaitwe, M., Adriko, M., Mwesigwa, G., Nabonge, J., Kabatereine, N. B., Sutherland, C. J. & Stothard,

J. R. Detection of persistent Plasmodium spp. infections in Ugandan children after artemether-lumefantrine treatment. *Parasitology* 1–11 (2014). doi:10.1017/S003118201400033X

10. Fançony, C., Gamboa, D., Sebastião, Y., Hallett, R., Sutherland, C., Sousa-Figueiredo, J. C. & Nery, S. V. Various pfcrt and pfmdr1 genotypes of Plasmodium falciparum cocirculate with P. malariae, P. ovale spp., and P. vivax in Northern Angola. *Antimicrob. Agents Chemother.* **56,** 5271–5277 (2012).
11. Proietti, C., Pettinato, D. D., Kanoi, B. N., Ntege, E., Crisanti, A., Riley, E. M., Egwang, T. G., Drakeley, C. & Bousema, T. Continuing intense malaria transmission in northern Uganda. *Am. J. Trop. Med. Hyg.* **84,** 830–837 (2011).
12. Sutherland, C. Trends in Parasitology Persistent parasitism : the adaptive biology of malariae and ovale malaria. *Trends Parasitol.* **Submitted,** (2016).
13. Dinko, B., Oguike, M. C., Larbi, J., Bousema, T. & Sutherland, C. J. Persistent detection of Plasmodium falciparum , P . malariae , P . ovale curtisi and P. ovale wallikeri after ACT treatment of asymptomatic Ghanaian school-children. *Int. J. Parasitol. Drugs Drug Resist.* 45–50 (2013).
14. Florens, L., Washburn, M. P., Raine, J. D., Anthony, R. M., Grainger, M., Haynes, J. D., Moch, J. K., Muster, N., Sacci, J. B., Tabb, D. L., Witney, A. A., Wolters, D., Wu, Y., Gardner, M. J., Holder, A. A., Sinden, R. E., Yates, J. R. & Carucci, D. J. A proteomic view of the Plasmodium falciparum life cycle. *Nature* **419,** 520–6 (2002).
15. Le Roch, K. G., Johnson, J. R., Florens, L., Zhou, Y., Santrosyan, A., Grainger, M., Yan, S. F., Williamson, K. C., Holder, A. A., Carucci, D. J., Yates, J. R. & Winzeler, E. A. Global analysis of transcript and protein levels across the Plasmodium falciparum life cycle. *Genome Res.* **14,** 2308–18 (2004).
16. Sherrard-Smith, E., Sala, K. A., Betancourt, M., Upton, L. M., Angrisano, F., Morin, M. J., Ghani, A. C., Churcher, T. S. & Blagborough, A. M. Synergy in anti-malarial pre-erythrocytic and transmission-blocking antibodies is achieved by reducing parasite density. *Elife* **7,** (2018).
17. Churcher, T. S., Sinden, R. E., Edwards, N. J., Poulton, I. D., Rampling, T. W., Brock, P. M., Griffin, J. T., Upton, L. M., Zakutansky, S. E., Sala, K. A., Angrisano, F., Hill, A. V. S. & Blagborough, A. M. Probability of

Transmission of Malaria from Mosquito to Human Is Regulated by Mosquito Parasite Density in Naïve and Vaccinated Hosts. *PLOS Pathog.* **13,** e1006108 (2017).

18. Masterson, K. M. *The Malaria Project: The U.S. Government's Secret Mission to Find a Miracle Cure*. (Penguin Group, 2014).
19. Parise, M. E., Ayisi, J. G., Nahlen, B. L., Schultz, L. J., Roberts, J. M., Misore, A., Muga, R., Oloo, A. J. & Steketee, R. W. Efficacy of sulfadoxine-pyrimethamine for prevention of placental malaria in an area of Kenya with a high prevalence of malaria and human immunodeficiency virus infection. *Am. J. Trop. Med. Hyg.* **59,** 813–22 (1998).
20. Challis, K., Osman, N. B., Cotiro, M., Nordahl, G., Dgedge, M. & Bergstrom, S. Impact of a double dose of sulphadoxine-pyrimethamine to reduce prevalence of pregnancy malaria in southern Mozambique. *Trop. Med. Int. Heal.* **9,** 1066–1073 (2004).
21. Radeva-Petrova, D., Kayentao, K., ter Kuile, F. O., Sinclair, D. & Garner, P. Drugs for preventing malaria in pregnant women in endemic areas: any drug regimen versus placebo or no treatment. *Cochrane database Syst. Rev.* **10,** CD000169 (2014).
22. Eisele, T. P., Larsen, D. & Steketee, R. W. Protective efficacy of interventions for preventing malaria mortality in children in Plasmodium falciparum endemic areas. *Int. J. Epidemiol.* **39 Suppl 1,** i88-101 (2010).
23. Shulman, C. E., Dorman, E. K., Cutts, F., Kawuondo, K., Bulmer, J. N., Peshu, N. & Marsh, K. Intermittent sulphadoxine-pyrimethamine to prevent severe anaemia secondary to malaria in pregnancy: a randomised placebo-controlled trial. *Lancet (London, England)* **353,** 632–6 (1999).
24. Hill, A. V. S. Vaccines against malaria. *Phil. Trans. R. Soc. B* **366,** 2806–2814 (2011).
25. Foquet, L., Hermsen, C. C., van Gemert, G.-J., Van Braeckel, E., Weening, K. E., Sauerwein, R., Meuleman, P. & Leroux-Roels, G. Vaccine-induced monoclonal antibodies targeting circumsporozoite protein prevent Plasmodium falciparum infection. *J. Clin. Invest.* **124,** 140–4 (2014).
26. Heppner, D. G., Kester, K. E., Ockenhouse, C. F., Tornieporth, N., Ofori, O., Lyon, J. A., Stewart, V. A., Dubois, P., Lanar, D. E., Krzych, U., Moris, P., Angov, E., Cummings, J. F., Leach, A., Hall, B. T., Dutta, S., Schwenk, R.,

Hillier, C., Barbosa, A., *et al.* Towards an RTS,S-based, multi-stage, multi-antigen vaccine against falciparum malaria: progress at the Walter Reed Army Institute of Research. *Vaccine* **23,** 2243–50 (2005).

27. Efficacy and safety of RTS,S/AS01 malaria vaccine with or without a booster dose in infants and children in Africa: final results of a phase 3, individually randomised, controlled trial. *Lancet* **386,** 31–45 (2016).
28. Epstein, J. E., Paolino, K. M., Richie, T. L., Sedegah, M., Singer, A., Ruben, A. J., Chakravarty, S., Stafford, A., Ruck, R. C., Eappen, A. G., Li, T., Billingsley, P. F., Manoj, A., Silva, J. C., Moser, K., Nielsen, R., Tosh, D., Cicatelli, S., Ganeshan, H., *et al.* Protection against Plasmodium falciparum malaria by PfSPZ Vaccine. *JCI Insight* **2,** (2017).
29. Rénia, L., Grüner, A. C., Mauduit, M. & Snounou, G. Vaccination using normal live sporozoites under drug treatment. *Methods Mol. Biol.* **923,** 567–576 (2013).
30. Raghavendra, K., Barik, T. K., Reddy, B. P. N., Sharma, P. & Dash, A. P. Malaria vector control: From past to future. *Parasitol. Res.* **108,** 757–779 (2011).
31. Alout, H., Yameogo, B., Djogbenou, L. S., Chandre, F., Dabire, R. K., Corbel, V. & Cohuet, A. Interplay between Plasmodium infection and resistance to insecticides in vector mosquitoes. *J. Infect. Dis.* **210,** 1464–1470 (2014).
32. Alout, H., Ndam, N. T., Sandeu, M. M., Dj??gbe, I., Chandre, F., Dabir??, R. K., Djogb??nou, L. S., Corbel, V. & Cohuet, A. Insecticide Resistance Alleles Affect Vector Competence of Anopheles gambiae s.s. for Plasmodium falciparum Field Isolates. *PLoS One* **8,** (2013).
33. Weidhaas, D. E. Chemical Sterilization of Mosquitoes. *Nature* **195,** 786–787 (1962).
34. Helinski, M. E. H., Parker, A. G. & Knols, B. G. J. Radiation-induced sterility for pupal and adult stages of the malaria mosquito Anopheles arabiensis. *Malar. J.* **5,** 41 (2006).
35. Alphey, L., Benedict, M., Bellini, R., Clark, G. G., Dame, D. A., Service, M. W. & Dobson, S. L. Sterile-insect methods for control of mosquito-borne diseases: an analysis. *Vector Borne Zoonotic Dis.* **10,** 295–311 (2010).
36. Hammond, A., Galizi, R., Kyrou, K., Simoni, A., Siniscalchi, C., Katsanos, D., Gribble, M., Baker, D., Marois, E., Russell, S., Burt, A., Windbichler, N.,

Crisanti, A. & Nolan, T. A CRISPR-Cas9 gene drive system targeting female reproduction in the malaria mosquito vector Anopheles gambiae. *Nat. Biotechnol.* **advance on,** (2015).

37. Russell, C. L., Sallau, A., Emukah, E., Graves, P. M., Noland, G. S., Ngondi, J. M., Ozaki, M., Nwankwo, L., Miri, E., McFarland, D. A., Richards, F. O. & Patterson, A. E. Determinants of Bed Net Use in Southeast Nigeria following Mass Distribution of LLINs: Implications for Social Behavior Change Interventions. *PLoS One* **10,** e0139447 (2015).
38. Ngonghala, C. N., Del Valle, S. Y., Zhao, R. & Mohammed-Awel, J. Quantifying the impact of decay in bed-net efficacy on malaria transmission. *J. Theor. Biol.* **363,** 247–61 (2014).
39. Ordinioha, B. The use and misuse of mass distributed free insecticide-treated bed nets in a semi-urban community in Rivers State, Nigeria. *Ann. Afr. Med.* **11,** 163–8 (2012).
40. Bradley, A. K., Greenwood, A. M., Byass, P., Greenwood, B. M., Marsh, K., Tulloch, S. & Hayes, R. Bed-Nets (Mosquito-Nets) and Morbidity From Malaria. *Lancet* **328,** 204–207 (1986).
41. Achan, J., Talisuna, A. O., Erhart, A., Yeka, A., Tibenderana, J. K., Baliraine, F. N., Rosenthal, P. J. & D'Alessandro, U. Quinine, an old anti-malarial drug in a modern world: role in the treatment of malaria. *Malar. J.* **10,** 144 (2011).
42. Warhurst, D. C., Craig, J. C., Adagu, I. S., Meyer, D. J. & Lee, S. Y. The relationship of physico-chemical properties and structure to the differential antiplasmodial activity of the cinchona alkaloids. *Malar. J.* **2,** 26 (2003).
43. da Silva, A. F. C. & Benchimol, J. L. Malaria and quinine resistance: a medical and scientific issue between Brazil and Germany (1907-19). *Med. Hist.* **58,** 1–26 (2014).
44. Croft, A. M. A lesson learnt: the rise and fall of Lariam and Halfan. *J. R. Soc. Med.* **100,** 170–4 (2007).
45. Jiang, J.-B., Guo, X.-B., Li, G.-Q., Cheung Kong, Y. & Arnold, K. ANTIMALARIAL ACTIVITY OF MEFLOQUINE AND QINGHAOSU. *Lancet* **320,** 285–288 (1982).
46. Pennie, R. A., Koren, G. & Crevoisier, C. Steady state pharmacokinetics of mefloquine in long-term travellers. *Trans. R. Soc. Trop. Med. Hyg.* **87,** 459–62 (1993).

47. Palmer, K. J., Holliday, S. M. & Brogden, R. N. Mefloquine. A review of its antimalarial activity, pharmacokinetic properties and therapeutic efficacy. *Drugs* **45,** 430–75 (1993).
48. Dow, G., Bauman, R., Caridha, D., Cabezas, M., Du, F., Gomez-Lobo, R., Park, M., Smith, K. & Cannard, K. Mefloquine Induces Dose-Related Neurological Effects in a Rat Model. *Antimicrob. Agents Chemother.* **50,** 1045–1053 (2006).
49. Sengupta, K. British armed forces set to ban most prescriptions of controversial anti-malarial drug Lariam. *The Independent* (2016).
50. Makanga, M. & Krudsood, S. The clinical efficacy of artemether/lumefantrine (Coartem). *Malar. J.* **8 Suppl 1,** S5 (2009).
51. Lefèvre, G., Looareesuwan, S., Treeprasertsuk, S., Krudsood, S., Silachamroon, U., Gathmann, I., Mull, R. & Bakshi, R. A clinical and pharmacokinetic trial of six doses of artemether-lumefantrine for multidrug-resistant Plasmodium falciparum malaria in Thailand. *Am. J. Trop. Med. Hyg.* **64,** 247–56
52. Antimalarial Drug Combination Therapy: Report of a WHO Technical Consultation. *World Heal. Organ. Geneva WHO* 4–5 (2001).
53. Premji, Z. G. Coartem: the journey to the clinic. *Malar. J.* **8 Suppl 1,** S3 (2009).
54. Raviña Rubira, E. *The evolution of drug discovery : from traditional medicines to modern drugs*. (Wiley-VCH, 2011).
55. Davis, T. M. E., Hung, T. Y., Sim, I. K., Karunajeewa, H. A. & Ilett, K. F. Piperaquine: A resurgent antimalarial drug. *Drugs* **65,** 75–87 (2005).
56. White, N. J. Malaria. in *Manson's Tropical Infectious Diseases* 532–600.e1 (Elsevier, 2014). doi:10.1016/B978-0-7020-5101-2.00044-3
57. Burckhalter, J. H., Tendick, F. H., Jones, E. M., Holcomb, W. F. & Rawlins, A. L. Aminoalkylphenols as Antimalarials. I. Simply Substituted α-Aminocresols. *J. Am. Chem. Soc.* **68,** 1894–1901 (1946).
58. Burckhalter, J. H., Tendick, F. H., Jones, E. M., Jones, P. A., Holcomb, W. F. & Rawlins, A. L. Aminoalkylphenols as Antimalarials. II. (Heterocyclic-amino)-α-amino-o-cresols. The Synthesis of Camoquin. *J. Am. Chem. Soc.* **70,** 1363–1373 (1948).
59. O'Neill, P. M., Barton, V. E., Ward, S. A. & Chadwick, J. 4-

Aminoquinolines: Chloroquine, Amodiaquine and Next-Generation Analogues. in *Treatment and Prevention of Malaria* 19–44 (Springer Basel, 2011). doi:10.1007/978-3-0346-0480-2_2

60. Cui, L. & Su, X. Discovery, mechanisms of action and combination therapy of artemisinin. *Expert Rev. Anti. Infect. Ther.* **7,** 999–1013 (2009).
61. Isba, R., Zani, B., Gathu, M. & Sinclair, D. Artemisinin-naphthoquine for treating uncomplicated Plasmodium falciparum malaria. *Cochrane database Syst. Rev.* **2,** CD011547 (2015).
62. Vale, N., Moreira, R. & Gomes, P. Primaquine revisited six decades after its discovery. *Eur. J. Med. Chem.* **44,** 937–953 (2008).
63. EDGCOMB, J. H., ARNOLD, J., YOUNT, E. H., ALVING, A. S., EICHELBERGER, L., JEFFERY, G. M., EYLES, D. & YOUNG, M. D. Primaquine, SN 13272, a new curative agent in vivax malaria; a preliminary report. *Journal. Natl. Malar. Soc.* **9,** 285–92 (1950).
64. Watson, J., Taylor, W. R., Menard, D., Kheng, S. & White, N. J. Modelling primaquine-induced haemolysis in G6PD deficiency. *Elife* **6,** (2017).
65. Palmer, M. & Wells, T. N. C. *Neglected diseases and drug discovery*. (Royal Society of Chemistry, 2011).
66. Vinayak, S., Alam, M. T., Mixson-Hayden, T., McCollum, A. M., Sem, R., Shah, N. K., Lim, P., Muth, S., Rogers, W. O., Fandeur, T., Barnwell, J. W., Escalante, A. A., Wongsrichanalai, C., Ariey, F., Meshnick, S. R. & Udhayakumar, V. Origin and Evolution of Sulfadoxine Resistant Plasmodium falciparum. *PLoS Pathog.* **6,** e1000830 (2010).
67. WHO | WHO Policy recommendation on intermittent preventive treatment during infancy with sulphadoxine-pyrimethamine (IPTi-SP) for Plasmodium falciparum malaria control in Africa. *WHO* (2010).
68. Cairns, M., Cheung, Y. B., Xu, Y., Asante, K. P., Owusu-Agyei, S., Diallo, D., Konate, A. T., Dicko, A., Chandramohan, D., Greenwood, B. & Milligan, P. Analysis of Preventive Interventions for Malaria: Exploring Partial and Complete Protection and Total and Primary Intervention Effects. *Am. J. Epidemiol.* **181,** 1008–1017 (2015).
69. Konaté, A. T., Yaro, J. B., Ouédraogo, A. Z., Diarra, A., Gansané, A., Soulama, I., Kangoyé, D. T., Kaboré, Y., Ouédraogo, E., Ouédraogo, A., Tiono, A. B., Ouédraogo, I. N., Chandramohan, D., Cousens, S., Milligan, P.

J., Sirima, S. B., Greenwood, B. & Diallo, D. A. Intermittent Preventive Treatment of Malaria Provides Substantial Protection against Malaria in Children Already Protected by an Insecticide-Treated Bednet in Burkina Faso: A Randomised, Double-Blind, Placebo-Controlled Trial. *PLoS Med.* **8,** e1000408 (2011).

70. Dicko, A., Diallo, A. I., Tembine, I., Dicko, Y., Dara, N., Sidibe, Y., Santara, G., Diawara, H., Conaré, T., Djimde, A., Chandramohan, D., Cousens, S., Milligan, P. J., Diallo, D. A., Doumbo, O. K. & Greenwood, B. Intermittent Preventive Treatment of Malaria Provides Substantial Protection against Malaria in Children Already Protected by an Insecticide-Treated Bednet in Mali: A Randomised, Double-Blind, Placebo-Controlled Trial. *PLoS Med.* **8,** e1000407 (2011).
71. Vanichtanankul, J., Taweechai, S., Yuvaniyama, J., Vilaivan, T., Chitnumsub, P., Kamchonwongpaisan, S. & Yuthavong, Y. Trypanosomal dihydrofolate reductase reveals natural antifolate resistance. *ACS Chem. Biol.* **6,** 905–11 (2011).
72. Yuvaniyama, J., Chitnumsub, P., Kamchonwongpaisan, S., Vanichtanankul, J., Sirawaraporn, W., Taylor, P., Walkinshaw, M. D. & Yuthavong, Y. Insights into antifolate resistance from malarial DHFR-TS structures. *Nat. Struct. Biol.* **10,** 357–365 (2003).
73. Vanichtanankul, J., Taweechai, S., Uttamapinant, C., Chitnumsub, P., Vilaivan, T., Yuthavong, Y. & Kamchonwongpaisan, S. Combined Spatial Limitation around Residues 16 and 108 of Plasmodium falciparum Dihydrofolate Reductase Explains Resistance to Cycloguanil. *Antimicrob. Agents Chemother.* **56,** 3928–3935 (2012).
74. Basco, L. K., Tahar, R. & Ringwald, P. Molecular basis of in vivo resistance to sulfadoxine-pyrimethamine in African adult patients infected with Plasmodium falciparum malaria parasites. *Antimicrob. Agents Chemother.* **42,** 1811–4 (1998).
75. de Koning-Ward, T. F., Fidock, D. A., Thathy, V., Menard, R., van Spaendonk, R. M., Waters, A. P. & Janse, C. J. The selectable marker human dihydrofolate reductase enables sequential genetic manipulation of the Plasmodium berghei genome. *Mol. Biochem. Parasitol.* **106,** 199–212 (2000).
76. van Schalkwyk, D. A., Moon, R. W., Blasco, B. & Sutherland, C. J.

Comparison of the susceptibility of Plasmodium knowlesi and Plasmodium falciparum to antimalarial agents. *J. Antimicrob. Chemother.* **72,** 3051–3058 (2017).

77. Arguin, P. M. & Magill, A. J. For the Record: A History of Malaria Chemoprophylaxis - Chapter 3 - 2018 Yellow Book | Travelers' Health | CDC. *CDC Traveler's Medicine* 1 (2017). Available at: https://wwwnc.cdc.gov/travel/yellowbook/2018/infectious-diseases-related-to-travel/emfor-the-record-a-history-of-malaria-chemoprophylaxisem. (Accessed: 4th January 2018)
78. Gaillard, T., Madamet, M. & Pradines, B. Tetracyclines in malaria. *Malar. J.* **14,** 445 (2015).
79. Lell, B. & Kremsner, P. G. Clindamycin as an Antimalarial Drug: Review of Clinical Trials. *Antimicrob. Agents Chemother.* **46,** 2315–2320 (2002).
80. Lim, L. & McFadden, G. I. The evolution, metabolism and functions of the apicoplast. *Philos. Trans. R. Soc. Lond. B. Biol. Sci.* **365,** 749–63 (2010).
81. Dahl, E. L. & Rosenthal, P. J. Multiple Antibiotics Exert Delayed Effects against the Plasmodium falciparum Apicoplast. *Antimicrob. Agents Chemother.* **51,** 3485–3490 (2007).
82. Yeh, E., DeRisi, J. L., Kappe, S. H. I., Hafalla, J. C. R. & Matuschewski, K. Chemical Rescue of Malaria Parasites Lacking an Apicoplast Defines Organelle Function in Blood-Stage Plasmodium falciparum. *PLoS Biol.* **9,** e1001138 (2011).
83. Shmuklarsky, M. J., Boudreau, E. F., Pang, L. W., Smith, J. I., Schneider, I., Fleckenstein, L., Abdelrahim, M. M., Canfield, C. J. & Schuster, B. Failure of doxycycline as a causal prophylactic agent against Plasmodium falciparum malaria in healthy nonimmune volunteers. *Ann. Intern. Med.* **120,** 294–9 (1994).
84. Madamet, M., Gaillard, T., Velut, G., Ficko, C., Houzé, P., Bylicki, C., Mérat, S., Houzé, S., Taudon, N., Michel, R., Pasquier, P., Rapp, C. & Pradines, B. Malaria Prophylaxis Failure with Doxycycline, Central African Republic, 2014. *Emerg. Infect. Dis.* **21,** 1485–1486 (2015).
85. Gaillard, T., Briolant, S., Houzé, S., Baragatti, M., Wurtz, N., Hubert, V., Lavina, M., Pascual, A., Travaillé, C., Le Bras, J., Pradines, B. & French National Reference Centre for Imported Malaria Study Group. PftetQ and

pfmdt copy numbers as predictive molecular markers of decreased ex vivo doxycycline susceptibility in imported Plasmodium falciparum malaria. *Malar. J.* **12,** 414 (2013).

86. Gaillard, T., Sriprawat, K., Briolant, S., Wangsing, C., Wurtz, N., Baragatti, M., Lavina, M., Pascual, A., Nosten, F. & Pradines, B. Molecular Markers and *In Vitro* Susceptibility to Doxycycline in Plasmodium falciparum Isolates from Thailand. *Antimicrob. Agents Chemother.* **59,** 5080–5083 (2015).
87. Gaillard, T., Wurtz, N., Houzé, S., Sriprawat, K., Wangsing, C., Hubert, V., Lebras, J., Nosten, F., Briolant, S., Pradines, B. & French National Reference Centre for Imported Malaria Study Group. Absence of association between Plasmodium falciparum small sub-unit ribosomal RNA gene mutations and in vitro decreased susceptibility to doxycycline. *Malar. J.* **14,** 348 (2015).
88. Faurant, C. From bark to weed: the history of artemisinin. *Parasite* **18,** 215–8 (2011).
89. Dogovski, C., Xie, S. C., Burgio, G., Bridgford, J., Mok, S., McCaw, J. M., Chotivanich, K., Kenny, S., Gnädig, N., Straimer, J., Bozdech, Z., Fidock, D. A., Simpson, J. A., Dondorp, A. M., Foote, S., Klonis, N. & Tilley, L. Targeting the Cell Stress Response of Plasmodium falciparum to Overcome Artemisinin Resistance. *PLOS Biol.* **13,** e1002132 (2015).
90. Xie, S. C., Dogovski, C., Hanssen, E., Chiu, F., Yang, T., Crespo, M. P., Stafford, C., Batinovic, S., Teguh, S., Charman, S., Klonis, N. & Tilley, L. Haemoglobin degradation underpins the sensitivity of early ring stage Plasmodium falciparum to artemisinins. *J. Cell Sci.* **129,** 406–416 (2016).
91. Klonis, N., Xie, S. C., Mccaw, J. M., Crespo-Ortiz, M. P., Zaloumis, S. G., Simpson, J. A. & Tilley, L. Altered temporal response of malaria parasites determines differential sensitivity to artemisinin. *Proc. Natl. Acad. Sci.* **110,** 5157–5162 (2013).
92. Delves, M. J., Ruecker, A., Straschil, U., Lelièvre, J., Marques, S., López-Barragán, M. J., Herreros, E. & Sinden, R. E. Male and female Plasmodium falciparum mature gametocytes show different responses to antimalarial drugs. *Antimicrob. Agents Chemother.* **57,** 3268–74 (2013).
93. Muwanguzi, J., Henriques, G., Sawa, P., Bousema, T., Sutherland, C. J. & Beshir, K. B. Lack of K13 mutations in Plasmodium falciparum persisting after artemisinin combination therapy treatment of Kenyan children. *Malar. J.*

**15,** 36 (2016).

94. Vijaykadga, S., Alker, A. P., Satimai, W., MacArthur, J. R., Meshnick, S. R. & Wongsrichanalai, C. Delayed Plasmodium falciparum clearance following artesunate-mefloquine combination therapy in Thailand, 1997–2007. *Malar. J.* **11,** 296 (2012).
95. Beshir, K. B., Sutherland, C. J., Sawa, P., Drakeley, C. J., Okell, L., Mweresa, C. K., Omar, S. a., Shekalaghe, S. a., Kaur, H., Ndaro, a., Chilongola, J., Schallig, H. D. F. H., Sauerwein, R. W., Hallett, R. L. & Bousema, T. Residual Plasmodium falciparum Parasitemia in Kenyan Children After Artemisinin-Combination Therapy Is Associated With Increased Transmission to Mosquitoes and Parasite Recurrence. *J. Infect. Dis.* **208,** 2017–2024 (2013).
96. Cooper, R. A., Conrad, M. D., Watson, Q. D., Huezo, S. J., Ninsiima, H., Tumwebaze, P., Nsobya, S. L. & Rosenthal, P. J. Lack of Artemisinin Resistance in Plasmodium falciparum in Uganda Based on Parasitological and Molecular Assays. *Antimicrob. Agents Chemother.* **59,** 5061–4 (2015).
97. Schallig, H. D., Tinto, H., Sawa, P., Kaur, H., Duparc, S., Ishengoma, D. S., Magnussen, P., Alifrangis, M. & Sutherland, C. J. Randomised controlled trial of two sequential artemisinin-based combination therapy regimens to treat uncomplicated falciparum malaria in African children: a protocol to investigate safety, efficacy and adherence. *BMJ Glob. Heal.* **2,** e000371 (2017).
98. McCarthy, J. S., Baker, M., O'Rourke, P., Marquart, L., Griffin, P., Hooft van Huijsduijnen, R. & Möhrle, J. J. Efficacy of OZ439 (artefenomel) against early Plasmodium falciparum blood-stage malaria infection in healthy volunteers. *J. Antimicrob. Chemother.* **71,** 2620–2627 (2016).
99. Baumgärtner, F., Jourdan, J., Scheurer, C., Blasco, B., Campo, B., Mäser, P. & Wittlin, S. In vitro activity of anti-malarial ozonides against an artemisinin-resistant isolate. *Malar. J.* **16,** 45 (2017).
100. Straimer, J., Gnädig, N. F., Stokes, B. H., Ehrenberger, M., Crane, A. A. & Fidock, D. A. Plasmodium falciparum K13 Mutations Differentially Impact Ozonide Susceptibility and Parasite Fitness In Vitro. *MBio* **8,** e00172-17 (2017).
101. Conway, D. J. Molecular epidemiology of malaria. *Clin. Microbiol. Rev.* **20,**

188–204 (2007).

102. Bopp, S. E. R., Manary, M. J., Bright, A. T., Johnston, G. L., Dharia, N. V, Luna, F. L., McCormack, S., Plouffe, D., McNamara, C. W., Walker, J. R., Fidock, D. A., Denchi, E. L. & Winzeler, E. A. Mitotic evolution of Plasmodium falciparum shows a stable core genome but recombination in antigen families. *PLoS Genet.* **9,** e1003293 (2013).
103. Hamilton, W. L., Claessens, A., Otto, T. D., Kekre, M., Fairhurst, R. M., Rayner, J. C. & Kwiatkowski, D. Extreme mutation bias and high AT content in Plasmodium falciparum. *Nucleic Acids Res.* **45,** 1889–1901 (2017).
104. Paget-Mcnicol, S. & Saul, A. Mutation rates in the dihydrofolate reductase gene of Plasmodium falciparum. *Parasitology* **122,** 497–505 (2001).
105. Claessens, A., Hamilton, W. L., Kekre, M., Otto, T. D., Faizullabhoy, A., Rayner, J. C. & Kwiatkowski, D. Generation of Antigenic Diversity in Plasmodium falciparum by Structured Rearrangement of Var Genes During Mitosis. *PLoS Genet.* **10,** (2014).
106. Brabin, B. J. Malaria's contribution to World War One – the unexpected adversary. *Malar. J.* **13,** 497 (2014).
107. Bloland, P. B. Drug resistance in malaria.
108. Kremsner, P. G., Winkler, S., Brandts, C., Neifer, S., Bienzle, U. & Graninger, W. Clindamycin in combination with chloroquine or quinine is an effective therapy for uncomplicated Plasmodium falciparum malaria in children from Gabon. *J. Infect. Dis.* **169,** 467–70 (1994).
109. Nosten, F., van Vugt, M., Price, R., Luxemburger, C., Thway, K. L., Brockman, A., McGready, R., ter Kuile, F., Looareesuwan, S. & White, N. J. Effects of artesunate-mefloquine combination on incidence of Plasmodium falciparum malaria and mefloquine resistance in western Thailand: a prospective study. *Lancet (London, England)* **356,** 297–302 (2000).
110. Witkowski, B., Iriart, X., Soh, P. N., Menard, S., Alvarez, M., Naneix-Laroche, V., Marchou, B., Magnaval, J.-F., Benoit-Vical, F. & Berry, A. pfmdr1 amplification associated with clinical resistance to mefloquine in West Africa: implications for efficacy of artemisinin combination therapies. *J. Clin. Microbiol.* **48,** 3797–9 (2010).
111. Gay, F., Binet, M. H., Bustos, M. D., Rouveix, B., Danis, M., Roy, C. & Gentilini, M. Mefloquine failure in child contracting falciparum malaria in

West Africa. *Lancet (London, England)* **335,** 120–1 (1990).

112. Cerutti, Jr., C., Durlacher, R. R., de Alencar, F. E. C., Segurado, A. A. C. & Pang, L. W. In Vivo Efficacy of Mefloquine for the Treatment of Falciparum Malaria in Brazil. *J. Infect. Dis.* **180,** 2077–2080 (1999).
113. Bukirwa, H. & Orton, L. C. Artesunate plus mefloquine versus mefloquine for treating uncomplicated malaria. in *Cochrane Database of Systematic Reviews* (ed. Bukirwa, H.) (John Wiley & Sons, Ltd, 2005). doi:10.1002/14651858.CD004531.pub2
114. de Souza-Lima, R. de C., Rodrigues, P. T., Ferreira, M. U., Bastos, M. S., Luz, F. das C. O., de Melo, G. N. P., Ladeia-Andrade, S. & Salla, L. C. No Clinical or Molecular Evidence of Plasmodium falciparum Resistance to Artesunate–Mefloquine in Northwestern Brazil. *Am. J. Trop. Med. Hyg.* **95,** 148–154 (2016).
115. Gutman, J., Green, M., Durand, S., Rojas, O. V., Ganguly, B., Quezada, W. M., Utz, G. C., Slutsker, L., Ruebush, T. K. & Bacon, D. J. Mefloquine pharmacokinetics and mefloquine-artesunate effectiveness in Peruvian patients with uncomplicated Plasmodium falciparum malaria. *Malar. J.* **8,** 58 (2009).
116. Bustos, M. D., Wongsrichanalai, C., Delacollette, C. & Burkholder, B. Monitoring antimalarial drug efficacy in the Greater Mekong Subregion: an overview of in vivo results from 2008 to 2010. *Southeast Asian J. Trop. Med. Public Health* **44 Suppl 1,** 201-30–7 (2013).
117. Na-Bangchang, K., Ruengweerayut, R., Mahamad, P., Ruengweerayut, K. & Chaijaroenkul, W. Declining in efficacy of a three-day combination regimen of mefloquine-artesunate in a multi-drug resistance area along the Thai-Myanmar border. *Malar. J.* **9,** 273 (2010).
118. Leang, R., Ros, S., Duong, S., Navaratnam, V., Lim, P., Ariey, F., Kiechel, J.-R., Ménard, D. & Taylor, W. R. Therapeutic efficacy of fixed dose artesunate-mefloquine for the treatment of acute, uncomplicated Plasmodium falciparum malaria in Kampong Speu, Cambodia. *Malar. J.* **12,** 343 (2013).
119. Phompradit, P., Muhamad, P., Wisedpanichkij, R., Chaijaroenkul, W. & Na-Bangchang, K. Four years' monitoring of in vitro sensitivity and candidate molecular markers of resistance of Plasmodium falciparum to artesunate-mefloquine combination in the Thai-Myanmar border. *Malar. J.* **13,** 23

(2014).

120. Cui, L., Wang, Z., Jiang, H., Parker, D., Wang, H., Su, X.-Z. & Cui, L. Lack of Association of the S769N Mutation in Plasmodium falciparum SERCA (PfATP6) with Resistance to Artemisinins. *Antimicrob. Agents Chemother.* **56,** 2546–2552 (2012).
121. Djimde, A. A., Makanga, M., Kuhen, K. & Hamed, K. The emerging threat of artemisinin resistance in malaria: focus on artemether-lumefantrine. *Expert Rev. Anti. Infect. Ther.* **13,** 1031–1045 (2015).
122. Macedo de Oliveira, A., Rachid Viana, G. M., Negreiros do Valle, S., Marchesini, P., Lucchi, N., Farias, S., Póvoa, M., Chenet, S., Holanda de Souza, T. M., Itoh, M. & Faria e Silva Santelli, A. C. Efficacy of Artemether–Lumefantrine for Uncomplicated Plasmodium falciparum Malaria in Cruzeiro do Sul, Brazil, 2016. *Am. J. Trop. Med. Hyg.* (2017). doi:10.4269/ajtmh.17-0623
123. Aponte, S., Guerra, Á. P., Álvarez-Larrotta, C., Bernal, S. D., Restrepo, C., González, C., Yasnot, M. F. & Knudson-Ospina, A. Baseline in vivo, ex vivo and molecular responses of Plasmodium falciparum to artemether and lumefantrine in three endemic zones for malaria in Colombia. *Trans. R. Soc. Trop. Med. Hyg.* **111,** 71–80 (2017).
124. Plucinski, M. M., Talundzic, E., Morton, L., Dimbu, P. R., Macaia, A. P., Fortes, F., Goldman, I., Lucchi, N., Stennies, G., MacArthur, J. R. & Udhayakumar, V. Reply to "no robust evidence of lumefantrine resistance". *Antimicrob. Agents Chemother.* **59,** 5867–8 (2015).
125. Hamed, K. & Kuhen, K. No robust evidence of lumefantrine resistance. *Antimicrob. Agents Chemother.* **59,** 5865–6 (2015).
126. Plucinski, M. M., Talundzic, E., Morton, L., Dimbu, P. R., Macaia, A. P., Fortes, F., Goldman, I., Lucchi, N., Stennies, G., MacArthur, J. R. & Udhayakumar, V. Efficacy of artemether-lumefantrine and dihydroartemisinin-piperaquine for treatment of uncomplicated malaria in children in Zaire and Uíge Provinces, angola. *Antimicrob. Agents Chemother.* **59,** 437–43 (2015).
127. Färnert, A., Ursing, J., Tolfvenstam, T., Rono, J., Karlsson, L., Sparrelid, E. & Lindegårdh, N. Artemether–lumefantrine treatment failure despite adequate lumefantrine day 7 concentration in a traveller with Plasmodium falciparum

malaria after returning from Tanzania. *Malar. J.* **11,** 176 (2012).

128. Ayalew, M. B. Therapeutic efficacy of artemether-lumefantrine in the treatment of uncomplicated Plasmodium falciparum malaria in Ethiopia: a systematic review and meta-analysis. *Infect. Dis. Poverty* **6,** 157 (2017).
129. Rasmussen, S. A., Ceja, F. G., Conrad, M. D., Tumwebaze, P. K., Byaruhanga, O., Katairo, T., Nsobya, S. L., Rosenthal, P. J. & Cooper, R. A. Changing Antimalarial Drug Sensitivities in Uganda. *Antimicrob. Agents Chemother.* **61,** e01516-17 (2017).
130. Sutherland, C. J., Lansdell, P., Sanders, M., Muwanguzi, J., van Schalkwyk, D. A., Kaur, H., Nolder, D., Tucker, J., Bennett, H. M., Otto, T. D., Berriman, M., Patel, T. A., Lynn, R., Gkrania-Klotsas, E. & Chiodini, P. L. Pfk13-independent treatment failure in four imported cases of Plasmodium falciparum malaria given artemether-lumefantrine in the UK. *Antimicrob. Agents Chemother.* **61,** (2017).
131. Krogstad, D. J., Gluzman, I. Y., Kyle, D. E., Oduola, A. M., Martin, S. K., Milhous, W. K. & Schlesinger, P. H. Efflux of chloroquine from Plasmodium falciparum: mechanism of chloroquine resistance. *Science* **238,** 1283–5 (1987).
132. Wilson, C. M., Serrano, A. E., Wasley, A., Bogenschutz, M. P., Shankar, A. H. & Wirth, D. F. Amplification of a gene related to mammalian mdr genes in drug-resistant Plasmodium falciparum. *Science* **244,** 1184–6 (1989).
133. Foote, S. J., Thompson, J. K., Cowman, A. F. & Kemp, D. J. Amplification of the multidrug resistance gene in some chloroquine-resistant isolates of P. falciparum. *Cell* **57,** 921–30 (1989).
134. Triglia, T., Foote, S. J., Kemp, D. J. & Cowman, A. F. Amplification of the multidrug resistance gene pfmdr1 in Plasmodium falciparum has arisen as multiple independent events. *Mol. Cell. Biol.* **11,** 5244–50 (1991).
135. Cowman, A. F., Karcz, S., Galatis, D. & Culvenor, J. G. A P-glycoprotein homologue of Plasmodium falciparum is localized on the digestive vacuole. *J. Cell Biol.* **113,** 1033–42 (1991).
136. Cowman, A. F., Galatis, D. & Thompson, J. K. Selection for mefloquine resistance in Plasmodium falciparum is linked to amplification of the pfmdr1 gene and cross-resistance to halofantrine and quinine. *Proc. Natl. Acad. Sci. U. S. A.* **91,** 1143–7 (1994).

137. Reed, M. B., Saliba, K. J., Caruana, S. R., Kirk, K. & Cowman, A. F. Pgh1 modulates sensitivity and resistance to multiple antimalarials in Plasmodium falciparum. *Nature* **403,** 906–909 (2000).
138. Price, R. N., Cassar, C., Brockman, A., Duraisingh, M., van Vugt, M., White, N. J., Nosten, F. & Krishna, S. The pfmdr1 gene is associated with a multidrug-resistant phenotype in Plasmodium falciparum from the western border of Thailand. *Antimicrob. Agents Chemother.* **43,** 2943–9 (1999).
139. Sidhu, A. B. S., Valderramos, S. G. & Fidock, D. A. pfmdr1 mutations contribute to quinine resistance and enhance mefloquine and artemisinin sensitivity in Plasmodium falciparum. *Mol. Microbiol.* **57,** 913–926 (2005).
140. Sidhu, A. B. S., Uhlemann, A., Valderramos, S. G., Valderramos, J., Krishna, S. & Fidock, D. A. Decreasing *pfmdr1* Copy Number in *Plasmodium falciparum* Malaria Heightens Susceptibility to Mefloquine, Lumefantrine, Halofantrine, Quinine, and Artemisinin. *J. Infect. Dis.* **194,** 528–535 (2006).
141. Veiga, M. I., Dhingra, S. K., Henrich, P. P., Straimer, J., Gnädig, N., Uhlemann, A.-C., Martin, R. E., Lehane, A. M. & Fidock, D. A. Globally prevalent PfMDR1 mutations modulate Plasmodium falciparum susceptibility to artemisinin-based combination therapies. *Nat. Commun.* **7,** 11553 (2016).
142. Fitch, C. D., Chan, R. L. & Chevli, R. Chloroquine resistance in malaria: accessibility of drug receptors to mefloquine. *Antimicrob. Agents Chemother.* **15,** 258–62 (1979).
143. Wong, W., Bai, X.-C., Sleebs, B. E., Triglia, T., Brown, A., Thompson, J. K., Jackson, K. E., Hanssen, E., Marapana, D. S., Fernandez, I. S., Ralph, S. A., Cowman, A. F., Scheres, S. H. W. & Baum, J. Mefloquine targets the Plasmodium falciparum 80S ribosome to inhibit protein synthesis. *Nat. Microbiol.* **2,** 17031 (2017).
144. Trape, J.-F. The Public Health Impact of Chloroquine Resistance in Africa. (2001).
145. Payne, D. Spread of chloroquine resistance in Plasmodium falciparum. *Parasitology Today* **3,** 241–246 (1987).
146. Trape, J. F., Pison, G., Preziosi, M. P., Enel, C., Du Loû, A. D., Delaunay, V., Samb, B., Lagarde, E., Molez, J. F. & Simondon, F. Impact of chloroquine resistance on malaria mortality. *Comptes Rendus l'Academie des Sci. - Ser. III* **321,** 689–697 (1998).

147. *Saving Lives, Buying Time: Economics of Malaria Drugs in an Age of Resistance*. (National Academies Press, 2004). doi:10.17226/11017
148. HOMEWOOD, C. A., WARHURST, D. C., PETERS, W. & BAGGALEY, V. C. Lysosomes, pH and the Anti-malarial Action of Chloroquine. *Nature* **235,** 50–52 (1972).
149. Trager, W. & Jensen, J. B. Human malaria parasites in continuous culture. *Science* **193,** 673–5 (1976).
150. Chou, A. C. & Fitch, C. D. Hemolysis of mouse erythrocytes by ferriprotoporphyrin IX and chloroquine. Chemotherapeutic implications. *J. Clin. Invest.* **66,** 856–8 (1980).
151. Banyal, H. S. & Fitch, C. D. Ferriprotoporphyrin IX binding substances and the mode of action of chloroquine against malaria. *Life Sci.* **31,** 1141–4 (1982).
152. Fitch, C. D. Ferriprotoporphyrin IX: role in chloroquine susceptibility and resistance in malaria. *Prog. Clin. Biol. Res.* **313,** 45–52 (1989).
153. Verdier, F., Le Bras, J., Clavier, F., Hatin, I. & Blayo, M. C. Chloroquine uptake by Plasmodium falciparum-infected human erythrocytes during in vitro culture and its relationship to chloroquine resistance. *Antimicrob. Agents Chemother.* **27,** 561–564 (1985).
154. Martin, S. K., Oduola, A. M. & Milhous, W. K. Reversal of chloroquine resistance in Plasmodium falciparum by verapamil. *Science* **235,** 899–901 (1987).
155. Djimde, A., Doumbo, O. K., Cortese, J. F., Kayentao, K., Doumbo, S., Diourte, Y., Dicko, A., Su, X.-Z., Nomura, T., Fidock, D. A., Wellems, T. E. & Plowe, C. V. A Molecular marker for chloroquine-resistant Falciparum malaria. *N Engl J Med* **344,** 257–263 (2001).
156. Martiney, J. A., Cerami, A. & Slater, A. F. Verapamil reversal of chloroquine resistance in the malaria parasite Plasmodium falciparum is specific for resistant parasites and independent of the weak base effect. *J. Biol. Chem.* **270,** 22393–8 (1995).
157. Adagu, I. S. & Warhurst, D. C. Association of cg2 and pfmdr1 genotype with chloroquine resistance in field samples of Plasmodium falciparum from Nigeria. *Parasitology* **119 ( Pt 4,** 343–8 (1999).
158. Su, X., Kirkman, L. A., Fujioka, H. & Wellems, T. E. Complex

Polymorphisms in an ~330 kDa Protein Are Linked to Chloroquine-Resistant P. falciparum in Southeast Asia and Africa. *Cell* **91,** 593–603 (1997).

159. Fidock, D. a, Nomura, T., Talley, A. K., Cooper, R. a, Dzekunov, S. M., Ferdig, M. T., Ursos, L. M., Sidhu, A. B., Naudé, B., Deitsch, K. W., Su, X. Z., Wootton, J. C., Roepe, P. D. & Wellems, T. E. Mutations in the P. falciparum digestive vacuole transmembrane protein PfCRT and evidence for their role in chloroquine resistance. *Mol. Cell* **6,** 861–71 (2000).
160. Fidock, D. A., Nomura, T., Cooper, R. A., Su, X., Talley, A. K. & Wellems, T. E. Allelic modifications of the cg2 and cg1 genes do not alter the chloroquine response of drug-resistant Plasmodium falciparum. *Mol. Biochem. Parasitol.* **110,** 1–10 (2000).
161. Cooper, R. a, Ferdig, M. T., Su, X.-Z., Ursos, L. M. B., Mu, J., Nomura, T., Fujioka, H., Fidock, D. a, Roepe, P. D. & Wellems, T. E. Alternative mutations at position 76 of the vacuolar transmembrane protein PfCRT are associated with chloroquine resistance and unique stereospecific quinine and quinidine responses in Plasmodium falciparum. *Mol. Pharmacol.* **61,** 35–42 (2002).
162. Chinappi, M., Via, A., Marcatili, P. & Tramontano, A. On the Mechanism of Chloroquine Resistance in Plasmodium falciparum. *PLoS One* **5,** e14064 (2010).
163. Pulcini, S., Staines, H. M., Lee, A. H., Shafik, S. H., Bouyer, G., Moore, C. M., Daley, D. a., Hoke, M. J., Altenhofen, L. M., Painter, H. J., Mu, J., Ferguson, D. J. P., Llinás, M., Martin, R. E., Fidock, D. a., Cooper, R. a. & Krishna, S. Mutations in the Plasmodium falciparum chloroquine resistance transporter, PfCRT, enlarge the parasite's food vacuole and alter drug sensitivities. *Sci. Rep.* **5,** 14552 (2015).
164. Martin, R. E., Marchetti, R. V, Cowan, A. I., Howitt, S. M., Bröer, S. & Kirk, K. Chloroquine Transport via the Malaria Parasite's Chloroquine Resistance Transporter.
165. Sa, J. M. & Twu, O. Protecting the malaria drug arsenal: halting the rise and spread of amodiaquine resistance by monitoring the PfCRT SVMNT type. *Malar. J.* **9,** 374 (2010).
166. Beshir, K., Sutherland, C. J., Merinopoulos, I., Durrani, N., Leslie, T., Rowland, M. & Hallett, R. L. Amodiaquine resistance in Plasmodium

falciparum malaria in Afghanistan is associated with the pfcrt SVMNT allele at codons 72 to 76. *Antimicrob. Agents Chemother.* **54,** 3714–6 (2010).

167. Ndung'u, L., Langat, B., Magiri, E., Ng'ang'a, J., Irungu, B., Nzila, A. & Kiboi, D. Amodiaquine resistance in Plasmodium berghei is associated with PbCRT His95Pro mutation, loss of chloroquine, artemisinin and primaquine sensitivity, and high transcript levels of key transporters. *Wellcome Open Res.* **2,** 44 (2017).
168. Chen, C. Development of antimalarial drugs and their application in China: a historical review. *Infect. Dis. poverty* **3,** 9 (2014).
169. Yang, H., Liu, D., Huang, K., Yang, Y., Yang, P., Liao, M. & Zhang, C. Assay of sensitivity of Plasmodium falciparum to chloroquine, amodiaquine, piperaquine, mefloquine and quinine in Yunnan province. *Chinese J. Parasitol. Parasit. Dis.* **17,** 43–5 (1999).
170. Leang, R., Barrette, A., Bouth, D. M., Menard, D., Abdur, R., Duong, S. & Ringwald, P. Efficacy of dihydroartemisinin-piperaquine for treatment of uncomplicated Plasmodium falciparum and Plasmodium vivax in Cambodia, 2008 to 2010. *Antimicrob. Agents Chemother.* **57,** 818–26 (2013).
171. Saunders, D. L., Vanachayangkul, P. & Lon, C. Dihydroartemisinin–Piperaquine Failure in Cambodia. *N. Engl. J. Med.* **371,** 484–485 (2014).
172. Imwong, M., Hien, T. T., Thuy-Nhien, N. T., Dondorp, A. M. & White, N. J. Spread of a single multidrug resistant malaria parasite lineage (PfPailin) to Vietnam. *Lancet. Infect. Dis.* **17,** 1022–1023 (2017).
173. Thanh, N. V., Thuy-Nhien, N., Tuyen, N. T. K., Tong, N. T., Nha-Ca, N. T., Dong, L. T., Quang, H. H., Farrar, J., Thwaites, G., White, N. J., Wolbers, M. & Hien, T. T. Rapid decline in the susceptibility of Plasmodium falciparum to dihydroartemisinin–piperaquine in the south of Vietnam. *Malar. J.* **16,** 27 (2017).
174. Pascual, A., Madamet, M., Bertaux, L., Amalvict, R., Benoit, N., Travers, D., Cren, J., Taudon, N., Rogier, C., Parzy, D., Pradines, B. & French National Reference Centre for Imported Malaria Study Group. In vitro piperaquine susceptibility is not associated with the Plasmodium falciparum chloroquine resistance transporter gene. *Malar. J.* **12,** 431 (2013).
175. Eastman, R. T., Dharia, N. V, Winzeler, E. A. & Fidock, D. A. Piperaquine resistance is associated with a copy number variation on chromosome 5 in

drug-pressured Plasmodium falciparum parasites. *Antimicrob. Agents Chemother.* **55,** 3908–16 (2011).

176. Dhingra, S. K., Redhi, D., Combrinck, J. M., Yeo, T., Okombo, J., Henrich, P. P., Cowell, A. N., Gupta, P., Stegman, M. L., Hoke, J. M., Cooper, R. A., Winzeler, E., Mok, S., Egan, T. J. & Fidock, D. A. A Variant PfCRT Isoform Can Contribute to Plasmodium falciparum Resistance to the First-Line Partner Drug Piperaquine. *MBio* **8,** e00303-17 (2017).
177. Ecker, A., Lehane, A. M., Clain, J. & Fidock, D. A. PfCRT and its role in antimalarial drug resistance. *Trends Parasitol.* **28,** 504–14 (2012).
178. Klemba, M., Beatty, W., Gluzman, I. & Goldberg, D. E. Trafficking of plasmepsin II to the food vacuole of the malaria parasite Plasmodium falciparum. *J. Cell Biol.* **164,** 47–56 (2004).
179. Silva, A. M., Lee, A. Y., Gulnik, S. V, Maier, P., Collins, J., Bhat, T. N., Collins, P. J., Cachau, R. E., Luker, K. E., Gluzman, I. Y., Francis, S. E., Oksman, A., Goldberg, D. E. & Erickson, J. W. Structure and inhibition of plasmepsin II, a hemoglobin-degrading enzyme from Plasmodium falciparum. *Proc. Natl. Acad. Sci. U. S. A.* **93,** 10034–9 (1996).
180. Witkowski, B., Duru, V., Khim, N., Ross, L. S., Saintpierre, B., Beghain, J., Chy, S., Kim, S., Ke, S., Kloeung, N., Eam, R., Khean, C., Ken, M., Loch, K., Bouillon, A., Domergue, A., Ma, L., Bouchier, C., Leang, R., *et al.* A surrogate marker of piperaquine-resistant Plasmodium falciparum malaria: a phenotype-genotype association study. *Lancet. Infect. Dis.* **17,** 174–183 (2017).
181. Amato, R., Lim, P., Miotto, O., Amaratunga, C., Dek, D., Pearson, R. D., Almagro-Garcia, J., Neal, A. T., Sreng, S., Suon, S., Drury, E., Jyothi, D., Stalker, J., Kwiatkowski, D. P. & Fairhurst, R. M. Genetic markers associated with dihydroartemisinin–piperaquine failure in Plasmodium falciparum malaria in Cambodia: a genotype–phenotype association study. *Lancet Infect. Dis.* **17,** 164–173 (2017).
182. Ashley, E. a., Dhorda, M., Fairhurst, R. M., Amaratunga, C., Lim, P., Suon, S., Sreng, S., Anderson, J. M., Mao, S., Sam, B., Sopha, C., Chuor, C. M., Nguon, C., Sovannaroth, S., Pukrittayakamee, S., Jittamala, P., Chotivanich, K., Chutasmit, K., Suchatsoonthorn, C., *et al.* Spread of Artemisinin Resistance in *Plasmodium falciparum* Malaria. *N. Engl. J. Med.* **371,** 411–423

(2014).

183. Noedl, H., Se, Y., Schaecher, K., Smith, B. L., Socheat, D. & Fukuda, M. M. Evidence of Artemisinin-resistant malaria in Western Cambodia. *N. Engl. J. Med.* **359,** 2619–2620 (2008).

184. Dondorp, A. M., Nosten, F., Yi, P., Das, D., Phyo, A. P., Tarning, J., Lwin, K. M., Ariey, F., Hanpithakpong, W., Lee, S. J., Ringwald, P., Silamut, K., Imwong, M., Chotivanich, K., Lim, P., Herdman, T., An, S. S., Yeung, S., Singhasivanon, P., *et al.* Artemisinin Resistance in Plasmodium falciparum Malaria. *N. Engl. J. Med.* **361,** 455–467 (2009).

185. Lu, F., Culleton, R., Zhang, M., Ramaprasad, A., von Seidlein, L., Zhou, H., Zhu, G., Tang, J., Liu, Y., Wang, W., Cao, Y., Xu, S., Gu, Y., Li, J., Zhang, C., Gao, Q., Menard, D., Pain, A., Yang, H., *et al.* Emergence of Indigenous Artemisinin-Resistant Plasmodium falciparum in Africa. *N. Engl. J. Med.* **376,** 991–993 (2017).

186. Nosten, F. & White, N. J. Artemisinin-Based Combination Treatment of Falciparum Malaria. *Am. J. Trop. Med. Hyg.* **77,** (2007).

187. de Vries, P. J. & Dien, T. K. Clinical pharmacology and therapeutic potential of artemisinin and its derivatives in the treatment of malaria. *Drugs* **52,** 818–36 (1996).

188. Witkowski, B., Khim, N., Chim, P., Kim, S., Ke, S., Kloeung, N., Chy, S., Duong, S., Leang, R., Ringwald, P., Dondorp, A. M., Tripura, R., Benoit-Vical, F., Berry, A., Gorgette, O., Ariey, F., Barale, J.-C., Mercereau-Puijalon, O. & Menard, D. Reduced Artemisinin Susceptibility of Plasmodium falciparum Ring Stages in Western Cambodia. *Antimicrob. Agents Chemother.* **57,** 914–923 (2013).

189. Klonis, N., Creek, D. J. & Tilley, L. Iron and heme metabolism in Plasmodium falciparum and the mechanism of action of artemisinins. *Curr. Opin. Microbiol.* **16,** 722–727 (2013).

190. Klonis, N., Crespo-Ortiz, M. P., Bottova, I., Abu-Bakar, N., Kenny, S., Rosenthal, P. J. & Tilley, L. Artemisinin activity against Plasmodium falciparum requires hemoglobin uptake and digestion. *Proc. Natl. Acad. Sci.* **108,** 11405–11410 (2011).

191. Elliott, D. A., McIntosh, M. T., Hosgood, H. D., Chen, S., Zhang, G., Baevova, P., Joiner, K. A. & Joiner, K. A. Four distinct pathways of

hemoglobin uptake in the malaria parasite Plasmodium falciparum. *Proc. Natl. Acad. Sci. U. S. A.* **105,** 2463–8 (2008).

192. Birnbaum, J., Flemming, S., Reichard, N., Soares, A. B., Mesén-Ramírez, P., Jonscher, E., Bergmann, B. & Spielmann, T. A genetic system to study Plasmodium falciparum protein function. *Nat. Methods* **14,** 450–456 (2017).
193. Siddiqui, G., Srivastava, A., Russell, A. S. & Creek, D. J. Multi-omics Based Identification of Specific Biochemical Changes Associated With PfKelch13-Mutant Artemisinin-Resistant Plasmodium falciparum. *J. Infect. Dis.* **215,** 1435–1444 (2017).
194. Carey, M. A., Papin, J. A. & Guler, J. L. Novel Plasmodium falciparum metabolic network reconstruction identifies shifts associated with clinical antimalarial resistance. *BMC Genomics* **18,** 543 (2017).
195. Hamilton, M. J., Lee, M. & Le Roch, K. G. The ubiquitin system: an essential component to unlocking the secrets of malaria parasite biology. *Mol. Biosyst.* **10,** 715–23 (2014).
196. Mbengue, A., Bhattacharjee, S., Pandharkar, T., Liu, H., Estiu, G., Stahelin, R. V, Rizk, S. S., Njimoh, D. L., Ryan, Y., Chotivanich, K., Nguon, C., Ghorbal, M., Lopez-Rubio, J.-J., Pfrender, M., Emrich, S., Mohandas, N., Dondorp, A. M., Wiest, O. & Haldar, K. A molecular mechanism of artemisinin resistance in Plasmodium falciparum malaria. *Nature* **520,** 683–690 (2015).
197. Tawk, L., Dubremetz, J.-F., Montcourrier, P., Chicanne, G., Merezegue, F., Richard, V., Payrastre, B., Meissner, M., Vial, H. J., Roy, C., Wengelnik, K. & Lebrun, M. Phosphatidylinositol 3-monophosphate is involved in toxoplasma apicoplast biogenesis. *PLOS Pathog.* **7,** e1001286 (2011).
198. Ebrahimzadeh, Z., Mukherjee, A. & Richard, D. A map of the subcellular distribution of phosphoinositides in the erythrocytic cycle of the malaria parasite Plasmodium falciparum. *Int. J. Parasitol.* (2017). doi:10.1016/j.ijpara.2017.08.015
199. McIntosh, M. T., Vaid, A., Hosgood, H. D., Vijay, J., Bhattacharya, A., Sahani, M. H., Baevova, P., Joiner, K. A. & Sharma, P. Traffic to the Malaria Parasite Food Vacuole. *J. Biol. Chem.* **282,** 11499–11508 (2007).
200. Bhattacharjee, S., Coppens, I., Mbengue, A., Suresh, N., Ghorbal, M., Slouka, Z., Safeukui, I., Tang, H.-Y., Speicher, D. W., Stahelin, R. V, Mohandas, N.

& Haldar, K. Remodeling of the malaria parasite and host human red cell by vesicle amplification that induces artemisinin resistance. *Blood* blood-2017-11-814665 (2018). doi:10.1182/blood-2017-11-814665

201. Boddey, J. A., O'Neill, M. T., Lopaticki, S., Carvalho, T. G., Hodder, A. N., Nebl, T., Wawra, S., van West, P., Ebrahimzadeh, Z., Richard, D., Flemming, S., Spielmann, T., Przyborski, J., Babon, J. J. & Cowman, A. F. Export of malaria proteins requires co-translational processing of the PEXEL motif independent of phosphatidylinositol-3-phosphate binding. *Nat. Commun.* **7,** 10470 (2016).
202. Zhang, M., Gallego-Delgado, J., Fernandez-Arias, C., Waters, N. C., Rodriguez, A., Tsuji, M., Wek, R. C., Nussenzweig, V. & Sullivan, W. J. Inhibiting the Plasmodium eIF2α Kinase PK4 Prevents Artemisinin-Induced Latency. *Cell Host Microbe* **22,** 766–776.e4 (2017).
203. Duvalsaint, M. & Kyle, D. E. Phytohormones, isoprenoids and role of the apicoplast in recovery from dihydroartemisinin-induced dormancy of Plasmodium falciparum. *Antimicrob. Agents Chemother.* AAC.01771-17 (2018). doi:10.1128/AAC.01771-17
204. Henriques, G., Martinelli, A., Rodrigues, L., Modrzynska, K., Fawcett, R., Houston, D. R., Borges, S. T., D'Alessandro, U., Tinto, H., Karema, C., Hunt, P. & Cravo, P. Artemisinin resistance in rodent malaria--mutation in the AP2 adaptor μ-chain suggests involvement of endocytosis and membrane protein trafficking. *Malar J* **12,** 118 (2013).
205. Henriques, G., Hallett, R. L., Beshir, K. B., Gadalla, N. B., Johnson, R. E., Burrow, R., van Schalkwyk, D. a., Sawa, P., Omar, S. a., Clark, T. G., Bousema, T. & Sutherland, C. J. Directional Selection at the pfmdr1, pfcrt, pfubp1, and pfap2mu Loci of Plasmodium falciparum in Kenyan Children Treated With ACT. *J. Infect. Dis.* **210,** 2001–2008 (2014).
206. Henriques, G., van Schalkwyk, D. A., Burrow, R., Warhurst, D. C., Thompson, E., Baker, D. A., Fidock, D. A., Hallett, R., Flueck, C. & Sutherland, C. J. The mu-subunit of Plasmodium falciparum clathrin-associated adaptor protein 2 modulates in vitro parasite response to artemisinin and quinine. *Antimicrob. Agents Chemother.* **59,** 2540–7 (2015).
207. Hunt, P., Martinelli, A., Modrzynska, K., Borges, S., Creasey, A., Rodrigues, L., Beraldi, D., Loewe, L., Fawcett, R., Kumar, S., Thomson, M., Trivedi, U.,

Otto, T. D., Pain, A., Blaxter, M. & Cravo, P. Experimental evolution, genetic analysis and genome re-sequencing reveal the mutation conferring artemisinin resistance in an isogenic lineage of malaria parasites. *BMC Genomics* **11,** 499 (2010).

208. Hunt, P., Afonso, A., Creasey, A., Culleton, R., Sidhu, A. B. S., Logan, J., Valderramos, S. G., McNae, I., Cheesman, S., Rosario, V. Do, Carter, R., Fidock, D. a. & Cravo, P. Gene encoding a deubiquitinating enzyme is mutated in artesunate- and chloroquine-resistant rodent malaria parasites. *Mol. Microbiol.* **65,** 27–40 (2007).
209. David-Bosne, S., Clausen, M. V., Poulsen, H., Møller, J. V., Nissen, P. & le Maire, M. Reappraising the effects of artemisinin on the ATPase activity of PfATP6 and SERCA1a E255L expressed in Xenopus laevis oocytes. *Nat. Struct. Mol. Biol.* **23,** 1–2 (2016).
210. Afonso, A., Hunt, P., Cheesman, S., Alves, A. C., Cunha, C. V, do V, R. & Cravo, P. Malaria parasites can develop stable resistance to artemisinin but lack mutations in candidate genes atp6 (encoding the sarcoplasmic and endoplasmic reticulum Ca2+ ATPase), tctp, mdr1, and cg10. *Antimicrob. Agents Chemother.* **50,** 480–489 (2006).
211. Ariey, F., Witkowski, B., Amaratunga, C., Beghain, J., Langlois, A.-C., Khim, N., Kim, S., Duru, V., Bouchier, C., Ma, L., Lim, P., Leang, R., Duong, S., Sreng, S., Suon, S., Chuor, C. M., Bout, D. M., Ménard, S., Rogers, W. O., *et al.* A molecular marker of artemisinin-resistant Plasmodium falciparum malaria. *Nature* **505,** 50–55 (2013).
212. Witkowski, B., Amaratunga, C., Khim, N., Sreng, S., Chim, P., Kim, S., Lim, P., Mao, S., Sopha, C., Sam, B., Anderson, J. M., Duong, S., Chuor, C. M., Taylor, W. R. J., Suon, S., Mercereau-Puijalon, O., Fairhurst, R. M. & Menard, D. Novel phenotypic assays for the detection of artemisinin-resistant Plasmodium falciparum malaria in Cambodia: In-vitro and ex-vivo drug-response studies. *Lancet Infect. Dis.* **13,** 1043–1049 (2013).
213. Yang, T., Xie, S. C., Cao, P., Giannangelo, C., McCaw, J., Creek, D. J., Charman, S. A., Klonis, N. & Tilley, L. Comparison of the Exposure Time Dependence of the Activities of Synthetic Ozonide Antimalarials and Dihydroartemisinin against K13 Wild-Type and Mutant Plasmodium falciparum Strains. *Antimicrob. Agents Chemother.* **60,** 4501–4510 (2016).

214. Alberts, B., Johnson, A., Lewis, J., Raff, M., Roberts, K. & Walter, P. *Molecular biology of the cell*. (Garland Science, 2002).
215. Kaksonen, M. & Roux, A. Mechanisms of clathrin-mediated endocytosis. *Nat. Rev. Mol. Cell Biol.* **19,** 313–326 (2018).
216. Kirchhausen, T. Adaptors for Clathrin-Mediated Traffic. *Annu. Rev. Cell Dev. Biol.* **15,** 705–732 (1999).
217. Bakar, N. A., Klonis, N., Hanssen, E., Chan, C., Tilley, L., Abu Bakar, N., Klonis, N., Hanssen, E., Chan, C. & Tilley, L. Digestive-vacuole genesis and endocytic processes in the early intraerythrocytic stages of Plasmodium falciparum. *J. Cell Sci.* **123,** 441–450 (2010).
218. Lazarus, M. D., Schneider, T. G. & Taraschi, T. F. A new model for hemoglobin ingestion and transport by the human malaria parasite Plasmodium falciparum. *J. Cell Sci.* **121,** 1937–49 (2008).
219. Smythe, W. A., Joiner, K. A. & Hoppe, H. C. Actin is required for endocytic trafficking in the malaria parasite Plasmodium falciparum. *Cell. Microbiol.* **0,** 071018055442001–??? (2007).
220. Milani, K. J., Schneider, T. G. & Taraschi, T. F. Defining the morphology and mechanism of the hemoglobin transport pathway in Plasmodium falciparum-infected erythrocytes. *Eukaryot. Cell* **14,** 415–26 (2015).
221. Rodriguez, M. H. & Jungery, M. A protein on Plasmodium falciparum-infected erythrocytes functions as a transferrin receptor. *Nature* **324,** 388–391 (1986).
222. Sanchez-Lopez, R. & Haldar, K. A transferrin-independent iron uptake activity in Plasmodium falciparum-infected and uninfected erythrocytes. *Mol. Biochem. Parasitol.* **55,** 9–20 (1992).
223. Yap, C. C. & Winckler, B. Adapting for endocytosis: roles for endocytic sorting adaptors in directing neural development. *Front. Cell. Neurosci.* **9,** 119 (2015).
224. Park, S. Y. & Guo, X. Adaptor protein complexes and intracellular transport. *Biosci. Rep.* **34,** (2014).
225. Hirst, J., Irving, C. & Borner, G. H. H. Adaptor Protein Complexes AP-4 and AP-5: New Players in Endosomal Trafficking and Progressive Spastic Paraplegia. *Traffic* **14,** 153–164 (2013).
226. Hirst, J., D. Barlow, L., Francisco, G. C., Sahlender, D. A., Seaman, M. N. J.,

Dacks, J. B. & Robinson, M. S. The Fifth Adaptor Protein Complex. *PLoS Biol.* **9,** e1001170 (2011).

227. Collins, B. M., McCoy, A. J., Kent, H. M., Evans, P. R. & Owen, D. J. Molecular architecture and functional model of the endocytic AP2 complex. *Cell* **109,** 523–35 (2002).

228. Brodsky, F. M., Chen, C.-Y., Knuehl, C., Towler, M. C. & Wakeham, D. E. Biological Basket Weaving: Formation and Function of Clathrin-Coated Vesicles. *GSR Annu. Rev. Cell Dev. Biol* **15305,** 517–68 (2001).

229. Howles, S., Nesbit, M. A., Hannan, F., Rogers, A., Piret, S., Rust, N. & Thakker, R. Adaptor protein-2 sigma subunit mutations causing familial hypocalciuric hypercalcaemia type 3 exert dominant-negative effects. *Endocr. Abstr.* (2014). doi:10.1530/endoabs.34.OC4.1

230. Tarpey, P. S., Stevens, C., Teague, J., Edkins, S., O'Meara, S., Avis, T., Barthorpe, S., Buck, G., Butler, A., Cole, J., Dicks, E., Gray, K., Halliday, K., Harrison, R., Hills, K., Hinton, J., Jones, D., Menzies, A., Mironenko, T., *et al.* Mutations in the gene encoding the Sigma 2 subunit of the adaptor protein 1 complex, AP1S2, cause X-linked mental retardation. *Am. J. Hum. Genet.* **79,** 1119–24 (2006).

231. Popova, N. V, Deyev, I. E. & Petrenko, A. G. Clathrin-mediated endocytosis and adaptor proteins. *Acta Naturae* **5,** 62–73 (2013).

232. Jackson, L. P., Kelly, B. T., McCoy, A. J., Gaffry, T., James, L. C., Collins, B. M., Höning, S., Evans, P. R. & Owen, D. J. A large-scale conformational change couples membrane recruitment to cargo binding in the AP2 clathrin adaptor complex. *Cell* **141,** 1220–9 (2010).

233. Robinson, M. S. Adaptable adaptors for coated vesicles. *Trends Cell Biol.* **14,** 167–174 (2004).

234. Venugopal, K., Werkmeister, E., Barois, N., Saliou, J.-M., Poncet, A., Huot, L., Sindikubwabo, F., Hakimi, M. A., Langsley, G., Lafont, F. & Marion, S. Dual role of the Toxoplasma gondii clathrin adaptor AP1 in the sorting of rhoptry and microneme proteins and in parasite division. *PLOS Pathog.* **13,** e1006331 (2017).

235. Kaderi Kibria, K. M., Rawat, K., Klinger, C. M., Datta, G., Panchal, M., Singh, S., Iyer, G. R., Kaur, I., Sharma, V., Dacks, J. B., Mohmmed, A. & Malhotra, P. A role for adaptor protein complex 1 in protein targeting to

rhoptry organelles in Plasmodium falciparum. *Biochim. Biophys. Acta - Mol. Cell Res.* **1853,** 699–710 (2015).

236. Thomas Sosa, R., Weber, M. M., Wen, Y. & O'Halloran, T. J. A Single β Adaptin Contributes to AP1 and AP2 Complexes and Clathrin Function in Dictyostelium. *Traffic* **13,** 305–316 (2012).
237. Pickart, C. M. Mechanisms Underlying ubiquitination. *Annu. Rev. Biochem.* **70,** 503–33 (2001).
238. Miranda, M. & Sorkin, A. Regulation of receptors and transporters by ubiquitination: new insights into surprisingly similar mechanisms. *Mol. Interv.* **7,** 157–167 (2007).
239. Peng, J., Schwartz, D., Elias, J. E., Thoreen, C. C., Cheng, D., Marsischky, G., Roelofs, J., Finley, D. & Gygi, S. P. A proteomics approach to understanding protein ubiquitination. *Nat. Biotechnol.* **21,** 921–926 (2003).
240. Komander, D. The emerging complexity of protein ubiquitination. *Biochem. Soc. Trans.* **37,** 937–953 (2009).
241. Nagy, V. & Dikic, I. Ubiquitin ligase complexes: From substrate selectivity to conjugational specificity. *Biol. Chem.* **391,** 163–169 (2010).
242. Ponts, N., Saraf, A., Chung, D.-W. D., Harris, A., Prudhomme, J., Washburn, M. P., Florens, L. & Le Roch, K. G. Unraveling the Ubiquitome of the Human Malaria Parasite. *J. Biol. Chem.* **286,** 40320–40330 (2011).
243. Park, D. J., Lukens, A. K., Neafsey, D. E., Schaffner, S. F., Chang, H.-H., Valim, C., Ribacke, U., Tyne, D. Van, Galinsky, K., Galligan, M., Becker, J. S., Ndiaye, D., Mboup, S., Wiegand, R. C., Hartl, D. L., Sabeti, P. C., Wirth, D. F. & Volkman, S. K. Sequence-based association and selection scans identify drug resistance loci in the Plasmodium falciparum malaria parasite. *Proc. Natl. Acad. Sci.* **109,** 13052–13057 (2012).
244. Gendrot, M., Fall, B., Madamet, M., Fall, M., Wade, K. A., Amalvict, R., Nakoulima, A., Benoit, N., Diawara, S., Diémé, Y., Diatta, B., Wade, B. & Pradines, B. Absence of Association between Polymorphisms in the RING E3 Ubiquitin Protein Ligase Gene and Ex Vivo Susceptibility to Conventional Antimalarial Drugs in Plasmodium falciparum Isolates from Dakar, Senegal. *Antimicrob. Agents Chemother.* **60,** 5010–3 (2016).
245. Wilkinson, K. D. Ubiquitination and deubiquitination: Targeting of proteins for degradation by the proteasome. *Semin. Cell Dev. Biol.* **11,** 141–148

(2000).

246. Wei, R., Liu, X., Yu, W., Yang, T., Cai, W., Liu, J., Huang, X., Xu, G., Zhao, S., Yang, J. & Liu, S. Deubiquitinases in cancer. *Oncotarget* **6,** 12872–89 (2015).

247. Hussain, S., Zhang, Y. & Galardy, P. DUBs and cancer: The role of deubiquitinating enzymes as oncogenes, non-oncogenes and tumor suppressors. *Cell Cycle* **8,** 1688–1697 (2009).

248. Deu, E. Proteases as antimalarial targets: strategies for genetic, chemical, and therapeutic validation. *FEBS J.* **284,** 2604–2628 (2017).

249. Artavanis-Tsakonas, K., Misaghi, S., Comeaux, C. A., Catic, A., Spooner, E., Duraisingh, M. T. & Ploegh, H. L. Identification by functional proteomics of a deubiquitinating/deNeddylating enzyme in Plasmodium falciparum. *Mol. Microbiol.* **61,** 1187–95 (2006).

250. Artavanis-Tsakonas, K., Weihofen, W. A., Antos, J. M., Coleman, B. I., Comeaux, C. A., Duraisingh, M. T., Gaudet, R. & Ploegh, H. L. Characterization and structural studies of the Plasmodium falciparum ubiquitin and Nedd8 hydrolase UCHL3. *J. Biol. Chem.* **285,** 6857–66 (2010).

251. Borrmann, S., Straimer, J., Mwai, L., Abdi, A., Rippert, A., Okombo, J., Muriithi, S., Sasi, P., Kortok, M. M., Lowe, B., Campino, S., Assefa, S., Auburn, S., Manske, M., Maslen, G., Peshu, N., Kwiatkowski, D. P., Marsh, K., Nzila, A., *et al.* Genome-wide screen identifies new candidate genes associated with artemisinin susceptibility in Plasmodium falciparum in Kenya. *Sci. Rep.* **3,** 3318 (2013).

252. Winzeler, E. a & Manary, M. J. Drug resistance genomics of the antimalarial drug artemisinin. *Genome Biol.* **15,** 544 (2014).

253. Modrzynska, K. K., Creasey, A., Loewe, L., Cezard, T., Trindade Borges, S., Martinelli, A., Rodrigues, L., Cravo, P., Blaxter, M., Carter, R., Hunt, P., Modrzynska, K. K., Creasey, A., Loewe, L., Cezard, T., Borges, S. T., Martinelli, A., Rodrigues, L., Cravo, P., *et al.* Quantitative genome re-sequencing defines multiple mutations conferring chloroquine resistance in rodent malaria. *BMC Genomics* **13,** 106 (2012).

254. Chung, D.-W. D., Ponts, N., Prudhomme, J., Rodrigues, E. M. & Le Roch, K. G. Characterization of the ubiquitylating components of the human malaria parasite's protein degradation pathway. *PLoS One* **7,** e43477 (2012).

255. Tonkin, C. J., Kalanon, M. & McFadden, G. I. Protein Targeting to the Malaria Parasite Plastid. *Traffic* **0,** 071115150434001–??? (2007).

256. Fellows, J. D., Cipriano, M. J., Agrawal, S. & Striepen, B. A Plastid Protein That Evolved from Ubiquitin and Is Required for Apicoplast Protein Import in Toxoplasma gondii. *MBio* **8,** e00950-17 (2017).

257. Spork, S., Hiss, J. A., Mandel, K., Sommer, M., Kooij, T. W. A., Chu, T., Schneider, G., Maier, U. G. & Przyborski, J. M. An unusual ERAD-like complex is targeted to the apicoplast of Plasmodium falciparum. *Eukaryot. Cell* **8,** 1134–45 (2009).

258. Baum, J., Papenfuss, A. T., Mair, G. R., Janse, C. J., Vlachou, D., Waters, A. P., Cowman, A. F., Crabb, B. S. & de Koning-Ward, T. F. Molecular genetics and comparative genomics reveal RNAi is not functional in malaria parasites. *Nucleic Acids Res.* **37,** 3788–3798 (2009).

259. Kolev, N. G., Tschudi, C. & Ullu, E. RNA interference in protozoan parasites: achievements and challenges. *Eukaryot. Cell* **10,** 1156–63 (2011).

260. Nkrumah, L. J., Muhle, R. A., Moura, P. A., Ghosh, P., Hatfull, G. F., Jacobs, W. R. & Fidock, D. A. Efficient site-specific integration in Plasmodium falciparum chromosomes mediated by mycobacteriophage Bxb1 integrase. *Nat. Methods* **3,** 615–621 (2006).

261. Adjalley, S. H., Lee, M. C. S. & Fidock, D. A. A Method for Rapid Genetic Integration into Plasmodium falciparum Utilizing Mycobacteriophage Bxb1 Integrase. in *Methods in molecular biology (Clifton, N.J.)* **634,** 87–100 (2010).

262. Straimer, J., Gnadig, N. F., Witkowski, B., Amaratunga, C., Duru, V., Ramadani, a. P., Dacheux, M., Khim, N., Zhang, L., Lam, S., Gregory, P. D., Urnov, F. D., Mercereau-Puijalon, O., Benoit-Vical, F., Fairhurst, R. M., Menard, D. & Fidock, D. a. K13-propeller mutations confer artemisinin resistance in Plasmodium falciparum clinical isolates. *Science (80-. ).* **347,** 428–431 (2014).

263. Ghorbal, M., Gorman, M., Macpherson, C. R., Martins, R. M., Scherf, A. & Lopez-Rubio, J.-J. Genome editing in the human malaria parasite Plasmodium falciparum using the CRISPR-Cas9 system. *Nat. Biotechnol.* **32,** 819–821 (2014).

264. Wagner, J. C., Platt, R. J., Goldfless, S. J., Zhang, F. & Niles, J. C. Efficient CRISPR-Cas9–mediated genome editing in Plasmodium falciparum. *Nat.*

*Methods* **11,** 915–8 (2014).

265. Ratner, H. K., Sampson, T. R. & Weiss, D. S. Overview of CRISPR–Cas9 Biology. *Cold Spring Harb. Protoc.* **2016,** pdb.top088849 (2016).
266. Jones, M. L., Das, S., Belda, H., Collins, C. R., Blackman, M. J. & Treeck, M. A versatile strategy for rapid conditional genome engineering using loxP sites in a small synthetic intron in Plasmodium falciparum. *Sci. Rep.* **6,** 21800 (2016).
267. Doench, J. G., Hartenian, E., Graham, D. B., Tothova, Z., Hegde, M., Smith, I., Sullender, M., Ebert, B. L., Xavier, R. J. & Root, D. E. Rational design of highly active sgRNAs for CRISPR-Cas9–mediated gene inactivation. *Nat. Biotechnol.* **32,** 1262–1267 (2014).
268. Zetsche, B., Gootenberg, J. S., Abudayyeh, O. O., Slaymaker, I. M., Makarova, K. S., Essletzbichler, P., Volz, S. E., Joung, J., Van Der Oost, J., Regev, A., Koonin, E. V. & Zhang, F. Cpf1 Is a Single RNA-Guided Endonuclease of a Class 2 CRISPR-Cas System. *Cell* **163,** 759–771 (2015).
269. Moll, K., Kaneko, A., Scherf, A. & Wahlgren, M. *Methods in Malaria Research*. (EVIMalaR, 2013).
270. Zhang, Z., Chung, T. D. Y. & Oldenburg, K. R. A Simple Statistical Parameter for Use in Evaluation and Validation of High Throughput Screening Assay. *J. Biomol. Screen.* **4,** 67–73 (1999).
271. Saul, A. & Battistutta, D. Codon usage in Plasmodium falciparum. *Mol. Biochem. Parasitol.* **27,** 35–42 (1988).
272. Taylor, H. M., McRobert, L., Grainger, M., Sicard, A., Dluzewski, A. R., Hopp, C. S., Holder, A. A. & Baker, D. A. The malaria parasite cyclic GMP-dependent protein kinase plays a central role in blood-stage schizogony. *Eukaryot. Cell* **9,** 37–45 (2010).
273. Zhang, M., Wang, C., Otto, T. D., Oberstaller, J., Liao, X., Adapa, S. R., Udenze, K., Bronner, I. F., Casandra, D., Mayho, M., Brown, J., Li, S., Swanson, J., Rayner, J. C., Jiang, R. H. Y. & Adams, J. H. Uncovering the essential genes of the human malaria parasite Plasmodium falciparum by saturation mutagenesis. *Science* **360,** eaap7847 (2018).
274. Winkler, W. C., Nahvi, A., Roth, A., Collins, J. A. & Breaker, R. R. Control of gene expression by a natural metabolite-responsive ribozyme. *Nature* **428,** 281–286 (2004).

275. Prommana, P., Uthaipibull, C., Wongsombat, C., Kamchonwongpaisan, S., Yuthavong, Y., Knuepfer, E., Holder, A. A., Shaw, P. J., Technologies, E., Bissati, K. El, Zufferey, R., Witola, W., Carter, N., Ullman, B., Combe, A., Giovannini, D., Carvalho, T., Spath, S., Boisson, B., *et al.* Inducible Knockdown of Plasmodium Gene Expression Using the glmS Ribozyme. *PLoS One* **8,** e73783 (2013).
276. Huh, W.-K., Falvo, J. V., Gerke, L. C., Carroll, A. S., Howson, R. W., Weissman, J. S. & O'Shea, E. K. Global analysis of protein localization in budding yeast. *Nature* **425,** 686–691 (2003).
277. Martzoukou, O., Amillis, S., Zervakou, A., Christoforidis, S. & Diallinas, G. The AP-2 complex has a specialized clathrin-independent role in apical endocytosis and polar growth in fungi. *Elife* **6,** (2017).
278. Nesterov, A., Carter, R. E., Sorkina, T., Gill, G. N. & Sorkin, A. Inhibition of the receptor-binding function of clathrin adaptor protein AP-2 by dominant-negative mutant mu2 subunit and its effects on endocytosis. *EMBO J.* **18,** 2489–99 (1999).
279. Traub, L. M. Sorting it out: AP-2 and alternate clathrin adaptors in endocytic cargo selection. *J. Cell Biol.* **163,** 203–8 (2003).
280. Neveu, G., Barouch-Bentov, R., Ziv-Av, A., Gerber, D., Jacob, Y. & Einav, S. Identification and targeting of an interaction between a tyrosine motif within hepatitis C virus core protein and AP2M1 essential for viral assembly. *PLoS Pathog.* **8,** e1002845 (2012).
281. Tian, Y., Chang, J. C., Fan, E. Y., Flajolet, M. & Greengard, P. Adaptor complex AP2/PICALM, through interaction with LC3, targets Alzheimer's APP-CTF for terminal degradation via autophagy. doi:10.1073/pnas.1315110110
282. Avinoam, O., Schorb, M., Beese, C. J., Briggs, J. A. G. & Kaksonen, M. Endocytic sites mature by continuous bending and remodeling of the clathrin coat. *Science* **348,** 1369–72 (2015).
283. Hutagalung, A. H. & Novick, P. J. Role of Rab GTPases in membrane traffic and cell physiology. *Physiol. Rev.* **91,** 119–49 (2011).
284. Rached, F. Ben, Ndjembo-Ezougou, C., Chandran, S., Talabani, H., Yera, H., Dandavate, V., Bourdoncle, P., Meissner, M., Tatu, U. & Langsley, G. Construction of a Plasmodium falciparum Rab-interactome identifies CK1

and PKA as Rab-effector kinases in malaria parasites. *Biol. Cell* **104,** 34–47 (2012).

285. Woodman, P. G. Biogenesis of the sorting endosome: the role of Rab5. *Traffic* **1,** 695–701 (2000).
286. Ebine, K., Hirai, M., Sakaguchi, M., Yahata, K., Kaneko, O. & Saito-Nakano, Y. Plasmodium Rab5b is secreted to the cytoplasmic face of the tubovesicular network in infected red blood cells together with N-acylated adenylate kinase 2. *Malar. J.* **15,** 323 (2016).
287. Ezougou, C. N., Ben-Rached, F., Moss, D. K., Lin, J., Black, S., Knuepfer, E., Green, J. L., Khan, S. M., Mukhopadhyay, A., Janse, C. J., Coppens, I., Yera, H., Holder, A. A. & Langsley, G. Plasmodium falciparum Rab5B is an N-terminally myristoylated Rab GTPase that is targeted to the parasite's plasma and food vacuole membranes. *PLoS One* **9,** e87695 (2014).
288. Krai, P., Dalal, S. & Klemba, M. Evidence for a Golgi-to-Endosome Protein Sorting Pathway in Plasmodium falciparum. *PLoS One* **9,** e89771 (2014).
289. Agop-Nersesian, C., Naissant, B., Ben Rached, F., Rauch, M., Kretzschmar, A., Thiberge, S., Menard, R., Ferguson, D. J. P., Meissner, M. & Langsley, G. Rab11A-Controlled Assembly of the Inner Membrane Complex Is Required for Completion of Apicomplexan Cytokinesis. *PLoS Pathog.* **5,** e1000270 (2009).
290. Kononenko, N. L., Claßen, G. A., Kuijpers, M., Puchkov, D., Maritzen, T., Tempes, A., Malik, A. R., Skalecka, A., Bera, S., Jaworski, J. & Haucke, V. Retrograde transport of TrkB-containing autophagosomes via the adaptor AP-2 mediates neuronal complexity and prevents neurodegeneration. *Nat. Commun.* **8,** 14819 (2017).
291. Pisciotta, J. M., Coppens, I., Tripathi, A. K., Scholl, P. F., Shuman, J., Bajad, S., Shulaev, V., Sullivan, D. J. & Jr. The role of neutral lipid nanospheres in Plasmodium falciparum haem crystallization. *Biochem. J.* **402,** 197–204 (2007).
292. Jackson, K. E., Klonis, N., Ferguson, D. J. P., Adisa, A., Dogovski, C. & Tilley, L. Food vacuole-associated lipid bodies and heterogeneous lipid environments in the malaria parasite, Plasmodium falciparum. *Mol. Microbiol.* **54,** 109–122 (2004).
293. Peyroche, A., Antonny, B., Robineau, S., Acker, J., Cherfils, J. & Jackson, C.

L. Brefeldin A Acts to Stabilize an Abortive ARF–GDP–Sec7 Domain Protein Complex: Involvement of Specific Residues of the Sec7 Domain. *Mol. Cell* **3,** 275–285 (1999).

294. Nebenführ, A., Gallagher, L. A., Dunahay, T. G., Frohlick, J. A., Mazurkiewicz, A. M., Meehl, J. B., Staehelin, L. A., Lerouge, P., Faye, L. & Hawes, C. Stop-and-Go Movements of Plant Golgi Stacks Are Mediated by the Acto-Myosin System. *Plant Physiol.* **121,** 1127–1141 (1999).
295. Martínez-Mená Rguez, J. A., Geuze, H. J., Slot, J. W. & Klumperman, J. Vesicular Tubular Clusters between the ER and Golgi Mediate Concentration of Soluble Secretory Proteins by Exclusion from COPI-Coated Vesicles. *Cell* **98,** 81–90 (1999).
296. Kyung, J. W., Cho, I. H., Lee, S., Song, W. K., Ryan, T. A., Hoppa, M. B. & Kim, S. H. Adaptor Protein 2 (AP-2) complex is essential for functional axogenesis in hippocampal neurons. *Sci. Rep.* **7,** 41620 (2017).
297. Mitsunari, T., Nakatsu, F., Shioda, N., Love, P. E., Grinberg, A., Bonifacino, J. S. & Ohno, H. Clathrin Adaptor AP-2 Is Essential for Early Embryonal Development. *Mol. Cell. Biol.* **25,** 9318–9323 (2005).
298. Collins, C. R., Das, S., Wong, E. H., Andenmatten, N., Stallmach, R., Hackett, F., Herman, J.-P., Müller, S., Meissner, M. & Blackman, M. J. Robust inducible Cre recombinase activity in the human malaria parasite *Plasmodium falciparum* enables efficient gene deletion within a single asexual erythrocytic growth cycle. *Mol. Microbiol.* **88,** 687–701 (2013).
299. Knuepfer, E., Napiorkowska, M., van Ooij, C. & Holder, A. A. Generating conditional gene knockouts in Plasmodium – a toolkit to produce stable DiCre recombinase-expressing parasite lines using CRISPR/Cas9. *Sci. Rep.* **7,** 3881 (2017).
300. Andenmatten, N., Egarter, S., Jackson, A. J., Jullien, N., Herman, J.-P. & Meissner, M. Conditional genome engineering in Toxoplasma gondii uncovers alternative invasion mechanisms. *Nat. Methods* **10,** 125–127 (2013).
301. Jullien, N., Sampieri, F., Enjalbert, A. & Herman, J.-P. Regulation of Cre recombinase by ligand-induced complementation of inactive fragments. *Nucleic Acids Res.* **31,** e131 (2003).
302. Zhang, X., Tolzmann, C. A., Melcher, M., Haas, B. J., Gardner, M. J., Smith, J. D. & Feagin, J. E. Branch point identification and sequence requirements

for intron splicing in Plasmodium falciparum. *Eukaryot. Cell* **10,** 1422–8 (2011).

303. Ridzuan, M. A. M., Moon, R. W., Knuepfer, E., Black, S., Holder, A. A. & Green, J. L. Subcellular Location, Phosphorylation and Assembly into the Motor Complex of GAP45 during Plasmodium falciparum Schizont Development. *PLoS One* **7,** e33845 (2012).
304. Kiontke, S., Langemeyer, L., Kuhlee, A., Schuback, S., Raunser, S., Ungermann, C. & Kümmel, D. Architecture and mechanism of the late endosomal Rab7-like Ypt7 guanine nucleotide exchange factor complex Mon1–Ccz1. *Nat. Commun.* **8,** 14034 (2017).
305. Randazzo, P. A. & Hirsch, D. S. Arf GAPs: multifunctional proteins that regulate membrane traffic and actin remodelling. *Cell. Signal.* **16,** 401–13 (2004).
306. Agop-Nersesian, C., Egarter, S., Langsley, G., Foth, B. J., Ferguson, D. J. P. & Meissner, M. Biogenesis of the inner membrane complex is dependent on vesicular transport by the alveolate specific GTPase Rab11B. *PLoS Pathog.* **6,** e1001029 (2010).
307. Cerqueira, G. C., Cheeseman, I. H., Schaffner, S. F., Nair, S., McDew-White, M., Phyo, A. P., Ashley, E. A., Melnikov, A., Rogov, P., Birren, B. W., Nosten, F., Anderson, T. J. C. & Neafsey, D. E. Longitudinal genomic surveillance of Plasmodium falciparum malaria parasites reveals complex genomic architecture of emerging artemisinin resistance. *Genome Biol.* **18,** 78 (2017).
308. Lian, Y.-F., Yuan, J., Cui, Q., Feng, Q.-S., Xu, M., Bei, J.-X., Zeng, Y.-X. & Feng, L. Upregulation of KLHDC4 Predicts a Poor Prognosis in Human Nasopharyngeal Carcinoma. *PLoS One* **11,** e0152820 (2016).
309. Moon, R. W., Hall, J., Rangkuti, F., Ho, Y. S., Almond, N., Mitchell, G. H., Pain, A., Holder, A. A. & Blackman, M. J. Adaptation of the genetically tractable malaria pathogen Plasmodium knowlesi to continuous culture in human erythrocytes. *Proc. Natl. Acad. Sci. U. S. A.* **110,** 531–6 (2013).
310. Pain, A., Böhme, U., Berry, A. E., Mungall, K., Finn, R. D., Jackson, A. P., Mourier, T., Mistry, J., Pasini, E. M., Aslett, M. A., Balasubrammaniam, S., Borgwardt, K., Brooks, K., Carret, C., Carver, T. J., Cherevach, I., Chillingworth, T., Clark, T. G., Galinski, M. R., *et al.* The genome of the

simian and human malaria parasite Plasmodium knowlesi. *Nature* **455,** 799–803 (2008).

311. Li, J., Ni, M., Lee, B., Barron, E., Hinton, D. R. & Lee, A. S. The unfolded protein response regulator GRP78/BiP is required for endoplasmic reticulum integrity and stress-induced autophagy in mammalian cells. *Cell Death Differ.* **15,** 1460–1471 (2008).
312. Liu, Y., Lok, C.-N., Ko, B. C.-B., Shum, T. Y.-T., Wong, M.-K. & Che, C.-M. Subcellular Localization of a Fluorescent Artemisinin Derivative to Endoplasmic Reticulum. *Org. Lett.* **12,** 1420–1423 (2010).
313. Jensen, A. N., Chindaudomsate, W., Thitiananpakorn, K., Mongkolsuk, S. & Jensen, L. T. Improper protein trafficking contributes to artemisinin sensitivity in cells lacking the KDAC Rpd3p. *FEBS Lett.* **588,** 4018–4025 (2014).
314. Rao, R. V, Hermel, E., Castro-Obregon, S., del Rio, G., Ellerby, L. M., Ellerby, H. M. & Bredesen, D. E. Coupling endoplasmic reticulum stress to the cell death program. Mechanism of caspase activation. *J. Biol. Chem.* **276,** 33869–74 (2001).
315. Teske, B. F., Wek, S. A., Bunpo, P., Cundiff, J. K., McClintick, J. N., Anthony, T. G. & Wek, R. C. The eIF2 kinase PERK and the integrated stress response facilitate activation of ATF6 during endoplasmic reticulum stress. *Mol. Biol. Cell* **22,** 4390–405 (2011).
316. Pandey, K., Ferreira, P. E., Ishikawa, T., Nagai, T., Kaneko, O. & Yahata, K. Ca2+ monitoring in Plasmodium falciparum using the yellow cameleon-Nano biosensor. *Sci. Rep.* **6,** 23454 (2016).
317. Rzechorzek, N. M., Connick, P., Patani, R., Selvaraj, B. T. & Chandran, S. Hypothermic Preconditioning of Human Cortical Neurons Requires Proteostatic Priming. *EBioMedicine* **2,** 528–535 (2015).
318. Morimoto, N., Oida, Y., Shimazawa, M., Miura, M., Kudo, T., Imaizumi, K. & Hara, H. Involvement of endoplasmic reticulum stress after middle cerebral artery occlusion in mice. *Neuroscience* **147,** 957–967 (2007).
319. Liu, X., Wang, M., Chen, H., Guo, Y., Ma, F., Shi, F., Bi, Y. & Li, Y. Hypothermia protects the brain from transient global ischemia/reperfusion by attenuating endoplasmic reticulum response-induced apoptosis through CHOP. *PLoS One* **8,** e53431 (2013).

320. Lee, J. K., Wang, B., Reyes, M., Armstrong, J. S., Kulikowicz, E., Santos, P. T., Lee, J.-H., Koehler, R. C. & Martin, L. J. Hypothermia and Rewarming Activate a Macroglial Unfolded Protein Response Independent of Hypoxic-Ischemic Brain Injury in Neonatal Piglets. *Dev. Neurosci.* **38,** 277–294 (2016).
321. George, P. M. & Steinberg, G. K. Novel Stroke Therapeutics: Unraveling Stroke Pathophysiology and Its Impact on Clinical Treatments. *Neuron* **87,** 297–309 (2015).
322. Saraste, J., Palade, G. E. & Farquhar, M. G. Temperature-sensitive steps in the transport of secretory proteins through the Golgi complex in exocrine pancreatic cells. *Proc. Natl. Acad. Sci. U. S. A.* **83,** 6425–9 (1986).
323. Parapini, S., Olliaro, P., Navaratnam, V., Taramelli, D. & Basilico, N. Stability of the antimalarial drug dihydroartemisinin under physiologically relevant conditions: implications for clinical treatment and pharmacokinetic and in vitro assays. *Antimicrob. Agents Chemother.* **59,** 4046–52 (2015).
324. Muralidharan, V. & Goldberg, D. E. Asparagine repeats in Plasmodium falciparum proteins: good for nothing? *PLoS Pathog.* **9,** e1003488 (2013).
325. Reverdy, C., Conrath, S., Lopez, R., Planquette, C., Atmanene, C., Collura, V., Harpon, J., Battaglia, V., Vivat, V., Sippl, W. & Colland, F. Discovery of Specific Inhibitors of Human USP7/HAUSP Deubiquitinating Enzyme. *Chem. Biol.* **19,** 467–477 (2012).
326. Turnbull, A. P., Ioannidis, S., Krajewski, W. W., Pinto-Fernandez, A., Heride, C., Martin, A. C. L., Tonkin, L. M., Townsend, E. C., Buker, S. M., Lancia, D. R., Caravella, J. A., Toms, A. V., Charlton, T. M., Lahdenranta, J., Wilker, E., Follows, B. C., Evans, N. J., Stead, L., Alli, C., *et al.* Molecular basis of USP7 inhibition by selective small-molecule inhibitors. *Nature* **550,** 481–486 (2017).
327. Li, M., Chen, D., Shiloh, A., Luo, J., Nikolaev, A. Y., Qin, J. & Gu, W. Deubiquitination of p53 by HAUSP is an important pathway for p53 stabilization. *Nature* **416,** 648–653 (2002).
328. Talman, A. M., Blagborough, A. M. & Sinden, R. E. A Plasmodium falciparum Strain Expressing GFP throughout the Parasite's Life-Cycle. *PLoS One* **5,** e9156 (2010).
329. Royle, S. J. The cellular functions of clathrin. *Cell. Mol. Life Sci.* **63,** 1823–32

(2006).

# Appendix I: Molecular modelling of PfAP2µ and PfUbp1

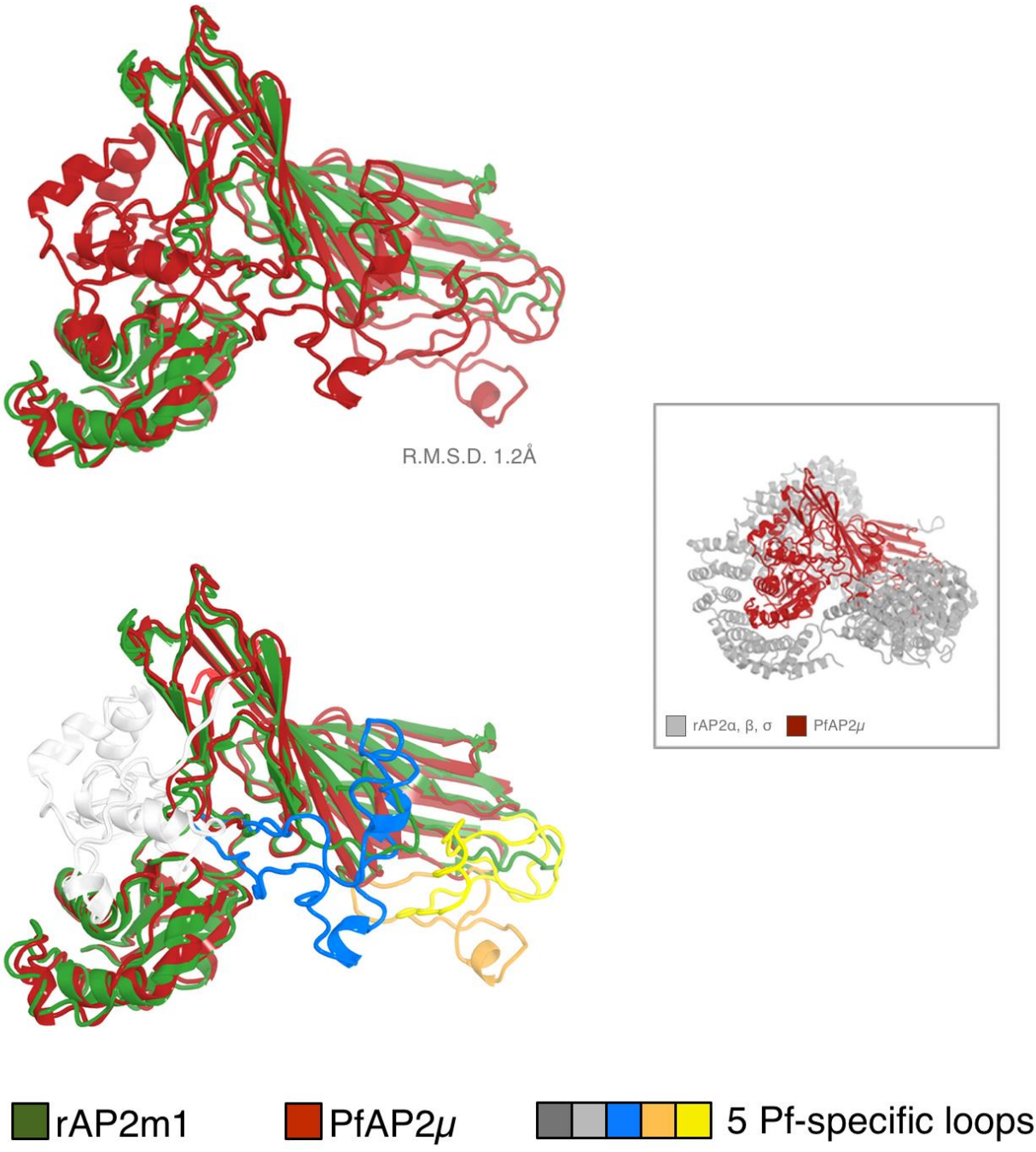


Molecular model of the *Plasmodium falciparum* µ2 subunit (red) generated using molecular threading (I-TASSER) through the *Rattus norvegicus* AP2m1 subunit (green) co-crystallised as the heterotetrameric AP-2 complex (RCSB: 2VGL). Five non-homologous *Plasmodium*-specific loops project out of the core *Plasmodium falciparum* µ2 fold, which aligns well with the mammalian homologue (RMSD = 1.2A over backbone atoms).

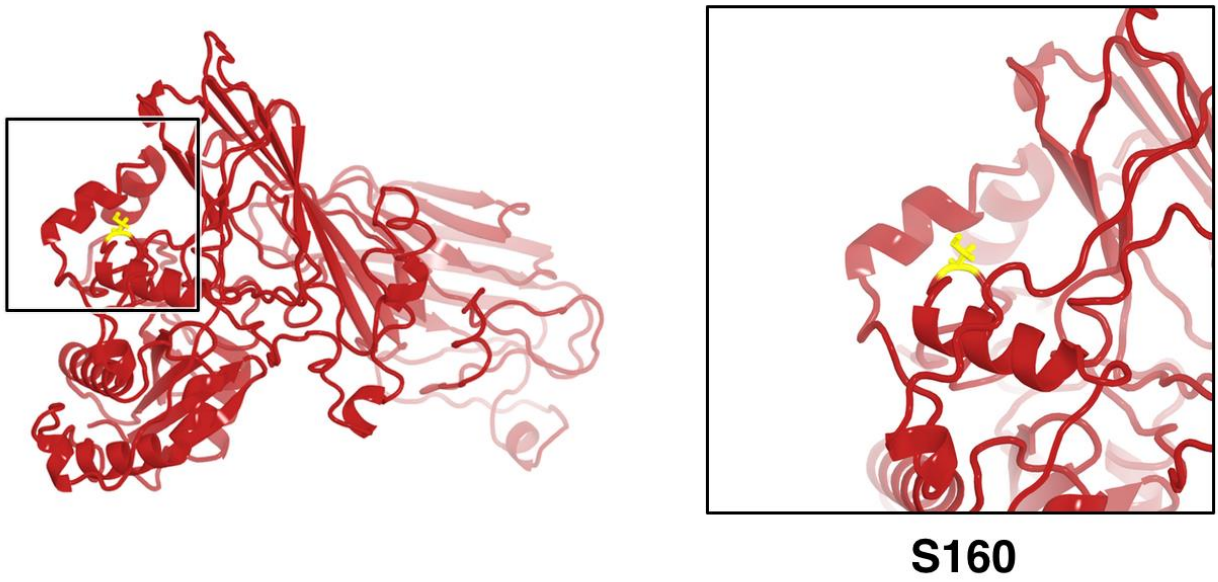


Spatial examination of the two *pfap2mu* mutations discussed in this thesis. S160 is located on the first loop connecting the core beta-sheet and sigma-homology domain, projecting into solvent-exposed space and is not spatially nearby the other complex subunits (top). I592 is a semi-conserved buried residue between the layered beta-sheets of the core µ2 fold (bottom). I592 is not solvent-exposed and instead resides within a hydrophobic pocket where it is predicted to mediate major van der Waals contacts holding the layers together.

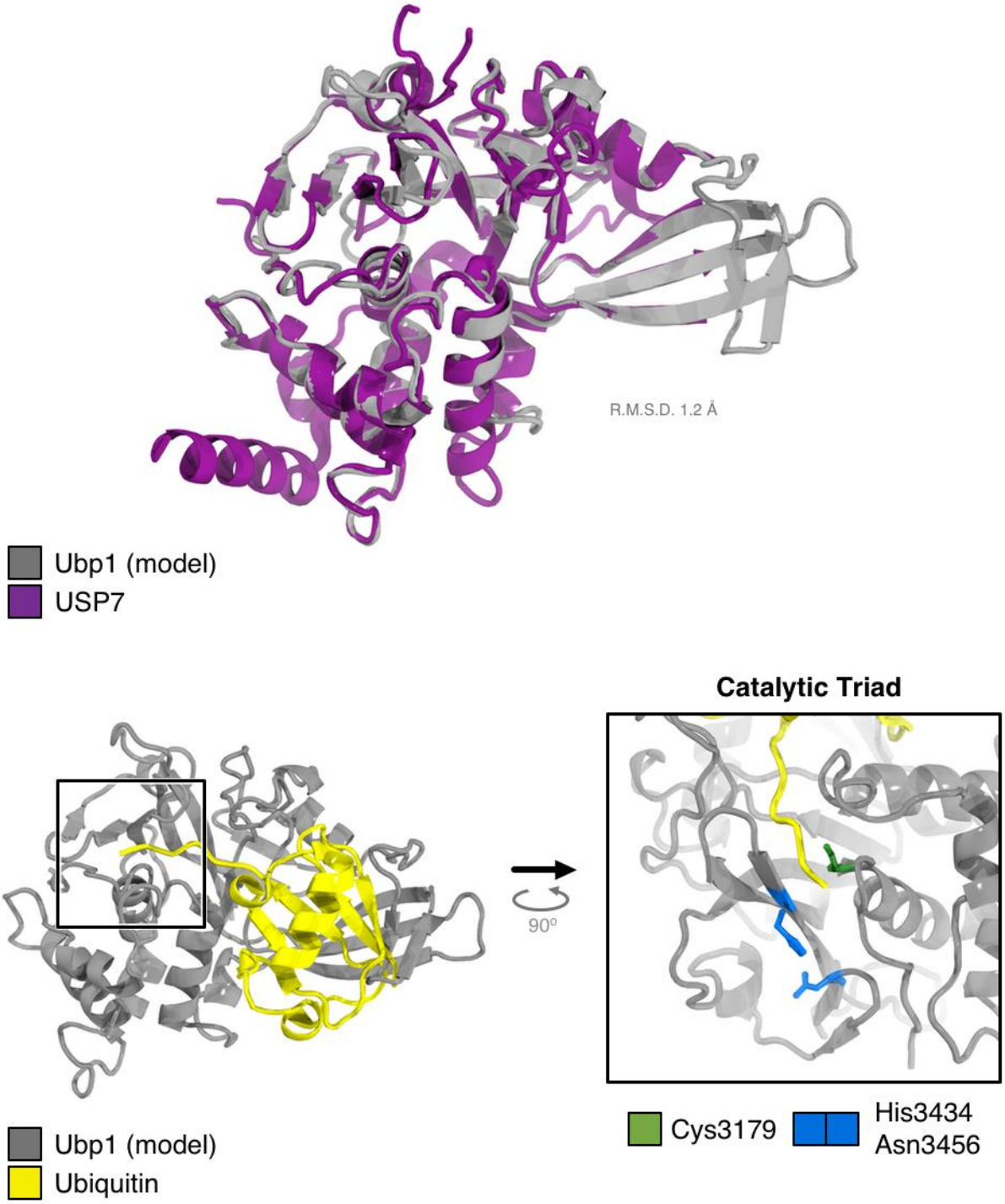


Molecular model of the *Plasmodium falciparum* Ubp1 putative catalytic domain (grey) generated using molecular threading (I-TASSER) through the human USP7 catalytic domain (purple) co-crystallised with ubiquitin (yellow, RCSB: 1NBF). Three conserved residues that constitute a catalytic triad are positioned as expected in the modelled structure with respect to the C-terminal tail of ubiquitin (catalytic Cys, green; supporting residues, blue).

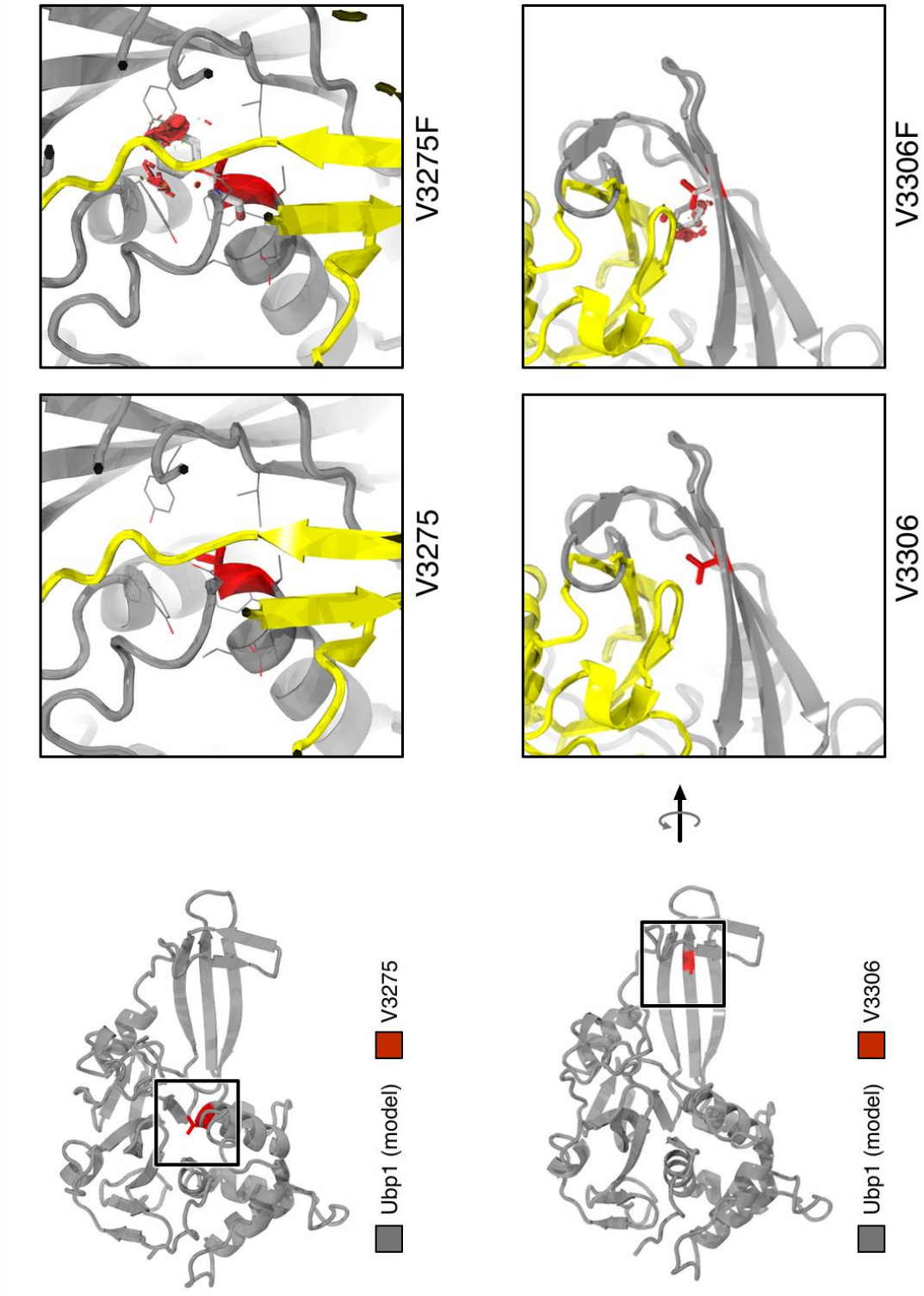


Spatial examination of the two *pfubp1* mutations identified from the *P. chabaudi* study[208]. V3275 is located in a hydrophobic pocket which positions the C-terminal tail of ubiquitin for hydrolysis. V3306 resides in the ubiquitin-binding "hand"- like domain. V3306 is predicted to make contacts with ubiquitin. Mutation of both residues is expected to cause steric clash with neighbouring residues and disrupt catalytic activity (red bubbles, right inset boxes).

# Appendix II: Transfection of recently culture-adapted clinical isolates

A secondary goal of this thesis is to evaluate the impacts of the mutations characterised above in recently culture-adapted clinical isolates. Examining the phenotypes of mutations in robust laboratory strains like 3D7 is technically established. Transfection protocols are well described in the literature. However, these parasite lines have never been exposed to artemisinin combination therapies and do not represent the genetic backgrounds that currently circulate in the field. We know that drug resistance, especially artemisinin resistance, involves many loci, and interrogating a mutation in one gene in the absence of potentially many other unknown background mutations (i.e. in a laboratory strain) may obscure some phenotypic consequences of that mutation of interest. For SNPs like the µ2(I592T) or Ubp1 mutations discussed above, examining these mutations in clinical isolates is less important because they have not been observed in human infections. However, the µ2(S160N) mutation was only observed in natural infections, and therefore it should be examined in a representative clinical isolate before being written off as having no phenotypic consequence.

Because the µ2(S160N) mutation was identified in Kenya around the late 2000s and again in this thesis work in the early 2010s, I decided to also characterise this mutation in the HL1402 *P. falciparum* strain in our laboratory. HL1402 was culture adapted by Dr Donnelly van Schalkwyk from a blood sample from a symptomatic patient who contracted malaria after visiting a similar region of Kenya in 2014.

At the time of these experiments, no publications had described the transfection of a recently adapted African clinical isolate. The Cam3.I and Cam3.II

series parasites described by researchers in Prof David Fidock's laboratory are clinical isolates but are also robust parasites that grow well under normal culture conditions. Our stable of African isolates typically do not propagate unless cultured in medium supplemented with human serum, and even under these conditions may still expand slowly. Given that CRISPR-Cas9 editing in *P. falciparum* involves two biological bottlenecks, transfection of plasmid DNA and successful chromosomal targeting, cleavage, and repair, I sought to determine whether HL1402 could be transfected under our current protocols and techniques.

HL1402 was transfected with the pEFGFP reporter construct described by Talman *et al*, which expresses GFP under the control of the *pfeF1α* promoter, using the schizont-stage Nucleofection, ring-stage electroporation, and spontaneous uptake of DNA methods described in Section 3.4.3[328]. The laboratory strain Dd2 was also transfected alongside HL1402 in these methods. While GFP-expressing parasites were obtained from all methods in the Dd2 strain, GFP-expressing HL1402 were only observed in the spontaneous DNA uptake transfections despite additional

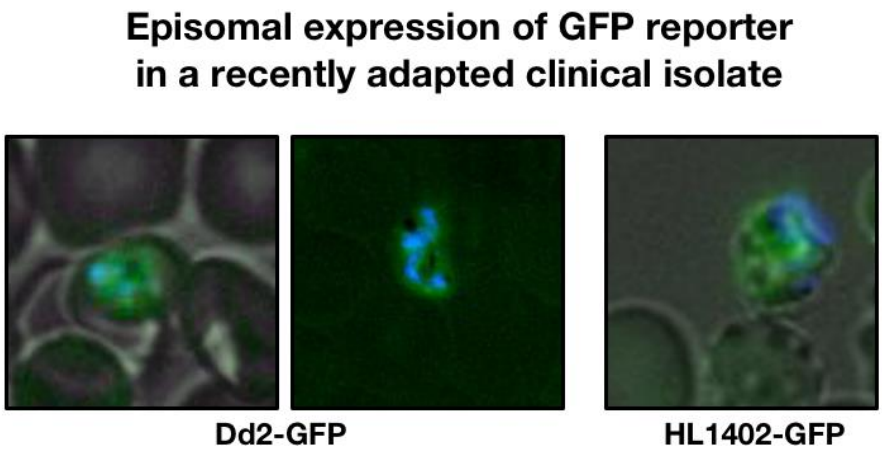


**Figure 78 Episomal expression of a GFP reporter into a recently adapted clinical isolate**
HL1402 is a recently culture-adapted *P. falciparum* clinical isolate collected from a patient who was infected while traveling in Kenya. To establish whether clinical isolates can be transfected, several transfection methods were used to introduce the pEFGFP reporter construct, which expresses GFP under the control of the eF1α promoter. The spontaneous DNA uptake method was the only transfection method that yielded modified parasites after WR99210 selection. The Dd2 parasite line, which grows robustly and is readily transfectable, was included alongside as a transfection control.

attempts with the other methods. Transfectants were selected for 14 days with 2.5 nM WR99210, and GFP-expressing transfectants were observed in culture after 4 weeks. Despite parasites recovering from drug selection, many parasites in the culture were not green, suggesting a subset of the parasites had been successfully transfected (Fig 38). HL1402, like all of our culture-adapted clinical isolates, is polyclonal. So far, we have not been able to successfully clone these parasites by limiting dilution. Therefore, it may be that certain clones are more robust than others, and these clones were the ones transfected. However, this experiment serves as proof of principle that at least a subpopulation of HL1402 can be successfully transfected, and the spontaneous DNA uptake method is the only suitable transfection method, probably because it is gentler on the parasites themselves than the electroporation methods. Therefore, the spontaneous DNA uptake method was used for transfecting genome editing constructs into HL1402.

### Generation of a transgenic *P. falciparum* strain harbouring a μ2 mutation from a recent African clinical isolate

Based on the reporter transfection experiments discussed above in Section 4.7, the spontaneous DNA uptake method was used for transfecting 100 μg of pL6-AP2μ(S160N)-sgDNA and 100 μg of pUF1-Cas9 into HL1402 to install the μ2(S160N) mutation. DNA-loaded red cells were exposed to Percoll-enriched HL1402 schizonts for 96 hours before selection with WR99210 was begun. Parasites were visible by Giemsa stain after 3 weeks. Several frozen stabilates were prepared once the culture exceeded 1% parasitaemia. PCR-RLFP mapping confirmed the

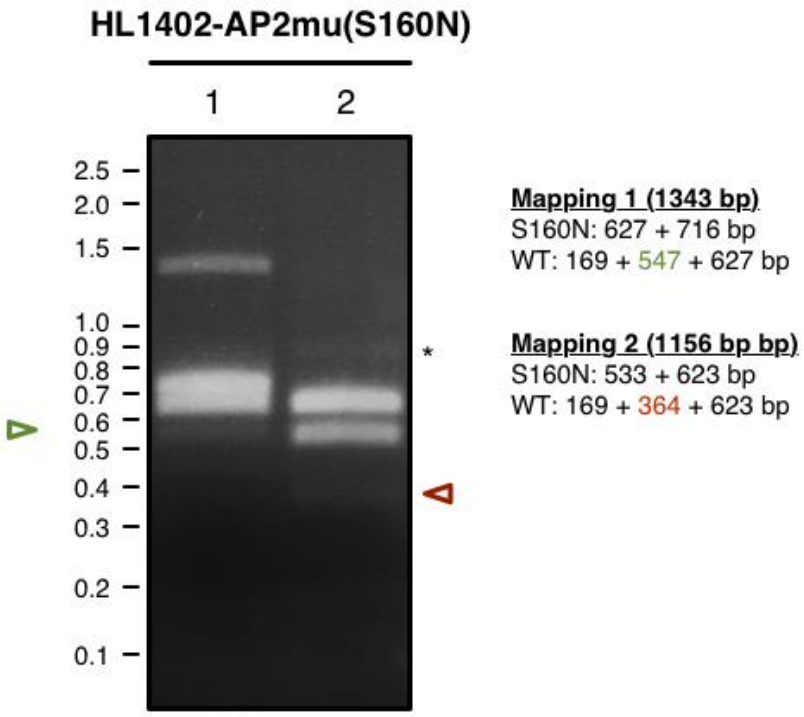


**Figure 79 PCR-RFLP mapping of transgenic HL1402 bearing *pfap2mu(S160N)***
PCR-RFLP mapping was performed to determine the genotype of transfected HL1402 parasites and estimate the proportion of unmodified parasites in the uncloned culture using two different sets of primers, both annealing outside the 5' and 3' homology regions of the Cas9 repair template. PCR products (1343 bp and 1156 bp) were digested with 0.5 units SnaBI and XbaI for 4 hours at 37ºC. Green and red arrows annotate low abundance RFLP fragments indicating the presence of low-level wild type genomes in the uncloned culture. * indicates possible incomplete WT digestion product.

presence of the mutant locus but also revealed the presence of unedited parasites in the culture (Fig 41). So far, our laboratory has not been able to successfully clone the parasites in our stable of culture-adapted African clinical parasite isolates because they do not yet grow robustly.

To attempt to derive a cloning protocol for these strains, I first used HL1212, one of our laboratory's best-growing strains. HL1212 was isolated in 2012 from a patient who was infected while traveling in Nigeria, and although it requires medium supplemented with 5% (v/v) human serum to grow well *in vitro*, its rate of expansion is similar to that of our laboratory strains. Previous attempts to clone HL1212 by

limiting dilution using the standard protocol by others in our laboratory had failed. I wondered whether culture medium supplemented with conditioned medium would simulate a parasite-dense culture environment and promote the growth of single clones. At high parasitaemia, conditioned medium provokes gametocytogenesis; however anecdotally, medium supplemented with small amounts of conditioned medium stimulates parasite growth in other laboratories. Under this rationale, I attempted to clone HL1212 using the standard limiting dilution cloning protocol with either 10% or 25% (v/v) conditioned medium in fresh complete medium. All medium for culturing clinical isolates contains either 10% (v/v) equine serum or 5% (v/v) human serum; in our hands, there is no significant difference in parasite growth between either serum (data not shown). For these cloning experiments, 10% (v/v) equine serum was used.

After 20 days, 10 wells of the 96-well cloning plate treated with 10% (v/v) conditioned medium were positive for parasite growth by the LDH colourimetric assay. These clones were expanded into a 1 ml culture at 2% haematocrit in a 24-well plate. No parasites were observed by Giemsa staining after a further 2 weeks in culture, and there were no positive wells in the plate treated with 25% (v/v) conditioned medium. When the original positive wells from the 96 well plate were smeared and examined by Giemsa staining, some gametocytes were observed as well as some asexual parasites. Since the establishment of a robust protocol for cloning clinical isolates was not one of the primary aims of this thesis, this work was not pursued further. It is possible that conditioned medium supports cloning at in the first few weeks but then begins to provoke terminal gametocytogenesis as the parasites reach a higher density in each well. An optimal protocol might blend the use of conditioned and unconditioned medium.

Because Hl402-*pfap2mu(S160N)* parasites have not been cloned, the sensitivity of these parasites to frontline chemotherapies was not determined. Any observed phenotype would be an average of genotypes in the culture, and since it is also unclear which parental subclone(s) was/were transfected, appropriate controls for any drug sensitivity comparison cannot be selected. Further work should aim to resolve these issues and characterise the drug sensitivity profile of this parasite line.

# Appendix III: µ2 interactome

| PFID | Name | Location | CHAPS Enrichment |
|---|---|---|---|
| PF3D7_0910800 | Cytosolic Fe-S cluster assembly factor NBP35, putative | Apicoplast | 6.33E+08 |
| PF3D7_0826100 | HECT-like E3 ubiquitin ligase, putative | Cytosol | 1.55E+10 |
| PF3D7_1124600 | ethanolamine kinase | Cytosol | 4.50E+09 |
| PF3D7_1138800 | WD repeat-containing protein, putative | Cytosol | 3.12E+09 |
| PF3D7_1453800 | glucose-6-phosphate dehydrogenase-6-phosphogluconolactonase | Cytosol | 2.97E+09 |
| PF3D7_1431600 | succinyl-CoA ligase [ADP-forming] subunit beta, putative | Cytosol | 1.04E+09 |
| PF3D7_0413900 | ubiquitin carboxyl-terminal hydrolase 13, putative | Cytosol | 6.24E+08 |
| PF3D7_1462800 | glyceraldehyde-3-phosphate dehydrogenase | Cytosol | 8.13E+00 |
| PF3D7_1034700 | ADP-ribosylation factor, putative | Cytosol | 4.33E+09 |
| PF3D7_1407900 | plasmepsin I | Digestive Vacuole | 8.48E+00 |
| PF3D7_1443900 | heat shock protein 90, putative | ER | 2.71E+09 |
| PF3D7_0306800 | T-complex protein 1 subunit beta | ER | 1.01E+02 |
| PF3D7_1229500 | T-complex protein 1 subunit gamma | ER | 1.76E+01 |
| PF3D7_1357800 | T-complex protein 1 subunit delta | ER | 1.44E+01 |
| PF3D7_1132200 | T-complex protein 1 subunit alpha | ER | 1.31E+01 |
| PF3D7_0320300 | T-complex protein 1 subunit epsilon | ER | 1.16E+01 |
| PF3D7_1211400 | heat shock protein DNAJ homologue Pfj4 | ER | 8.48E+00 |
| PF3D7_0708400 | heat shock protein 90 | ER | 7.42E+00 |
| PF3D7_0621900 | signal recognition particle subunit SRP68, putative | ER | 7.35E+00 |
| PF3D7_0608700 | T-complex protein 1 subunit zeta | ER | 7.32E+00 |
| PF3D7_0409400 | chaperone protein DnaJ | ER | 6.83E+00 |
| PF3D7_1361800 | glideosome-associated connector | IMC | 5.80E+09 |
| PF3D7_0616800 | malate:quinone oxidoreductase, putative | Mitochondria | 1.74E+09 |
| PF3D7_1015600 | heat shock protein 60 | Mitochondria | 8.00E+00 |
| PF3D7_1035700 | duffy binding-like merozoite surface protein | Periphery/Exported | 4.80E+09 |
| PF3D7_0104200 | StAR-related lipid transfer protein | Periphery/Exported | 1.99E+09 |
| PF3D7_0935900 | ring-exported protein 1 | Periphery/Exported | 9.62E+00 |
| PF3D7_1471100 | Exported protein 2 | Periphery/Exported | 7.46E+00 |
| PF3D7_1033200 | early transcribed membrane protein 10.2 | Periphery/Exported | 6.61E+00 |
| PF3D7_1248900 | 26S protease regulatory subunit 8, putative | Proteasome | 2.10E+01 |
| PF3D7_0205900 | 26S proteasome regulatory subunit RPN1, putative | Proteasome | 1.09E+01 |
| PF3D7_1008400 | 26S protease regulatory subunit 4, putative | Proteasome | 1.06E+01 |
| PF3D7_1311500 | 26S protease regulatory subunit 7, putative | Proteasome | 8.13E+00 |
| PF3D7_0608500 | proteasome subunit alpha type-2, putative | Proteasome | 7.85E+00 |
| PF3D7_1118100 | AP-1 complex subunit sigma, putative | Traffic | 2.75E+09 |
| PF3D7_0906100 | vacuolar protein sorting-associated protein 46, putative | Traffic | 2.46E+09 |
| PF3D7_1246200 | actin I | Traffic | 2.32E+01 |
| PF3D7_0903700 | alpha tubulin 1 | Traffic | 1.66E+01 |
| PF3D7_1020900 | ADP-ribosylation factor | Traffic | 1.64E+01 |
| PF3D7_1008700 | tubulin beta chain | Traffic | 1.45E+01 |
| PF3D7_0416800 | small GTP-binding protein sar1 | Traffic | 1.18E+01 |
| PF3D7_1222300 | endoplasmin, putative | unknown | 1.02E+01 |
| PF3D7_1446200 | M17 leucyl aminopeptidase | unknown | 9.88E+00 |
| PF3D7_0726800 | dolichyl-phosphate-mannose--protein mannosyltransferase, putative | unknown | 8.61E+00 |
| PF3D7_0826700 | receptor for activated c kinase | unknown | 7.70E+00 |

Identified µ2 interacting factors unique to CHAPS-based extraction condition (20 mM HEPES, 250 mM sodium citrate, 0.1% (w/v) CHAPS, 1 mM $MgCl_2$, 10 mM $CaCl_2$, pH 7.4). Factors are grouped by putative location as listed on MPMP.

| PFID | Name | Location | Triton Enrichment |
|---|---|---|---|
| PF3D7_0727200 | cysteine desulfurase, putative | Apicoplast | 8.79E+08 |
| PF3D7_1360800 | falcilysin | Apicoplast | 8.24E+00 |
| PF3D7_1033400 | haloacid dehalogenase-like hydrolase | Cytosol | 3.77E+09 |
| PF3D7_1332600 | apurinic/apyrimidinic endonuclease Apn1, putative | Cytosol | 3.50E+09 |
| PF3D7_0709700 | prodrug activation and resistance esterase | Cytosol | 2.86E+09 |
| PF3D7_1472900 | dihydroorotase, putative | Cytosol | 1.94E+09 |
| PF3D7_0926700 | glutamine-dependent NAD(+) synthetase, putative | Cytosol | 1.37E+09 |
| PF3D7_0934800 | cAMP-dependent protein kinase catalytic subunit | Cytosol | 1.34E+09 |
| PF3D7_0306400 | FAD-dependent glycerol-3-phosphate dehydrogenase, putative | Cytosol | 9.92E+08 |
| PF3D7_0708300 | EKC/KEOPS complex subunit BUD32 | Cytosol | 9.77E+08 |
| PF3D7_0925800 | armadillo repeat protein, putative | Cytosol | 8.66E+08 |
| PF3D7_0829200 | prohibitin, putative | Cytosol | 8.44E+08 |
| PF3D7_0317200 | cdc2-related protein kinase 4 | Cytosol | 7.33E+08 |
| PF3D7_0801800 | mannose-6-phosphate isomerase, putative | Cytosol | 6.25E+01 |
| PF3D7_1434600 | methionine aminopeptidase 2 | Cytosol | 1.69E+01 |
| PF3D7_1412800 | glycylpeptide N-tetradecanoyltransferase | Cytosol | 9.54E+00 |
| PF3D7_1244800 | cytoplasmic translation machinery associated protein, putative | Cytosol | 9.10E+00 |
| PF3D7_1004300 | E3 ubiquitin-protein ligase, putative | Cytosol | 2.46E+09 |
| PF3D7_0704600 | E3 ubiquitin-protein ligase | Cytosol | 1.93E+09 |
| PF3D7_1458000 | cysteine proteinase falcipain 1 | Digestive Vacuole | 3.80E+09 |
| PF3D7_0704400 | phosphoinositide-binding protein, putative | ER | 3.70E+09 |
| PF3D7_0320700 | signal peptidase complex subunit SPC2, putative | ER | 2.70E+09 |
| PF3D7_0106300 | calcium-transporting ATPase | ER | 2.61E+09 |
| PF3D7_0322000 | peptidyl-prolyl cis-trans isomerase | ER | 2.30E+09 |
| PF3D7_0934500 | V-type proton ATPase subunit E, putative | ER | 2.07E+09 |
| PF3D7_1341900 | V-type proton ATPase subunit D, putative | ER | 1.51E+09 |
| PF3D7_1442900 | protein transport protein SEC7, putative | ER | 1.27E+09 |
| PF3D7_1229100 | multidrug resistance-associated protein 2 | ER | 7.40E+08 |
| PF3D7_1214100 | GPI ethanolamine phosphate transferase 3, putative | ER | 6.77E+08 |
| PF3D7_1432100 | voltage-dependent anion-selective channel protein, putative | ER | 6.65E+08 |
| PF3D7_1438100 | secretory complex protein 62 | ER | 6.36E+08 |
| PF3D7_0704900 | peptide chain release factor 2 | ER | 3.98E+08 |
| PF3D7_0212300 | peptide chain release factor subunit 1, putative | ER | 2.60E+01 |
| PF3D7_1108700 | heat shock protein J2 | ER | 1.23E+01 |
| PF3D7_0621800 | nascent polypeptide-associated complex subunit alpha, putative | ER | 1.10E+01 |
| PF3D7_0726500 | ubiquitin carboxyl-terminal hydrolase, putative | ER | 3.50E+00 |
| PF3D7_0316700 | protein YOP1, putative | Mitochondria | 4.19E+00 |
| PF3D7_0804900 | GTPase-activating protein, putative | Golgi | 4.85E+10 |
| PF3D7_1465100 | conserved oligomeric Golgi complex subunit 6, putative | Golgi | 7.04E+09 |
| PF3D7_0522600 | inner membrane complex protein | IMC | 2.40E+09 |
| PF3D7_0918100 | cytochrome b5-like heme/steroid binding protein, putative | Mitochondria | 8.40E+09 |
| PF3D7_0823900 | dicarboxylate/tricarboxylate carrier | Mitochondria | 2.45E+09 |
| PF3D7_1457200 | thioredoxin 1 | Mitochondria | 1.02E+09 |
| PF3D7_1416500 | NADP-specific glutamate dehydrogenase | Mitochondria | 1.88E+08 |
| PF3D7_1345100 | thioredoxin 2 | Mitochondria | 7.74E+00 |
| PF3D7_0113000 | glutamic acid-rich protein | Periphery/Exported | 1.00E+10 |
| PF3D7_0731300 | Plasmodium Periphery/Exported protein (PHISTb), unknown functior | Periphery/Exported | 8.55E+09 |
| PF3D7_0805700 | serine/threonine protein kinase, FIKK family | Periphery/Exported | 7.98E+09 |
| PF3D7_0113200 | Plasmodium Exported protein, unknown function | Periphery/Exported | 6.90E+09 |
| PF3D7_0301600 | Plasmodium Exported protein (hyp1), unknown function | Periphery/Exported | 3.32E+09 |
| PF3D7_0207600 | serine repeat antigen 5 | Periphery/Exported | 1.13E+09 |
| PF3D7_1001700 | Plasmodium Exported protein (PHISTc), unknown function | Periphery/Exported | 4.95E+08 |
| PF3D7_0201900 | erythrocyte membrane protein 3 | Periphery/Exported | 4.39E+08 |
| PF3D7_0207500 | serine repeat antigen 6 | Periphery/Exported | 7.64E+00 |
| PF3D7_0202000 | knob-associated histidine-rich protein | Periphery/Exported | 4.71E+00 |
| PF3D7_1437900 | HSP40, subfamily A | Periphery/Exported | 4.69E+00 |
| PF3D7_1471100 | Exported protein 2 | Periphery/Exported | 7.46E+00 |
| PF3D7_1033200 | early transcribed membrane protein 10.2 | Periphery/Exported | 6.61E+00 |

Identified μ2 interacting factors unique to Triton-based extraction condition (20 mM HEPES, 100 mM NaCl, 0.1% (w/v) Triton X-100, pH 7.4). Factors are grouped by putative location as listed on MPMP. (Continued on next page)

| PFID | Name | Location | Triton Enrichment |
|---|---|---|---|
| PF3D7_0715800 | drug/metabolite transporter DMT1, putative | Plasma Membrane | 1.04E+09 |
| PF3D7_1466300 | 26S proteasome regulatory subunit RPN2, putative | Proteasome | 3.08E+09 |
| PF3D7_1306400 | 26S protease regulatory subunit 10B, putative | Proteasome | 2.48E+09 |
| PF3D7_0807500 | proteasome subunit alpha type-6, putative | Proteasome | 2.05E+09 |
| PF3D7_0108000 | proteasome subunit beta type-3, putative | Proteasome | 1.14E+09 |
| PF3D7_1353800 | proteasome subunit alpha type-4, putative | Proteasome | 5.97E+08 |
| PF3D7_1366400 | rhoptry protein RHOP148 | Rhoptry | 7.48E+08 |
| PF3D7_0935200 | vacuolar protein sorting-associated protein 33, putative | Traffic | 1.43E+09 |
| PF3D7_1104100 | syntaxin, Qa-SNARE family | Traffic | 1.22E+09 |
| PF3D7_1242800 | rab specific GDP dissociation inhibitor | Traffic | 1.10E+09 |
| PF3D7_1250300 | vacuolar protein sorting-associated protein 26, putative | Traffic | 7.72E+08 |
| PF3D7_0319400 | kinesin-8, putative | Traffic | 6.39E+08 |
| PF3D7_1329100 | myosin F, putative | Traffic | 4.95E+00 |
| PF3D7_0728000 | eukaryotic translation initiation factor 2 subunit alpha, putative | Translation | 9.38E+09 |
| PF3D7_0111800 | eukaryotic translation initiation factor 4E, putative | Translation | 3.51E+09 |
| PF3D7_0319600 | elongation factor 1-delta, putative | Translation | 5.15E+08 |
| PF3D7_1233000 | elongation factor G | Translation | 4.77E+08 |
| PF3D7_1204300 | eukaryotic translation initiation factor 5A | Translation | 2.96E+01 |
| PF3D7_1010600 | eukaryotic translation initiation factor 2 subunit beta | Translation | 1.52E+01 |
| PF3D7_0607000 | translation initiation factor IF-2, putative | Translation | 1.40E+01 |
| PF3D7_1143400 | translation initiation factor eIF-1A, putative | Translation | 1.28E+01 |
| PF3D7_1438000 | eukaryotic translation initiation factor eIF2A, putative | Translation | 9.16E+00 |
| PF3D7_1410600 | eukaryotic translation initiation factor 2 subunit gamma, putative | Translation | 5.26E+00 |
| PF3D7_0612100 | eukaryotic translation initiation factor 3 subunit L, putative | Translation | 4.97E+00 |
| PF3D7_1451100 | elongation factor 2 | Translation | 4.26E+00 |
| PF3D7_0319700 | ABC transporter I family member 1, putative | Transporter | 1.23E+10 |
| PF3D7_1132800 | aquaglyceroporin | Transporter | 2.00E+09 |
| PF3D7_0525400 | G-protein coupled receptor, putative | Transporter | 1.06E+09 |

Identified μ2 interacting factors unique to Triton-based extraction condition (20 mM HEPES, 100 mM NaCl, 0.1% (w/v) Triton X-100, pH 7.4). Factors are grouped by putative location as listed on MPMP. (Continued from previous page)

# Appendix IV: Expression of µ2 and K13 in HeLa cells

The divergence of µ2 localisation and function in the *Plasmodium* genus with that observed in other cells was so unexpected that I wondered whether PfAP2µ retained the ability to localise properly in mammalian cells. It is reasonable to propose that the AP-2 complex is recruited to membranes of vesicular origin by other factors. Therefore, it could be that these factors are actually the ones that have evolutionarily diverged and µ2 is simply following these recruitment factors and may not be intrinsically diverged. To investigate this question, I cloned the Pfµ2-3xHA CDS into the pTriEx mammalian expression system, transfected the resulting pTriEx-Pfµ2-3xHA construct into $1x10^6$ HeLa cells with Lipofectamine 3000, and examined the localisation of µ2-3xHA by immunofluorescence.

Interestingly, Pfµ2 was localised mainly at the cell periphery (Fig 80). Currently, we do not have further reagents to probe the localisation of Pfµ2 in human cells, but these data tentatively suggest Pfµ2 may be capable of functionality similar to the human orthologue, and the non-canonical behaviour reported here in *Plasmodium* may be due to divergence at a different level of the vesicle formation process. Structural modelling suggests Pfµ2 may occupy a similar folded conformation to the mammalian factor and would support this hypothesis (Appendix II). Though hµ2 and Pfµ2 only share 35% sequence homology over their entire sequences, there is clear conservation in long tracts which map to architectural structures in the µ subunit core, which provides further support for possible conservation of the molecule between species, even though the species-specific function may be diverged. Alignments are provided in Appendix IV.

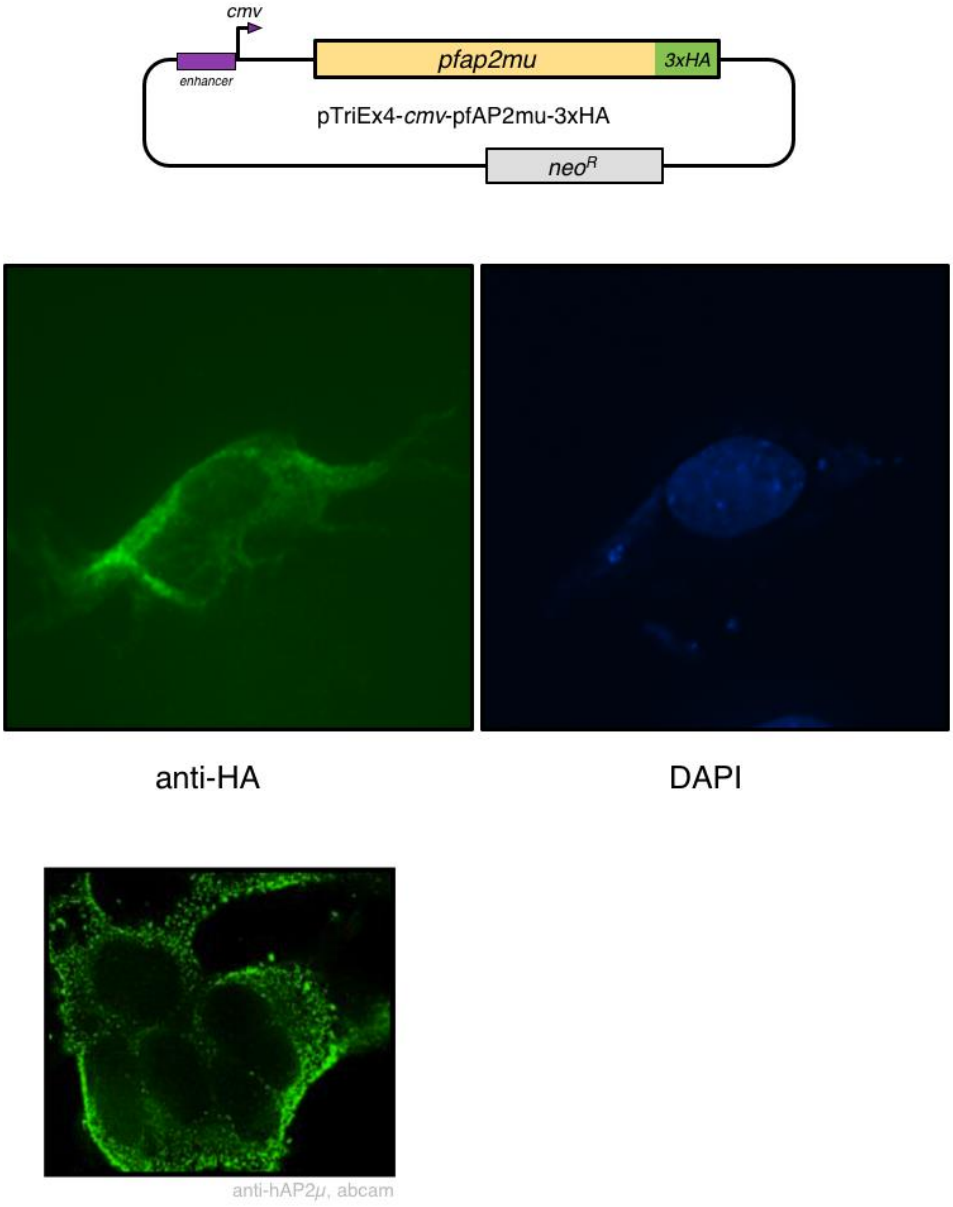


**Figure 80 Transient transfection and localisation of Pfμ2-HA into HeLa cells**
The *pfap2mu-3xHA* coding sequence was amplified from modified 3D7-μ2-3xHA-*glmS* parasites and cloned into the pTriEx4 expression vector under the control of the *cmv* promoter and enhancer (Merck; top panel). This construct was transiently transfected into $1x10^6$ HeLa cells with Lipofectamine 3000, and localisation of Pfμ2-3xHA was examined 24 hours after transfection by indirect immunofluorescence. Anti-HA immunostaining (rat, Sigma 3F10, 1:150) with anti-rat-488 (Invitrogen, 1:150) detected Pfμ2-3xHA at the periphery of HeLa cells, consistent with the localisation of hμ2 observed in other human cells (lower panel; image from Abcam).

I similarly expressed PfK13 in HeLa cells to explore its localisation. Unlike Pfμ2, PfK13 exhibited no similarity with previously reported localisations of its putative homologue, hKEAP1. hKEAP1 has been previously reported to localise predominantly to the cytosol, whereas PfK13 is clearly in distinct foci in the nucleus of transfected HeLa cells (Fig 81). It is difficult to read too far into these data as K13 and KEAP1 only share 21% sequence homology. Outside of the annotated, but

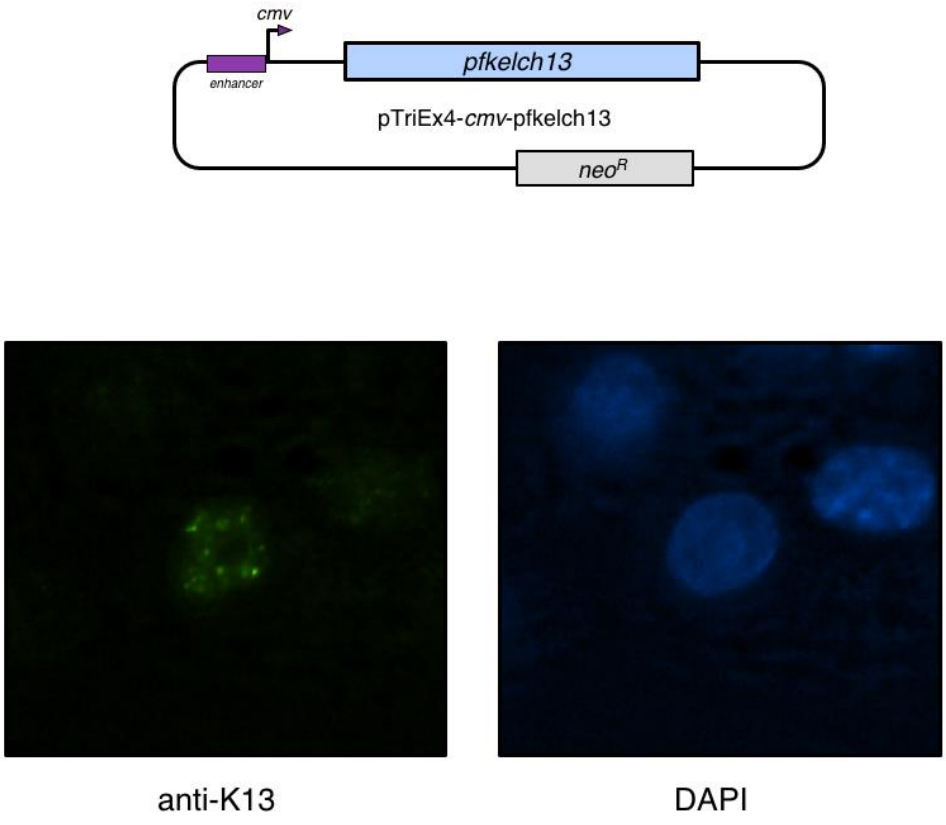


**Figure 81 Transient transfection and localisation of PfK13 into HeLa cells**
The *pfkelch13* coding sequence was amplified from 3D7 parasites and cloned into the pTriEx4 expression vector under the control of the *cmv* promoter and enhancer (Merck; top panel). This construct was transiently transfected into $1x10^6$ HeLa cells with Lipofectamine 3000, and localisation of PfK13 was examined 24 hours after transfection by indirect immunofluorescence. Anti-K13 immunostaining (mouse, D. Fidock laboratory, 1:150) with anti-mouse-488 (Invitrogen, 1:150) detected PfK13 in the nucleus of HeLa cells.

barely homologous, BTB/POZ and kelch repeat domains in PfK13, there is little expectation that PfK13 and hKEAP1 would function similarly.

Overall, these studies were aimed to be preliminary and exploratory, and future work could aim to further validate this evolutionary divergence by pulling down Pfμ2-3xHA from transgenic HeLa lysates and probing interactions with other known hAP-2 components or attempting to rescue a conditional hμ2 knockout with Pfμ2. Alternatively, hμ2 could be introduced into *Plasmodium* for similar experiments.

# Appendix V: Alignments of selected *Plasmodium* proteins of interest and their human orthologues

## Alignment of PfAP2µ and hAP2m1 protein sequences

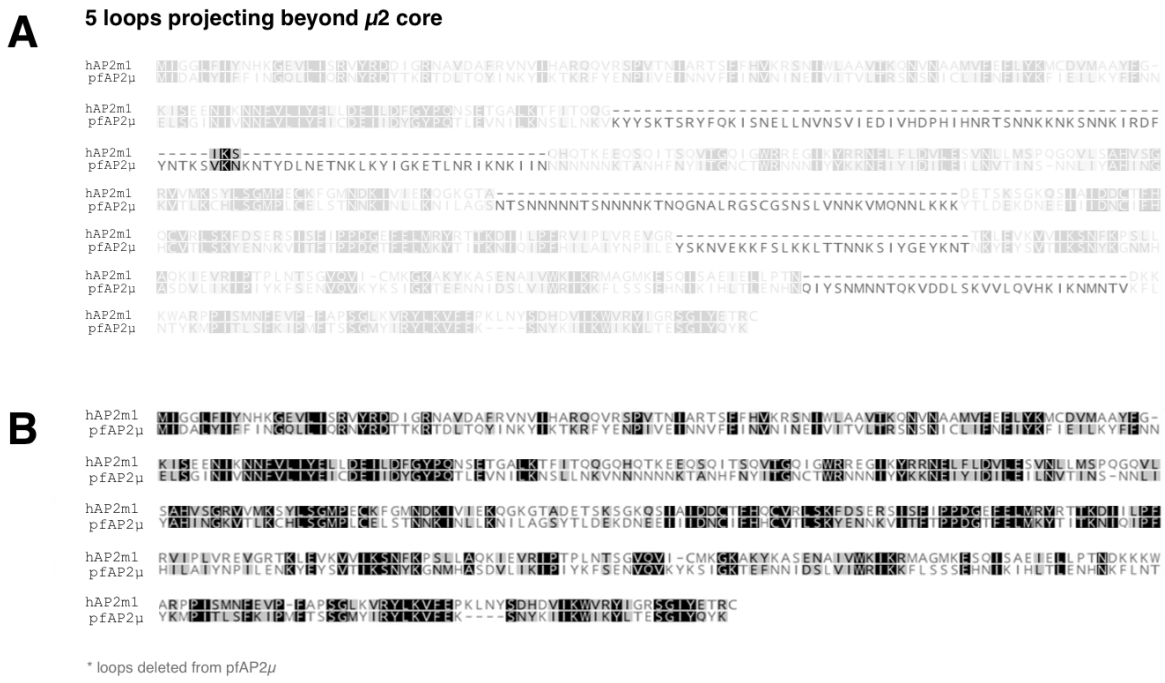


## Alignment of PfAP2σ and hAP2s1 protein sequences

## Alignment of PfAP2α and hAP2a1 protein sequences

## Alignment of PfAP1β and hAP1b protein sequences

## Alignment of PfCLC and hCLCA protein sequences

## Alignment of PfCHC and hCLH1 protein sequences

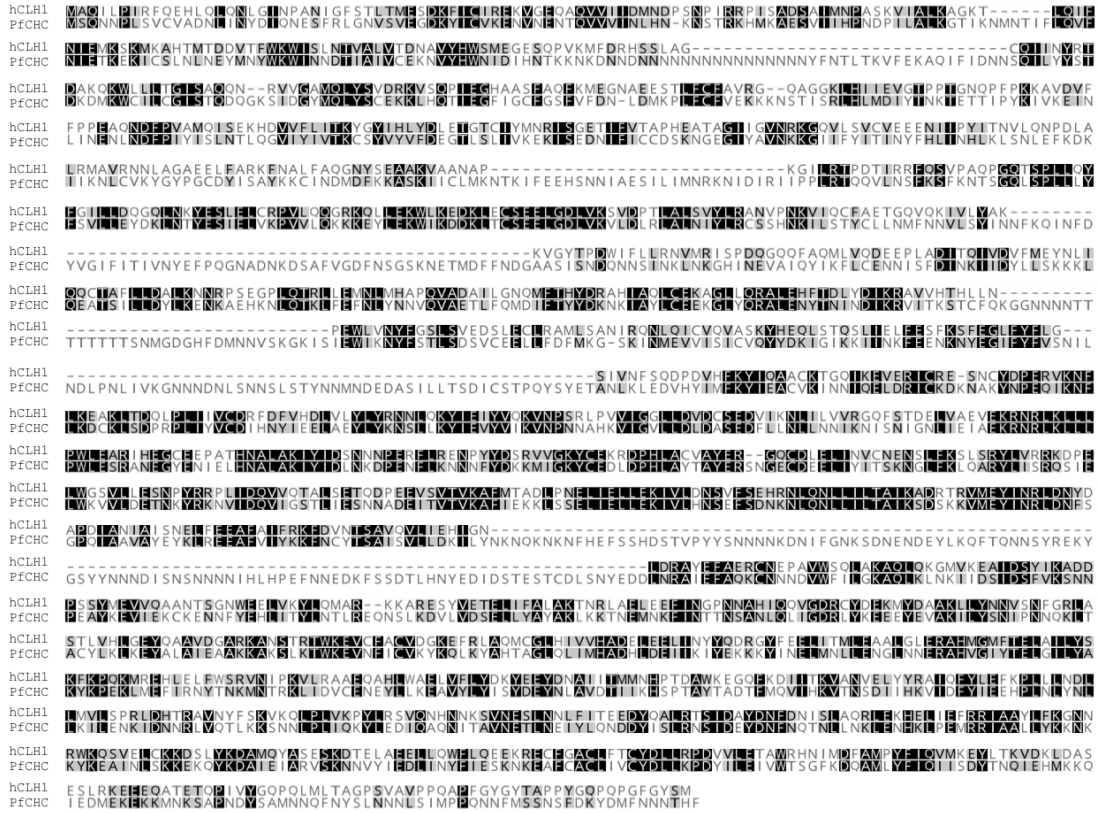


## Alignment of PfK13 and hKEAP1 protein sequences

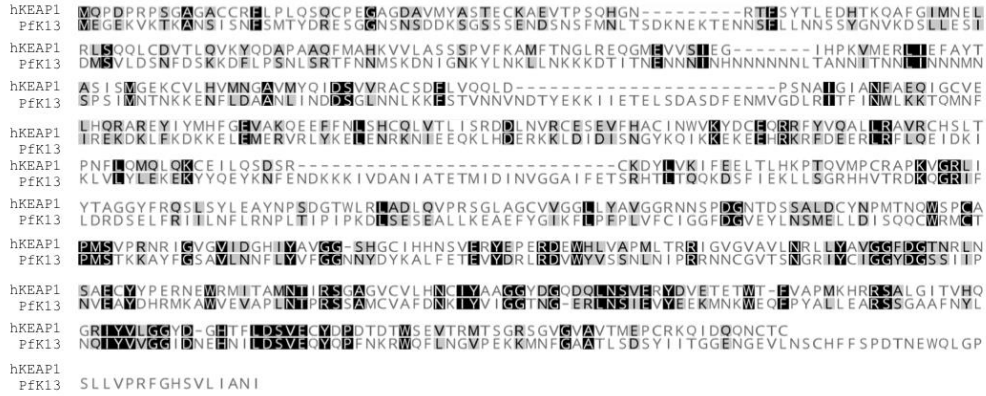

**Alignment of PfUbp1(3166-3486) and hUSP7(210-531) protein sequences (catalytic core)**

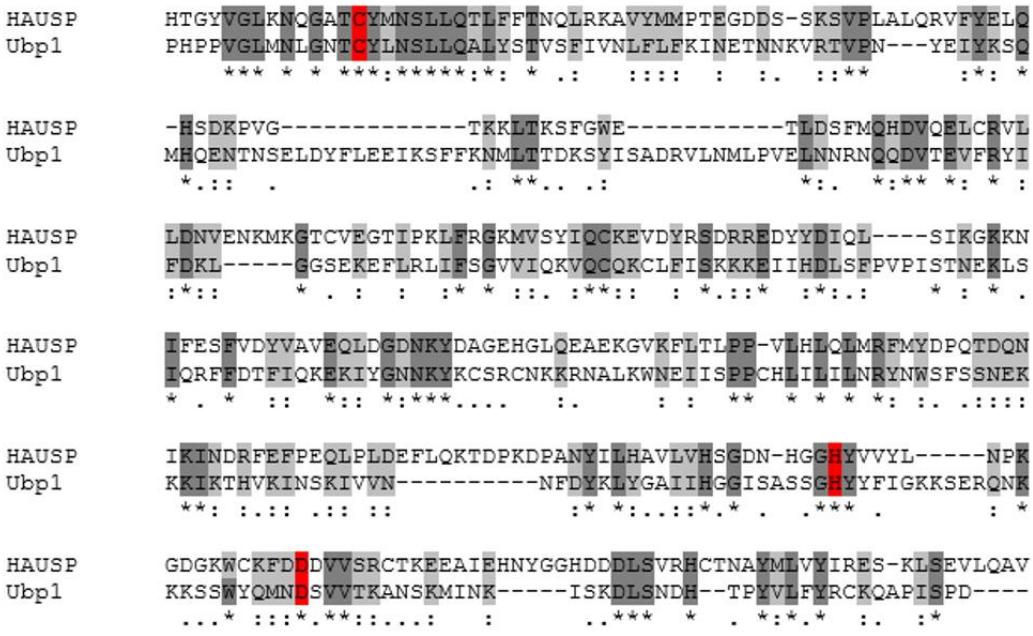


* catalytic triad is highlighted in red.

# Appendix VI: A brief characterisation of Clathrin Heavy Chain in *Plasmodium falciparum*

*Foreword:*

*During the course of the production of this thesis and the investigation of the AP-2 complex, my experiments began with roots in clathrin-mediated trafficking dogma. However, as we came to realise, AP-2 in Plasmodium may not interact with clathrin. While AP-2 is near the ER, clathrin appeared peripheral. Therefore, given the lack of knowledge about clathrin in Plasmodium and the importance of endocytosis to parasite biology, I decided to undertake a brief characterisation of clathrin heavy chain. The parasite lines and antibodies described here are attributed to those who created or supplied them.*

## Clathrin in *Plasmodium falciparum*

As described in Section 1.8, clathrin cages participate in several trafficking routes in higher order eukaryotes. They are often found at the plasma membrane where they participate in clathrin-mediated endocytosis, typically of receptor-bound cargo[329]. Clathrin also participates in traffic between various endosomal compartments downstream from the Golgi. Canonically, clathrin interacts with one of the large subunits of the clathrin adaptor protein complexes (AP complexes), which recognise and aggregate cargo molecules during vesicle formation[215,231]. After several molecular processes including cage polymerisation and actin scaffold formation, the budding vesicle is cleaved from the origin membrane, and clathrin and the associated molecules disassemble from the nascent vesicle.

Structurally, clathrin cages are made up of two core components: clathrin heavy chain and clathrin light chain[228]. The heavy chain is a unique, high molecular weight molecule that forms a three-legged triskelion structure, with each leg consisting of two jointed limbs fused by a central hub domain. By comparison, the light chain is small, typically less than 20 kDa, and associates with the heavy chain in the polyhedral cage structure at triskelion junctions[228]. Both components are nearly universally found in higher order eukaryotic organisms. In *Plasmodium*, PF3D7_1219100 is annotated as clathrin heavy chain, and PF3D7_1435500 is annotated as clathrin light chain.

To our knowledge, there is no existing characterisation, in part or in full, of clathrin in *Plasmodium falciparum*. One would expect that it participates in similar roles in the cell, but based on the surprising and divergent function of the AP-2 complex demonstrated in Chapter 5, it is conceivable that clathrin function is similarly diverged. In the process of investigating the AP-2 complex, we received a

parasite line expressing an endogenously GFP-tagged clathrin heavy chain and a monoclonal antibody against clathrin from the laboratories of Tobias Spielmann and Frances Brodsky, respectively, with which I pursued a preliminary molecular characterisation.

## Localisation of Clathrin Heavy Chain in *Plasmodium falciparum*

The localisation and distribution of clathrin in the GFP-tagged parasite line was examined via live microscopy. Consistent with clathrin being one of the most abundant proteins in the cell, the endogenously-integrated clathrin-GFP fusion was readily visible in all parasite stages (Fig 82). Throughout the lifecycle, clathrin is predominantly localised to the parasite periphery in discrete foci. In ring stages, a single clathrin focus exists at the plasma membrane. As the parasite matures, additional foci appear at the plasma membrane and in the parasite cytoplasm in close proximity to the digestive vacuole. In segmented schizonts, merozoites seem to receive a single clathrin-labelled structure. In contrast to the AP-2 complex, clathrin in ring stages is much further away from the nucleus and never observed in a perinuclear space consistent with the ER. The localisation of clathrin in trophozoites was not consistent between trophozoites, suggesting a changing localisation.

In mammalian systems, clathrin-coated vesicles form and bud quickly. In yeast, these processes have been better characterised and visualised and seem to take place over the course of 30 seconds to a few minutes. To better understand the dynamics of clathrin in trophozoites, live microscopy was performed on poly-L

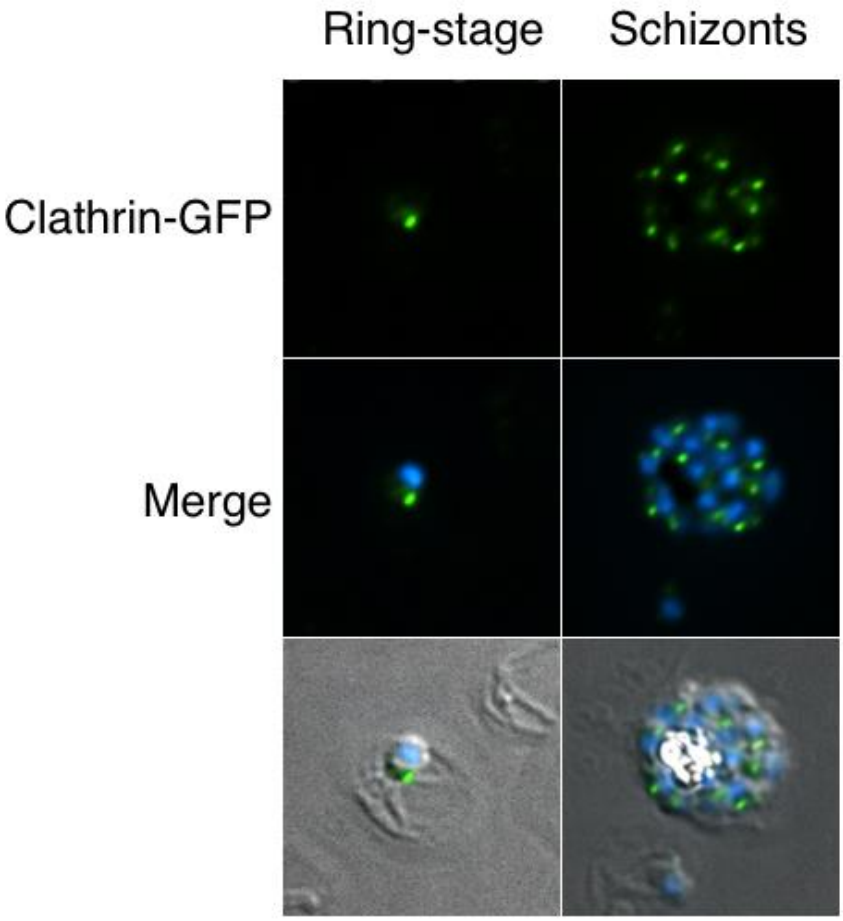


**Figure 82 Localisation of clathrin heavy chain in fixed cells**
The localisation of clathrin heavy chain was examined in live cells in ring stages and in schizonts. Trophozoites are not displayed because clathrin localisation is highly variable due to the putatively dynamic nature of clathrin-coated vesicles. In ring stages, clathrin-2xFKBP-GFP is clearly at a single punctate location at the cell periphery. In schizonts, clathrin exists as multiple punctae. Each merozoite seems to inherit a single clathrin-labeled structure.

lysine-immobilised, infected red cells. The microscope stage was sealed, heated, and gassed to 5% $CO_2$ to mimic standard culture conditions, and 3D7-CHC-2xFKBP-GFP trophozoites were observed prior to nuclear replication. In each cell, there were many GFP foci throughout the cell periphery and in the cytosol, in contrast to ring

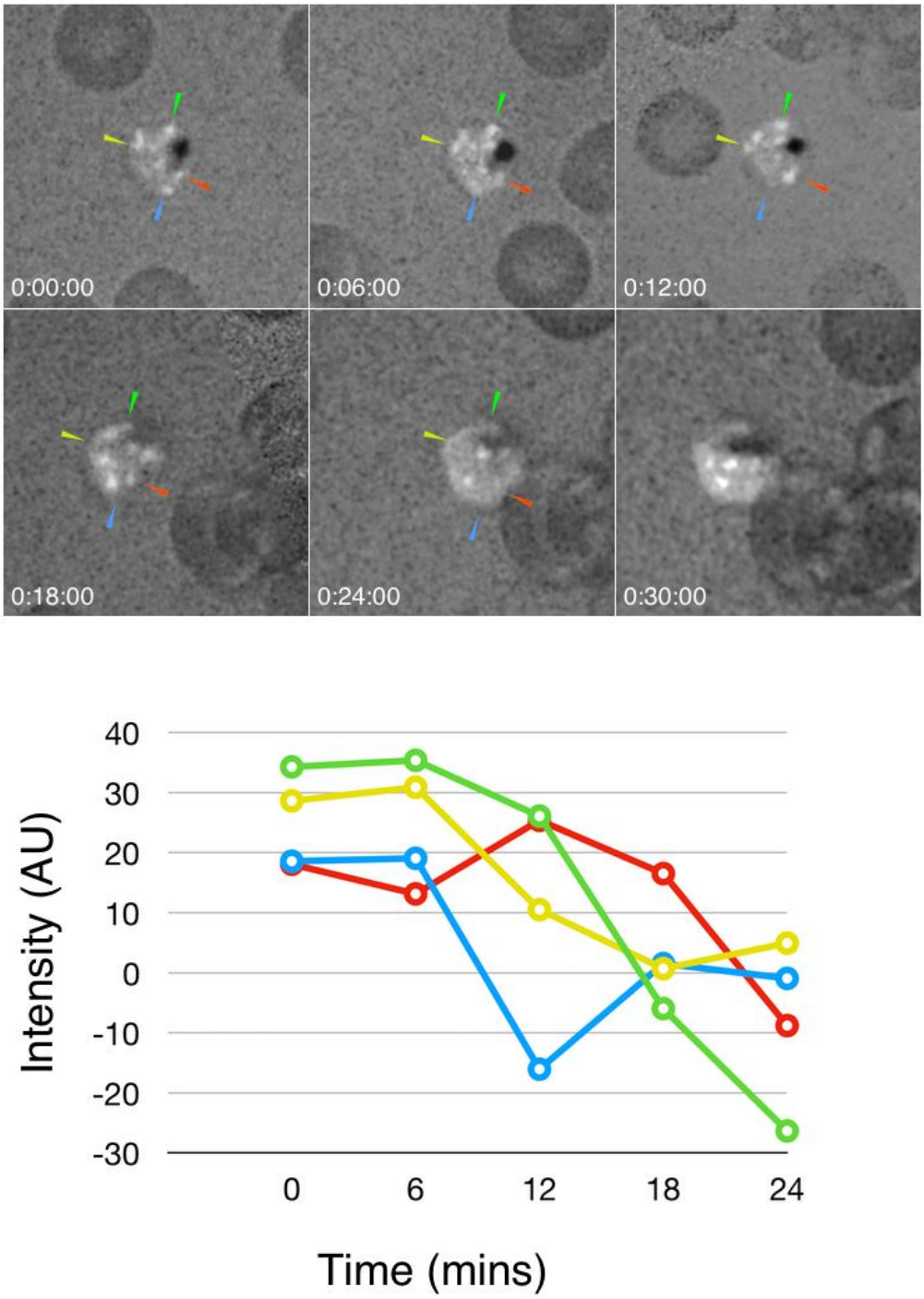


**Figure 83 Visualisation of clathrin-GFP dynamics in live trophozoites**
Clathrin in immobilised 3D7-CHC-2xFKBP-GFP trophozoites was imaged by live microscopy. Serial Z-stacks (0.1µm steps) were acquired through green and white light channels every 6 minutes and overlaid in Nikon Advanced Research Elements software (top panel). 3D stacks were projected into a 2D image using ImageJ. The average intensity of several GFP spots in the cell were quantitated and plotted over time (lower panel).

stages which clearly possessed a single peripheral focus (Fig 83, top panel). When observed continuously, fluorescent signal for any signal focus seemed to fade over roughly 30 seconds, however during this time, no new foci appeared suggesting this is more due to photobleaching than vesicle budding and clathrin disassembly. Instead, Z-stack images of immobilised trophozoites were collected every 6 minutes for several hours to capture broad changes in clathrin-GFP distribution in the cell over time. 2-dimensional projections of these Z-stacks were generated, and the average intensities of single foci were calculated using 11px diameter circular ROIs in ImageJ. These intensities were plotted over time, and it seems that once a vesicle forms, it may complete the budding process within 15 minutes (Fig 83, lower panel). Further characterisation is required to better time this process, but this initial characterisation highlights the dynamic nature of the clathrin-coated architecture in the cell, and suggests a role for clathrin at the cell periphery and in the cytosol, consistent with the role of clathrin in vesicular traffic at these locations in other eukaryotes.

## Examination of Clathrin Heavy Chain in *Plasmodium falciparum* by immunoelectron microscopy

To better characterise the localisation of clathrin, thin sections of 3D7-CHC-2xFKBP-GFP trophozoites were imaged by immunoelectron microscopy (Fig 84-87). These images supported the localisation of clathrin at the cell periphery and in vesicles as observed in the previous section.

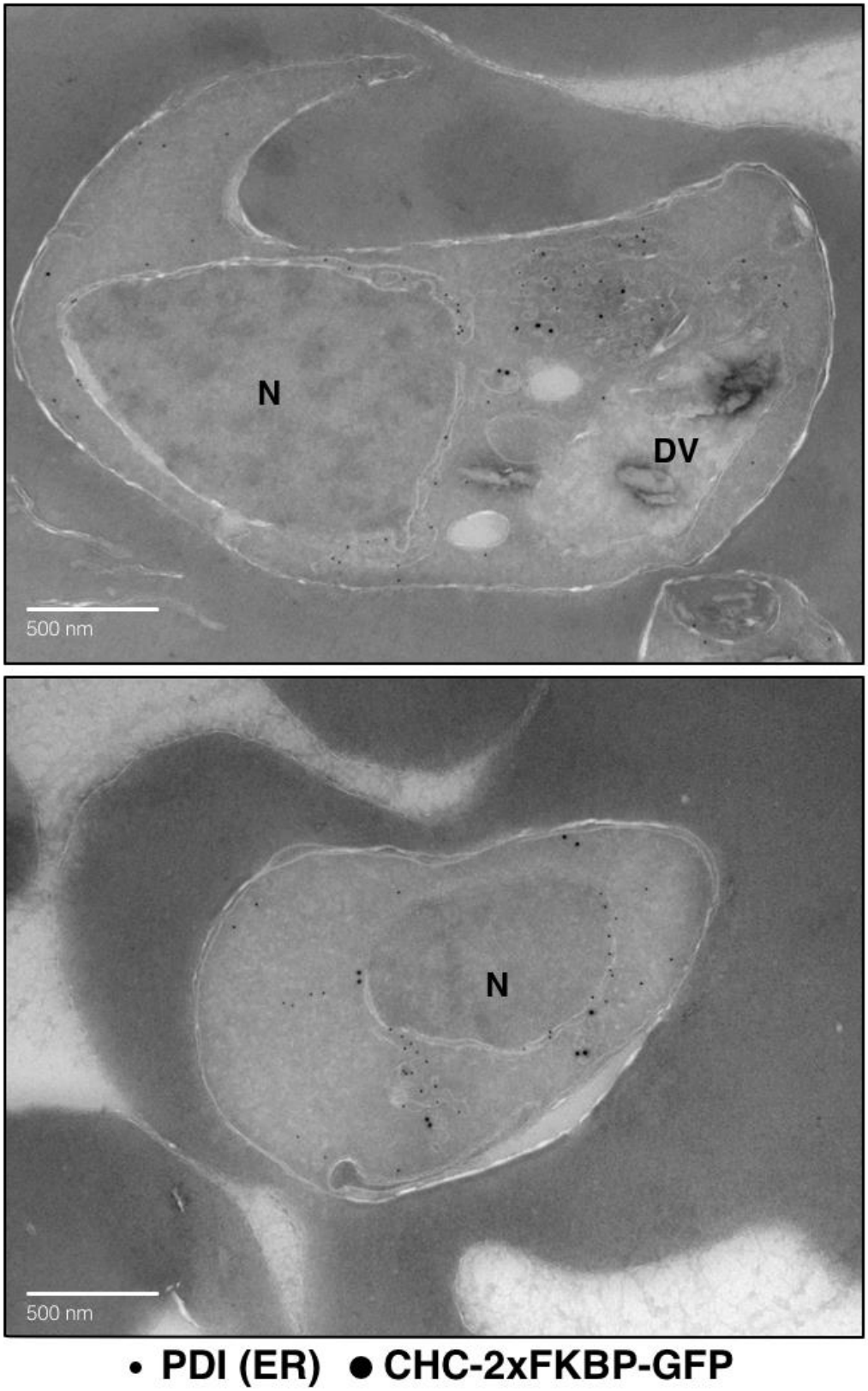


**Figure 84 Immunoelectron micrographs of clathrin in the cytosol in *Plasmodium falciparum* trophozoites**
Localisation of CHC-2xFKBP-GFP by immunoelectron microscopy in trophozoites. Clathrin (18 nm particles) is located in vesicular structures near the ER (anti-PDI, 12 nm particles) and at the plasma membrane (Fig 85). Visualised at 20,000x magnification. N: nucleus; DV: digestive vacuole.

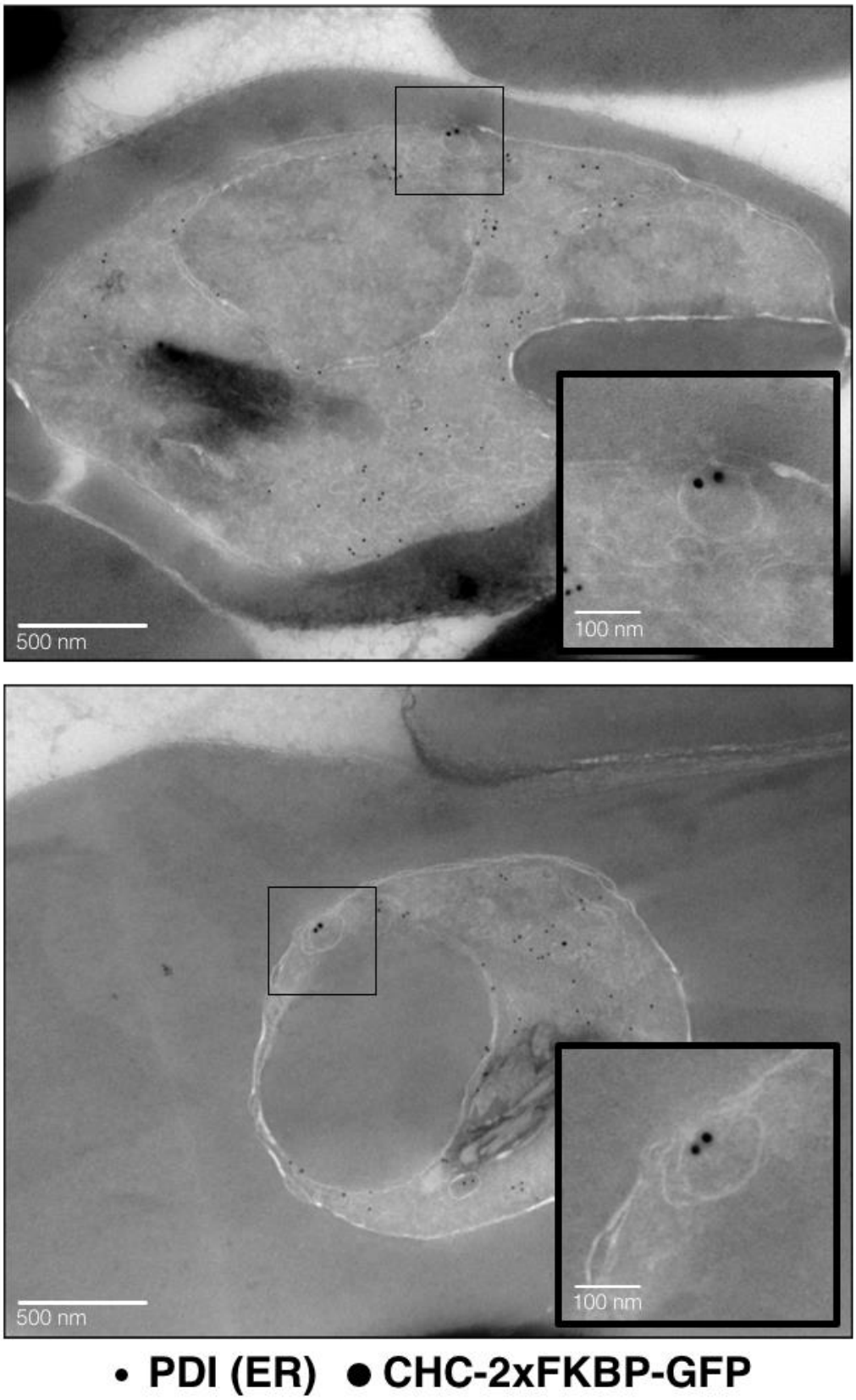


**Figure 85 Localisation of clathrin at the plasma membrane of infected erythrocytes by IEM**
Localisation of CHC-2xFKBP-GFP (anti-GFP; 18 nm particles) at the parasite plasma membrane (inset boxes) and ER structures (anti-PDI; 12 nm particles) by immunoelectron microscopy in trophozoites. Visualised at 20,000x magnification. N: nucleus; DV: digestive vacuole. Inset boxes show Type I (top panel) and Type II (bottom panel) vesicles.

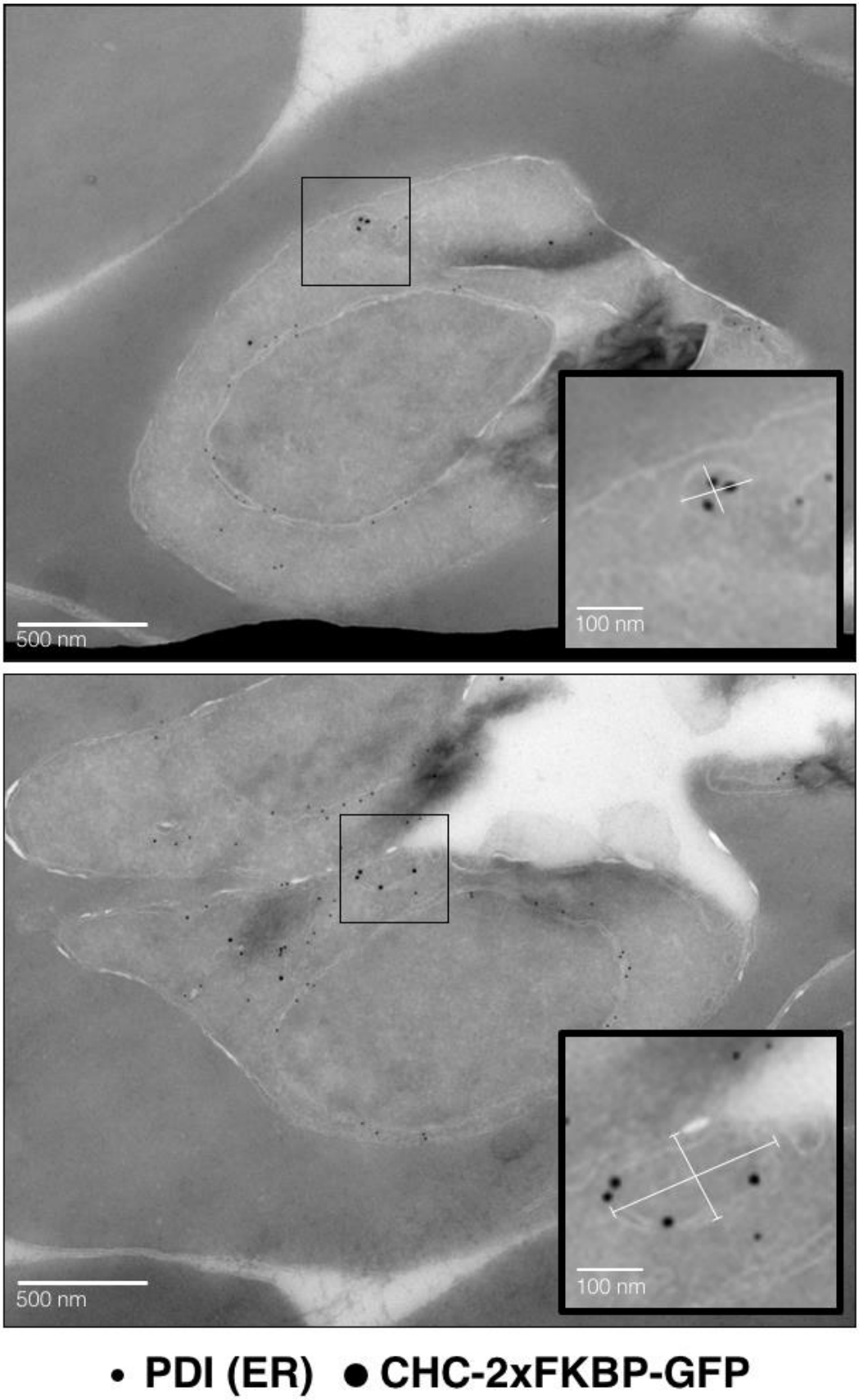


**Figure 86 Type I and Type II clathrin-coated vesicles**
Immunoelectron micrographs of "Type I" and "Type II" clathrin-coated vesicles (18 nm particles). Top panel: characteristic Type I vesicle. Bottom Panel: characteristic Type II vesicle. Major and minor axes were measured in ImageJ as depicted. 12 nm particles represent anti-PDI (ER lumen). Visualised at 20,000x magnification. Inset indicates major and minor axis measurements.

Interestingly, sections colabeled with antibodies against protein disulfide isomerase (PDI, 12 nm particles), a luminal ER folding chaperone, reveal some colocalisation between PDI and clathrin (18 nm particles). This is surprising because canonically, clathrin is located in the endosomal and Golgi network and at the plasma membrane, not the ER. Traffic out of the ER is typically mediated by elements of the COPII complex.

Additionally, several sections revealed what appears to be vesicular structures labelled with clathrin. Some of these vesicular structures are located near the ER and some seem contiguous with at least the parasite plasma membrane. Greater resolution and membrane preservation is needed to clarify this observation and determine whether the parasitophorous vacuole membrane is also invaginated into these budding structures. Near-ER vesicular structures could be the Golgi. Because *Plasmodium spp.* do not have stacked Golgi cisternae, identifying the Golgi without a Golgi-specific antibody is difficult.

Additionally, when observing these labelled micrographs, there seemed to be two different sized clathrin-labelled vesicles (Fig 87). Neither of these structures were labelled with anti-PDI, indicating they are likely not extensions of the ER. To provide additional clarity on this, straight-line diameter measurements were taken in ImageJ. Possibly because of the sectioning process, some clathrin-labelled vesicular structures appeared more elliptical than others, so a single diameter measurement fails to capture the dimensions of structure. Therefore, to better compare the size of these vesicles, the major and minor axes of the labelled vesicles were measured and plotted and clustered using K-means clustering (K = 2). As expected, the majority of vesicles ("Type I") cluster around average dimensions of 100 nm x 80 nm, with an

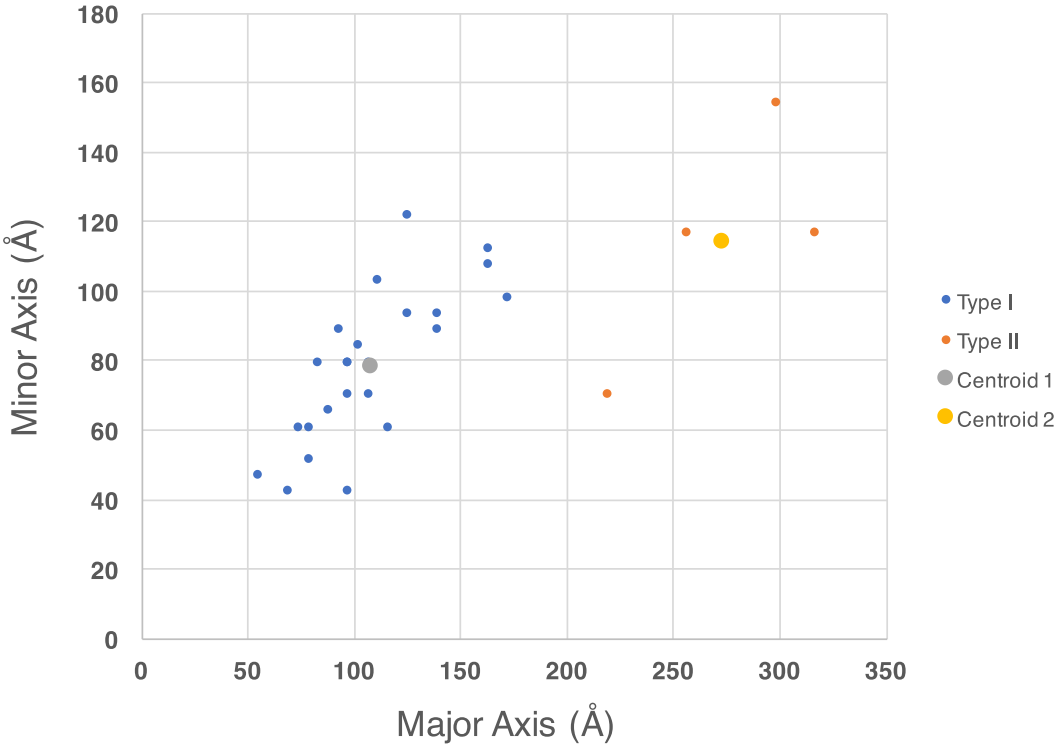


**Figure 87 K-means clustering of elliptical dimensions of clathrin-coated vesicles**
Scatterplot of major and minor axis measurements of clathrin coated vesicles identified by immunoelectron micrographs. Measurements were analysed by K-means clustering with K = 2. Centroids identified for two clusters are plotted. Type I vesicles (blue points) cluster around Centroid I (grey), and Type II vesicles (orange points) cluster around Centroid 2 (yellow). Vesicles were clustered by distance to each centroid.

elliptical cross-sectional area of approximately 6,000 $nm^2$. The remaining larger "Type II" vesicles cluster around average dimensions of 270 nm x 115 nm, with an approximate cross-sectional area of 25,000 $nm^2$. The cellular distribution of these potential sub-types of vesicles does not seem to point to a particular functional role (i.e. more often at the PM or near the ER, etc.). However, it is interesting to note the existence of this difference, and future imaging will clarify whether this clustering is artefactual or if there are real differences in the localisation and potential roles of these structures.

## Characterisation of clathrin-interactors by immunoprecipitation and mass spectrometry

Because the data presented in this chapter suggest clathrin may participate in endocytic events at the plasma membrane and transcytosis events throughout the cytosol and given the importance of understanding these processes, the same IP-MS pipeline used to characterise AP2µ-HA by cryomilling was applied to reveal interacting partners of CHC-2xFKBP-GFP.

Trophozoite stage lysates were prepared using the same CHAPS-based extraction buffer used in Section 5.7 (20 mM HEPES, 250 mM sodium citrate, 0.1% (w/v) CHAPS, 1 mM $MgCl_2$, 10 mM $CaCl_2$, pH 7.4, protease inhibitors). These lysates were incubated with custom magnetic (DynaBeads) anti-GFP nanobody beads, generated by the Field lab, for 1 hour at 4$^{o}$C. The beads were washed several times with extraction buffer, and bound material was eluted and processed for mass spectrometry as described in Section 3.3.4. Control pulldowns were performed using lysates from untagged 3D7 lysates.

As with the µ2 interactome, these experiments are still ongoing. At the time of the printing of this thesis, only one dataset was available for analysis. Therefore, it is important not to over-analyse the identified proteins, but instead consider the broad patterns of potential interacting factors. Identified ribosomal subunits and nuclear factors were omitted from this analysis for the reasons described in Section 5.7.

When examining the putative localisation or function of the identified clathrin heavy chain interactors from this single experiment, the vast majority of the identified proteins reside along the secretory pathway, centred around the Golgi. Of the 227 factors identified, more than 25% are putatively involved in intracellular

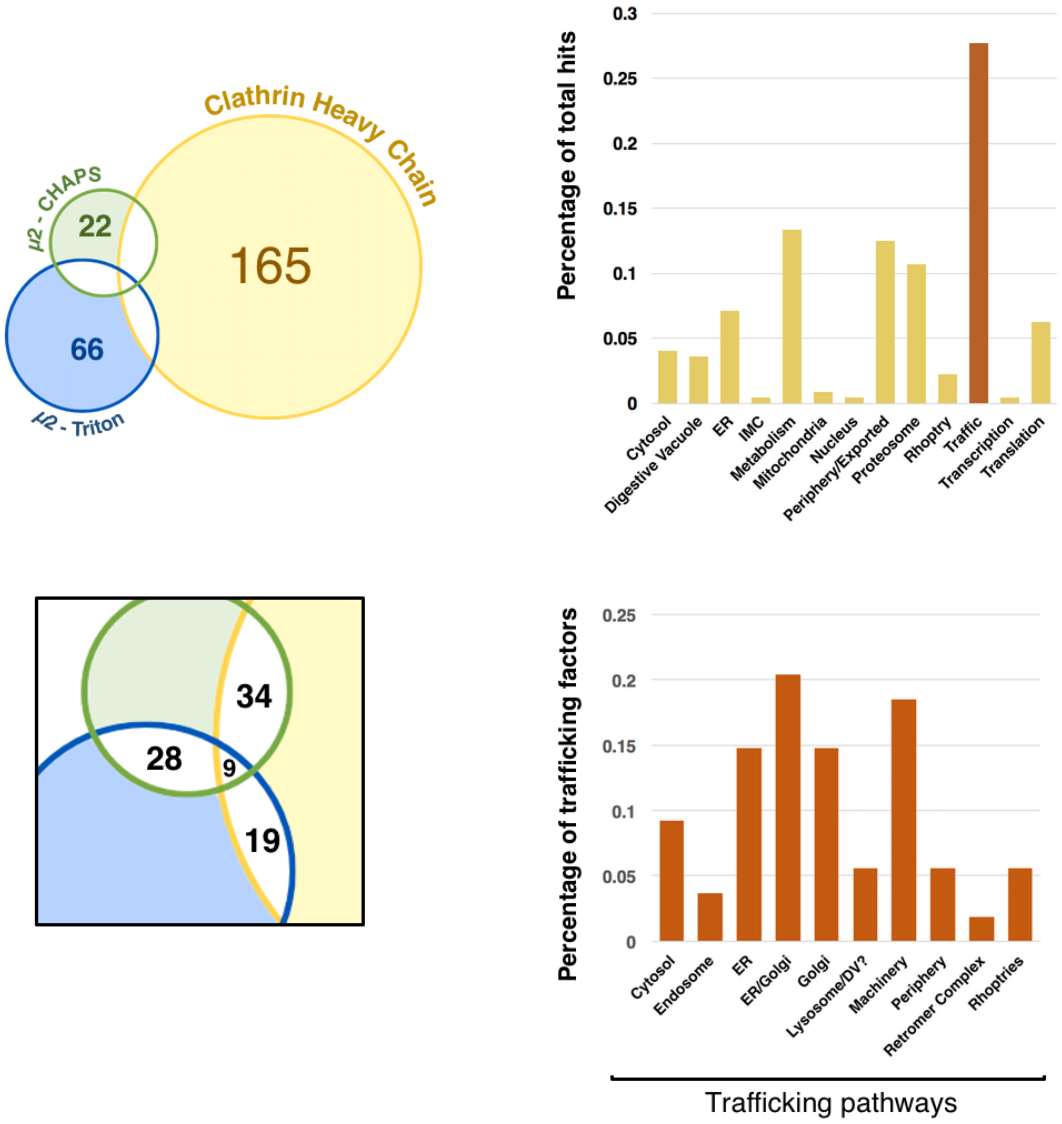


**Figure 88 Overview of a preliminary clathrin heavy chain interactome**
227 potential interacting factors were identified from a single replicate of a clathrin heavy chain-2xFKBP-GFP pulldown. Within this dataset, trafficking factors were highly enriched, accounting for nearly 30% of the identified proteins. These trafficking factors map to many secretory organelles including the rhoptries, endosomal system, digestive vacuole, and cell periphery. Additionally, elements of endosomal recycling and ER-to-Golgi traffic were also identified, supporting the localisation presented above. Left panels show the overlap of this clathrin interactome with the two interactomes generated for μ2 in Section 5.7, revealing 36% overlap between the datasets resulting from extractions performed in the same CHAPS-based extraction buffer. Proteins were identified by MASCOT and filtered against known contaminants using MaxQuant and Perseus. Putative function and localisation was assigned using the Malaria Parasite Molecular Pathways (MPMP) database.

**Table 10 Grouping of CHC-interacting trafficking factors**

| PFID | Name | Enrichment | Location | μ2 CHAPS? | μ2 Triton? |
|---|---|---|---|---|---|
| PF3D7_1015600 | Heat Shock Protein 60 | 1.36E+00 | Apicoplast | Y | |
| PF3D7_1117100 | Deubiquinating/Deneddylating Enzyme | 1.73E+09 | Cytosol | | |
| PF3D7_1136500 | Casein Kinase 1 | 8.78E+08 | Cytosol | | |
| PF3D7_0217500 | Calcium-Dependent Protein Kinase 1 | 8.70E+08 | Cytosol | | |
| PF3D7_0904600 | Ubiquitin Specific Protease, Putative | 2.99E+08 | Cytosol | | |
| PF3D7_1232100 | 60 Kda Chaperonin | 1.79E+00 | Cytosol | | |
| PF3D7_0826100 | Hect-Like E3 Ubiquitin Ligase, Putative | 1.25E+00 | Cytosol | Y | |
| PF3D7_0505800 | Small Ubiquitin-Related Modifier | 3.67E+09 | Cytosol | | |
| PF3D7_1466100 | Protein Phosphatase Containing Kelch-Like Domains | 1.17E+09 | Cytosol | | |
| PF3D7_0826700 | Receptor For Activated C Kinase | 9.28E-01 | Cytosol | Y | |
| PF3D7_1408000 | Plasmepsin II | 1.38E+00 | Digestive Vacuole | | |
| PF3D7_0629200 | DnaJ Protein, Putative | 2.90E+10 | ER | Y | |
| PF3D7_1134100 | Protein Disulfide Isomerase | 1.67E+00 | ER | | |
| PF3D7_1108600 | Endoplasmic Reticulum-Resident Calcium Binding Protein | 1.46E+00 | ER | | |
| PF3D7_1211400 | Heat Shock Protein Dnaj Homologue Pfj4 | 1.24E+00 | ER | Y | |
| PF3D7_1134000 | Heat Shock Protein 70 | 1.20E+00 | ER | | |
| PF3D7_0818900 | Heat Shock Protein 70 | 1.08E+00 | ER | | |
| PF3D7_1222300 | Endoplasmin, Putative | 1.10E+00 | ER | Y | |
| PF3D7_0609800 | Palmitoyltransferase, Putative | 2.17E+09 | IMC | | |
| PF3D7_1446200 | M17 Leucyl Aminopeptidase | 1.44E+10 | Metabolism | Y | |
| PF3D7_1124600 | Ethanolamine Kinase | 5.94E+09 | Metabolism | Y | |
| PF3D7_0922600 | Glutamine Synthetase, Putative | 3.17E+09 | Metabolism | | |
| PF3D7_1469600 | Biotin Carboxylase Subunit Of Acetyl Coa Carboxylase | 2.32E+09 | Metabolism | | |
| PF3D7_1033400 | Haloacid Dehalogenase-Like Hydrolase | 2.28E+09 | Metabolism | Y | Y |
| PF3D7_0610800 | Transketolase | 1.04E+09 | Metabolism | | |
| PF3D7_0605900 | Long Chain Polyunsaturated Fatty Acid Elongation Enzyme | 5.51E+03 | Metabolism | | |
| PF3D7_0624000 | Hexokinase | 4.38E+00 | Metabolism | Y | Y |
| PF3D7_0627800 | Acetyl-CoA Synthetase, Putative | 2.58E+00 | Metabolism | | |
| PF3D7_1308200 | Carbamoyl Phosphate Synthetase | 2.57E+00 | Metabolism | | |
| PF3D7_1015900 | Enolase | 2.02E+00 | Metabolism | | |
| PF3D7_1361000 | Protein Arginine N-Methyltransferase 5, Putative | 1.53E+00 | Metabolism | | |
| PF3D7_1343000 | Phosphoethanolamine N-Methyltransferase | 1.53E+00 | Metabolism | | |
| PF3D7_0626800 | Pyruvate Kinase | 1.44E+00 | Metabolism | | |
| PF3D7_1444800 | Fructose-Bisphosphate Aldolase | 1.39E+00 | Metabolism | | |
| PF3D7_0922200 | S-Adenosylmethionine Synthetase | 1.38E+00 | Metabolism | | |
| PF3D7_0922500 | Phosphoglycerate Kinase | 1.21E+00 | Metabolism | Y | |
| PF3D7_0621200 | Pyridoxine Biosynthesis Protein Pdx1 | 1.16E+00 | Metabolism | | |
| PF3D7_1120100 | Phosphoglycerate Mutase, Putative | 1.08E+00 | Metabolism | | |
| PF3D7_0218000 | Replication Factor C Subunit 2, Putative | 6.16E+09 | Nucleus | | |
| PF3D7_0811300 | CCR4-Associated Factor 1 | 4.07E+09 | Nucleus | | |
| PF3D7_1315900 | Exportin-T, Putative | 3.86E+09 | Nucleus | | |
| PF3D7_1027300 | Peroxiredoxin | 3.49E+09 | Nucleus | Y | |
| PF3D7_1330600 | Elongation Factor Tu, Putative | 2.07E+09 | Nucleus | Y | |
| PF3D7_1355800 | Splicing Factor 3B Subunit 5, Putative | 2.15E+00 | Nucleus | Y | |
| PF3D7_0910100 | Exportin-7, Putative | 1.39E+11 | Periphery/Exported | | |
| PF3D7_1129100 | Parasitophorous Vacuolar Protein 1 | 4.28E+10 | Periphery/Exported | Y | Y |
| PF3D7_0500800 | Mature Parasite-Infected Erythrocyte Surface Antigen | 4.15E+10 | Periphery/Exported | | |
| PF3D7_0801000 | Plasmodium Exported Protein (Phistc), Unknown Function | 4.14E+10 | Periphery/Exported | | |
| PF3D7_1121600 | Exported Protein 1 | 1.96E+10 | Periphery/Exported | | |
| PF3D7_0424600 | Plasmodium Exported Protein (Phistb), Unknown Function | 1.42E+10 | Periphery/Exported | | |
| PF3D7_0402000 | Plasmodium Exported Protein (Phista), Unknown Function | 1.16E+10 | Periphery/Exported | Y | Y |
| PF3D7_0301600 | Plasmodium Exported Protein (Hyp1), Unknown Function | 1.05E+10 | Periphery/Exported | | Y |
| PF3D7_1401400 | Early Transcribed Membrane Protein 14.1 | 4.78E+09 | Periphery/Exported | | |
| PF3D7_0401800 | Plasmodium Exported Protein (Phistb), Unknown Function | 4.11E+09 | Periphery/Exported | | |
| PF3D7_0532300 | Plasmodium Exported Protein (Phistb), Unknown Function | 3.96E+09 | Periphery/Exported | | |
| PF3D7_0730900 | Emp1-Trafficking Protein | 1.99E+09 | Periphery/Exported | Y | Y |
| PF3D7_1149000 | Antigen 332, Dbl-Like Protein | 5.78E+08 | Periphery/Exported | Y | |
| PF3D7_0532100 | Early Transcribed Membrane Protein 5 | 3.35E+00 | Periphery/Exported | Y | Y |
| PF3D7_0936800 | Plasmodium Exported Protein (Phistc), Unknown Function | 2.89E+00 | Periphery/Exported | | |
| PF3D7_0703500 | Erythrocyte Membrane-Associated Antigen | 2.08E+00 | Periphery/Exported | | |
| PF3D7_1353200 | Membrane Associated Histidine-Rich Protein | 1.87E+00 | Periphery/Exported | | |
| PF3D7_0102200 | Ring-Infected Erythrocyte Surface Antigen | 1.41E+00 | Periphery/Exported | | Y |
| PF3D7_1016300 | Gbp130 Protein | 2.77E-01 | Periphery/Exported | | |
| PF3D7_0501300 | Skeleton-Binding Protein 1 | 3.76E+10 | Periphery/Exported | | |
| PF3D7_0501100 | Heat Shock Protein 40, Type II | 5.19E+09 | Periphery/Exported | | |
| PF3D7_0830400 | Cra Domain-Containing Protein, Putative | 2.14E+09 | Periphery/Exported | | |
| PF3D7_0113000 | Glutamic Acid-Rich Protein | 1.15E+09 | Periphery/Exported | | Y |

CHC interacting factors were filtered for those with putative functions relating to intracellular traffic. These factors were then sub-classified based on data available on MPMP for the location of their associated trafficking pathway. These factors were also cross-referenced against the μ2 interactome datasets generated using the same CHAPS-based condition as described here and an alternative, triton-based extraction condition. (Table continues on next page)

| PFID | Name | Enrichment | Location | μ2 CHAPS? | μ2 Triton? |
|---|---|---|---|---|---|
| PF3D7_0317000 | Proteasome Subunit Alpha Type-3, Putative | 2.53E+10 | Proteosome | | |
| PF3D7_0727400 | Proteasome Subunit Alpha Type-5, Putative | 1.57E+10 | Proteosome | | |
| PF3D7_1402300 | 26S Proteasome Regulatory Subunit Rpn6 | 1.08E+10 | Proteosome | | |
| PF3D7_1368100 | 26S Proteasome Regulatory Subunit Rpn11, Putative | 5.93E+09 | Proteosome | | |
| PF3D7_1017900 | 26S Proteasome Regulatory Subunit P55, Putative | 5.80E+09 | Proteosome | | |
| PF3D7_1030500 | 26S Proteasome Regulatory Subunit Rpn9, Putative | 5.25E+09 | Proteosome | | |
| PF3D7_1328100 | Proteasome Subunit Beta Type-7, Putative | 2.79E+09 | Proteosome | Y | Y |
| PF3D7_0912900 | 26S Proteasome Regulatory Subunit Rpn8, Putative | 2.24E+09 | Proteosome | | |
| PF3D7_0907700 | Proteasome Activator 28 Subunit Beta, Putative | 1.37E+09 | Proteosome | | |
| PF3D7_0803800 | Proteasome Subunit Beta Type-4 | 3.32E+00 | Proteosome | | |
| PF3D7_1248900 | 26S Protease Regulatory Subunit 8, Putative | 2.90E+00 | Proteosome | Y | |
| PF3D7_1130400 | 26S Protease Regulatory Subunit 6A, Putative | 2.57E+00 | Proteosome | | |
| PF3D7_1311500 | 26S Protease Regulatory Subunit 7, Putative | 2.35E+00 | Proteosome | Y | |
| PF3D7_1306400 | 26S Protease Regulatory Subunit 10B, Putative | 1.76E+00 | Proteosome | | Y |
| PF3D7_1008400 | 26S Protease Regulatory Subunit 4, Putative | 1.74E+00 | Proteosome | Y | |
| PF3D7_1129200 | 26S Proteasome Regulatory Subunit Rpn7, Putative | 1.72E+00 | Proteosome | | |
| PF3D7_0205900 | 26S Proteasome Regulatory Subunit Rpn1, Putative | 1.70E+00 | Proteosome | Y | |
| PF3D7_1466300 | 26S Proteasome Regulatory Subunit Rpn2, Putative | 1.26E+00 | Proteosome | | Y |
| PF3D7_0108000 | Proteasome Subunit Beta Type-3, Putative | 1.05E+00 | Proteosome | | Y |
| PF3D7_1353900 | Proteasome Subunit Alpha Type-7, Putative | 1.01E+00 | Proteosome | | |
| PF3D7_0608500 | Proteasome Subunit Alpha Type-2, Putative | 7.30E-01 | Proteosome | Y | |
| PF3D7_0817700 | Rhoptry Neck Protein 5 | 1.59E+09 | Rhoptry | | |
| PF3D7_1252100 | Rhoptry Neck Protein 3 | 1.30E+00 | Rhoptry | | |
| PF3D7_0929400 | High Molecular Weight Rhoptry Protein 2 | 1.16E+00 | Rhoptry | | |
| PF3D7_0302100 | Serine/Threonine Protein Kinase | 5.20E+10 | Signaling | | |
| PF3D7_1443000 | Serine/Threonine Protein Kinase | 2.45E+09 | Signaling | | |
| PF3D7_1246200 | Actin I | 4.85E+11 | Traffic | Y | |
| PF3D7_1008700 | Tubulin Beta Chain | 1.66E+11 | Traffic | Y | |
| PF3D7_0903700 | Alpha Tubulin 1 | 5.51E+10 | Traffic | Y | |
| PF3D7_1016200 | Rab3 Gtpase-Activating Protein Non-Catalytic Subunit | 3.34E+10 | Traffic | | |
| PF3D7_1472100 | Protein Transport Protein Yip1, Putative | 7.03E+09 | Traffic | | |
| PF3D7_0503400 | Actin-Depolymerizing Factor 1 | 6.72E+09 | Traffic | | |
| PF3D7_1465100 | Conserved Oligomeric Golgi Complex Subunit 6, Putative | 2.46E+09 | Traffic | | |
| PF3D7_1130500 | Conserved Oligomeric Golgi Complex Subunit 2, Putative | 2.16E+09 | Traffic | | |
| PF3D7_1250300 | Vacuolar Protein Sorting-Associated Protein 26, Putative | 2.08E+09 | Traffic | | |
| PF3D7_0109400 | Tubulin-Specific Chaperone A, Putative | 1.12E+09 | Traffic | | |
| PF3D7_1435500 | Clathrin Light Chain, Putative | 5.30E+00 | Traffic | | |
| PF3D7_0905900 | Coatomer Subunit Beta, Putative | 3.68E+00 | Traffic | | |
| PF3D7_0808400 | Coatomer Subunit Epsilon, Putative | 3.31E+00 | Traffic | | |
| PF3D7_1219100 | Clathrin Heavy Chain, Putative | 3.02E+00 | Traffic | | |
| PF3D7_1429800 | Coatomer Subunit Beta, Putative | 2.98E+00 | Traffic | | |
| PF3D7_1020900 | Adp-Ribosylation Factor | 2.75E+00 | Traffic | Y | |
| PF3D7_0606700 | Coatomer Alpha Subunit, Putative | 2.66E+00 | Traffic | | |
| PF3D7_1455500 | Ap-1 Complex Subunit Gamma, Putative | 2.23E+00 | Traffic | | |
| PF3D7_0308200 | T-Complex Protein 1 Subunit Eta | 1.95E+00 | Traffic | Y | Y |
| PF3D7_1145100 | Coatomer Subunit Gamma, Putative | 1.83E+00 | Traffic | | |
| PF3D7_0306800 | T-Complex Protein 1 Subunit Beta | 1.69E+00 | Traffic | Y | |
| PF3D7_1134800 | Coatomer Subunit Delta | 1.68E+00 | Traffic | | |
| PF3D7_1311400 | Ap-1 Complex Subunit Mu-1 | 1.56E+00 | Traffic | | |
| PF3D7_0528100 | Ap-1 Complex Subunit Beta, Putative | 1.31E+00 | Traffic | Y | |
| PF3D7_1229500 | T-Complex Protein 1 Subunit Gamma | 1.31E+00 | Traffic | Y | |
| PF3D7_1230700 | Protein Transport Protein Sec13 | 1.19E+00 | Traffic | | |
| PF3D7_0214100 | Protein Transport Protein Sec31 | 1.18E+00 | Traffic | | |
| PF3D7_1132200 | T-Complex Protein 1 Subunit Alpha | 1.07E+00 | Traffic | Y | |
| PF3D7_0415400 | Coatomer Subunit Zeta, Putative | 1.06E+00 | Traffic | | |
| PF3D7_1357800 | T-Complex Protein 1 Subunit Delta | 8.20E-01 | Traffic | Y | |
| PF3D7_0418200 | Eukaryotic Translation Initiation Factor 3 Subunit | 3.73E+09 | Translation | | |
| PF3D7_1410600 | Eukaryotic Translation Initiation Factor 2 Subunit | 2.05E+09 | Translation | | Y |
| PF3D7_1312900 | Eukaryotic Translation Initation Factor 4 Gamma | 1.69E+00 | Translation | | |
| PF3D7_1019000 | Eukaryotic Translation Initiation Factor Subunit E | 1.63E+00 | Translation | | |
| PF3D7_0716800 | Eukaryotic Translation Initiation Factor 3 Subunit I | 1.59E+00 | Translation | | |
| PF3D7_1212700 | Eukaryotic Translation Initiation Factor 3 Subunit A | 1.32E+00 | Translation | | |
| PF3D7_1357100 | Elongation Factor 1-Alpha | 1.25E+00 | Translation | | |
| PF3D7_1338300 | Elongation Factor 1-Gamma, Putative | 1.24E+00 | Translation | | |
| PF3D7_0315100 | Eukaryotic Translation Initiation Factor 4E | 1.06E+00 | Translation | | |
| PF3D7_1451100 | Elongation Factor 2 | 8.75E-01 | Translation | | Y |
| PF3D7_1468700 | Eukaryotic Initiation Factor 4A | 8.52E-01 | Translation | Y | |
| PF3D7_0612100 | Eukaryotic Translation Initiation Factor 3 Subunit L | 7.10E-01 | Translation | | Y |
| PF3D7_1208400 | Amino Acid Transporter, Putative | 5.66E+09 | Transporter | | |
| PF3D7_1368200 | Abc Transporter E Family Member 1, Putative | 2.12E+09 | Transporter | Y | Y |
| PF3D7_1421900 | Copper Transporter, Putative | 7.61E+08 | Transporter | | |
| PF3D7_0932800 | Importin Alpha Re-Exporter, Putative | 1.79E+00 | Transporter | | |
| PF3D7_0814300 | Aaa Family Atpase, Putative | 1.32E+00 | Transporter | | |
| PF3D7_0706000 | Importin-7, Putative | 9.97E-01 | Transporter | | |
| PF3D7_0815200 | Importin Beta, Putative | 6.52E+10 | Transporter | | |
| PF3D7_1038000 | Antigen Ub05 | 1.32E+10 | Unknown | | |
| PF3D7_1409800 | CUGBP Elav-Like Family Member 2, Putative | 7.26E+09 | Unknown | | |
| PF3D7_0309800 | YTH Domain-Containing Protein, Putative | 3.54E+09 | Unknown | | |
| PF3D7_0620500 | Cleavage Stimulation Factor Subunit 1, Putative | 3.04E+09 | Unknown | | |
| PF3D7_1249300 | Protein Phosphatase PPM4, Putative | 9.77E+08 | Unknown | | |
| PF3D7_0914900 | Bsd-Domain Protein, Putative | 9.12E+08 | Unknown | Y | |
| PF3D7_1231800 | Asparagine-Rich Protein, Putative | 8.74E-01 | Unknown | | |
| PF3D7_1118200 | Heat Shock Protein 90, Putative | 5.33E-01 | Unknown | Y | |

traffic, including adaptins, GTPases, secretory complex subunits, and other trafficking machinery. Importantly, the putative clathrin light chain was also identified.

Separating specific clathrin-heavy chain interactors will be difficult because clathrin is one of the most abundant proteins in the cell may be inherently sticky because clathrin heavy chain is abundant in the control pulls, and only present at 5-fold enrichment in the anti-GFP pulldown. By comparison, µ2-3xHA was identified at $10^{11}$-fold enrichment between anti-HA and control pulldowns. These clathrin-GFP pulldowns and their wild type controls were not cross-contaminated during preparation, and the eluted material was separated on separate gels before submission for mass spectrometry. Therefore, it may not be possible to identify low abundance, specific interactors because these will also be present in the control pulldowns.

## Discussion

To the best of our knowledge, these data are the first characterisation of clathrin heavy chain in *Plasmodium* falciparum. These data show for the first time that clathrin is located at several locations in the parasite cell, including the plasma membrane and the cytosol, consistent with known roles for clathrin in endocytosis and post-Golgi traffic.

By indirect immunofluorescence, as the parasite develops, the clathrin system also develops from a single peripheral structure in the ring stage to dynamic and short-lived structures throughout the cell in trophozoites, ultimately culminating with a single clathrin focus in each merozoite. Immunoelectron microscopy supports

this localisation pattern and shows clathrin as localised near the ER in vesicles and what may be tubular ER extensions. These micrographs also show clathrin at the cell periphery.

Interestingly, these micrographs suggest a possible role for clathrin at or near the ER. Clathrin has never been reported in the early secretory pathway, but the colocalisation observed in several images with protein disulfide isomerase, a known luminal ER factor, suggests there may be some clathrin-mediated traffic out of or near this organelle. These observations require further study. One alternative interpretation is that the anti-PDI antibody used in the electron microscopy imaging, meant to exclusively stain the ER lumen, may also be labelling aspects of the Golgi. Therefore, further experiments should explore other markers of the ER and Golgi in IEM to clarify the localisation of clathrin.

The immunoprecipitation and mass spectrometry work performed in this chapter support the notion that clathrin is involved in may transport steps throughout the parasite cell, as it is in other eukaryotes. The interactome we generated, which requires further refinement with additional datasets and controls, shows a strong enrichment in the interactome for trafficking factors that may serve several secretory organelles in the cell. Upon further functional classification, the identified putative trafficking factors suggest clathrin may be involved in transport to many organelles including the rhoptries, cell periphery, post-Golgi endosomal system, and digestive vacuole. While this list initially seems like essentially every compartment in the cell, at least the mitochondria, apicoplast, and micronemes are all conspicuously missing from the list. As some preliminary validation, clathrin has already been shown to be involved in traffic to the rhoptries in Plasmodium falciparum and Toxoplasma

gondii, and the localisation presented above in Section 8.2 is supported by the identification of peripheral, cytosolic, and ER trafficking factors.

The data in this chapter may shed light on clathrin dependence of the AP-2 complex as characterised in Chapter 5. While the entire AP-1 and AP-3 complexes and elements of the AP-4 complex are present in this list of potential CHC interactors, no AP-2 complex elements, other than AP-1β, were identified. One would not necessarily expect to find all of the AP-2 subunits, but the presence of μ subunits of the other complexes and not AP-2 is intriguing. On one hand, by immunoelectron microscopy, clathrin heavy chain seems to have a similar localisation to μ2, and there is significant overlap in the μ2 interactome and this preliminary CHC interactome. In the CHAPS-based extraction condition, 36% of the μ2 interacting factors (34 out of 93) were shared with the CHC interactome. Yet paradoxically, no AP-2 components have been identified as interacting with clathrin so far, despite the presence of other adaptor complex subunits, including μ subunits, in my preliminary CHC interactome, and no experimental data presented in either Chapter 5 or Appendix VIfirmly suggest an interaction between AP-2 and clathrin. Further experiments are required to explore these observations and clarify whether AP-2 and clathrin interact. A full list of the interacting partners identified in this experiment are listed in Appendices III and VI.

It will be very interesting to probe the function of the AP-3 and AP-4 complexes and ultimately generate an adaptor complex “roadmap” that accurately reflects the dynamics of clathrin-mediated transport within the parasite cell.

Additionally, the identification of two possible sub-types of clathrin-coated vesicles (Type I and Type II) based on their dimensions and elliptical area warrants further investigation as these structures may have functional significance in parasite

development. Given the size of these vesicles, SEM could be done to better examine vesicle morphology and the organisation of the clathrin cage. Overall, this chapter provides more questions than answers and should serve as a jumping off point for further research.


## Acknowledgement of reagents

The work in this chapter was made possible by the generous donation of the 3D7-Clathrin Heavy Chain-2xFKBP-GFP parasite line by Prof Tobias Spielmann. His laboratory generated this line using the selection linked integration platform (SLI) as I used to generate a Ubp1-GFP-expressing parasite line. Mislocalisation experiments using the knock-sideways system are underway to further explore the cellular role of the CHC molecule. Additionally, as in Chapter 5, the immunoelectron microscopy described in this chapter was made possible by our collaboration with Prof Audrey Odom-John and Dr Rachel Edwards at Washington University, St. Louis in the United States. Immunoprecipitation and mass spectrometry experiments were performed with expertise and assistance from Dr Martin Zoltner and Prof Mark Field at the University of Dundee.